Pedro Miguel Palma Rendas
Licenciado em Ciências de Engenharia Mecânica

Fixture Design and Process Development for High Pressure Compressor Rotor Blades Measuring in Turbofan Engine Maintenance

Dissertação para obtenção do Grau de Mestre em Engenharia Mecânica

Orientador: João Manuel Vicente Fradinho, Prof. Auxiliar, FCT/UNL
Co-orientador(es): Mário Almeida Santos, Eng.

FACULDADE DE CIÊNCIAS E TECNOLOGIA
UNIVERSIDADE NOVA DE LISBOA

Setembro 2020

Pedro Miguel Palma Rendas
Licenciado em Ciências de Engenharia Mecânica

Fixture Design and Process Development for High Pressure Compressor Rotor Blades Measuring in Turbofan Engine Maintenance

Dissertação para obtenção do Grau de Mestre em Engenharia Mecânica

Orientador: João Manuel Vicente Fradinho, Prof. Auxiliar, FCT/UNL
Co-orientador: Mário Almeida Santos, Eng.

Fixture Design and Process Development for High Pressure Compressor Rotor Blades Measuring in Turbofan Engine Maintenance

À minha avó e ao meu pai, pelo vosso orgulho e carinho,

Agradecimentos

Esta dissertação representa o culminar de todo um percurso escolar e académico do qual me posso orgulhar. No entanto, este percurso representa também para mim grandes desafios não só a nível académico e profissional, mas principalmente a nível pessoal. Neste sentido, acredito que grande parte deste sucesso não seria possível sem o apoio de todos aqueles que me acompanharam, tanto no desenvolvimento deste trabalho como ao longo de todo este percurso. A estas pessoas, gostaria de deixar os meus sinceros agradecimentos por todo o apoio e disponibilidade.

Primeiramente, gostaria de agradecer à Oficina de Motores da TAP por confiarem em mim o desenvolvimento deste trabalho. Agradeço a toda a engenharia, em particular à Eng. Sara e ao Eng. Daniel por toda a disponibilidade e acompanhamento. Agradeço também a toda a equipa de inspeção dimensional, em especial ao Emanuel, André, José António, João Pedro e Nuno, por todo o tempo que dedicaram tanto ao meu trabalho e pelos conhecimentos transmitidos.

A nível académico, quero agradecer a todos os professores do Departamento de Engenharia Mecânica e Industrial da FCT-NOVA que deixaram a sua marca neste meu percurso. Em especial aos professores António Mourão, Bruno Soares e Rui Martins pela oportunidade de trabalhar como monitor do Núcleo de Projeto Mecânico e ao Prof. João Fradinho pelo seu acompanhamento como orientador desta dissertação. Agradeço também ao Eng. Mário Almeida Santos que, como orientador desta tese, contribuiu ativamente para o seu desenvolvimento e cujo acompanhamento foi essencial, sobretudo dada a situação de pandemia atual.

A todos os meus amigos agradeço todo o apoio e paciência. Ao Mourato, à Carolina, ao Filipe e ao Chico por fazerem de mim um melhor aluno e proporcionarem grandes momentos de descompressão. Aos rapazes Ivo, Miguel, Esquilo, Rafa, Primo, Niko, Cunha, Kikas, Vasco e Leça, não podia deixar de vos mencionar um por um pelo vosso suporte. E por último, mas não menos importante, à minha namorada e melhor amiga, Cláudia pelo apoio que palavras não conseguem descrever.

Finalmente e acima de tudo, à minha família, pai, mãe, irmã e avós por me tornarem na pessoa que sou hoje e por toda a paciência. Convosco, nenhum objetivo é demasiado grande e nenhum percurso será demasiado difícil. Obrigado.

Resumo

A TAP *Maintenance and Engineering* disponibiliza serviços de manutenção para motores de aviação comercial. Para tal, os diversos componentes do motor são inspecionados com o intuito de realizar sua reparação e/ou substituição de forma a restaurar alguma da *performance* e eficiência no consumo de combustível do motor.

Nestes motores, acredita-se que o HPC (Compressor de Alta Pressão) tem um grande impacto na sua *performance*. Por isso, a oficina de motores da TAP tem grande interesse em adquirir conhecimentos mais aprofundados acerca da relação entre as pás do compressor de alta e os resultados de *performance* do motor em banco de testes.

O trabalho desenvolvido procura responder a esta necessidade, disponibilizando à oficina os meios necessários para uma inspeção detalhada das dimensões das pás do compressor de alta. Desta forma, engenheiros da TAP poderão adquirir a informação necessária para estudar a correlação descrita acima e consequentemente melhorar os processos de manutenção e reparação do compressor de alta.

Para este efeito, será necessária medição com recurso a uma CMM (Máquina de Medição de Coordenadas) dada a complexidade de algumas geometrias, o nível de precisão exigido por este estudo e ainda a quantidade elevada de pás que constituem o conjunto do rotor do compressor de alta. Assim o trabalho desenvolvido irá focar-se nas duas primeiras fases de implementação deste método de medição, sendo estas o desenvolvimento de modelos CAD de referência para as pás do compressor e o projeto de uma ferramenta de fixação de um conjunto de pás no plano de granito da CMM. Só depois, com base neste trabalho, será possível criar o programa de inspeção automático.

Os modelos CAD das pás foram desenvolvidos no software *SolidWorks* a partir de uma nuvem de pontos captada por um scanner 3D, foram depois usados como referência para o projeto da ferramenta e podem ainda vir a ser essenciais para a programação da inspeção através da CMM com recurso a modelos virtuais.

Adicionalmente, como a secção mais aprofundada desta tese, o projeto da ferramenta de fixação teve em conta tanto os requisitos de inspeção dimensional das pás como a própria manufatura da ferramenta. Assim, este trabalho irá também resultar na documentação necessária para a manufatura destas ferramentas permitindo à TAP iniciar o desenvolvimento do programa automático de inspeção das pás através da CMM.

Palavras-chave: Manutenção de Motores Turbofan; Pás do Rotor do Compressor de Alta; Inspeção Dimensional; Ferramenta de Fixação; Máquina de Medição de Coordenadas.

Abstract

TAP Maintenance and Engineering provides repair and overhaul services for a commercial aircraft's engines. For this, TAP's shop disassembles and inspects the engine's parts to determine which repairs and replacements should be performed in order to restore the engine's performance and fuel efficiency and meet client's requirements.

In these engine's, the HPC (High Pressure Compressor) is thought to have a large impact in the overall engine's performance. Concerning this, TAP Engine's shop has great interest in better understanding the correlation between the HPC Rotor blades and the engine's performance which could improve the results of the engine's overhaul.

This work tries to answer this by providing the shop the means to perform detailed dimensional inspection for HPC Rotor blades which will provide TAP's engineers real data necessary to perform a correlation study between the HPC blades' condition and the engine's efficiency.

To achieve this, a CMM (Coordinate Measuring Machine) based inspection procedure would have to be implemented given the level of detail and the sheer number of blades assembled in the HPC rotor.

The work developed focuses on the first two stages of this project, the development of CAD models of the blade from each compressor stage and the design of a fixture tool to display the blades for CMM inspection. The third stage, which is only introduced in the final segment of this work, corresponds to the development of the CMM's automatic blade inspection program.

The CAD models of the blades were developed in SolidWorks software based on a point cloud obtained from a 3D scanner. These models were then used to design the fixture tools and may be essential for the CMM programming using CAD data.

The fixture tools were designed to meet the blade inspection functional requirements. This design, as the more in-depth segment of this work, was developed concerning both the blade inspection procedure using the CMM and the tool's manufacturing.

This work will result in the blade's CAD models and the correspondent fixture tools' files for manufacturing thus providing TAP Engine Shop with the initial framework to develop the CMM inspection program.

Keywords: Turbofan Engine Maintenance; High Pressure Compressor Rotor Blades; Dimensional Inspection; Fixture Tool; Coordinate Measuring Machine.

Index

1 Introduction 1

1.1 Motivation 1

1.2 Objectives 2

1.3 Contents 2

2 Company, Engine and Process Description 5

2.1 TAP Maintenance & Engineering 5

2.2 TurboFan Engine – CFM56-5B 6

2.2.1 The TurboFan Engine 6

2.2.2 CFM56 Engine Family 8

2.2.3 *CFM56-5B* TurboFan Engine 10

2.3 HPC Rotor Blade Inspection and Maintenance 14

3 Literature Review 17

3.1 HPC Deterioration and Effects on Blade Geometry 18

3.2 HPC Blade Geometry and Leakage Effect on Performance 21

3.3 TAP M&E Past Work 26

4 Reference Blade Model and dimensions 29

4.1 HPC Blade's Reference Dimensions 29

4.1.1 Reference Dimensions for Modelling 30

4.1.2 HPC Blade's Serviceable and Repairable Dimensions 31

4.2 HPC Blade CAD Model Development 33

4.2.1 HPC Blade Scanning 33

4.2.2 HPC Blade CAD Model Development 38

5 Fixture Design for HPC Blade's Dimensional Inspection Using the CMM 47

5.1 Functional Requirements 48

5.2 Design Constraints 51

5.3 Design Features 55

5.3.1 Blade's fastening mechanism 56

5.3.2 Blade's display configuration 68

5.3.3 Fixture Tool's positioning features 77

5.3.4 Fixture Tool's Early Prototyping and Design Adjustments 81

5.3.5 Design Adjustments for Manufacturing 86

5.3.6 Fixture Tool's handling Features 93

5.4 Geometric Dimensioning and Tolerancing 106

5.4.1 Dowel Pin Fitting and Tolerancing 106

5.4.2 Bolted Connection Tolerancing 109

5.4.3 Blade Slot's Profile Tolerancing 111

5.4.4 Reference Surfaces Dimensional Tolerancing 116
6 HPC Blade Dimensional Inspection using the Coordinate Measuring Machine.....121
6.1 *Mitutoyo*'s Coordinate Measuring Machine and Equipment Brief Description 122
6.2 *Mitutoyo*'s software for CMM programing 126
6.2.1 CAT1000P – Creating GEOPAK Part Program with Help of CAD Data 126
6.2.2 MAFIS – Airfoil Profile Analysis 130
7 Conclusions 133
7.1 Achievements 134
7.2 Future Work 136
References……..139
Appendix……141
Appendix I……...143
Appendix II……...147
Appendix III……...155
Appendix IV……...169
Appendix V……...173
Appendix VI……...179
Appendix VII……....183
Appendix VIII……....191
Appendix IX……....195
Appendix X……....199
Appendix XI……....203
Appendix XII……....207
Appendix XIII……....211
Appendix XIV……...215
Appendix XV……....219
Appendix XVI……....223
Appendix XVII……....227
Appendix XVIII……...231
Appendix XIX……....235
Appendix XX……....239
Appendix XXI……....243
Appendix XXII……....247
Appendix XXIII……...251
Appendix XXIV……...255
Appendix XXV……....259
Appendix XXVI……...263
Appendix XXVII……....267
Appendix XXVIII……....271

Index of Figures

Figure 2.1 - Propulsive Efficiency of Different Turbine Engines [27] 6
Figure 2.2 - Pratt & Whitney JT8D Low-Bypass Turbofan Cross Section [33] 7
Figure 2.3 - Pratt & Whitney PW400 High-Bypass Turbofan's Cross Section [33] 7
Figure 2.4 - Flows and Drives of Turbofan Engine (Adapted from [5]) 8
Figure 2.5 - CFM56-5B Major Modules (Adapted From [5]) 10
Figure 2.6 - CFM56 Engine's Modular Composition (Adapted From [31]) 11
Figure 2.7 - CFM56-5B Core Major Module View [5] 12
Figure 2.8 - CFM56-5B HPC Module Exploded View [5] 13
Figure 2.9 - CFM56-5B Core MM Cross Section (Adapted From [5]) 13
Figure 2.10 - Go/No Go Tool for Chord Length Dimensional Inspection 15
Figure 2.11 - Go/No Go Tool for Edge Thickness Inspection 15
Figure 2.12 - Exhaust Gas Temperature Variation in relation to Outside Air Temperature [29] 16
Figure 3.1 - Airfoil Nomenclature [23] 18
Figure 3.2 - Airfoil Section Dimensions 18
Figure 3.3 - Leading Edge Profile Categories 19
Figure 3.4 - HPC Rotor Blade's Measurements [12] 20
Figure 3.5 - Airfoil Cascade Arrangement Experiment [8] 22
Figure 3.6 - Edge Deterioration Classification [8] 23
Figure 3.7 - Schlieren Photograph from Cascade Experiment [8] 23
Figure 3.8 - Different Chord Blade Configurations [26] 24
Figure 3.9 - Cascade Arrangement Experiment to study secondary flows [10] 25
Figure 3.10 - Results of HPC efficiency for different New/Overhauled Blade Combinations [3] – Appendix I 26
Figure 3.11 - Updated HPC Rotor Blade Maintenace Plan [3] 27
Figure 4.1 - Dimensional specifications for coating repair procedures for Stage 1 Blades – Appendix II 30
Figure 4.2 - Dovetail Profile Angle of Aperture for Stage 1 Blades – Appendix III 30
Figure 4.3 - Pressure face specification for 4-9 Stage Blades - Appendix III 31
Figure 4.4 - Dimensionl inspection specifications for stage 1 blades. – Appendix III 32
Figure 4.5 - Creaform's HandySCAN 3D 34
Figure 4.6 - 3D Scanning Stages Diagram 34
Figure 4.7 - Scanning Workspace 35
Figure 4.8 - Blade Scanning Positions Rendered Image 36
Figure 4.9 - Mesh Model Edge's Irregularities 37
Figure 4.10 - Mesh Model's Available Points and Lines 39
Figure 4.11 - Mesh Model's Reference Planes 40
Figure 4.12 - Blade's Dovetail and Platform Longitudinal Profile Tracing 41
Figure 4.13 - Blade's Dovetail and Platform Lateral Profile 41
Figure 4.14 - Mesh to CAD Model Dovetail and Platform Correspondence After Profile Tracing 42
Figure 4.15 - Mesh to CAD Model Dovetail amd Platform Correspondence After Edge Fillet 42
Figure 4.16 - Mesh Model Airfoil Cross Section Profile 43
Figure 4.17 - Airfoil Profile Tracing in CAD Model 43
Figure 4.18 - Airfoil Profiles for Solidworks' "Loft Boss/Base" Feature 44
Figure 4.19 - Blade's CAD Model Tip Profile Adjustment 44
Figure 5.1 - Main Stages of the Functional and Physical Design Domains 47
Figure 5.2 - HPC Blade Airfoil Chord (left) and Thickness (right) Sectioning 49
Figure 5.3 - Fixture Tool's Design Functional Domain 51
Figure 5.4 - HPC Blades with damaged RTV Silicone 52
Figure 5.5 - CMM Workvolume Display [7] 52
Figure 5.6 - CMM Workvolume Illustration with Dimensions [7] 53
Figure 5.7 - CMM's *X* and *Y* Axis Illustration [7] 53
Figure 5.8 - Available Volume for Tool Design 54
Figure 5.9 - HPC Blade's Available Surface for Tool Attachment 56
Figure 5.10 - 3-2-1 Mating System 57
Figure 5.11 - HPC Blade's Dovetail Fastening Principle 58
Figure 5.12 - Blade's Dovetail Fastening through Upwards Force 59
Figure 5.13 - Blade's Slot Dimensions for Tool Design 59

Figure 5.14 – 1st Stage Blade's Longitudinal Angle of Inclination 60
Figure 5.15 – 1st Stage Blade's Dotevail's Tilt Angle 60
Figure 5.16 - Tool's Slot Profile Compatability with 4th and 5th Stage Blades 61
Figure 5.17 - CMM Probing Force Diagram 62
Figure 5.18 - Conventional CMM's Touch Trigger Mechanism [35] 63
Figure 5.19 - Experiment for Force *P* Estimation 63
Figure 5.20 - Blade's Spring-based Fastening Mechanism 65
Figure 5.21 - *Lesjöfors* Spring's Dimensions [11] - Appendix IV 66
Figure 5.22 - Lesjöfors Spring's Specifications [11] - Appendix IV 66
Figure 5.23 - Tool Dimensioning for Spring Housing 67
Figure 5.24 - *RENISHAW*'s REVO-2 RSP2-RSH250 System [24] 69
Figure 5.25 - *RENISHAW*'s Stylus Specifications [25] 69
Figure 5.26 - *RENISHAW*'s Probe CAD Mock Model with Overall Dimensions 70
Figure 5.27 - Probe's Rotation around its *Y* Axis 71
Figure 5.28 - Probe's Rotation around its *Z* Axis 71
Figure 5.29 - Blade's Distance Influence on the Probe's Accessability 72
Figure 5.30 - Blade's Height Influence on the Probe's Accessability 72
Figure 5.31 - Blade Distance Dimensions with Two-dimensional Approach 73
Figure 5.32 – *SolidWorks'* Minumum Distance Feature 73
Figure 5.33 - Blade Distance Dimensions with Three-dimensional Approach 74
Figure 5.34 – 1st Stage Tool Design Final Blade Display 76
Figure 5.35 - Blade Display Dimensions for 1st Stage Tool 76
Figure 5.36 - CMM's Part Alignment Options [17] 77
Figure 5.37 - Tool's Plane-Line-Line Corresponding Features 78
Figure 5.38 - Tool's Defined Co-ordinate System 79
Figure 5.39 - Tool's Bolted Pin Positioning Feature 80
Figure 5.40 - Tool's Early Prototypes for Slot Testing 81
Figure 5.41 - Blade Slot Profile Dimensions Adjusted for Spacer 82
Figure 5.42 - Designed Spacers for 1st Stage Tool (left) and Remaining Stages (right) 82
Figure 5.43 - RTV Clearance Provided by the Spacer 83
Figure 5.44 - 1st Stage Tool Prototype completed with the Spacer 83
Figure 5.45 - Bar and Spring's Fault Demonstrated through 2nd Stage Tool Prototype 84
Figure 5.46 - Tool Design Adjustment for Bar Movement Constriction 84
Figure 5.47 - Blade Distance Validation Prototypes 85
Figure 5.48 - Tool's Division in Top and Bottom Components 86
Figure 5.49 - Reference Plane for the Component's Separation 87
Figure 5.50 - Shear Stress in the Thread Fillets fo the Bolted Connection 88
Figure 5.51 - Thread Dimensions 89
Figure 5.52 - Bolted Connection Design Illustration 90
Figure 5.53 - Pressure on the Thread Fillet Surfaces for the Bolted Connection 91
Figure 5.54 - Threaded Holes Display on the Top Component 92
Figure 5.55 - Dowel Pin Holes Display on the Top Component 93
Figure 5.56 - 1st Stage Tool with Lifting Eye Bolts 95
Figure 5.57 - Loads to be avoided according to *DIN 580:2010* [14] 96
Figure 5.58 - Lifting Eye Bolts' Force Diagram 96
Figure 5.59 - Weight Lifting Capacity per Lifting Eye Bolt - Appendix VI 97
Figure 5.60 - Shear Stress in the Thread Fillets for the Lifting Eye Bolted Connection 98
Figure 5.61 - Pressure on the Thread Fillet Surfaces for the Lifting Eye Bolted Connection 99
Figure 5.62 - 1st Stage Tool's Assembly Exploded View 100
Figure 5.63 - 1st Stage Tool with Handle Bars and Caster Wheels 101
Figure 5.64 - Designed Handle Bars' Dimensions 101
Figure 5.65 - Tool's Lifting Force Diagram 102
Figure 5.66 - Tool's Lifting Two-Dimensional Force Diagram with Dimensions 102
Figure 5.67 - Handle Bars' Bolted Connection Force Diagram 103
Figure 5.68 - Forces on the Bolted Connection Illustration 104
Figure 5.69 - Dowel Pin Holes Geometric Tolerancing 109
Figure 5.70 - Clearance for the Bolted Connection's True Position Tolerance Calculation 110
Figure 5.71 - Bolted Connection Hole's Geometric Tolerancing 111
Figure 5.72 - Slot's Profile Toleranced Angle 112
Figure 5.73 - Slot's Angle Deviation effects on Blade Attachment 112

Figure 5.74 - Blade Slot Geometric Tolerances Representation 114
Figure 5.75 - Blade Slot's Symmetry Plane Geometric Tolerancing 115
Figure 5.76 - 1st Stage Blade Slot's Angle of Inclination Tolerancing 116
Figure 5.77 - Top and Bottom Component's Mating Surfaces' Geometric Tolerances Representation 117
Figure 5.78 - Top and Bottom Component's Mating Surfaces' Geometric Tolerancing 119
Figure 5.79 - Top Component's Refference Surfaces Geometric Tolerancing 120
Figure 6.1 - *Mitutoyo*'s CMM Available in TAP's Engine's Shop 122
Figure 6.2 - CMM's Co-ordinate System Referential [7] 123
Figure 6.3 - CMM's *A* Rotation Axis Orientation [7] 123
Figure 6.4 - CMM's *B* Rotation Axis Orientation [7] 124
Figure 6.5 - *RENISHAW*'s Manual Command Unit 124
Figure 6.6 - CMM's Probe Storage Rack 125
Figure 6.7 - *CAT1000P*'s Line Element Pop-up Window [16] 127
Figure 6.8 - *CAT1000*'s Tree View Selection [16] 128
Figure 6.9 - HPC Blade's Inspection Suggested Reference Surfaces for *CAT1000* Programming 128
Figure 6.10 - *CAT1000*'s Probe Movement Simulation [16] 129
Figure 6.11 - Airfoil Profile Data From *SCANPAK*-based Inspection [15] 130
Figure 6.12 - *MAFIS* Airfoil Profile Analisys Output [15] 131
Figure 6.13 - *MAFIS* Profile Analisys Settings [15] 131
Figure 7.1 - Early Stage Developments for Airfoil Dimensional Data Acquisition 133
Figure 7.2 - HPC Blade's and Engine's Performance Correlation Study End Stages 134
Figure 7.3 - Rendered Imagem of HPC Blade's CAD Reference Models (Stages 1 to 5) 135
Figure 7.4 - Rendered Images of the Designed Fixture Tools (Stage 1 and Stage4/5) 136
Figure 7.5 - Rendered Image of Fixture Tool with Blades Assembled 137

Index of Tables

Table 2-1 - CFM56 Engine Family Overview [31] 9
Table 2-2 - CFM Delivered Engines [5] 9
Table 4-1 - Dimensional Inspection Specifications for Stage 1 HPC -5B/P Blades 32
Table 5-1 - HPC Blade's Set Weight 55
Table 5-2 - Scale Measurements for Force P Estimation 64
Table 5-3 - Force F Calculation Values 64
Table 5-4 - Blade Distance Calculation and Measured Dimensions 75
Table 5-5 - Metric Thread Dimensions – M6 (*Desenho Técnico* Tabela 15.10 [34]) 90
Table 5-6 – Aluminium 6061's Properties (Consulted from [13]) 94
Table 5-7 - Tool's weight and dimensions by HPC stage 94
Table 5-8 - Hoist force on the Lifting Eye bolt by angle β for the 1st Stage tool 97
Table 5-9 - Metric Thread Dimensions– M8 (*Desenho Técnico* Tabela 15.10 [34]) 100
Table 5-10 - Pin-Hole Fitting Tolerances 107
Table 5-11 - Hole Adjusted Standard Tolerances 107
Table 5-12 - Slot Length Tolerance Class Analysis 113
Table 5-13 - Surface Height Tolerance Class Analysis 113
Table 5-14 - Flatness Tolerance Values Comparison 118

Acronyms

AR	Aspect Ratio
BR	*Bypass Ratio*
CAD	Computer Assisted Design
CC	Combustion chamber
CMM	Coordinate Measuring Machine
CNC	Computer Numerical Control
EGT	Exhaust Gas Temperature
FCT	Faculdade de Ciências e Tecnologias
HPC	High pressure compressor
HPT	High pressure compressor
IGV	Inlet Guide Vane
LE	Leading Edge
LLP	Life Limited Part
LPC	Low pressure compressor (também denominado *Booster*)
LPT	Low pressure compressor
M&E	Maintenance and Engineering
MM	Major Module
MRO	Maintenance Repair and Overhaul
OAT	Outside Air temperature
PR	*Pressure Ratio*
RTV	Room Temperature Vulcanizing
SFC	Specific Fuel Consumption
SM	*Stall Margin*
TAP	Transportes Aéreos Portugueses
UNL	Universidade Nova de Lisboa
VSV	Variable Stator Vane

1 Introduction

As is well known, aircraft travelling is one of the major contributors to globalization as it has allowed to travel across the globe in a matter of hours. Due to this the evolution of commercial air travelling is considered one of the major facilitators for economic growth, world trade, international investment and tourism causing an increase on demand for flight passes to all over the world.

Thanks to this increase in demand, airline companies are looking to offer cheaper and almost hourly flights to major cities across the globe. Therefore, in addition to the well-known concern about flight safety, appeared a concern about flight economic and environmental efficiency, as fuel efficiency and aircraft pollution reduction became the major focus of innovation regarding aircraft engine design.

With this in mind, there is a great interest in maintaining the fuel efficiency of the aircraft engine through its whole life as some engine deterioration is inevitable and results in an increase in fuel consumption. This is possible through engine MRO (Maintenance Repair and Overhaul) when a shop visit can restore the engine's fuel efficiency to some extent thus reducing airline companies costs.

1.1 Motivation

In commercial aircrafts today, the most common type of engine is the turbofan engine which can be seen as an evolution of the propeller and turbojet engines used in the early models. These engines are designed to have greater bypass ratios and higher-pressure ratios than their predecessors. With this, engines improve in fuel efficiency, thus lowering pollution emissions and reducing noise.

The HPC (High Pressure Compressor) is believed to have a strong influence in the performance of these engines. Therefore, because of deterioration of engine components during operation time, there is a great interest in performing engine overhaul focused on HPC components which include rotor blades, stator vanes and others that will be described in more detail ahead.

However, the geometry of some of these components and assemblies may prove to be very difficult to inspect and, although there is some research focused in describing which characteristics or specific geometries have an influence in engine performance, the processes and tools used for dimensional inspection are still rather rudimentary in some MRO shops.

With somewhat recent advances in technology, there are tools and machines available that allow us to inspect and even model the most complex geometries in three dimensions, but these tools also require a more in-depth knowledge to be put into use. This way, there is an opportunity for engineers to develop the methods and tools to perform these inspections using the latest technologies

1.2 Objectives

Considering the abovementioned, the main goal of this work is to make use of the technology available in shop namely the CMM (Coordinate Measuring Machine) and the, recently acquired, 3D Scanner, to evaluate the various blade geometries and correlate them with the engine's performance.

This suggests the need to design a fixture tool that allows the positioning of a full set of HPC rotor blades with special attention to geometric design and tolerances to minimize the measuring errors that can derive from the tool's geometric flaws. Thereafter, in order make use of the CMM, a reference model will be created with the intent of mapping the components in position to serve as reference to the CMM.

Furthermore, an automated CNC program should be created that measures and evaluates the fundamental dimensions of the rotor blades making it possible to determine the overall condition of the blades in order to develop a correlation study between the blades and the engine's performance.

In addition to this, this work should also include guidelines to the use of the tools and processes developed as its objective is to be implemented in future shop work and improvement of MRO efficiency and quality.

1.3 Contents

This thesis is organized in seven chapters as well as bibliographic references and appendix sections. The present chapter offers an introduction to the topics covered by this work while also providing an explanation to the motivation and main objectives behind it. It also contains this section where the outline of this thesis is described chapter by chapter.

The second chapter consists of an over-the-top description of the company, more specifically the engine's maintenance and engineering department. This also includes a brief description of the services provided by the company and its commitment to costumers and a segment that describes the turbofan engine focusing on *CFM* engine models which are the models more common in the shop.

With the engine representation comes a brief description of the engine's major modules and their components as well as their functionality in order to provide a better understanding of some of the topics that may be addressed in other chapters. This chapter also contains the procedures that are currently in place for compressor rotor blade dimensional inspection.

The third chapter reviews some literature namely some articles published by ASME, International Journal of Gas Turbines and others regarding the compressor blade airfoil geometry and its relation to compressor efficiency and engine SFC (Specific Fuel Consumption). This chapter

also addresses some of the investigation work previously done at the company by other mastets' students that enrolled in programs similar to this and that also addressed the correlation between compressor rotor blades and engine efficiency yet overlooked the procedures for dimensional inspection.

The fourth chapter documents the known blade reference dimensions and contains the development of a reference CAD model for HPC blades based on a 3D scanned model. This chapter will cover the *SolidWorks* software features used and will be described in a sort of step by step manner so it can be replicated for the compressor's latter stages or even other engine components.

Then, the fifth chapter uses this information abovementioned and presents an in-depth design report for a fixture tool to support the blades during CMM operation. This includes the definition of design parameters to meet the tool's requirements and will also cover the tool's tolerancing and geometric design concerning manufacturing.

The sixth chapter briefly covers the *Mitutoyo'*s CMM software with greater potential to be combined with both the fixture tool and blade reference models. This chapter intends to provide the baseline to continue the developments of this work.

At last, the seventh and final chapter provides a conclusion to the work done as well as some of its achievements concerning the broader project for the correlation study. This chapter also addresses some of the future work that may be done in order to complete and give continuity to the work of this thesis, and also some acknowledgment of where there is room for further improvement or some design flaws that should be addressed.

2 Company, Engine and Process Description

2.1 TAP Maintenance & Engineering

TAP Maintenance and Engineering offers a wide range of MRO (Maintenance Repair and Overhaul) services to commercial aircraft both from the TAP airline fleet and third-party airline fleets. As part of the TAP group, TAP M&E which completed this past year 50 years of operation, offers the advantages of a complete set of integrated services such as aircraft maintenance, engine repair and overhaul, component repair, continuing airworthiness management and a variety of engineering services.

Located in Lisbon, Portugal, the company employs around 2000 people including highly qualified technicians and engineering staff while also providing training and internship programs for engineering students. Over the years, both TAP air Portugal and TAP M&E have received international recognition for their quality and reliability from costumers and manufactures such as Airbus, FedEx and NATO.

As part of somewhat recent changes, the Care²Quality concept was adopted by TAP M&E as a mean to establish Safety, Quality and Relationship as the main focuses of the company towards its interested parties as well as providing an overview of the commercial services that the company has to offer. This concept covers four main services provided by TAP M&E, these being the following:

- Care²Airframe – Providing baseline maintenance to aircraft frame as well as some structural repairs and modifications. In this section, TAP M&E was the first European Aircraft MRO Company to perform the sharklets retrofit to their Airbus A320's as a mean to improve the aircraft aerodynamics and reducing fuel consumption.
- Care²Engines – Providing engine repair and overhaul for the CFM56 engine family and General Electric CF6 engine. In-house repair capability for over 80% of engine parts and APU (Accessory Power Unit) and Thrust Reverser Overhaul.
- Care²Components – Overhaul, repair, test and modifications for over 15000 components ranging from avionics or mechanical components to pneumatic/hydraulic, fuel and oil system components.
- Care²Engineering – Providing engineering, technical and logistical services tailored to the TAP Air Portugal's fleet specific needs. TAP M&E also provides a series of training programs and technical laboratory services.

2.2 TurboFan Engine – CFM56-5B.

A brief introduction to both the engine components and manufacturer is considered to be important as it allows to have a better grasp on the importance of the work that is going to be done as well as providing a base knowledge of the engine's operation and its dependence on the performance of some of its components.

2.2.1 The TurboFan Engine

The turbofan engine is the most common type of engine in commercial aircraft. This engine has greater fuel efficiency due to its capability of accelerating a very large mass of air through the fan duct at relatively lower velocity. This high mass-low velocity airflow is more propulsive efficient than the high velocity jet produced at a turbojet's exhaust nozzle. This propulsive efficiency results in an engine with lower specific fuel consumption making the turbofan engine more fuel efficient.

In the turbofan engine, the gas turbine is powered by the primary air flow which acts as a driver of the ducted fan producing over 70% of the total thrust consisting of cold low-velocity bypass air. The commercial Turbofan, a turbojet engine with high bypass ratios, has been proven to be the most propulsive efficient engine for subsonic high Mach number flights (between about 500 and approx. 760 m.p.h.) as it is shown in Figure 2.1 below.

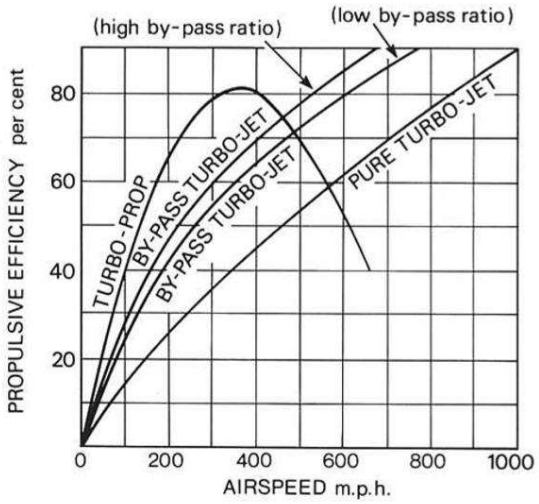

Figure 2.1 - Propulsive Efficiency of Different Turbine Engines [27]

The turbofan engine usefulness in commercial aircraft propulsion systems is attributed to the engine's lower fuel consumption which allows companies to lower transportation costs. In addition to this, lower fuel consumption is also associated with lower pollutant gas emissions and lower noise, making these engines the appropriate choice.

The turbofan engine is capable of producing lower noise values partly because of the extra turbine stages needed to drive the fan which result on lower velocity and lower pressure exhaust gases. Due to these advantages, the turbofan engine has evolved with currently used models in commercial aircraft providing higher bypass ratios and higher-pressure ratios.

The CFM56 engine family, which we are going to cover ahead in this chapter, presents bypass ratios of approximately 6:1 and pressure ratios greater than 30:1 as opposed to the bypass ratios of 1:1 and pressure ratios below 20:1 for earlier turbofan engine models. These engines' cross section comparison between earlier (1960's) and more recent (1980's) *Pratt&Whitney's* turbofan engine models can be observed in Figures 2.2 and 2.3 respectively, where the difference in ratios between the fan duct and primary flow as well as reduction in transversal section area in compressor stages are clear.

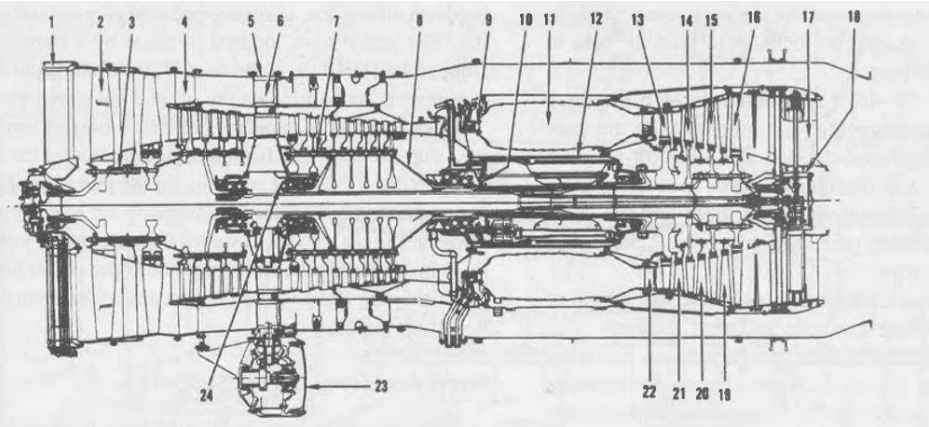

Figure 2.2 - Pratt & Whitney JT8D Low-Bypass Turbofan Cross Section [33]

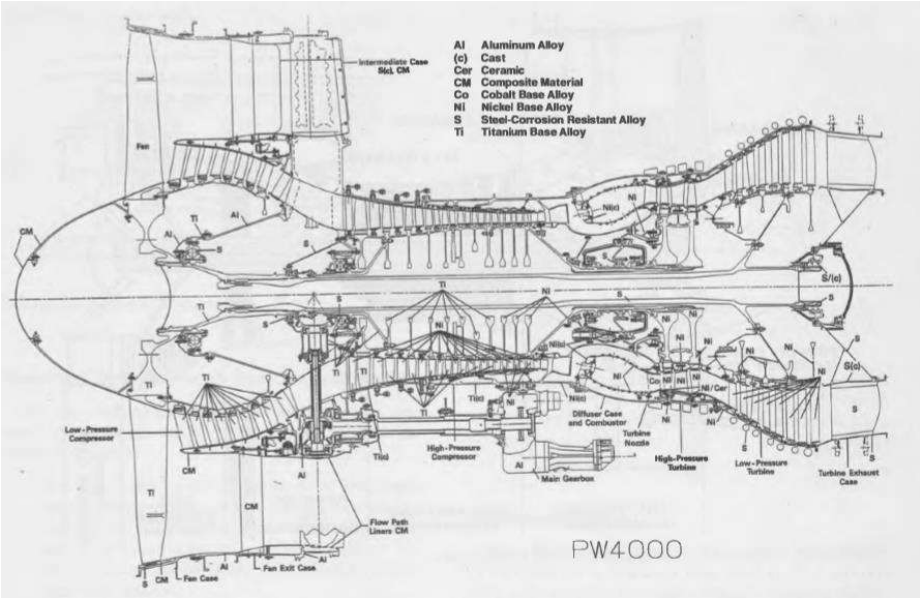

Figure 2.3 - Pratt & Whitney PW400 High-Bypass Turbofan's Cross Section [33]

The turbofan mode of operation can be described very simply. The primary air flow passes through a fan and both the low pressure (LPC) and high pressure compressors (HPC), pressurizing and preheating the air, preparing it to enter the combustion chamber. In the combustion chamber the air is the mixed with fuel and ignited to heat and expand the air, increasing airflow velocity and moving the high pressure (HPT) and low pressure turbines (LPT).

For this, the turbofan engine rotates at two different speeds. The fan and low pressure compressor rotate slower at N1 RPM, in some cases producing nearly 80% of the engine's Take-off Thrust, powered by the LPT and the HPC rotates at a higher N2 RPM, powered by the HPT. Figure 2.4 can provide a more graphical explanation of this simple approach to the turbofan engine's operation.

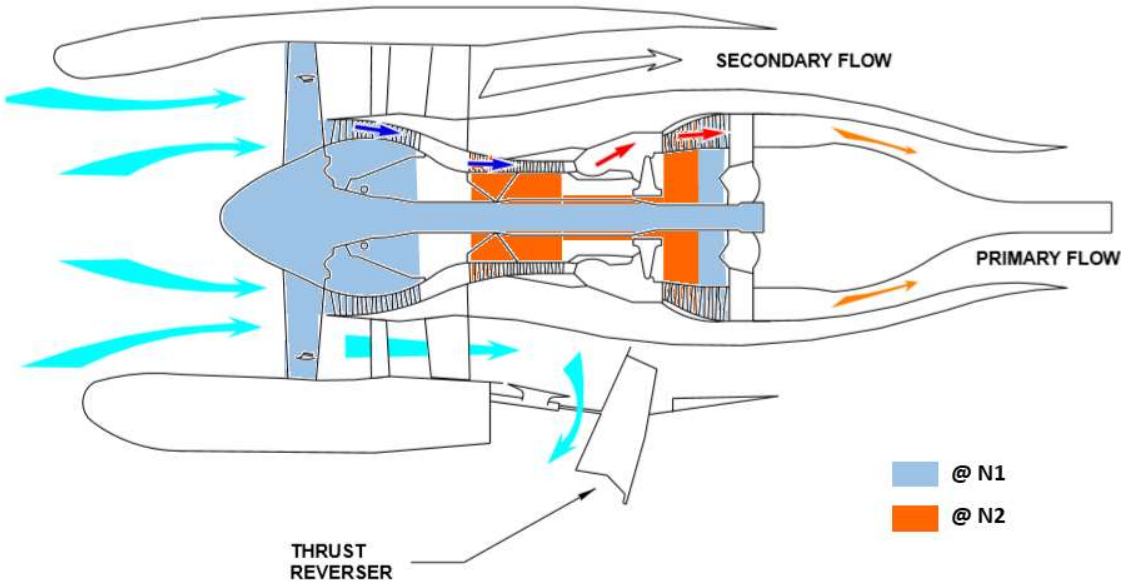

Figure 2.4 - Flows and Drives of Turbofan Engine (Adapted from [5])

2.2.2 CFM56 Engine Family

CFM International was born in a joint venture between the French company *Snecma*, now a part of the *Safran Group*, and the well-known American company *General Electric Aviation. CFM* went on to produce the world's best-selling engines for commercial aircraft propulsion systems, the *CFM56* engine with more than 30.000 engines delivered to a span of over 550 operators worldwide, as these engines are used to power a variety of aircraft models as listed in Table 2-1. Their latest engine, the *LEAP*, leverages from the successful *CFM56* engine family and displays a whopping 15% improvement in fuel consumption with further improvements in reliability, durability, and environmental impact.

Table 2-1 - CFM56 Engine Family Overview [31]

CFM56	Max TO Thrust [lb]	Fan Diameter [in]	Aircraft
-2	24000	68.3	Boeing E3 AWACS Boeing KC135 Douglas DC8-70
-3	23500	60	B737-300/400/500
-5A	26500	68.3	A319 A320
-5B	32000	68.3	A318 A319 A320 A321
-5C	34000	72.3	A340
-7B	27300	61	B737NG

As listed in the table above the *CFM56* engine family is comprised of the -2 through -7 models with variations in dimensions and Take-Off (TO) thrust outputs. Table 2 below provides further details on the models delivered by CFM.

Table 2-2 - CFM Delivered Engines [5]

Engine Model	Aircraft	Engines	Operators
CFM56-2 (-2A/-2B/-2C)	621	2,684	20
CFM56-3	1,989	4,496	235
CFM56-5A	535	1,191	48
CFM56-5B	3,278	7,014	180
CFM56-5C	247	1,133	45
CFM56-7B	5,593	11,943	210
Total	12,263	24,461	738

As we can see, the *CFM56-7B* is the model with the most engines in operation as of 2015 and this is one of the reasons why this model was the second to be overhauled by TAP M&E despite not being operated on TAP fleet. For the purpose of this work, we will pay special attention to the *CFM56-5B* model as it is one of the models overhauled more frequently in the shop. A brief introduction to this model's main components and their respective functions can be found in the following section.

2.2.3 *CFM56-5B* TurboFan Engine

The *CFM56-5B* (and other CFM56) engines can be divided into four Major Modules (MM), the Fan and Booster MM, the Core MM, the Low Pressure Turbine MM and the Accessory Drive MM. These modules also represent the first stage of engine disassembly as it is separated into these four modules for further dismantling. The Major Modules position in the engine's assembly is provided in the exploded view of the engine in Figure 2.5 as we will continue to cover the modules main components and their role in the engine performance.

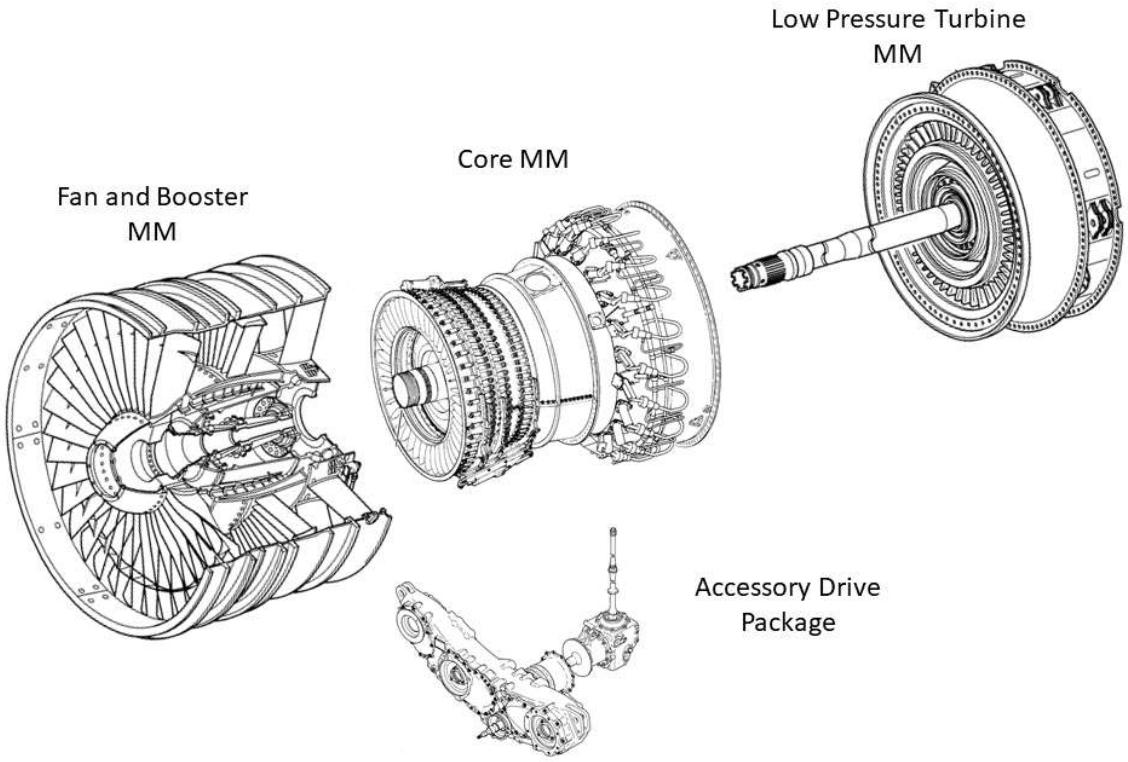

Figure 2.5 - CFM56-5B Major Modules (Adapted From [5])

The Fan MM, as other Major modules, is comprised of smaller assemblies which represent smaller modules. This modular constitution is typical of an improved design and is very important as it provides an easier access to the engine's multiple components, simplifying workscopes in MRO facilities and facilitating module and part replacement.

An illustration of the engine's module modular composition can be seen in Figures 2.6. In this figure, the modules numbering can be attributed to each one of the major modules as modules 1 to 4 belong to the Fan MM, modules' 5 to 12 belong to the Core MM, modules 13 to 15 to the Low Pressure Turbine MM and finally modules 16 and 17 to the Accessory drive MM. In the following paragraphs we are going to cover briefly each one of these 17 modules and some of their components in hope of attaining a more complete, although simple, understanding of the turbofan engine and the *CFM56-5B* in particular.

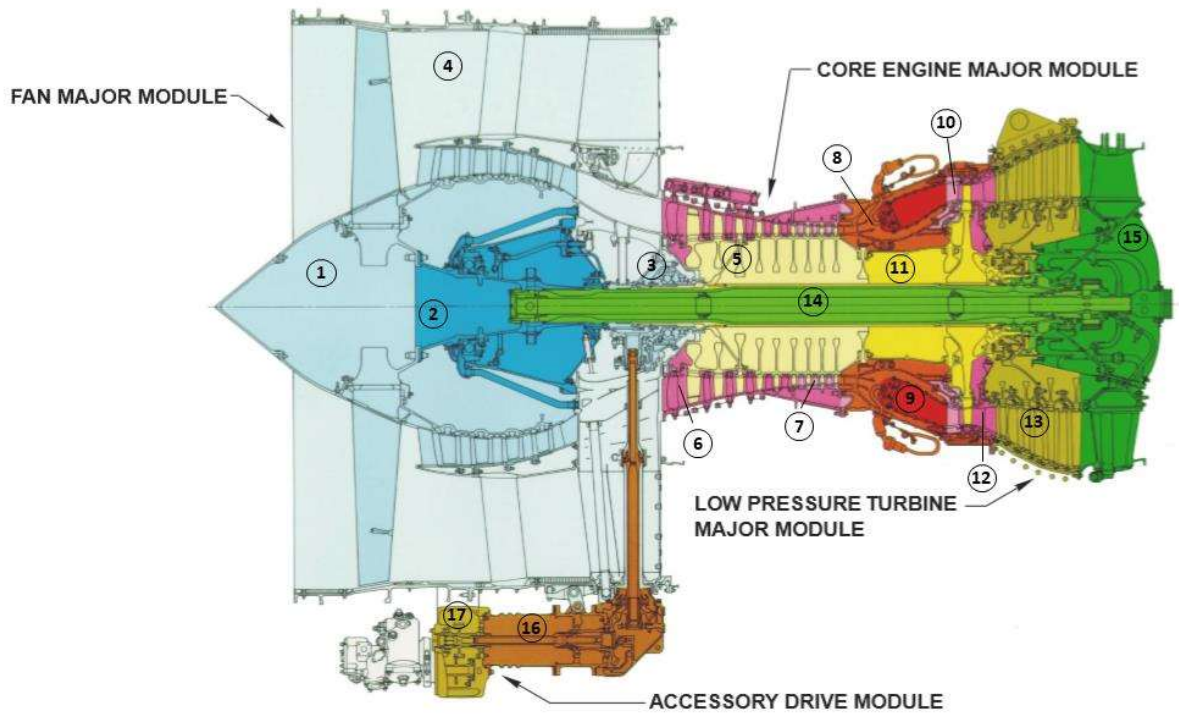

Figure 2.6 - CFM56 Engine's Modular Composition (Adapted From [31])

The Fan and Booster (LPC) Module, number 1 in Figure 6, is comprised mainly by the front and rear spinner, the fan rotor as well as the booster rotor and stator. The front spinner acts as diffuser to the airflow and is designed to prevent ice build-up while the rear spinner allows to control the balance of the N1 rotating components through weight calibrated bolts. The fan rotor produces the vast majority of take-off thrust and provides airflow to the thrust reverser, while the Booster (also known as Low Pressure Compressor) accomplishes the precompression of the primary airflow as it enters the HPC.

Modules number 2, 3 and 4 are mainly structural. Module 2 provides support to the N1 rotating parts and Module 3 to the N2 rotating front parts through both ball and roller bearings. Module 3 also provides transmission to the shaft that drives the Transfer Gearbox (TGB – Module 16) and module 4 allows for the engine's frontal support transmitting the loads and thrust to the aircraft.

Modules 5 to 7 are comprised by the HPC rotor and HPC front and rear cases respectively which are going to be covered in more detail ahead, since these modules are the ones where we will focus most of the work done in this thesis.

The HPC cases represent the stator and outer stationary parts of the HPC, consisting of the inlet and outlet guide vanes (IGV's and OGV's), as well as the stator vanes between stages. Is important to notice that the first three stator cases (including IGV's) are variable, therefore, in addition to the stator vanes main

purpose, which is to guide the airflow through the HPC stages, these first stages also allow to control the amount of airflow entering the HPC through an actuator associated with lever mechanisms.

The HPC rotor consists of 9 stages with blades decreasing in height, width and angle of attack through the stages as the transversal area for the airflow path decreases as we move further along the compressor. HPC Blades in stages 1 and 2 are fixed in axial slots to a spool, stage 3 blades are also fixed in axial slot in this case to a disk and stages 4 to 9 are fixed in circumferential slots. similar to a rail, along the spool. This circumferential slot type of assembly assures the position of the blades through bolted locks between blade sets which may present some clearance between the blade's platforms. Therefore, these blades must be assembled arranged in sets of wide and narrow platform blades in order to minimize that clearance. This is one of the possible clearances relevant to compressor efficiency and is something that is important to notice regarding this work. Figure 2.7 illustrates the location of the HPC in the Core MM while Figures 2.8 and 2.9 demonstrate the HPC rotor general assembly as well as rotor blades slots description.

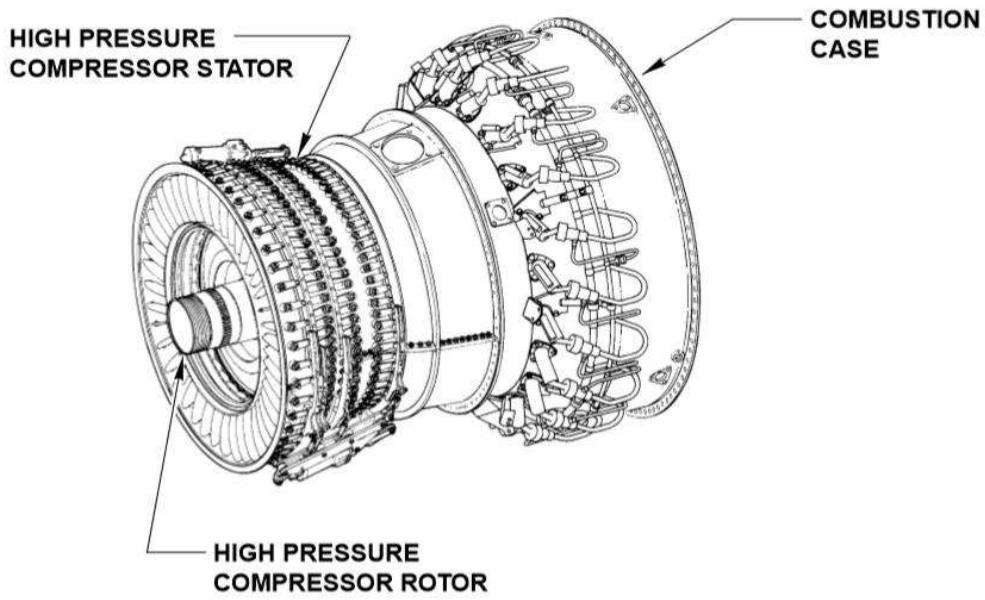

Figure 2.7 - CFM56-5B Core Major Module View [5]

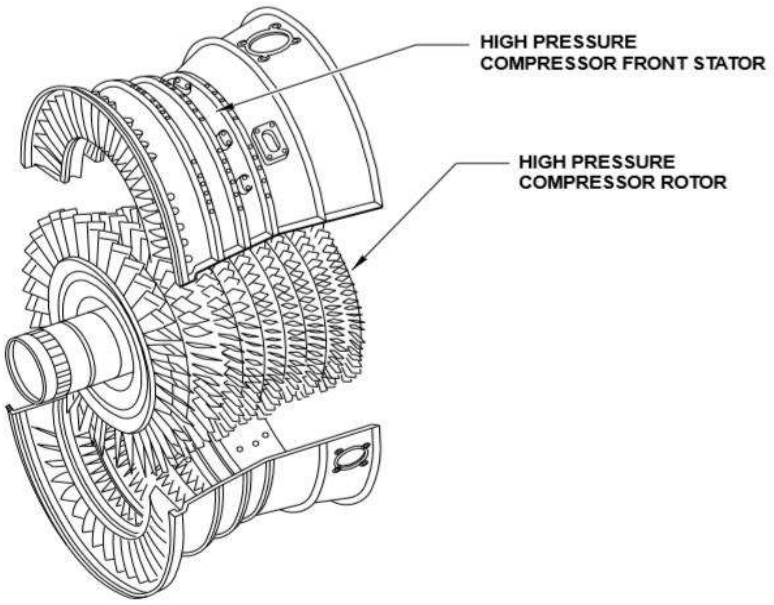

Figure 2.8 - CFM56-5B HPC Module Exploded View [5]

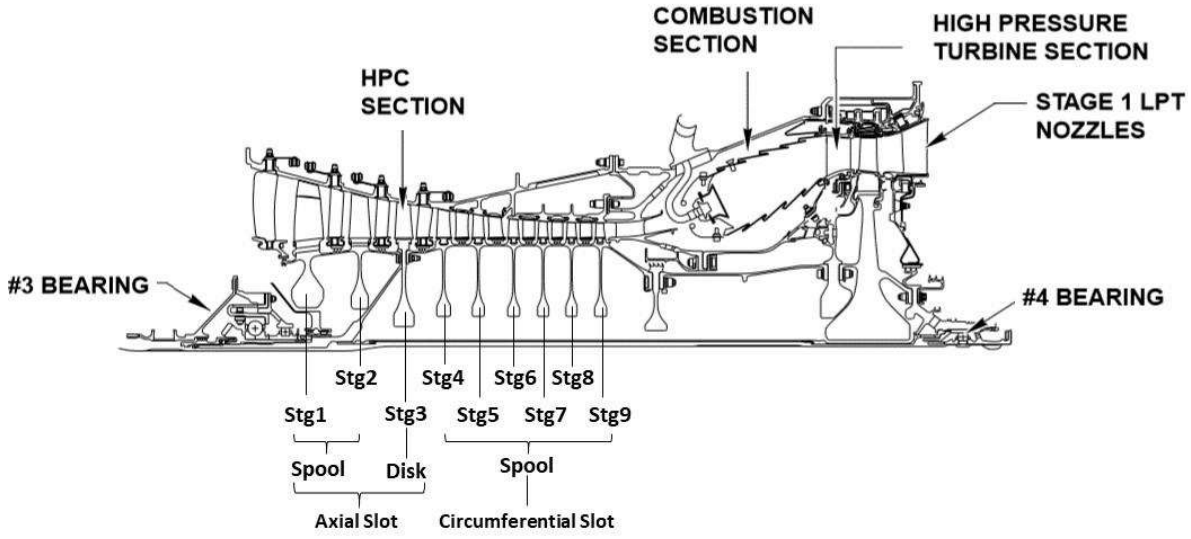

Figure 2.9 - CFM56-5B Core MM Cross Section (Adapted From [5])

Still in the Core MM, modules 8 and 9 correspond to the Combustion chamber which contain HPT stationary seal, support components, the combustion case and the fuel manifold. The *CFM56-5B* has two configurations available for the fuel manifold them being single annular or dual annular. These modules are designed to assure an optimal fuel-air mixture critical to engine performance.

Modules 10 to 12 are attributed to the HPT, namely the turbine nozzles, rotor and shroud support. These module's components endure the harshest conditions in all of the engine and are specially designed to be able to sustain high temperatures and high pressures through use of specialty components such as pressure seals, retainers and air cooling mechanisms. The following modules 13 to 15 are a part of the LPT MM and include the LPT rotor and stator as well as the Turbine Rear Frame (TRF) and LPT shaft which goes all the way through to module 2, Nr1 & Nr2 Bearing support, rotating at N1. These modules are also very important as they extract the remaining energy necessary from the primary airflow to power the LPC and the Fan which, as we know, produces the majority of the engine's thrust. The components in these modules are specially designed to prevent overspeed by causing contact between the rotor and stator.

Finally, the Accessory Drive MM can be divided in two modules, number 16 the Transfer Gearbox (TGB) and number 17, the Accessory Gearbox (AGB). The TGB assures torque transmission between the Inlet Gearbox (IGB) and the AGB, receiving rotation from the radial drive shaft and transferring it through bevel gears to the horizontal drive shaft which connects to the AGB. The AGB then uses the torque to power other aircraft and engine accessories.

The engine also includes several other systems to maintain the engine's required operating conditions such as air-cooling systems, lubrication systems and exhaust systems.

2.3 HPC Rotor Blade Inspection and Maintenance

TAP M&E performs full Core MM disassembly in order to overhaul all the module's components. As far as HPC rotor blades, the company doesn't have the certification necessary to repair non-serviceable yet repairable blades so, it is common for HPC blades that don't meet the specified requirements to be sent back to the manufacturer or certified MRO facilities to be repaired/overhauled. These blades are then received in a new or overhauled state by TAP M&E, which proceeds to inspect the overhauled blades as a precaution to guarantee the assembled blades condition.

HPC blade inspections consists mostly of visual inspection. CFM specifies a variety of subtasks regarding the visual inspection, most of them being referent to FOD (Foreign Object Damage) in the various blade geometries. FOD inspection includes blade defects such as cracks, nicks, dents, pits, scratches, tears and so on. Visual inspection also refers to particle deposits on the blade, surface finish quality and edge geometry (blunt or sharp). Visual inspection is often complemented by touch as edge geometry and FOD depth can be identified better using hand touch.

As far as dimensional inspection goes, the manufacturer does not specify all of the blade's dimensions, but they indicate some minimum dimensions required for serviceable blades namely chord length, leading and trailing edge thickness, and also blade height. Blade nomenclature and geometries will be described with more detail in the following pages.

Dimensional inspection procedures implemented by TAP M&E in order to ensure overhauled blade serviceability include the verification of minimum chord length through the use of a *Go/No Go* tool as shown in Figure 2.10. This tool allows to verify the chord length of the blade at the specified height with ease as the HPC blade quantity and number of stages imply that blade dimensional inspection in detail through conventional methods would be impractical. The use of a *Go/No Go* Tool is also required for the dimensional inspection of leading and trailing edge thickness. However, this practice is not very common at TAP M&E despite the tool being available. Figure 2.11 details the edge dimensional inspection tool.

Figure 2.10 - Go/No Go Tool for Chord Length Dimensional Inspection

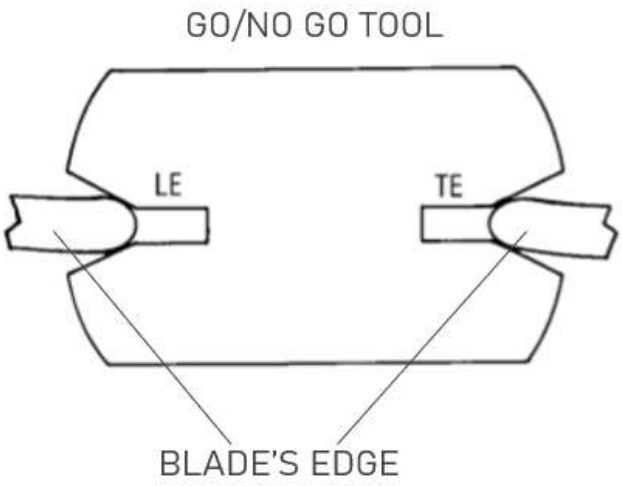

Figure 2.11 - Go/No Go Tool for Edge Thickness Inspection

After dimensional inspection, the blades are accepted by TAP M&E and registered for assembly. Sets of blades are then arranged to be mounted in the spool/disk and proceed for tip grinding and rotor balancing.

Exhaust Gas Temperature (EGT) is one of the main indicators of the engine's performance deterioration and the margin for this indicator, as depicted in Figure 2.12, is often set by contract for MRO services.

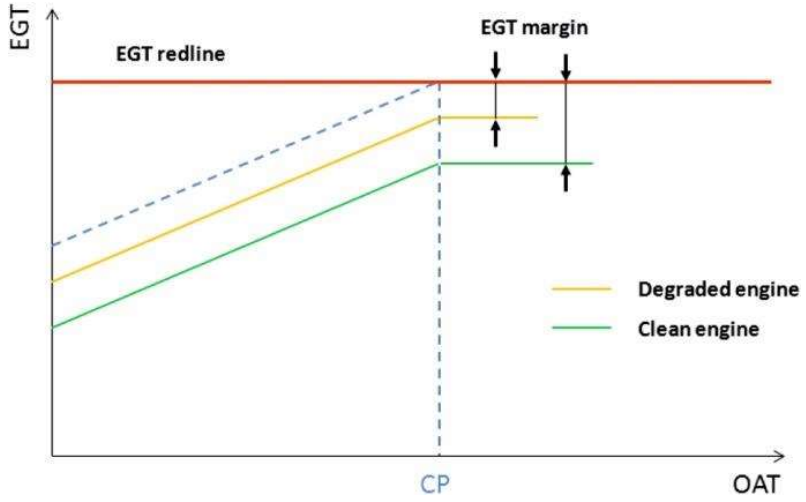

Figure 2.12 - Exhaust Gas Temperature Variation in relation to Outside Air Temperature [29]

TAP M&E has manifested great interest in determining the correlation between the status of the sets of blades assembled with the engine's performance in order to improve de capability of improving Exhaust Gas Temperature (EGT) margin by arranging serviceable blades in different conditions in the same set. For this, more than Go/No Go tools will be necessary in order to document the blade dimensions with greater detail.

3 Literature Review

With the inevitable evolution of air travelling, airline companies have looked to push the limits of commercial aircraft engine's performance. During on-wing time, the turbofan engines are susceptible to inevitable engine's part deterioration (mainly in airfoils) which leads to a decrease in engine performance. However, restoring the original engine's performance is very difficult and very unpractical as this would require replacing almost every airfoil component in the engine.

This way, airline companies and engine manufacturers have established that the engine needs to be overhauled when it reaches a specified Exhaust Gas Temperature (EGT) limit, allowing for restoration of engine's performance to a great extent, more specifically lowering EGT and TSFC (Thrust Specific Fuel Consumption) to a certain value often set by contract with MRO Facilities.

Regarding these interests, many studies have been conducted in order to determine engine deterioration and its effects on the engine's overall performance. One example, Sallee et al. [28] provides a complete study on the turbofan engine's performance deterioration, describing in detail the in-service alterations found in engine components as well as the effects these alterations have on performance. This study [28] also provides some data regarding MRO material consumption and repair rates of some engines as well as engine performance tests, going as far as presenting a proposed test program to determine the engine's condition.

In any case, as it was already stated in chapter one, the High Pressure Compressor is a crucial section of the turbofan engine, as the pressure ratio plays an important role in the engine's energetic efficiency. In addition to this, HPC's components are also subject to considerable deterioration which means that performing repair and overhaul in this module's components will normally have a positive impact in the engine's performance.

In this regard, the articles reviewed will cover mostly the HPC rotor deterioration and its effects on performance. Some articles regarding other rotor parts such as fan and turbine blades are also going to be taken into consideration in order to include more detailed data.

This way, the literature review will be separated into three main segments, the first describing the HPC blades deterioration characteristics and the second describing the effects of leakage or geometric variances of HPC blades on compressor/engine performance. Lastly, the third segment is referred to past work conducted at TAP M&E regarding CFM engine's HPC performance, more specifically the HPC rotor blades impact on the engine's performance.

3.1 HPC Deterioration and Effects on Blade Geometry

Obtaining a good correlation between erosion effects and HPC rotor blade geometry is very important to improve HPC maintenance and overhaul as it allows for a more focused inspection of the complex airfoil geometry. For a better understanding of the blade's geometry and nomenclature that is going to be used in this chapter, Figures 3.1 and 3.2 depict the different geometries in more detail.

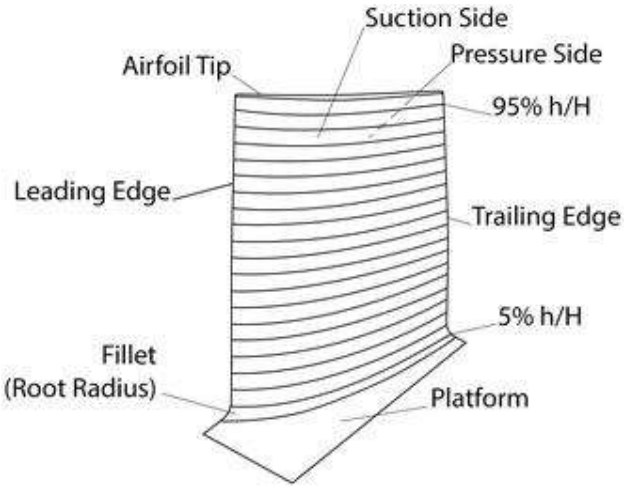

Figure 3.1 - Airfoil Nomenclature [23]

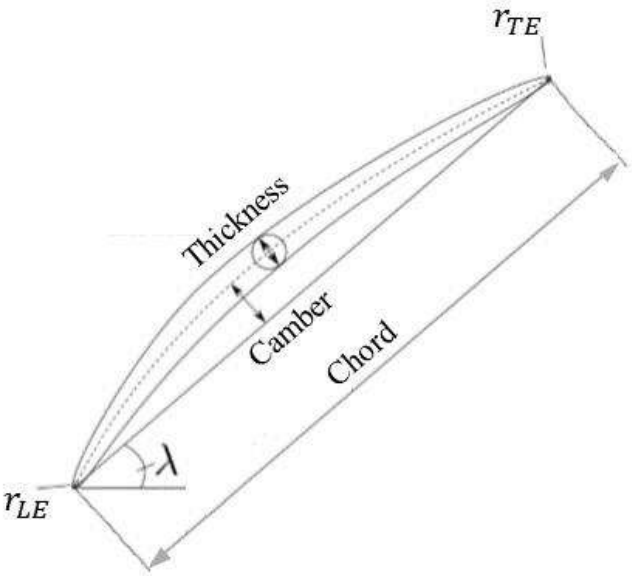

Figure 3.2 - Airfoil Section Dimensions

As described above, Sallee et al. [28] documents the typical effects of deterioration in the turbofan engine. This study points out typical damages in fan/compressor blades such as nicks, tears as types of Foreign Object Damage (FOD) and surface roughness, as well as blunt edges and lack of blade camber due to airflow particle erosion. Although presenting a broader study of turbofan engine deterioration, one particular detail described by the works of Sallee et al. [28] is the fact that blade wear caused by abrasive particles present in the airflow seems to localize near the tip of the blade due to centrifugation.

Dedicated more exclusively to HPC deterioration and it's correlation to engine performance, Marx et al. [12] conducted a study which took measurements from more than 1400 used HPC blades and more than 300 new ones digitized by structured-light 3D scanning to determine the geometric variations of both manufacturing processes and on-wing deterioration. This study proves that variations caused by deterioration are greater than variations due to manufacturing and that airfoil geometries are often a result of the combination of both these variations. Marx et al. [12] also discriminates between the blade stages in order to determine the difference in geometry between the front and rear stages. The study concludes that the front stage blades feature a sharper Leading Edge (LE) when compared to a blunter LE presented by the rear stage blades. The distinction between both geometries is clear can be seen in Figure 3.3.

Additionally, the results obtained by the study regarding HPC rotor blade deterioration are portrayed in Figure 3.4, which demonstrates the variations in the relevant airfoil dimensions for 10 compressor stages. As its observable, excluding other situations, the first compressor stages consistently present variations close to 100% in most dimensions, while the leading edge thickness and radius dimensions display greater variations when compared to other airfoil dimensions.

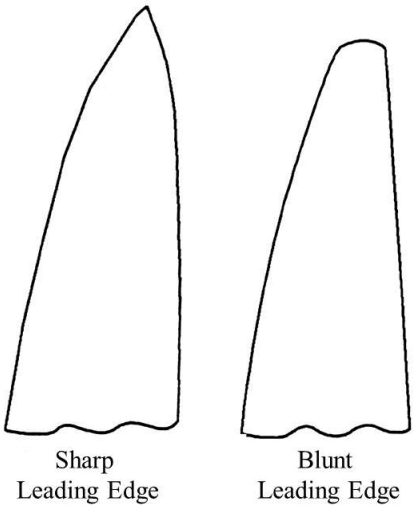

Figure 3.3 - Leading Edge Profile Categories

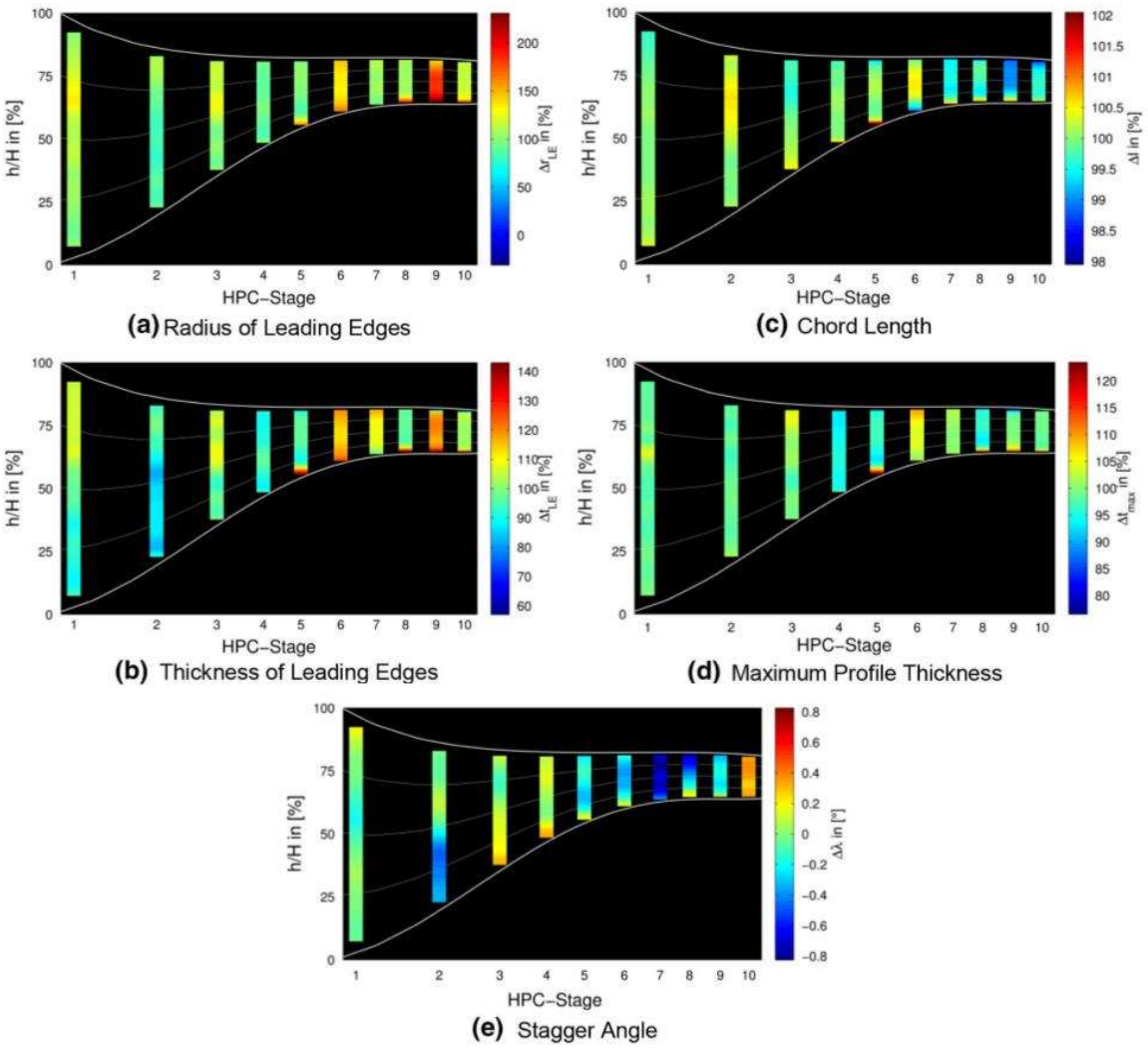

Figure 3.4 - HPC Rotor Blade's Measurements [12]

This conclusion is also supported by the works of Reitz et al. [22] which, based on the measurements taken by Marx et al. [12], used correlation coefficients to determine the relation between different types of airfoil geometry presented by used blades. Reitz et al. [22] concluded that, as expected, a large amount of blade abrasion takes place at the leading edge, more specifically the pressure side of the airfoil, which results in a thinner and more asymmetric LE geometry. Furthermore, Reitz et al. [22] also confirms that, as described by Marx et al. [12], this asymmetry is characteristic of the front stages as the rear stages present blunt LE.

To summarize the works of both Marx et al. [12] and Reitz et al. [22], HPC blade deterioration is characterized mainly by LE erosion as the compressor front stages present a thinner, sharper leading edge with asymmetry towards the blade suction side and the rear stages present a blunt LE with nearly homogenous material removal.

Reitz et al [22] even goes as far as pointing out that a decreased chord length in conjunction with increase in LE thickness (as LE thickness is measured at 5% chord length) may provide proof that the airfoil is severely eroded and is no longer serviceable. This note is of great importance as chord length and LE thickness are two simple dimensions that allow for a somewhat precise assessment of the blade's condition when compared to the all dimensions that define the complex geometry of the airfoil such as blade twist and camber.

3.2 HPC Blade Geometry and Leakage Effect on Performance

Several studies have been conducted in order to determine the influence of HPC blade geometry in the overall compressor's or engine's performance. Most of the studies conducted make use of Computational Fluid Dynamics (CFD) simulation in order to observe the behaviour of airflow through one blade segment. Other studies conducted experiments with blade cascade arrangements to observe the behaviour of airflow through blade stages.

However, by trying to isolate the behaviour of compressor blades, these studies neglect the influence of other engine's components and how these might influence the behaviour of the compressor itself. Nonetheless, these experiments provide great insight on how airflow behaves when going through the compressor stages and what might affect it.

Reitz and Friedrichs [21] focused on the procedure to analyse the flow through compressor blades using CFD simulation. Considering the conditions of a front stage HPC rotor and stator row, the simulation was done to different airfoil geometries as a profile modifier was applied that allowed to manipulate leading and trailing edge dimensions, as well as maximum profile thickness and its chordwise position. The simulation demonstrated that variations in blade geometry resembling blade deterioration resulted in a drop of isentropic efficiency of as much as 0,39% and a variation in pressure coefficients of almost 0,64% for single stage performance.

Similar work was done by Reitz, Marx et al. [23] with further CFD simulation using 5 different blade samples varying in profile/LE thickness and stagger angle. This study confirmed leading edge profile thickness as the main factor in single stage decrease in performance and profile thickness second in relevance. This study also concluded that stagger angle (angle between airfoil's chord and the engine's axis or rotation) is not relevant to the compressor's single stage performance as large deformations seemed to barely affect performance.

Other works, such as Krone et al. [9] also conclude that, with leading edges less altered than those presented in the work of Marx et al. [12], the effects on performance are fairly noticeable as a decrease in peak efficiency as great as 1,2% was observed. Additionally, Tabakoff et al. [30] determined that blunt leading edges may cause an increase in SFC of 0,38% and 0,13% by surface roughness. This study

was conducted with the goal to determine the effects of erosion in multistage compressors EHM (Engine Health Monitoring) and used experimental data to calculate the effects of deterioration for individual stage characteristics. A stage stacking technique was then used to extrapolate results to the effects on multistage compressor, which determined a decrease in both pressure and mass flow rate due to deterioration, namely reduced chord length and blunt LE. Tabakoff et al. [30] also described that the effects of the front stages are of most impact as their effects carry on through the next stages affecting the overall compressor performance more than the rear stages.

Giebmanns et al. [8], one of the most cited papers regarding this subject, described the effects of degraded fan blades by analysing transonic fan blades by means of 2D and 3D simulations and cascade measurements as shown in Figure 3.5. It is important to notice that, although this study was conducted considering fan blades in a cascade arrangement, the analysis of airflow characteristics through the cascade can safely translate to the compressor blade's operation.

Figure 3.5 - Airfoil Cascade Arrangement Experiment [8]

Categorizing blades in five different types: 1 - Blunt leading edge (representing an eroded blade); 2 - Variation of clearance gap height; 3 - Blunt leading edge with reduced chord length (representing a long-term eroded blade (Fig. 3.6 - left); 4 - Reduced chord length but reshaped leading edge (representing a long-term eroded but repaired blade (Fig. 3.6 - right); 5 - Blending in transonic part of the blade.

Giebmanns et al. [8] concludes that the disturbances to airflow are significant and mainly caused by blunt leading edges as Figure 3.7 illustrates by showing an intensified expansion around the defected

leading edge in the cascade arrangement wind tunnel experiment. This study also determined that blades with reduced chord length but rounded leading edges performed as well as the original blades suggesting that the main geometry affecting compressor performance is leading edge geometry and not chord length. Therefore, this study suggests that airfoil dimensional inspection should focus on leading edge profile more than chord length or leading edge thickness, an observation of great relevance to this work.

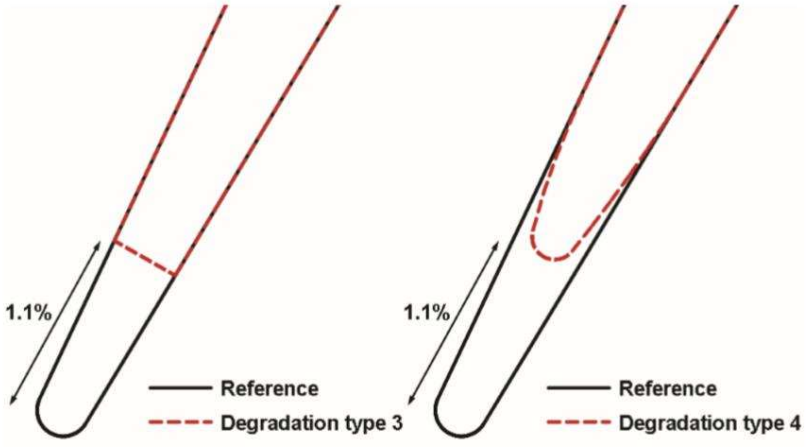

Figure 3.6 - Edge Deterioration Classification [8]

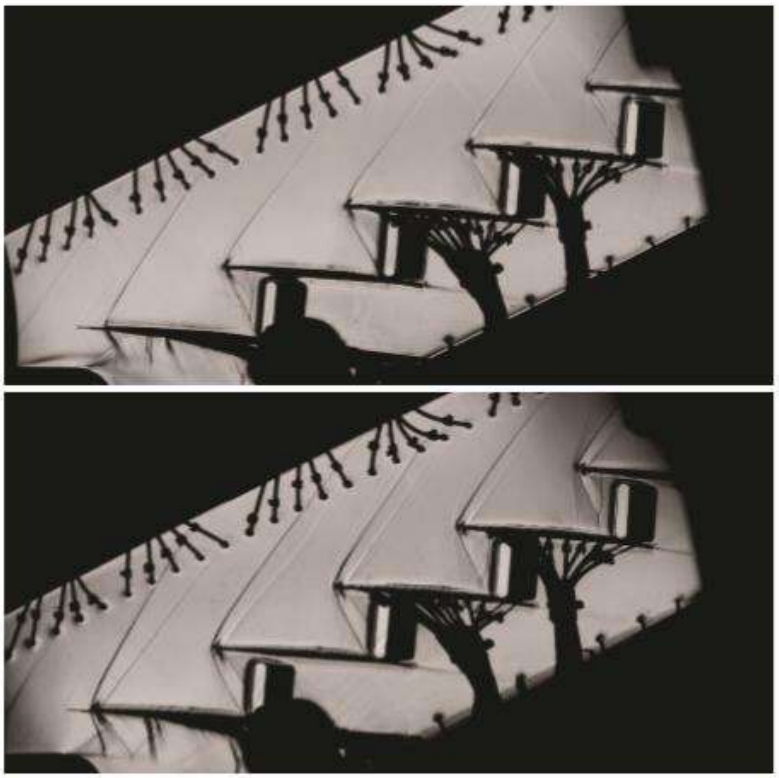

Figure 3.7 - Schlieren Photograph from Cascade Experiment [8]

So far, all the articles we've reviewed have described the effects of HPC rotor blade geometry in performance concluding that the leading edge profile is the main geometry of influence. However, as blade chord length is perhaps the easiest and more controlled dimension in overhaul facilities, therefor a study of the effects of chord length in compressor performance would be very useful for MRO procedure applications. Roberts, W. et al. [26] presented a study of the effects of variable chord length in transonic axial compressor performance which translates very well to the one of the objectives of this work. In this study, erosion was simulated to 50% of the blades and then a compressor rotor disk was used to assemble the blades with variable chord length in three dispositions as demonstrated in Figure 3.8, halves, quadrants and alternating.

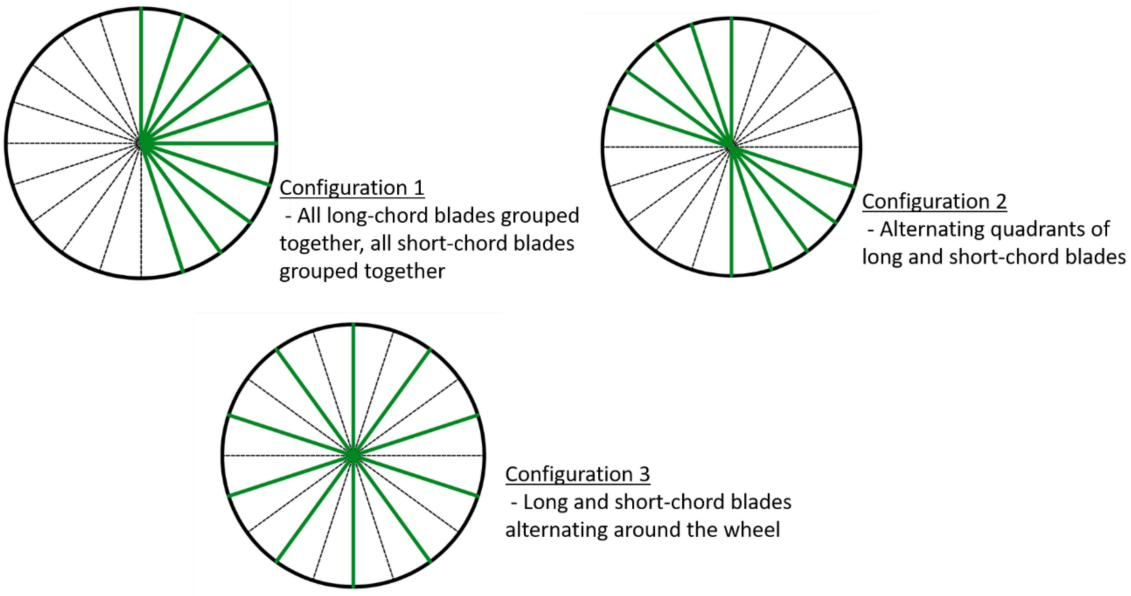

Figure 3.8 - Different Chord Blade Configurations [26]

Roberts, W. et al. [26] then proceeded to perform an experiment using a single-stage transonic rotor test facility to determine the effects of these three configurations on the Pressure Ratio (PR), Temperature Ratio (TR) and Adiabatic Efficiency (AE). The study concluded that, although all configurations had a negative impact in PR and AE when compared with the rotor with solely non-eroded blades, the best results in performance where observed with the alternating configuration. This study also brings up the fact that blades with restored chord length do not perform as well as expected suggesting that there are other geometries in play as was confirmed by the studies abovementioned.

At last, having determined the effects of compressor blade's geometries, we are left wondering what other factors may cause disruptions of airflow through an axial compressor thus decreasing pressure ratios. Concerning this, some studies have tried to describe the behaviour of airflow disrupted by leakages in the compressor or surface roughness on the blades.

One example of these studies is Lackshminarayana and Horlock [10] which described in detail the behaviour of airflow through a cascade type of blade arrangement as shown in Figure 3.9. This study provided some insight regarding the disruptions caused by leakage in the blade's tip clearance and other secondary flows. Other example is the study of Bammert and Woelk [2] that documented the effects of blade surface roughness on airflow and concluded that surface roughness influences flow losses as much as 6% in total internal efficiency for a relatively standard roughness.

Figure 3.9 - Cascade Arrangement Experiment to study secondary flows [10]

Even tough tip leakage and surface roughness have been proven to be of relevance to axial compressor efficiency, rotor blade tip clearances and blade surface finish are two parameters well controlled by MRO facilities, including TAP M&E. However, inter-platform clearance has proven to be difficult to control especially when blades are assembled in spool's circumferential slots. Current procedures include combining blades with wider and narrower platforms between locks in order to minimize the clearance between blade's platforms. Very few studies were conducted regarding this matter and maybe none specifically to HPC rotor circumferential slot type of assembly, but Reid, K. et al. [20] presented a study that describes the interaction of inter-platform leakage flow with a turbine mainstream. Although this study focuses on the leakage through a gap between mating surfaces of individual stator units of a turbine, it provides us some insight on the possible impact of rotor blade platform leakage in an axial compressor even though leakage effects will always be greater in stator clearances (outer) due to centrifugation. This study described a difference in performance resulting in a 1,08% loss in efficiency when the clearance was present deeming inter-platform leakage relevant to the turbine's efficiency.

3.3 TAP M&E Past Work

Correlating between the different module's performance with the engine's overall performance is something of great relevance to TAP M&E and other MRO facilities as it is very common to spend several hours overhauling the engine's different modules down to their every component and still obtaining disappointing results regarding engine's performance test. Due to this difficulty TAP M&E, in conjunction with some Portuguese universities, has proposed some studies for students obtaining their masters' degree in engineering in order to obtain a better knowledge of the relation between the various engine components and the engine's performance and possibly improving MRO outcomes.

One of the studies developed at TAP M&E regarding engine performance, Baptista, F. M. C. [3] tried to determine the effects of the HPC in the overall engine performance by simulation using the software *GasTurb*® specially designed for gas turbine engines. This study confirmed the effects of HPC deterioration in the turbofan engine's performance stated by Marx et al. [12] and provides further proof to the conclusion of Tabakoff et al. [30] regarding the importance of the first stages in compressor performance as they seem to affect the overall performance the most.

Furthermore, this study provides the graph displayed in Figure 3.10 (provided in detail in Appendix 1) which demonstrates that, with different combinations of new and overhauled blade arrangements for different stages, different results in HPC efficiency were verified. As expected, the combination with the greater percentage of new blades displays the best efficiency but the combination with almost only first stage new blades also performed very well.

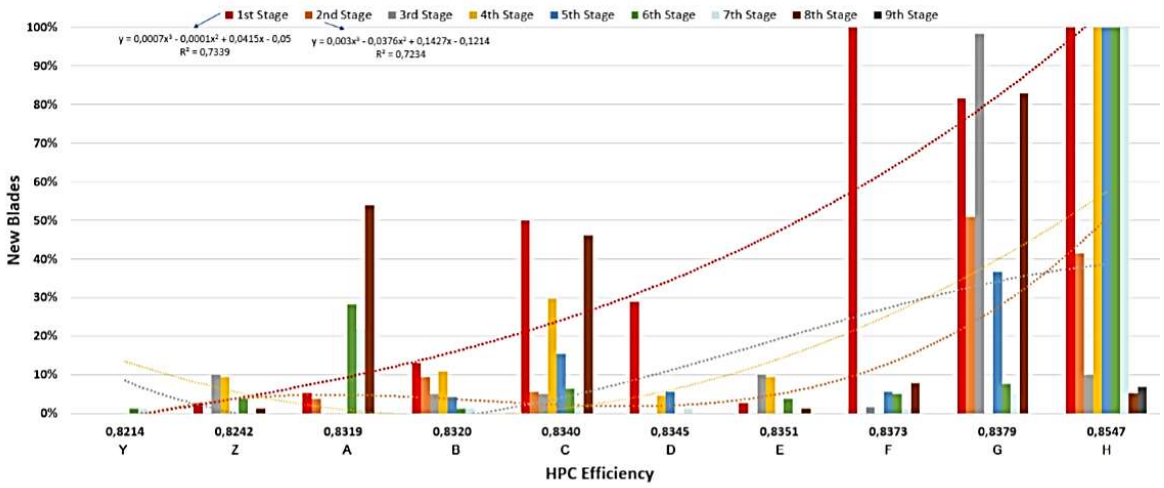

Figure 3.10 - Results of HPC efficiency for different New/Overhauled Blade Combinations [3] – Appendix I

Baptista, F. M. C.'s work [3] also presents a cost analysis regarding the advantages of controlling HPC rotor blade dimensions in order to obtain the best performance with minimum MRO costs going as far as providing a suggestion to an updated HPC maintenance/performance plan as shown in figure 24. This plan outlines some procedures that are going to be the focus of the work of this thesis as one of the objectives is to develop a procedure to determine the rotor blade's conditions with the best accuracy possible and obtaining a correlation between the blade's condition assessment and overall engine performance.

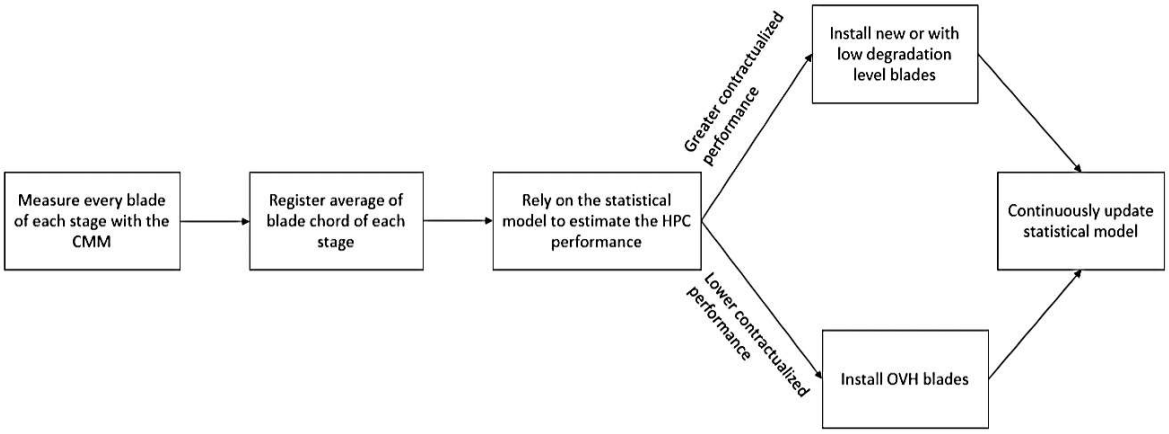

Figure 3.11 - Updated HPC Rotor Blade Maintenace Plan [3]

Another work developed at this company, Recrude, T. M. [19] was carried with a similar objective but with special focus on the HPC blades which was to determine the correlation between HPC blade dimensions and the HPC/engine performance. This study's approach was different as compressor blade chord measurements were taken in order to develop a case study which was analysed with the GasTurb® software. The chord measurements were taken manually, and a study was conducted in order to evaluate if there should be a new criterion to the acceptance of the blade's chord length. A tool to perform automatic measurements of blade's dimensions through the CMM was also developed but had some limitations regarding its utility as far as operability and CMM software development.

4 Reference Blade Model and dimensions.

HPC Rotor blades as well as Fan blades present complex geometries partly due to their design being focused on the airflow dynamics around these components. This makes it very unpractical to define all the geometries completely in order to obtain an exact reference model. Although TAP M&E has access to MRO manuals provided by the manufacturer, the manuals don't include all the nominal dimensions referent to the complete blade design. Despite this, the manuals do include some reference dimensions specified for dimensional inspection or repair procedures. The following subchapter presents a compilation of the provided reference dimensions as well as maximum and minimum serviceable values for chord length, leading and trailing edges along with platform to tip length.

This chapter also describes the process for the development of the HPC blade's reference model which includes some guidelines for the blade's 3D scanning and reverse engineering. The deviations between the blade's reference model and its real counterpart will also be covered in order to provide some validation for the reference models as well as the possible impact of these deviations in the CMM measurements.

4.1 HPC Blade's Reference Dimensions

As described above, most of the blade's dimensions are unknown and proprietary to the manufacturer which would require to develop the reference model based purely on the 3D scanning of a usable HPC blade. This procedure would only rely on the scanner's precision and would not account for the variations in dimensions due to manufacturing processes. Although the manufacturing variations may not be substantial for the CAD modelling process, most of the blades available in shop were in overhauled condition which means that the 3D scanned model would display serviceable dimensions presenting deviations greater than those caused by manufacturing.

In order to improve the precision of the scanner-based blade model's dimensions, it was necessary to compile some of the blade's reference dimensions available in the MRO manuals scattered through the HPC blade's dimensional inspection and repair procedures. Repair procedures include mostly details regarding the dovetail section of the blade while Dimensional Inspection procedures provide reference dimensions mostly for the airfoil geometry. Combining as much information as we can, will result in a more precise reference CAD model and will contribute to a better fixture design in the following chapter.

4.1.1 Reference Dimensions for Modelling

The reference dimensions available in the Engine Shop Manuals (ESM) are provided as specifications for repair procedures. Of all the blade's repairs specified in the manuals, those involving dovetail focused procedures were highlighted as these allow us to define the dovetail profile geometries which can be used as fixing points in the fixture design. Therefore, dovetail repairs such as plasma coating, RTV (Room Temperature Vulcanizing) silicone application, among others were reviewed in order to identify some reference dimensions. The compilation of these dimensions is provided in more detail in Appendix II.

Some of the dimensions identified include the dovetails angle of aperture and its positioning in the profile which defines the area of contact between the blade and the spool/disk in the rotor assembly as displayed in Figures 4.1 and 4.2 for the case of the stage 1 compressor blade. The same information can be acquired for the 2nd and 3rd stage blades as it is also provided in Appendix II.

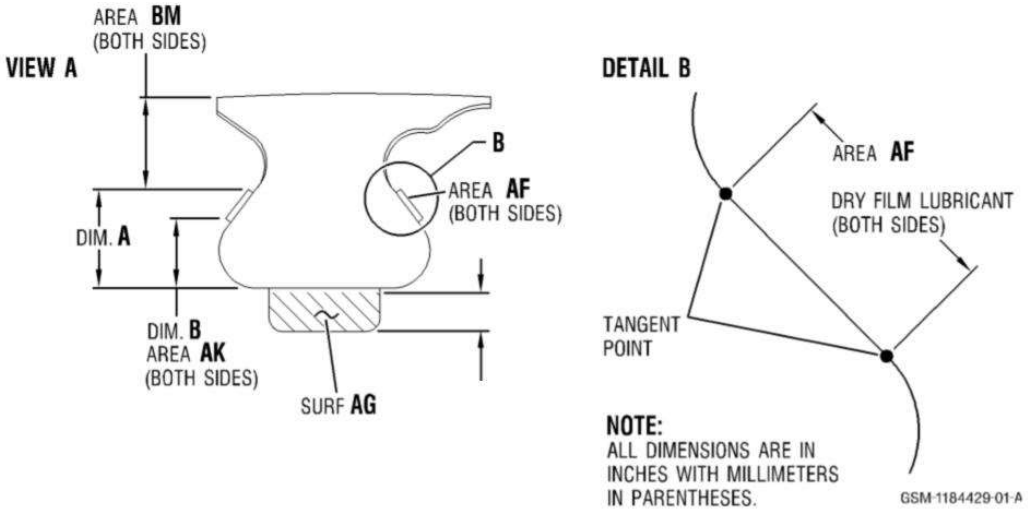

Figure 4.1 - Dimensional specifications for coating repair procedures for Stage 1 Blades – Appendix II

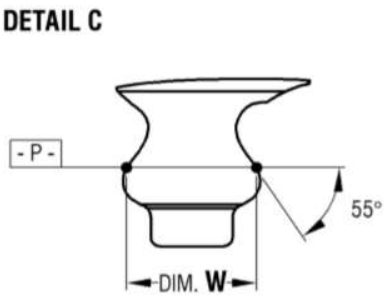

Figure 4.2 - Dovetail Profile Angle of Aperture for Stage 1 Blades – Appendix III

Information regarding the dovetail profile of the spool assembled blades of stages 4 to 9 is more sparse. Although the pressure face for the surface of contact between the blade and the spool is identified as shown in Figure 4.3, we do not have any specifications for the angle of aperture as we did for the first 3 stages. Information regarding stage 4 to 9 blade's reference dimensions is provided mostly in Appendix III which refers to dimensional inspection procedures.

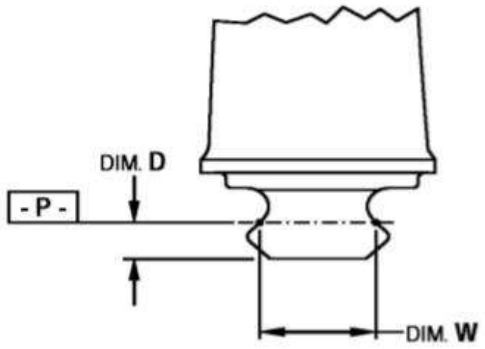

Figure 4.3 - Pressure face specification for 4-9 Stage Blades - Appendix III

4.1.2 HPC Blade's Serviceable and Repairable Dimensions

In order to develop a correlation study between the blade's airfoil dimensions and the overall engine's performance, the serviceable and repairable dimensions had to be documented. This information was organized and compiled into a single document provided as Appendix III.

Dimensional inspection consists mostly of four different blade dimensions, chord length (Dim. Y), leading edge thickness (Dim. LE), trailing edge thickness (Dim. TE) and tip length (Dim. H) as displayed in Figure 4.4 for the case of stage 1 blades. These dimensions refer to a specified blade height (Dim. SH) which places the measurements near the tip where deterioration is accentuated. Leading and trailing edge thickness also refer to a specified camber line length where this dimension should be measured.

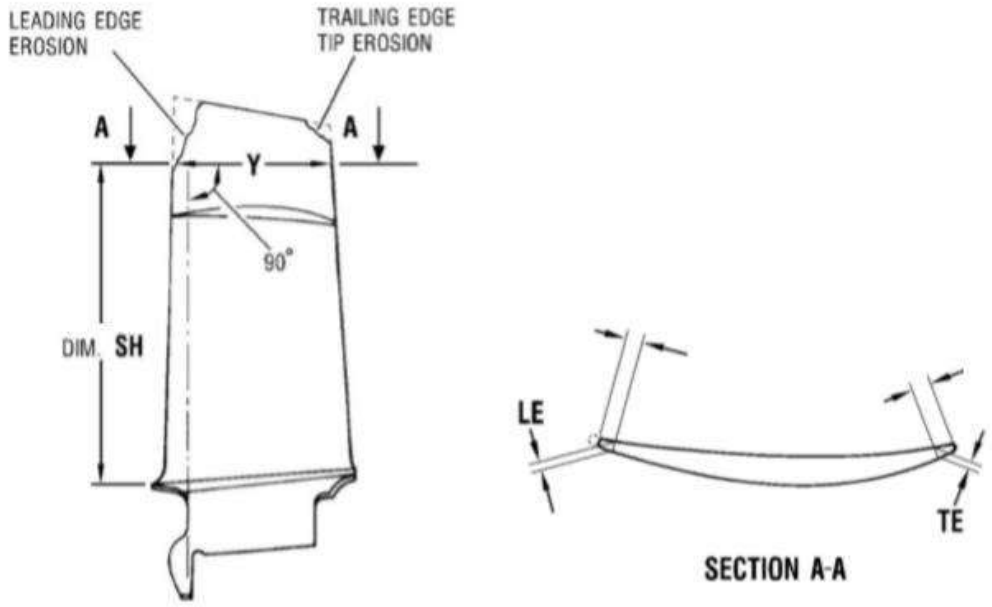

Figure 4.4 - Dimensionl inspection specifications for stage 1 blades. – Appendix III

It is important to notice that for the various stages, there are different types of blades with different specifications for serviceable and repairable dimensions. For the effects of this thesis, we will focus on the type -*5B/P* also specified in the tables displayed in Appendix III, as this is the model more commonly overhauled in the *TAP M&E* shop. Table 4-1 below displays the serviceable and repairable dimensions relevant for the stage 1 blade as an example.

Table 4-1 - Dimensional Inspection Specifications for Stage 1 HPC -5B/P Blades

	Min. Serviceable [in]	**Max. Serviceable [in]**	**Max. Repairable [in]**
Dim. Y (chord length)	2.277	—	Non Rep.
Dim. LE	0.025	0.037	Any if Y
Dim. TE	0.015	—	Any if Y
Dim. H (tip length)	3.761	—	3.636

As we can see, blade serviceability and repairability is highly dependent on chord length as the airfoil dimensions can be restored as long as chord length displays the minimum serviceable. A maximum limit is also specified for the leading edge thickness as this might be an indicator of an eroded and blunt leading edge.

Excluding tip length, the other three dimensions specified in dimensional inspection procedures, chord length, leading edge thickness and, maybe less relevant, trailing edge thickness will be the main focus of the correlation study. One of the objectives of the correlation study will be the development of new criteria for these dimensions in order to obtain a better output in engine performance test.

4.2 HPC Blade CAD Model Development

Reverse Engineering is a practice used throughout all sorts of industries as a mean to study and understand an objects design, obtaining knowledge that may be used to develop improvements to product designs and manufacturing processes. With the latest advances in 3D Scanning technologies, there has been a great interest in using this technology to develop virtual models that can be used for simulation studies.

The virtual model scanned may allow for a more detailed flow boundary in the case of Computacional Fluid Dynamics (CFD) or for an exact model for structural simulation. In this case, the CAD model in conjunction with the fixture tool's model may be useful as a reference for the CNC measuring program as they can be used to locate and define the points of measurement for the CMM through dedicated software.

The development of the HPC blade's CAD model requires a base template because most of the blade's geometries and their relative position to one another cannot be accurately measured or defined in a two-dimensional setting. This way, a 3D base model of the complete geometry of the blade will be very helpful for the blade modelling process as it will allow us to the trace the geometries of the dovetail, platform and airfoil in the CAD Software, in this case *SolidWorks*.

Both the blade scanning and blade modelling processes will be described in the following sections. These sections will include guidelines for each step of these processes in order for them to be replicated in future works for other compressor blades or even other engine parts.

4.2.1 HPC Blade Scanning

The equipment used for blade scanning, *HandySCAN 3D* by *Creaform* displayed in Figure 4.5 is a metrology grade portable 3D Scanner that allows for a scanning precision of about a thousandth of an inch (0.025mm). *Creaform* also provides the *VXelements* software package to support the *HandySCAN*'s operability which is comprised of three different modules: *VXscan* assists in the scanning process by displaying the point cloud acquired in the software's virtual environment and allows to adjust scanning parameters and merge scanned point clouds to fully define the model from every angle; *Vxmodel* which allows to improve the mesh quality by filling holes, smooth edges and eliminate any kind of mesh defects; And finally, *VXinspect* allows us to take measurements of the scanned model and even compare it to a reference model through a deviation analysis.

Figure 4.5 - Creaform's HandySCAN 3D

This scanner was recently acquired by TAP M&E as a dimensional inspection tool to compare scanned models to reference models. Although the precision allowed by this equipment may be very useful in determining the deviations between the scanned part and the reference model's geometries, this technology raises out some concerns regarding this procedure's utility as far as scanning/measuring times, scanned model validation or even other process requirements.

Scanning a part too small can lead to more defects in the scanned model which require greater mesh treatment and therefore, result in a less accurate scanned model. Scanning a part too big may require various scans to be merged which will require more computer processing capability and time.

This optical technology also depends on a various set of parameters such as part reflectivity, background illumination, target/part positioning amongst others which require optimization. Yet, despite all of these constrains, 3D scanning is the only technology that will grant us the complete part's geometric information and *HandySCAN* is able to do so with great precision.

This being said, the blade scanning process will follow a set of steps summarized in the diagram of Figure 4.6 which should grant us a mesh model with enough quality to be used as a CAD template. Each of these stages is going to be covered in more detail in the following segments.

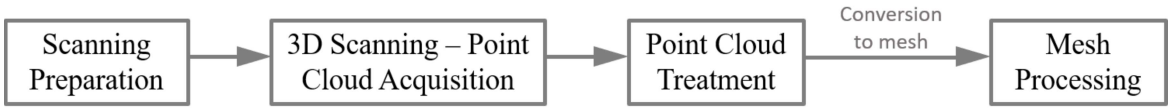

Figure 4.6 - 3D Scanning Stages Diagram

4.2.1.1 Point Cloud Acquisition

To initialize the scanning process, preparation of the workspace is required as Figure 4.7 illustrates where scanned objects are placed in a rotating table covered with unevenly spaced targets that position the object in the virtual environment. The surface where the part stands should be low in reflectivity and well illuminated in order to obtain a more precise point cloud with less background noise.

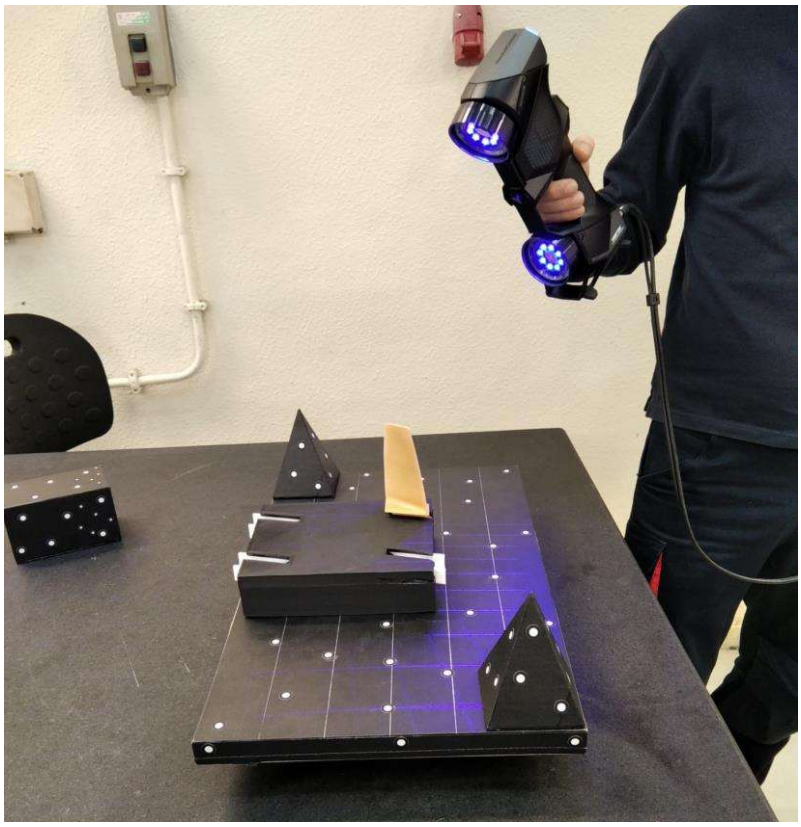

Figure 4.7 - Scanning Workspace

The positioning of the blade is also important as surfaces that reflect the structured light (laser grid) from the scanner are captured with greater detail. This way, in order to capture all the blade's geometries, two separate scans were performed with the blade laying down on either side so that all the dovetail and platform are captured with the best detail as exemplified in the left and middle of Figure 4.8 . A third scan with the blade standing up, demonstrated in the right of Figure 4.8, proved to be useful to detail the airfoil profiles better, namely the leading and trailing edge profiles. Each scan is then cleaned of all unnecessary information detailing only the surfaces respective to the blade. Figures XX to YY illustrate the blade scanning positions and their respective point cloud.

Figure 4.8 - Blade Scanning Positions Rendered Image

However, it is important to note that, as we scan smaller blades from latter compressor stages, the leading and trailing edges of the blade tend to be more difficult to scan due to their decreasing thickness. This will require the adjustment of scanner parameters to better capture these features and, still may result in mesh defects.

When all the scans are completed, the software allows for an automated merge of the point clouds from each scan. The *VXScan* software module provides a "best fit" merge tool, yet this tool is not always successful. For these cases, the creation of points of reference in each scan might be necessary in order to match the position of each point cloud, thus completing the merge. The end result should be a point cloud detailing the blade completely which will be converted to a mesh for further treatment.

4.2.1.2 Mesh Processing

Following the point cloud acquisition, the points are connected by lines converting into nodes and creating a surface mesh. This mesh may present some defects such as holes, spikes or irregularities which are a consequence of lack of information from the point cloud. This way, mesh defects will appear in the areas where the laser grid from the scanner is more difficult to reflect. This occurs typically on the edges and will be more common for smaller detailed geometries such as the ones of the latter compressor stage blades.

Various mesh processing tools are available in the *VXModel* software module to correct these defects and improve mesh quality. For example, the "fill holes" tool creates a surface by connecting the mesh's nodes with information from the adjacent surfaces. This tool works very well for small holes in the mesh but often results in mesh irregularities when filling larger holes that spread along edges as Figure 4.9 depicts.

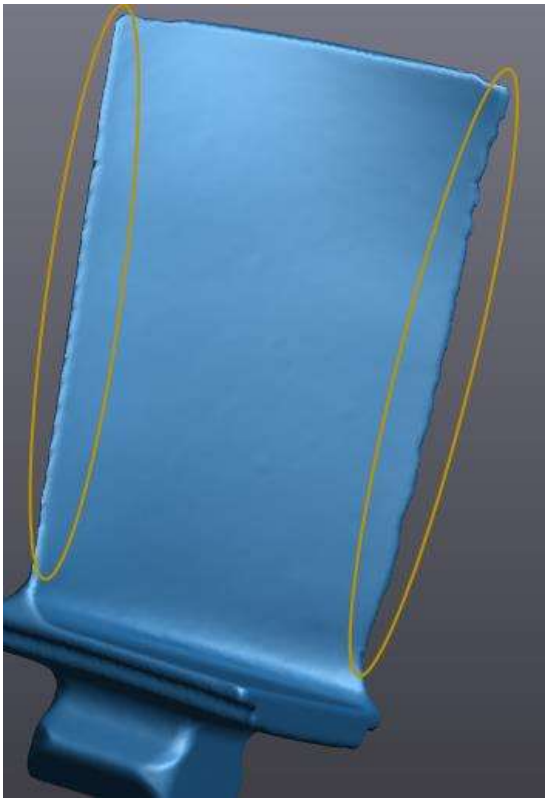

Figure 4.9 - Mesh Model Edge's Irregularities

Other mesh processing tools such as “smooth mesh” and “remove spike” reduce the mesh’s irregularities by taking information from the surfaces’ normal vector and reducing its variation in direction. This process results in a smoother mesh and gets rid of most of the mesh’s defects but still leaves some of the irregularities along the edges of the object scanned.

It is important to notice that mesh processing may result in deviations between the real object’s dimensions and the scanned model. These deviations are mostly inevitable and a direct result of the mathematical interpolation used in the described mesh processing tools. This means that, despite being mostly irrelevant, they will contribute for some percentage of the deviations between the computer designed model and its real counterpart. Therefore, the best way to minimize these deviations is to focus in the acquisition of a good quality point cloud thus reducing the necessary mesh processing.

Finally, the last step of the mesh processing is to eliminate any redundant information. This can be done by connecting elements with similar surface normal into one single element, greatly reducing de number of elements and nodes in the mesh. The “decimate” tool performs this, significantly reducing the toll on the computers processor and graphic card when using a CAD software to model using the mesh file as a template. After this mesh processing is completed, the model was exported as *.STL* mesh file format compatible with most of CAD software, namely *SolidWorks*.

4.2.2 HPC Blade CAD Model Development

As the second stage of the HPC blade's reference model development, the CAD reference model will allow us to define and adjust the blade's various geometries such as faces, edges and profiles according to the information documented in subchapter 4.1. However, most geometries will still rely on the mesh model obtained from de scanner and therefore, will inevitably present some defects/deviations from the real blade.

The CAD model developed will compensate some of the irregularities identified in the mesh file by rounding edges and create facets through the mesh's surfaces. Hopefully, this CAD model should be accurate enough to be used as reference for the position of the blade's different geometries when these will be measured by the CMM.

Although there are a variety of different licensed reverse engineering dedicated software programs that will allow us to develop CAD models based on 3D scanned data, these tend to require high computer processing and graphical capability in addition to the software's rather high license costs. Still, these types of software programs are not fully reliable as they would still require a mesh file with considerable quality and base understanding of the model's geometries in order to trace these features to a CAD model.

This being said, the CAD model was developed using only the basic features of SolidWorks with no need for premium features or add-ins. The CAD model developing process was then improved in order to minimize the deviations between the mesh file and reference model, making it possible to replicate this process for all the compressor stage blades or even other engine parts. A step-by-step description of this process is included in the following paragraphs with illustrative images of what to look for when developing the CAD model along with some guidelines for some of these steps.

The first step to create the CAD model is to generate reference planes in the base mesh file in order to align the features generated through profile extrusions with the mesh's surfaces. As *.STL* mesh format files are opened in SolidWorks, mesh information regarding its nodes and elements is not accessible as the file is opened as a surface body imported mesh by default.

For this, the "segment mesh" feature was found to be useful as this feature allows to extract some of the mesh's information mainly in the model's areas correspondent to edges or other distinct features. Figure 4.10 displays the model after the use of the "segment mesh" feature as dark lines represent the points and lines that are now accessible by the software's "Snap-On" features. This procedure is essential as it allows us to place reference planes in the three-dimensional coordinate system.

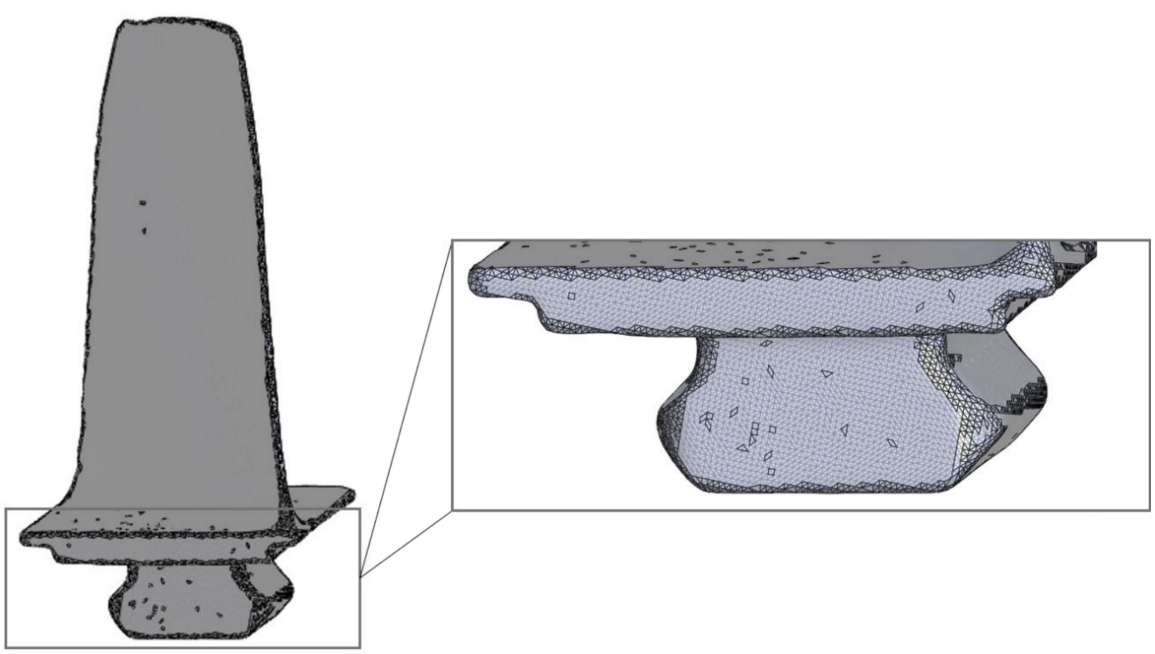

Figure 4.10 - Mesh Model's Available Points and Lines

These points will now be used to create the reference planes on which we will proceed to create the CAD model and may also be used to create other auxiliary planes or lines for the CAD features.

Firstly, three orthogonal planes will be necessary and therefore, to help the modelling process, the planes may be aligned with the blade's orthogonal features (if available), namely the dovetail profile. Figure 4.11 demonstrates the reference planes placement creating an implied point of origin at the intersection of the three planes. This figure also illustrates some auxiliary planes parallel to the platform plane that will later be used to trace the blade's airfoil profile.

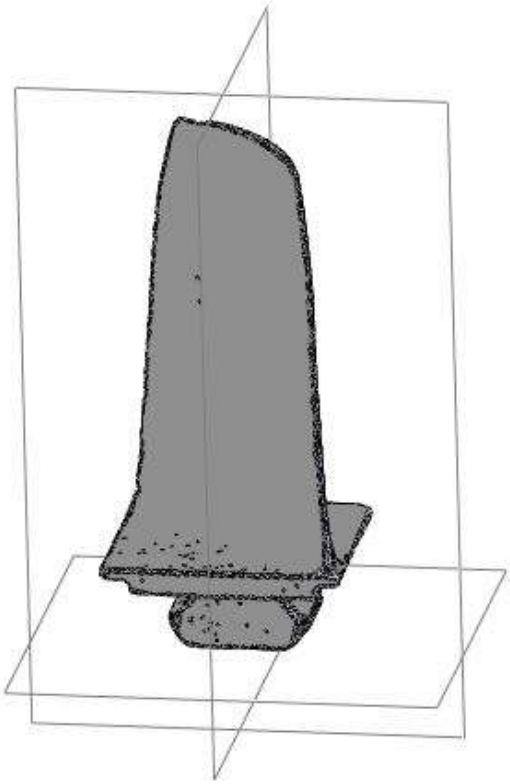

Figure 4.11 - Mesh Model's Reference Planes

These planes allow us to define practically almost all the blade's geometries as the dovetail section of the blades is orthogonal apart from the stage 1 blade which required other planes to fully define.

The following process of tracing the blade's geometries using *SolidWorks* consisted of basically four steps. First, the *Extrude Boss/Base* command of the dovetail's longitudinal section which required some dimensions referred in the subchapter above, regarding the blade's reference dimensions. For this step, as Figure 4.12 demonstrates, the angle of the surface of contact between the blade and the HPC disk/spool was used and the profile was traced using mostly lines and circumference arcs.

Notice that the scanned model's geometries regarding RTV placement were ignored in order to include only the blade's geometries. After obtaining the longitudinal profile, the body is cut tracing the dovetail geometry through the lateral reference plane, thus completing the dovetail geometry as displayed in Figure 4.13.

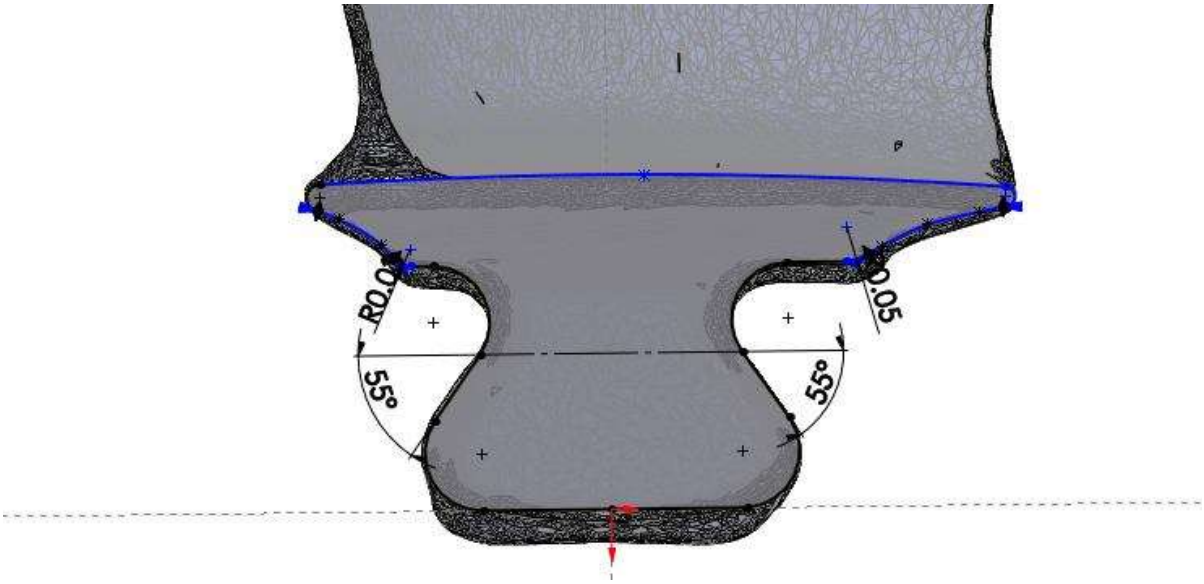

Figure 4.12 - Blade's Dovetail and Platform Longitudinal Profile Tracing

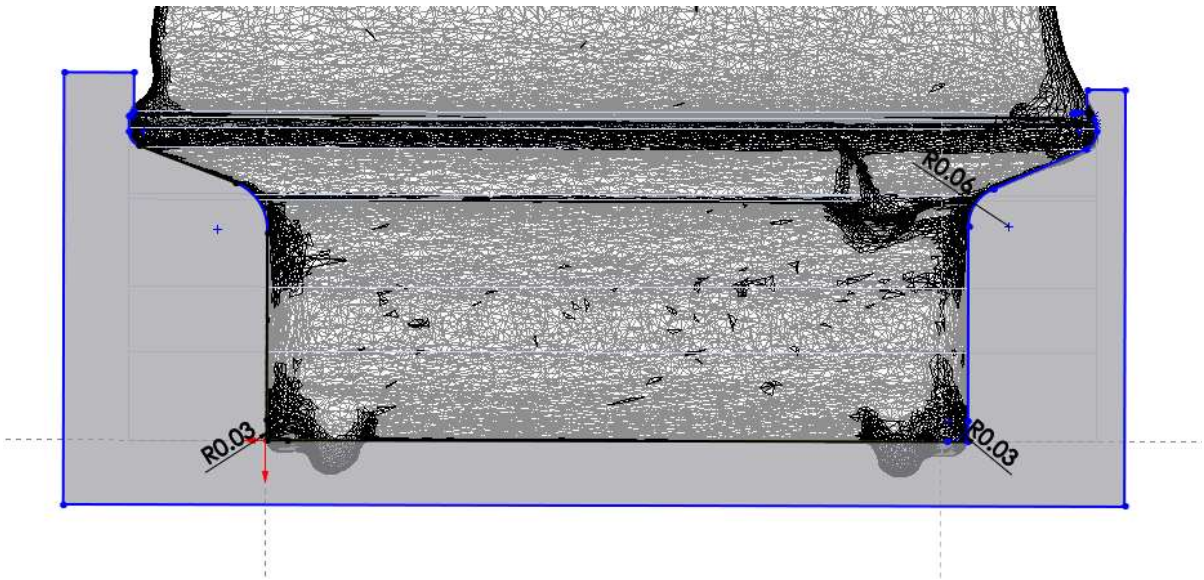

Figure 4.13 - Blade's Dovetail and Platform Lateral Profile

Figure 4.14 shows the generated CAD body in green overlapped with the mesh model. As displayed, the CAD almost exactly overlaps with the mesh body but the edges need to be rounded in order to obtain a more exact replica of de mesh model, which brings us to the third step, applying the "fillet" feature to the dovetail's edges, obtaining a better match between both models. The result of this step can be observed in Figure 4.15 with the CAD model still in green.

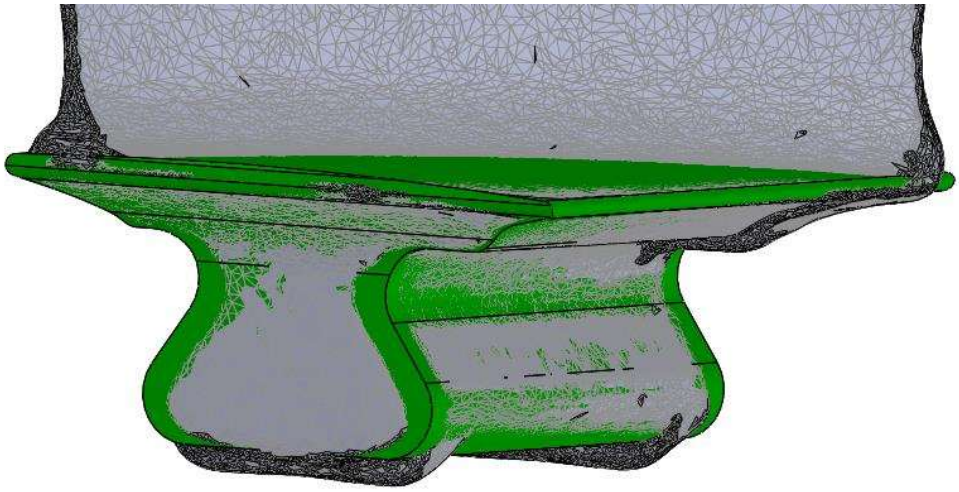

Figure 4.14 - Mesh to CAD Model Dovetail and Platform Correspondence After Profile Tracing

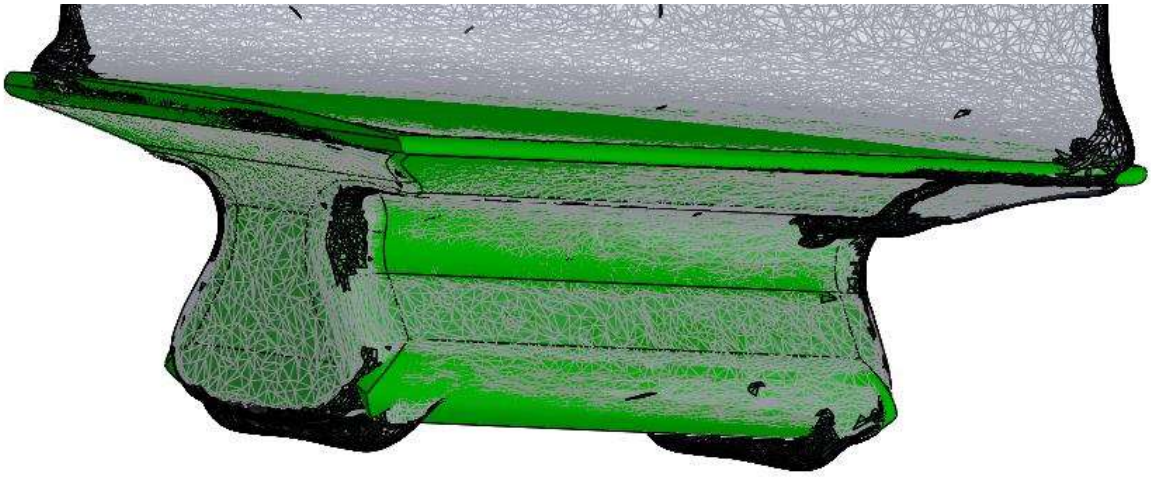

Figure 4.15 - Mesh to CAD Model Dovetail amd Platform Correspondence After Edge Fillet

Finally, the fourth step to complete the HPC blade model is focused on the airfoil section. For this step, the auxiliary reference planes parallel to the platform plane where used to perform a section view of the mesh model. Here the intersection between the section plane and the mesh is highlighted in blue as displayed in Figure 4.16. This profile will now serve as a reference to trace the airfoil profile.

The airfoil profile was traced simply by two curved lines (Splines in *SolidWorks*) connected at the edges by circumference arcs as Figure 4.17 demonstrates. This will allow us to correct both the irregularities in the mesh's surface and the thickness of leading and trailing edges with the reference dimensions.

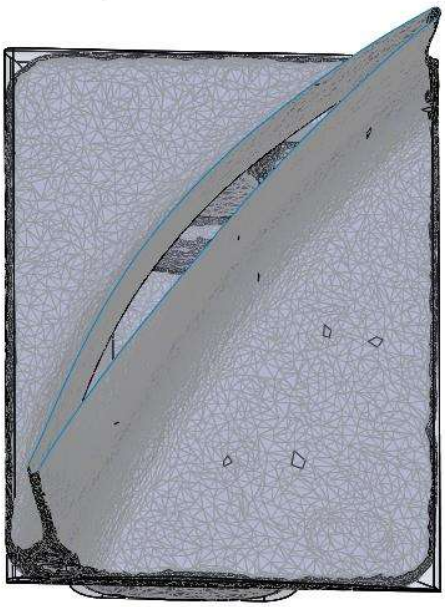

Figure 4.16 - Mesh Model Airfoil Cross Section Profile

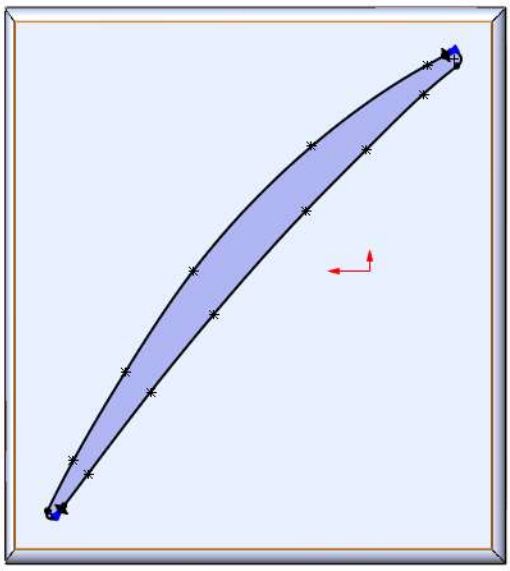

Figure 4.17 - Airfoil Profile Tracing in CAD Model

With airfoil profiles defined for different blade heights as shown in Figure 4.18, the blade's body was then generated through the "Lofted Boss/Base" feature as it allows us to create a body connecting different profiles. For this feature, the use of "guide lines" was found to be useful as a mean to help the software connect the numerous profiles as these lines provide further constrains to the computer iterations necessary to create the airfoil body.

Lastly, the tip of the blade will need to be adjusted as its geometry is not parallel to the platform plane. For this the blade's airfoil body is cut with a trace of the mesh's tip profile as it is demonstrated below in Figure 4.19.

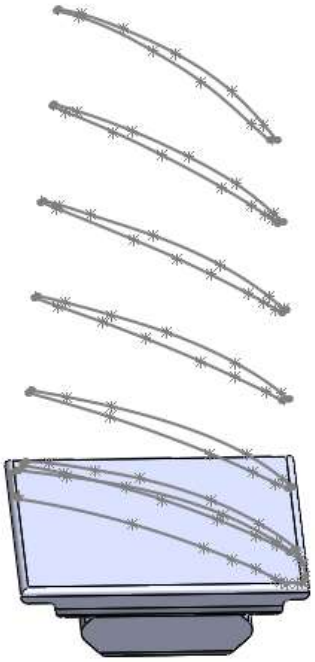

Figure 4.18 - Airfoil Profiles for Solidworks' "Loft Boss/Base" Feature

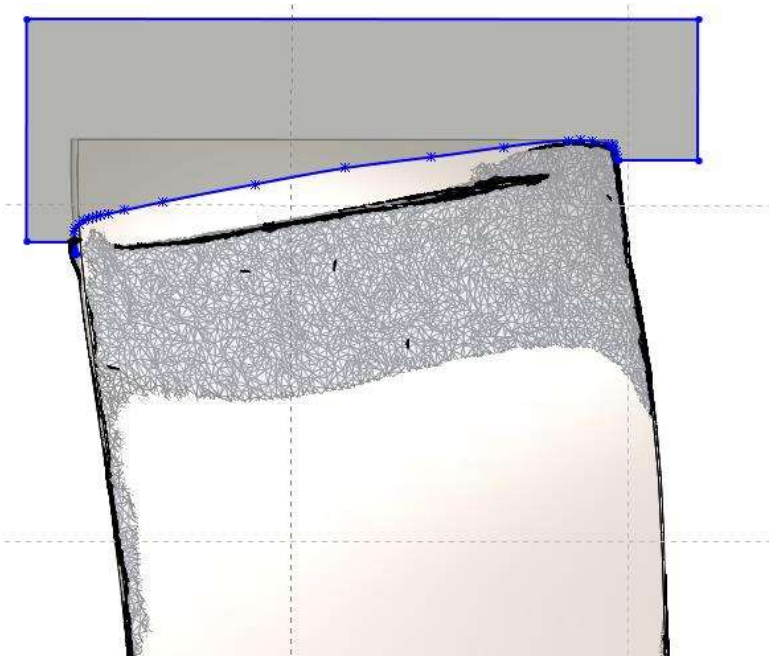

Figure 4.19 - Blade's CAD Model Tip Profile Adjustment

One important detail to notice is that the airfoil's body is generated mathematically to connect the traced profiles, therefore, this body is most accurate at intersection with the traced profile's planes. This allows us to somewhat control the accuracy of the CAD model's by placing the planes of intersection at the blade's height where the airfoil measurements through the CMM are desired or required.

At last, by completing this process, the final result should be a CAD model for the desired HPC blade, accurate enough to serve as a reference for the software that generates the CNC commands for the CMM. However, it is important to understand that the exact position of points of measurement is not that relevant as the dimensions registered by the CMM are relative to the exact distance between physical points measured by the probe. Regardless of that, there is in fact, the need to have the model designed within a certain interval of confidence as the deviations between the CAD model and the real blade shouldn't be so great that the probe misses the blade completely.

5 Fixture Design for HPC Blade's Dimensional Inspection Using the CMM

As one of the primary focuses of this thesis, the fixture's design was requested by TAP M&E with the goal of improving the HPC blade's inspection capability. As described in the third chapter, with the high pressure compressor playing a major role in the turbofan engine's performance, there is a vast interest in evaluating the blade's condition with greater detail. This may allow TAP Engine's Shop engineers to obtain better performance outputs by assembling arranged sets of blades based on their known condition.

To improve the blade's inspection capability in both its precision and measuring rate, there was the opportunity to rely on the Coordinate Measuring Machine (CMM) to run a computer guided program to measure entire blade sets with improved accuracy. However, although the CMM is a resource commonly available in shop, it was never used to inspect HPC blades since it would be very impractical to measure each blade through manual commands. This raised the necessity to create a fixture tool that would arrange and present the blades in the CMM table, thus giving the probe access to measure the required dimensions.

Regarding this matter, excluding the blade's CAD modelling as a prerequisite to this project's development, the functional requirements to improve TAP's blade inspection capability consist on the ability to arrange the blades on the CMM table and to inspect them using an automated CMM program. These requirements correspond directly to the fixture's design and the programming of the CMM in light of Axiomatic Design Correspondence between the functional requirements and design parameters as displayed in Figure 5.1.

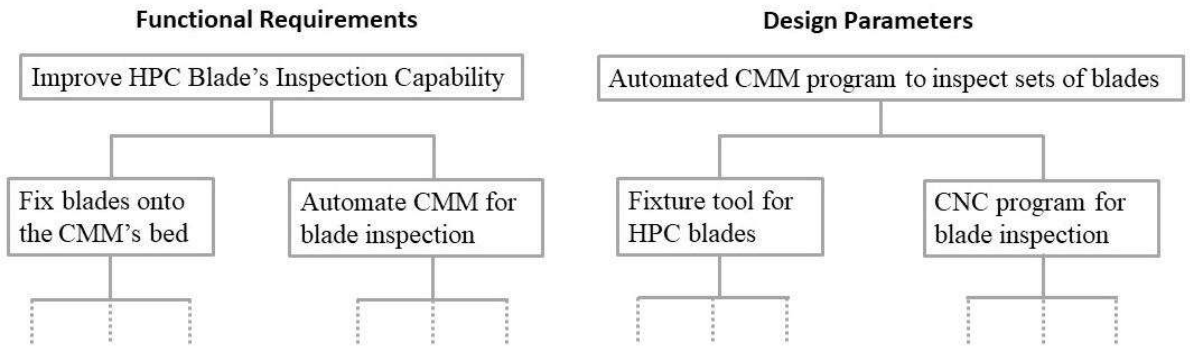

Figure 5.1 - Main Stages of the Functional and Physical Design Domains

This chapter is focused on the different stages regarding the fixture's design and will be organized following an Axiomatic Design inspired approach by documenting the fixture's functional requirements and constrains raised from stakeholder's recommendations and concerns.

However, this design's parameters will not attend to the Axiomatic Design recommendations, for example, concerning the "one-to-one" correspondence between functional requirements and design parameters, neither concerning the independence axiom. Instead, this approach is meant to provide a more structured view on this design stages by defining the tool's features that will meet all the defined functional requirements.

This way, this chapter will be comprised of three main sections concerning the fixture tool's functional requirements, design constrains and lastly, design features. This last section will include a more in-depth description of the development of each of the tool's features and geometries thus providing a clear view on the tool's design process. As a result, both the CAD models and the technical drawing of the tool's components and assembly will be provided allowing TAP to advance with the tool's manufacture if so desired.

5.1 Functional Requirements

As the fixture tool's goal is to improve the shop's dimensional inspection capability for HPC blades using the coordinate measuring machine, functional requirements and constraints derive not only from the shop's needs but also from the possibilities available with the CMM. This way, three main functional requirements for the fixture's design were raised regarding the improvement of the blade's dimensional inspection procedure. These three main requirements are: to increase the detail in the HPC blade's dimensional inspection; to improve the blade's set dimensional inspection's rate; and finally, to assure the fixture's manoeuvrability and the tool's ergonomics.

The current level of detail in the measurements taken from the airfoil geometry is rather low regarding the ESM's (Engine's Shop Manual) specification for dimensional inspection. To assure shop productivity, the manual specifies only chord length and leading/trailing edge thickness at a specific blade height maybe because these part's assembly quantity makes the blade's dimensional inspection procedure very time consuming. However, the possibility to evaluate the blade's condition beyond the measurements specified may be useful for better performance outputs. This way, the fixture tool is required to display the blade's in such way that it should be possible to perform all sorts of measurements available through the CMM.

There are different degrees of detail regarding the HPC blade's dimensional inspection. One of the possibilities is to simply increase the number of measurements taken, whether by varying the blade's height where chord length and edge thickness is measured (Figure 5.2 - left) or to increase the number of sections along the camber line where airfoil thickness will be measured (Figure 5.2 - right).

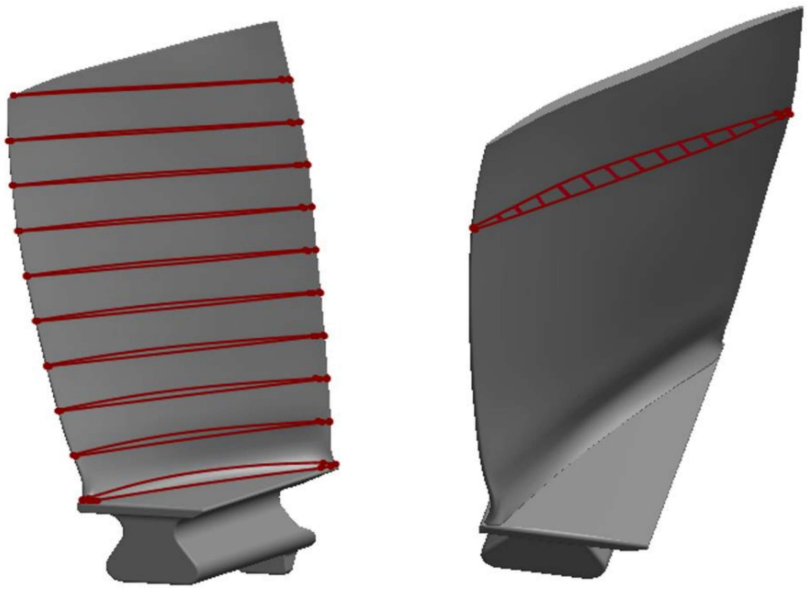

Figure 5.2 - HPC Blade Airfoil Chord (left) and Thickness (right) Sectioning

Other option is to detail the entire airfoil profile where the CMM sweeps the blade surface detecting all sorts of irregularities and providing all information regarding edge thickness, profile thickness, camber line, chord length and even blade twist (if the scanning is performed at different blade heights). This requirement is by far the most demanding as it implies not only a precise blade reference model but also a precise and robust blade positioning onto the tool.

Lastly, other way to add more scope to dimensional inspection of the operating status of HPC blades, is to inspect dovetail and platform dimensions. This option may, however, be associated with worse outcomes in performance outputs as these dimensions have less impact in compressor efficiency. Still, platform width as described in chapter three is especially relevant in blades from stages 4 to 9 and, therefore, the fixture tool for blades from these stages should allow for platform width measurement in order to reduce the gap between platforms upon assembly.

In short, to the increase detail in HPC blade's dimensional inspection is basically to extend the number of measurements to cover a wider surface area of the blade thus increasing the information regarding the blade's operational status. This obviously comes with a cost of time as the increase of the number of measurements per blade will translate into increases blade inspection time.

Therefore, there is an inherent trade-off between these two main functional requirements, blade's dimensional inspection detail and rate, which raises the question of which requirement is more relevant in face of the other. Despite this, it is important to notice that, as described in this chapter, detail does not equal precision, as detail portraits the amount of information obtained regarding the blade's dimensions and precision is solely reliant on the CMM measuring capability.

Regarding the HPC blade's dimensional inspection rate, as the shop currently inspects the blade by visual inspection and evaluates the chord length status using a *Go/No-Go* tool, it is fair to say that process's rate won't be reduced significantly. Still, it is relevant to note that, in comparison to current procedures, the level of information regarding the blade's status should increase and, as the inspection automated program is optimized, it will solely require the CMM as a resource, freeing dimensional inspection team members for other duties as the program runs.

This way, the fixture's design effect on the dimensional inspection rate should be mostly due to preparation/setup times. This rate can be improved by allowing the fixture to accommodate the full set of each blade stage or even sets from multiple stages. Despite this, the amount of blades accommodated in the CMM granite table is limited by the workspace volume that will be specified further ahead as a constraint. The fixture tool still has to be versatile enough to allow for all of the CMM measuring feature and the blades should be displayed closer enough in order to accommodate as many blades as possible yet, further enough to allow access for the CMM probe. This indicates that blade display is key to the fixture's design and will be discussed in the following chapter.

Other way to reduce setup times through the fixture's design is to allow for a quick blade fastening onto the tool. As some compressor stages comprised of up to 82 blades, if the assembly time for each blade is reduced it will have a great impact in the overall setup time. This fixation should be rigid blocking all the blade's degrees of freedom so that it does not compromise CMM readings. This is also valid for the tool's mounting and positioning onto the CMM table as the fixture should allow for a quick setup also reducing the machine's downtime.

Lastly, the fixture's design has to take into consideration the tool's manoeuvrability and ergonomics, not only because these concerns often prove to be impactful in improving productivity results in shop, but also because these directly affect setup times and are closely related to the functional requirements above. This means that, some features should be added in design for the fixture to become "worker friendly" such as simple fastening mechanisms for the blades and for the fixture's manoeuvrability. Therefore, the fixture's design is required to assure the tool's portability, whether manual transportation or by gantry (depending on the tool's weight), and to include ergonomic features.

To summarize, design functional requirements are displayed in a diagram format in Figure 5.3 below which should provide a clearer view of this design's functional domain. To ensure simplicity, functional requirements were restricted to the shop's main interests and, therefore, were not decomposed

any further. Despite this simplicity, these functional requirements should still guarantee most of dimensional inspection variations available with the CMM.

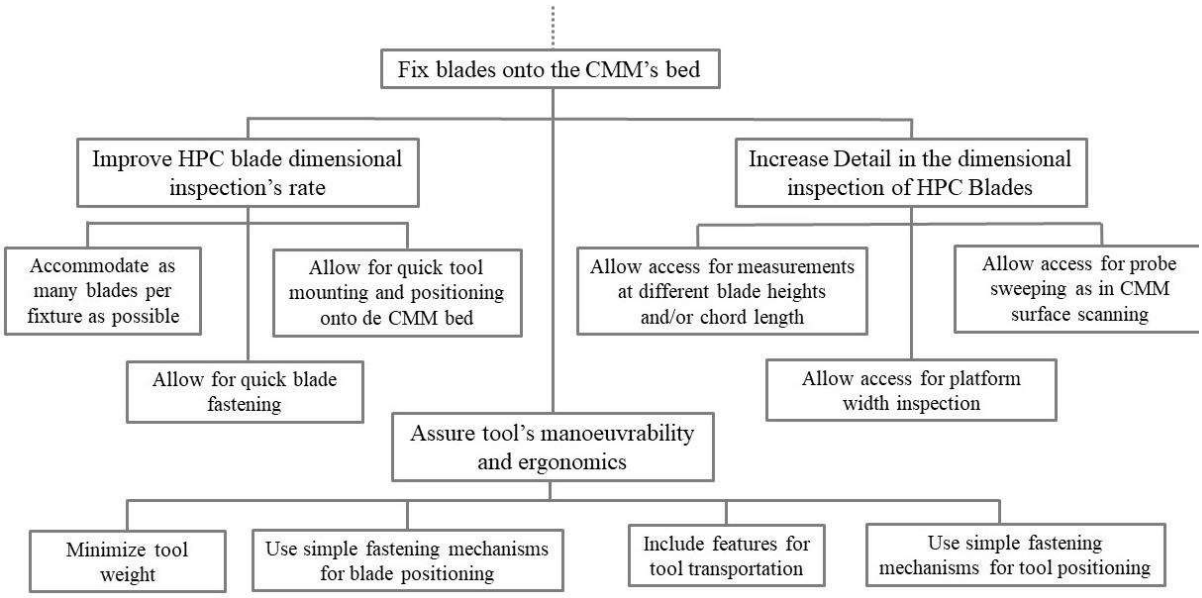

Figure 5.3 - Fixture Tool's Design Functional Domain

5.2 Design Constraints

As it was already stated, this project is focused on the inspection of HPC blades with the CMM. Since this is a project of great interest to TAP's engine maintenance shop, no cost constraints were initially considered for to the fixture's manufacturing respective to this preliminary design. Despite this, as good practice, cost reduction will be taken into consideration when designing the tool without compromising the tool's quality and longevity. Regardless of this, there are still some constraints to this work as the fixture tool's design is mostly limited by the CMM's operation and some shop requirements.

Regarding shop requirements, this project must attend all Engine Shop Manual's specifications, which means that both the tool and the CMM's inspection program should, at the very least, allow for the chord length and leading and trailing edge thickness serviceability and repairability inspection described in the subchapter 4.1.2 and the respective Appendix III.

Furthermore, the fixture tool must not compromise the blade's serviceable condition or mark the blade in any sort of way upon assembly. This means that the tool is required to consider the blade's repairs and preparations for service and that the blade's fastening mechanism is limited to some available surfaces of contact. One quick example of this is the RTV application to the dovetail section of the blade. Figure 5.4 portraits some blades where this orange RTV silicone application was damaged.

Figure 5.4 - HPC Blades with damaged RTV Silicone

Apart from the Engine's Shop Manual's specification, it is clear that the fixture tool must also be compatible with the CMM and is limited by the machine's available work-volume and other operational restrictions. This way, the CMM restricts the tool's design in both weight and dimensions as the tool's weight with the full set of blades assembled must not exceed 2000 kg and the tool must fit within the work-volume of 1200x1200x1000mm as displayed in Figures 5.5 and 5.6. However, these specifications do not represent exactly to the tool's design constraints and further assumptions must be made to clarify the exact values for weight and dimension that the tool must not exceed.

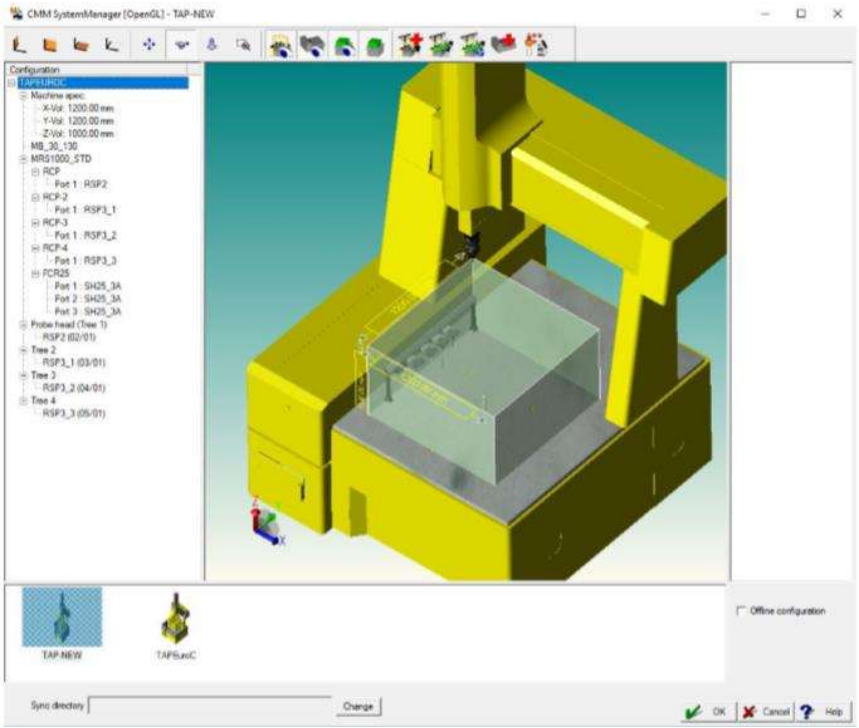

Figure 5.5 - CMM Workvolume Display [7]

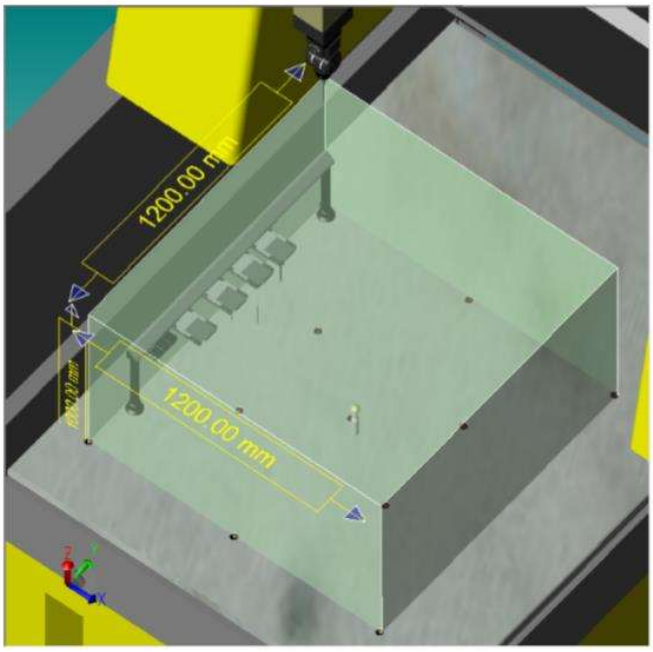

Figure 5.6 - CMM Workvolume Illustration with Dimensions [7]

Firstly, the work-volume described simply states the dimensions above the granite bed that are accessible to the CMM's probe. These dimensions did not take into consideration the location of the probe's storage rack and the tool must also guarantee the probe's access from all angles. This way, the tool's maximum dimensions will be a result of a reduction of this volume in the CMM's coordinate system *X* and *Y* directions as represented in Figure 5.7. In addition to this, to maximize the probes access to the blade's features, the blade's will most likely be displayed in the fixture standing, therefore, the maximum dimension in *Z* axis direction should not be a concern despite being a constraint, nevertheless.

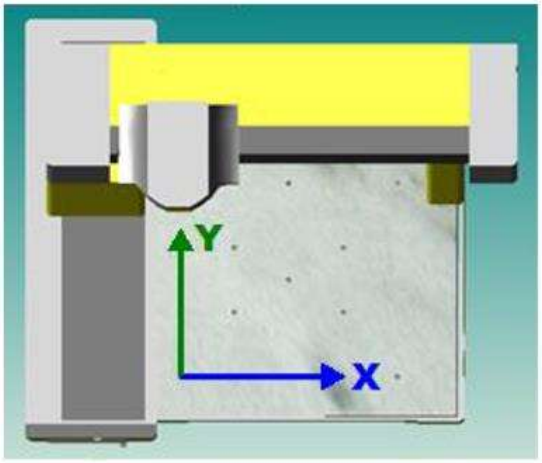

Figure 5.7 - CMM's *X* and *Y* Axis Illustration [7]

Taking the figures above as reference, the probe storage rack occupies the leftmost part of the granite bed and is only thick enough to store the stylus part of the probe. This way, the space available for the tool is limited by the probe rack only in the *X* direction as its Y position on the bed will not be considered in order to allow for future probe rack extensions. On that premise, the volume available for the tool was adjusted by 200*mm* accounting for the storage rack width, its distance from the very end of the CMM table and even some clearance to avoid any collisions.

Regarding the probe's access to the blades mounted in the fixture, one must consider both the CMM's arm and the probe's stylus dimensions. This is important to determine required spacing between blades but also to provide the CMM's probe enough clearance to access the blades from around the tool. Although the exact clearance necessary will be detailed further ahead on the blade display subchapter, for now a settled $150mm$ clearance around the tool should provide more than enough space for probe's access.

Consequently, the granite bed's available surface is shrunk down two-dimensionally to grant the probe's access to the blades from around the tool, thus resulting in a *700x900mm* constraint for the tool's *X* and *Y* dimensions respectively. Figure 5.8 illustrates this process of thought where the red highlighted area corresponds to the probe's storage rack available space, the green area to the available access form around the tool and, lastly, the blue highlighted area to the available dimensions for the tool's design.

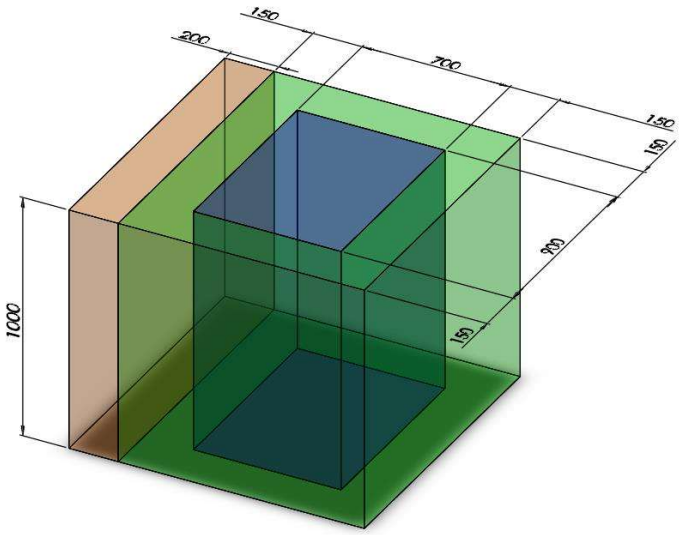

Figure 5.8 - Available Volume for Tool Design

Secondly, as described above, the weight constraint for the tool's design must consider the overall weight of the blades assembled. For this we need to estimate the weight of the blades from each stage which can be done through two different methods. One of them is to weight groups of blades from each stage and either consider the mean value or the heaviest in order to assure that weight limit isn't

surpassed. The other method, and the one that is going to be carried out for the purposes of this work, is based on the blade's developed CAD models. As the blade's titanium alloy's density is proprietary to the manufacturer, to assure safety, the heaviest alloy available in the *SolidWork'*s software was selected, with a mass density of 4820 kg/m^3 for a solution treated Titanium *Ti-13V-11Cr-3Al* alloy. The weight results for each stage per blade and per full set are displayed in Table 5-1 below. Weight estimates concern only the five compressor stages correspondent to the CAD models developed in this work.

Table 5-1 - HPC Blade's Set Weight

	Weight per blade [g]	**Blade Quantity per set**	**Full set weight [kg]**
Stage 1	128.27	38	4.88
Stage 2	51.13	53	2.71
Stage 3	27.33	60	1.64
Stage 4	16.27	68	1.11
Stage 5	11.60	75	0.87
Stage 6	—	82	—
Stage 7	—	82	—
Stage 8	—	80	—
Stage 9	—	76	—

As observed, blade weight is barely significant and, therefore, the fixture's weight is relevant as a functional requirement but not as a design constraint. Regardless of that, the tool's weight is officially limited at 1900kg considering approximately a 95kg margin between the tool's maximum weight allowed with a full set of first stage HPC blades assembled and the CMM's granite table weight limit.

5.3 Design Features

As the fixture tool's design is now properly framed, the following stage consists in the development of the different tool's features that meet all the functional requirements and respect this design's constrains as documented in the segments above.

This way, the tool's design was decomposed in the design of different features and design options that attend to the tool's functional requirements. These features include the blade's fastening mechanism; the blade's set display configuration on the tool; the tool's CMM positioning features and lastly the tool's portability/manoeuvrability features. Other design options that will also be approached in this chapter will be the tool's material choice and even some modifications for manufacture.

Lastly, a s the tool's features become fully defined, a segment on the assembly's geometric design and tolerancing will be provided thus resulting in this design's components and assembly technical drawings.

5.3.1 Blade's fastening mechanism

In order to come up with the proper fastening mechanism for the compressor blades, we should first determine which surfaces of the blade can be used for contact with the tool. This means that these surfaces will not be available for dimensional inspection and, therefore, the blade surfaces that are in fact necessary for inspection, must be exposed when the blade is attached to the tool.

Simply put, similarly to what happens in the compressor's rotor assembly, the dovetail section of the blade is available for fixation on the tool while the airfoil and platform sections of the blade need to be exposed for the probe's access. Figure 5.9 highlights in blue this section of the blade that is available to secure the blade to the tool.

Figure 5.9 - HPC Blade's Available Surface for Tool Attachment

The fastening mechanism is required to restrict all the blade's degrees of freedom which include all three of the directions of translational motion and all three rotation directions in its reference coordinate system. Another requirement for this mechanism is that the blade should always lock into the same position relative to the tool, thus allowing the CMM's automated inspection routine to encounter the blade's features every time.

Theoretically, the simplest way to achieve a fully defined geometric assembly between two parts, these must be mated firstly by a plane, then by a line and lastly by a point, granted that both the line and point chosen are not contained by the plane and that the point is not contained by the line. This type

of mating should restrict all the moving part's degrees of freedom. This system is commonly used when mating parts in CAD software.

When we are accounting for a part's geometric irregularities, the type of mating described above corresponds to the most precise way of assembling two parts and is may be referred to as a *3-2-1* mating system. Firstly, the moving part's surface is mated with three points of contact defining a plane, then slides to meet two more non-coplanar points which define a line and lastly, secured by a single point of contact. This is done through single points of contact because two surfaces are impossible to be perfectly mating as, in reality, it is impossible to achieve geometric perfection such as planarity or straightness. Figure 5.10 illustrates this mating system for the parallelogram's case with the plane defined by the three blue support points, the line defined by the two in green and the point defined by the one in orange.

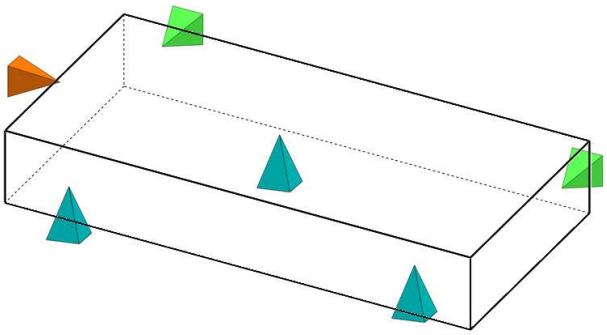

Figure 5.10 - 3-2-1 Mating System

However, to consider this type of mating system when designing fixture tools means extra design challenges. To emulate a single point of contact, curved surfaces need to be used which are more complicated to manufacture especially through machining processes. This way, this type of system is only reliable when the assembly requires the mating of surfaces with large areas, which is not the case of the blade's dovetail section.

This way, the decision was to emulate the mating system used in the compressor's rotor assembly utilizing the blade's dovetail profile. The blade is going to be secured firstly by mating one of the surfaces at the end of the dovetail section, then an upwards force will lock the blades into position by mating the blades lateral surfaces. Figure 5.11 illustrates this mating system highlighting the mating surfaces in blue.

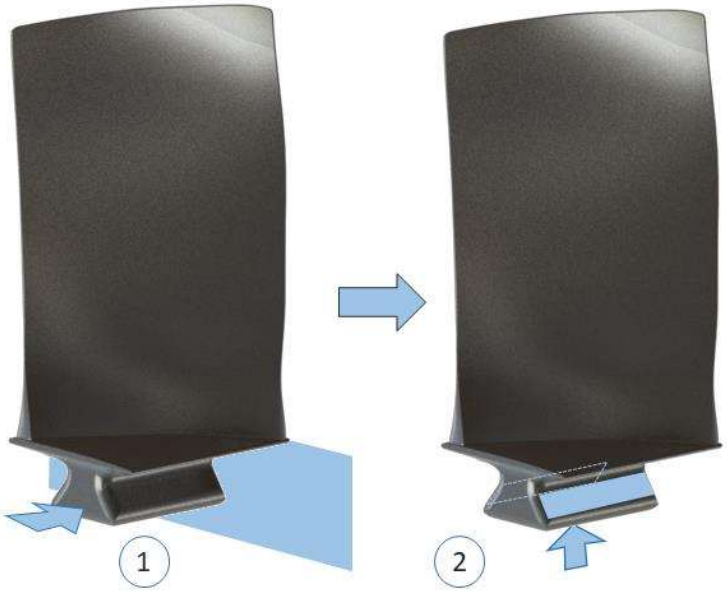

Figure 5.11 - HPC Blade's Dovetail Fastening Principle

The dovetail's lateral surfaces are key here as the upwards force locks the blade into the same position every time with considerable precision. This traced back to the blade's design itself, as this is similar to what happens during compressor operation, when centrifugal forces push the blades outwards securing the blade by its dovetail's lateral surfaces.

Considering all this, knowing the blade's dimensions, it is now possible to design a slot profile in which each stage blade should fit. For this, the dovetail's section angle of aperture referred to in section 4.1.1 of this document and registered in both Appendixes II and III will be very useful to attribute the slot's profile dimensions.

The slot profile should provide enough clearance for the blade's dovetail profile discarding the use of unnecessary profile tolerancing on the tool's design. The only geometric tolerances required will be for the mating surfaces which refer to the dovetail's angle of aperture. Figure 5.12 illustrates the outline of the slot's profile for the blade's sliding position (left) and and after the blade is fixed by the upward force (right).

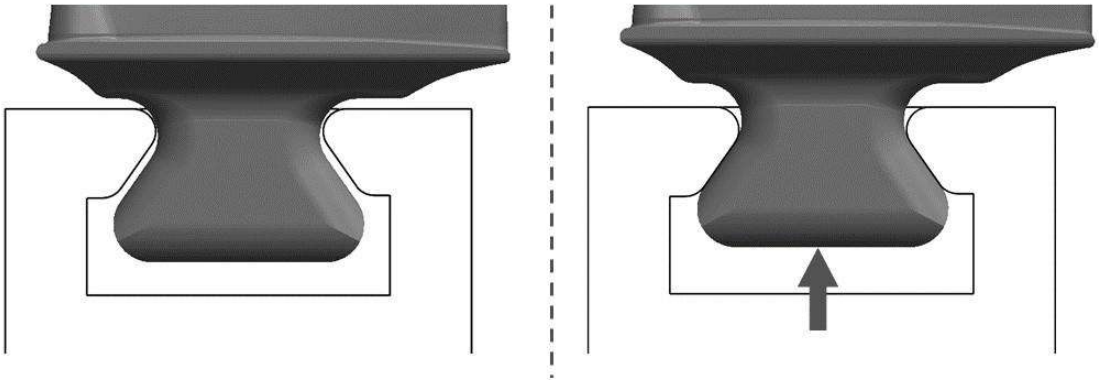

Figure 5.12 - Blade's Dovetail Fastening through Upwards Force

As displayed in the figure above, some fillets were added to the extremities of the tool's designated surface of contact. These features are considered essential as smooth edges will assure that the blades aren't damaged by tool's edges.

Figure 5.12 also illustrates the tool's profile that was outlined for design. This profile should vary according to the differences of each blade from stage to stage regarding the dimensions of the dovetail section. As displayed in Figure 5.13, the slot's profile is fully defined by six different dimensions. Angle β as already specified above is related directly to the dovetail's angle of aperture. Dimensions A and B are dependent on the blade's dovetail width and, in conjunction with angle β and the slot's dept, should dictate the area of contact between the tool and the blade. Other dimensions C, D and the fillet radius R are only required to provide enough clearance for a smooth blade assembly onto the fixture tool.

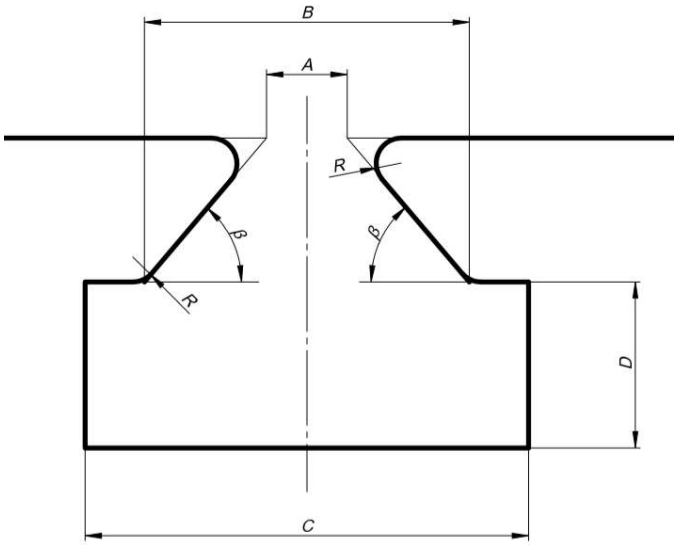

Figure 5.13 - Blade's Slot Dimensions for Tool Design

Of all these dimensions, the only reference available is for the angle β, which means that other dimensions will be based on the CAD reference models described in subchapter 4.2. Although the dimensional inspection specifications provide us with the dovetail's mid surface width (dimension W in appendixes II and III), this dimension will not be used as reference as it doesn't limit neither dimension *A* nor *B*.

One important note is that the dovetail section in stage 1 blades is not orthogonal, this means the slot should be defined by a seventh dimension, the dovetail's angle of inclination in the *XY* and YZ planes. Figures 5.14 and 5.15 display these dimensions in the top and right plane views of the stage 1 blade reference model respectively.

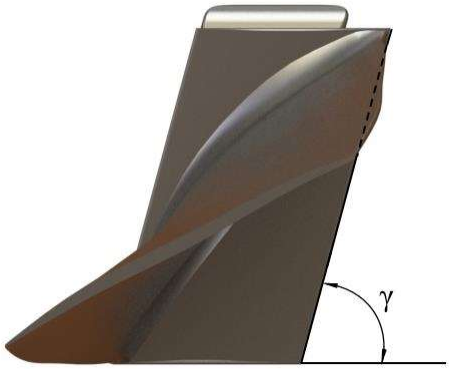

Figure 5.14 – 1st Stage Blade's Longitudinal Angle of Inclination

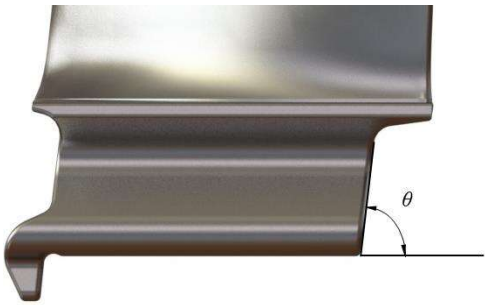

Figure 5.15 – 1st Stage Blade's Dotevail's Tilt Angle

Once again, there is no reference to these angles in Engine Shop Manual. Therefor these angles will be defined for the tool's design based on the blade's reverse engineered model. This could cause some issues with the fastening mechanism due incoherencies between the reference model and real blades. To counter these effects the slot geometries should be tested through prototypes in order to adjust these dimensions if needed.

On another note, the same slot geometry will be used for blades from compressor stages 4 and 5 due to the proximity in dovetail dimensions for blades of circumferential slot. This way, a single fixture tool can be designed for stages 4 and 5 as Figure 5.16 illustrates with the 5th stage blades assembled on the left and 4th stage blades assembled on the right.

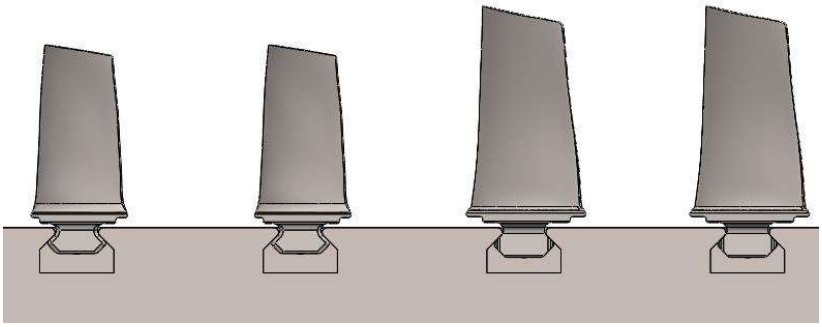

Figure 5.16 - Tool's Slot Profile Compatability with 4th and 5th Stage Blades

Finally, to complete the fastening mechanism design, the upwards force that locks the blade into position must be determined as well as how this force will be applied on the blade.

The upwards force's main requirements are to secure the blade into position without being disturbed by the CMM probe's contact and to provide an easy snap-in-place assembly of the blades onto the fixture tool.

For this there were a variety of possibilities but due to blade quantity, any solution that required longer setup times for dimensional inspection preparation was discarded. One example of this was to use threads and lock the blades into position by tightening screws. This was quickly discarded as tightening one of more screws for each blade in complete sets of blades would be very unpractical.

With this in mind, a clamp-like mechanism seemed to be the best option to minimize the efforts of the operator by making use of the energy stored in springs. This way, the blades could be simply slid into position where the springs apply the required upwards force.

For this, the springs needed to be preloaded on the tool in order to apply the required force. So, there are three steps for the spring-based design. First, the required force to fix the blades has to be determined. Next, the spring needs to be chosen according to the required force and finally, in accordance with the supplier's information, the assembly configuration of the springs onto the tool has to be designed.

As stated above the upwards force must counteract the force applied by the CMM's probe. This force must also take into consideration the blade's own weight as it is directly opposite to the force that is necessary to lock the blade into position. Figure 5.17 displays the free-body diagram of the blade

considering that the probe is touching the blade near its tip. This refers to the situation where the moment applied by the probe is the highest, as is this case the force $\vec{P}$ is applied the furthest away from the pivot point (marked in the dovetail section in bright red).

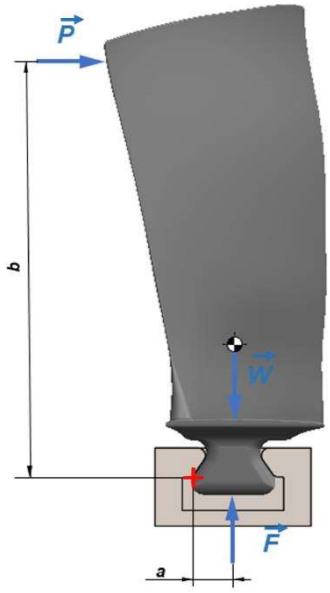

Figure 5.17 - CMM Probing Force Diagram

As displayed, the necessary force $\vec{F}$ has to produce a moment equivalent to the combinations of the moments produced by the blade's weight $\vec{W}$ and the force exerted by the probe $\vec{P}$. These moments are calculated in reference to the pivot point highlighted by the bright red '+' mark. With this, it is possible to determine the value of force *F* through the equilibrium of moments equation below.

$$F.a = W.a + P.b \tag{1}$$

From this, the required upwards force is easily determined as dimensions *a* and *b* derive from the blade's geometry, while *W* is obtained with the blade's mass and *P* depends on the CMM's probing mechanism. Equation (1) can now be simplified in order to determine *F*, as follows.

$$F = m.g + P.\frac{b}{a} \tag{2}$$

However, force $\vec{P}$ has yet to be determined. For this we need to understand that some CMM probes recognize touch through a displacement which causes contact between two conductors, thus emitting an electric signal. The force required to cause this displacement is determined by the rigidity of a spring inside the probe which correlates directly to force P. This mechanism is illustrated in Figure 5.18 with the spring and contact switches as described. In the case of the *RENISHAW's REVO-2 RSP2* system used in shop, a laser sensing trigger recognizes touch when the laser reflector is displaced which grants us a more accurate measuring system.

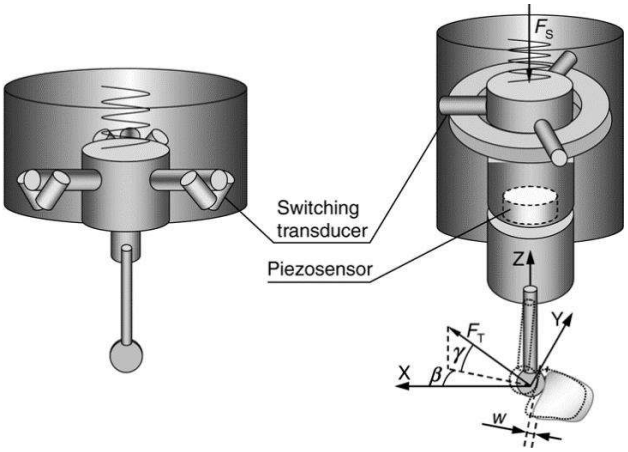

Figure 5.18 - Conventional CMM's Touch Trigger Mechanism [35]

However, we do not have the required information to determine force *P* as this probing mechanism specifications may be proprietary to the CMM's manufacturer or, in this case, the probe's manufacturer *RENISHAW*. Considering this, force P can be estimated by a quick experiment where a scale is placed on the CMM and a series of measurements are performed registering the values given by the scale.

This small experiment was conducted using two different styli available in the probe's storage rack where the probe touched the scale's plate in its geometric centre. The scale had a resolution of a tenth of a gram and the experiment was conducted at full movement speed for the measuring settings. The setup of this experiment is illustrated in Figure 5.19.

Figure 5.19 - Experiment for Force $\vec{P}$ Estimation

Table 5-2 - Scale Measurements for Force $\vec{P}$ Estimation

Measurement	Stylus 1 [g]	Stylus 2 [g]
1	470.43	15.25
2	455.04	18.60
3	346.52	19.19
4	306.76	—
5	515.84	—

As we can see there is a major difference in force $\vec{P}$ due to stylus specifications. Stylus 1 is bigger with a ball point diameter of 6mm and a length of 10mm connected to the RSP2-RSH250 adaptor, while stylus 2 is smaller with a ball diameter of 4mm and 10mm length connecting to the RSP2-RSH175 adaptor. While Stylus 1 is bigger, it was acquired by the shop specifically to support various measuring positions and had been recently calibrated to do so which makes it more appropriate for this experiment despite its values.

Due to the disparity of the values of the two probes tested, there was some concerns with the calibration of the CMM especially because the values obtained with stylus 1 were much higher than expected. Regardless of this, the max value obtained in this experiment will be used to define force P as 0.516 kgf which translates to about 5.1N of force with approximations by excess.

It is important to note that for further calculations, a safety factor won't be included as the value obtained for force P from the experiment abovementioned is an excessive estimate in itself. Even discarding the disparity of the values from different probes, we must account for the scale's springs displacement which increases the value registered on the scale before the probe detects the scale's surface.

With the value for force $\vec{P}$ estimated, we can now proceed to the calculation of the required upwards force $\vec{F}$ using expression (2). For this, dimensions a and b are based on the blade's reference models and were registered according to the CAD models as well as blade weight. The values obtained are documented in Table 5-3.

Table 5-3 - Force $\vec{F}$ Calculation Values

Blade Stage	Dim. a (mm)	Dim. b (mm)	m (grams)	F (N)
1	9.26	105.00	128.27	58.62
2	6.47	75.21	54.13	58.85
3	4.89	57.50	27.33	59.47
4	6.20	49.97	16.27	40.77
5	515.84	41.60	11.60	35.85

With the upwards force required to restrain the blades into place defined, the springs should be selected accordingly. Each blade slot will have two springs per lock, with respective housing. The springs will apply the force onto a bar which contacts with the blade's bottom surface. Figure 5.20 illustrates this type of mounting with the blade unattached (left) and with the blade attached (right).

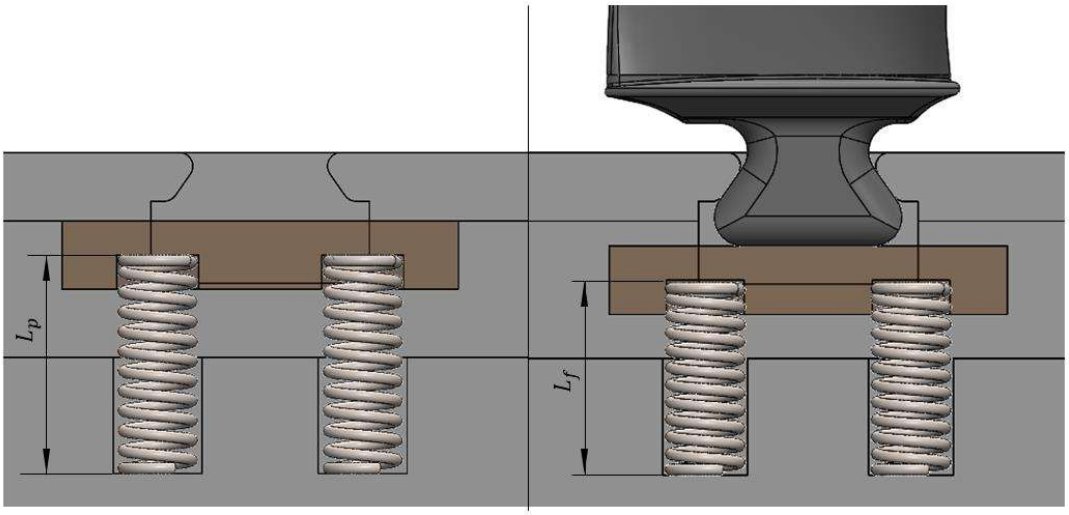

Figure 5.20 - Blade's Spring-based Fastening Mechanism

The spring is mounted on the tool with a preload compression when the blade is unattached which translates to spring length L_p. On the other end, when the blade is attached, the loaded length should correspond to a spring force equal or greater than *F* divided by 2 which is the required design force per spring on each blade slot. The length corresponding to the loaded spring will be referred to as L_f.

Considering $60N$ as the highest upwards force documented in Table 5-3, each spring is required to produce at least $30N$ of force (F_{req}) when the blade is mounted provided that the variation in spring length between the two positions is sufficient for the blade to slide through. For this, the *Lesjöfors Gas & Stock Springs* Catalogue [11] was used to select a stock compression spring available to match the required specifications which are categorized by the parameters displayed in Figure 5.21. Further information on the catalogue's spring specifications and more relevant information is listed in Appendix IV.

All dimensions are in mm

D_t = Wire diameter
D_m = Mean diameter
$D_{i\,min}$ = Inner diameter with smallest possible tolerance
L_o = Unloaded length
n_t = Total number of coils
L_n = Permitted loaded length for static load
F_n = Spring force in Newtons at L_n
R = Rate Newton / mm
P_o = Pitch
L_{st} = Solid length = $D_t \times n_t$
s = Deflection

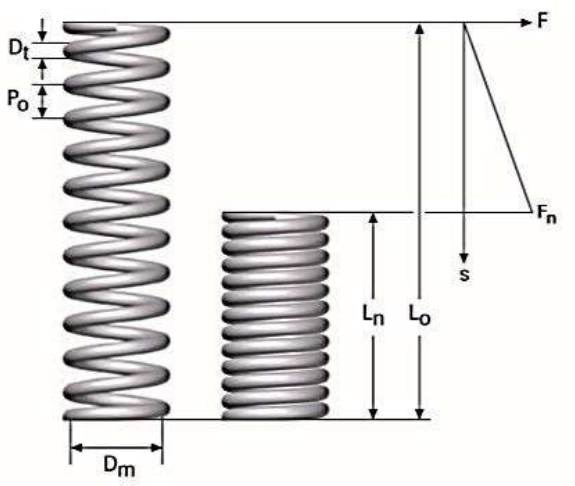

Figure 5.21 - *Lesjöfors* Spring's Dimensions [11] - Appendix IV

According to this information, to meet the design requirements, the spring should be selected according to the condition $F_n \geq F_{req}$. Then the housing for the spring should be properly dimensioned to match $L_n \leq L_f$ due to the spring's minimum permitted loaded length for static load. Lastly L_p should be dimensioned according to an established preload for the spring with the only required condition is $L_0 > L_p$.

For this effect, a spring with *5mm* of mean diameter was selected from the catalogue. The spring selected, highlighted in Appendix IV, corresponds to catalogue number 5960 and is fabricated from a *1.00mm* diameter unalloyed spring steel wire with end coils ground to ¾ revolutions. This spring, also highlighted in Figure 5.22, meets all the requirements described in the paragraph above and was selected especially due to the larger variation between loaded and unloaded length, $L_0 - L_n$ of *12mm*.

Material: EN 10270-1-SH								
d_t	D_m	$D_{i\,min}$	L_0	n_t	L_n	F_n	R	Cat.no
1,00	5,00	3,80	7,4	5,0	5,4	55	27	2914
1,00	5,00	3,80	8,5	5,5	6,0	59	23	5956
1,00	5,00	3,80	11	7,0	7,7	51	16	2915
1,00	5,00	3,80	12	7,5	8,3	55	15	5957
1,00	5,00	3,80	16	10,0	11	49	10	2916
1,00	5,00	3,80	17	10,5	12	51	9,6	5958
1,00	5,00	3,80	23	14,0	16	47	6,8	2917
1,00	5,00	3,80	24	14,5	16	51	6,5	5959
1,00	5,00	3,80	33	20,0	22	47	4,5	2918
1,00	5,00	3,80	35	20,5	23	50	4,4	5960

Figure 5.22 - Lesjöfors Spring's Specifications [11] - Appendix IV

With these settings, length L_f is calculated based on the spring's constant, k, which is referred to as rate *R (N/mm)* in the catalogue. Using Hooke's law (3) for linear behaviour springs, force $\vec{F}$ can be replaced by loaded force, $\overrightarrow{F_f}$ which corresponds to length $\overrightarrow{L_f}$. Similarly, any given design length, generically L_x, is related to x as it translates to spring length variation as displayed in expression (4). Therefore, expression (5) is result of the adapted Hooke's law which determines any given length L_x provided the required force, $\overrightarrow{F_x}$, and spring constant, R.

$$F = k.x \tag{3}$$

$$x = L_0 - L_x \tag{4}$$

$$F_x = R.(L_0 - L_x) \tag{5}$$

The required force for blade attachment, $\overrightarrow{F_f}$, was previously established as *30N*. With spring constant, R, as *4.4 N/mm* and L_0 as *35mm* both provided by the catalogue, length L_f is easily determined by (5) as approximately 28*mm* (approximation by defect in order to guarantee $F_f \geq 30N$).

With this in mind, L_p can be established as 2 mm greater than L_f in order to reduce the displacement necessary to mount the blade on the tool, which according to (5) with $L_p = 30mm$ corresponds to a preload of $22N$.

Lastly, the spring housing holes as illustrated in Figure 5.20 above should be dimensioned according to the spring's outer diameter and design lengths, which should also consider enough clearance for diameter expansion as a result of the spring's compression. Figure 5.23 displays these dimensions with the length of the housing hole on the tool and on the bar, $L_t$and L_b respectively.

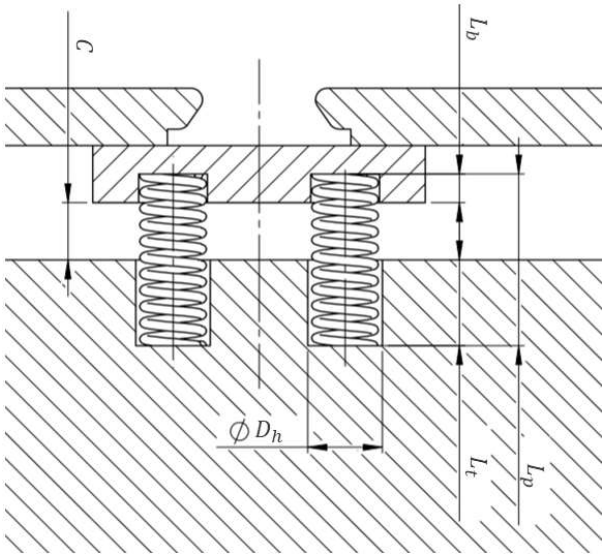

Figure 5.23 - Tool Dimensioning for Spring Housing

$$L_p = L_t + L_b + C \tag{6}$$

$$D_h = D_m + d_t + \Delta D \tag{7}$$

Clearance C should be great enough to accommodate the required displacement for mounting the blade (RTV included) and should be dimensioned according to condition (6). The housing holes diameter, D_h, is dimensioned based on the spring's mean diameter and wire diameter available in the catalogue as displayed in expression (7). This diameter also includes a clearance, ΔD, that should account for the spring's radial expansion when compressed. The spring's outer diameter after expansion is given by:

$$D_{exp} = \left[\sqrt{{D_m}^2 + \frac{p^2 - {d_t}^2}{\pi^2}} + d_t\right] \tag{8}$$

With p referring to the spring's pitch which can be determined by dividing the spring's unloaded length by its number of coils as in:

$$p = \frac{L_0}{n_t} \tag{9}$$

According to this, the spring's diameter after compression is approximately $6.02mm$ which is somewhat negligible for the housing hole dimensioning. However, clearance ΔD will be established as $0.5mm$ for good measure, which for the selected spring corresponds to a housing hole diameter D_h of $6.5mm$.

With these specifications, this concludes all the dimensions required for the blade's fastening mechanism design. With this, the fixture tool's mentioned features should be adequately dimensioned according to dimensions of the blades of the respective stage to fulfil the dimensional requirements established in this chapter. Additionally, each of the tools must be modelled in *SolidWorks* according to these parameters.

5.3.2 Blade's display configuration

The main parameter to consider when outlining the blade's display on the fixture tool is the spacing between blades. This must take into account the CMM probe's dimensions according to the type of dimensional inspection that we are looking to perform.

Regarding the blade's dimensional inspection, it was stated that the tool should consider all the CMM's available functionalities. This means that blade spacing should allow the probe's access to the airfoil dimensions at different blade heights and also for the CMM scanning feature where the probe sweeps the blade surface. This implies that the considered probe's operating position should be the one that requires the most spacing between blades.

In order to obtain the probe's dimensions, stylus 1 (as named in Table X) was considered which was the one used in the force *P* estimating experiment described in the subchapter above. The system considered for this probe was *RENISHAW*'s *REVO-2 RSP2* with *RSH250* connection with a ruby stylus with a ball diameter of 6mm and 10mm length. These system's dimensions are displayed in Figure 5.24 whereas the stylus dimension is displayed in Figure 5.25.

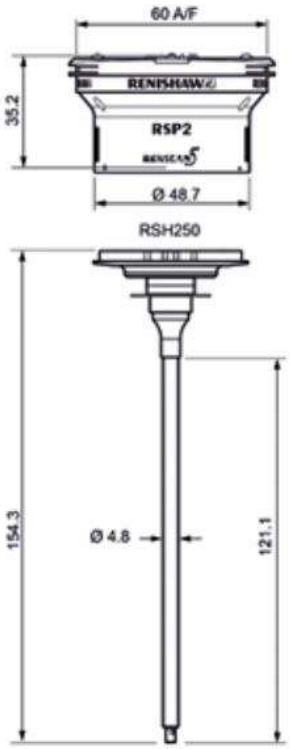

Figure 5.24 - *RENISHAW*'s REVO-2 RSP2-RSH250 System [24]

Ruby ball styli (stainless steel stems)

Ball material		Part number
Ruby		A-5000-4156
Silicon nitride		A-5004-0237
Zirconia		A-5004-2203
A	Ball dia. mm (in.)	6.0 (0.24)
B	Length mm (in.)	10.0 (0.40)
C	Stem dia. mm (in.)	2.5 (0.10)
D	EWL* mm (in.)	10.0 (0.40)
	Mass grammes	0.9
10 mm range		

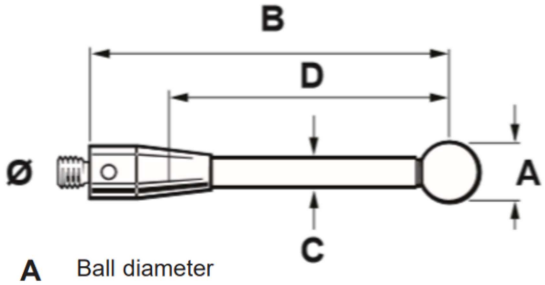

A Ball diameter
B Overall length
C Stem diameter
D Effective working length

Figure 5.25 - *RENISHAW*'s Stylus Specifications (Adapted from [25])

The *RSH250* connection implies that the probe's overall length from the probe's tip to the centre of rotation is 250mm. With this and the rest of the information conveyed in the images above, a 3D CAD mock model of the complete probe was constructed in order to analyse three-dimensionally the possible interferences between the probe and the mounted blades. Figure 5.26 displays a rendered image of this model which does not represent an exact replica of the CMM's probe, but it is still true to its overall dimensions.

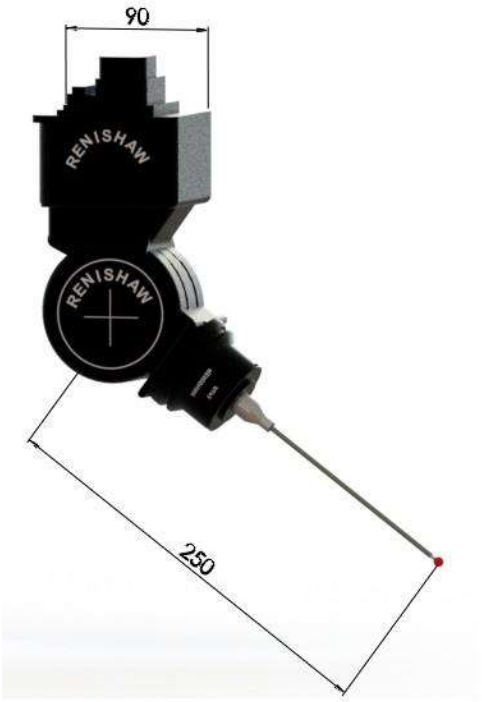

Figure 5.26 - *RENISHAW*'s Probe CAD Mock Model with Overall Dimensions

While the CMM's arm moves along the machines *X, Y* and *Z* axis, the *REVO-2* System enables the probe to rotate in two different directions making this a 5-axis system. *RENISHAW*'s *REVO-2* allows the probe to rotate around the probe's arm *Y* axis as displayed in Figure 5.27, and around its *Z* axis as displayed in Figure 5.28.

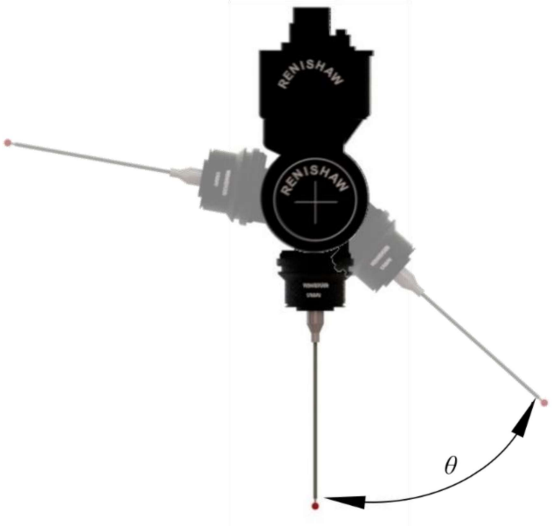

Figure 5.27 - Probe's Rotation around its *Y* Axis

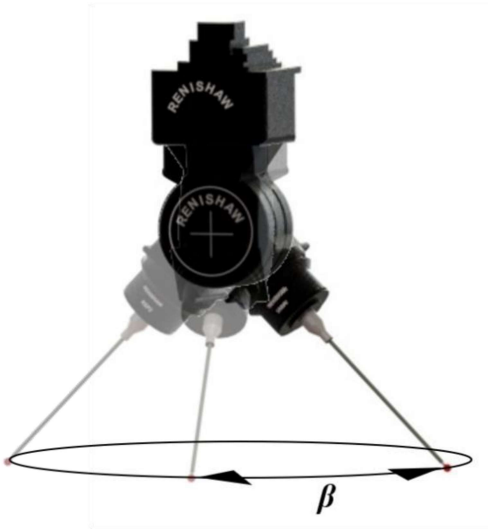

Figure 5.28 - Probe's Rotation around its *Z* Axis

Using this model, it is possible to visualise the different implications of the probe's position on blade spacing. For example, when performing edge thickness measurements on the base of the airfoil section of the blade, the angle θ of the probe's position in conjunction to blade height have a direct influence on the required blade distance. As Figure 5.29 displays for the case of stage 1 blades, the greater the angle θ the greater should be the distance between blades to allow for probe inspection. This image also shows that the position correspondent to $\measuredangle\theta = 0°$ results in an interference with the blade's geometry. Additionally, Figure 5.30 demonstrates the influence of blade height as, when the probe is at the same angle θ, stage 2 blades required about *2/3* of the distance required by stage 1 blades.

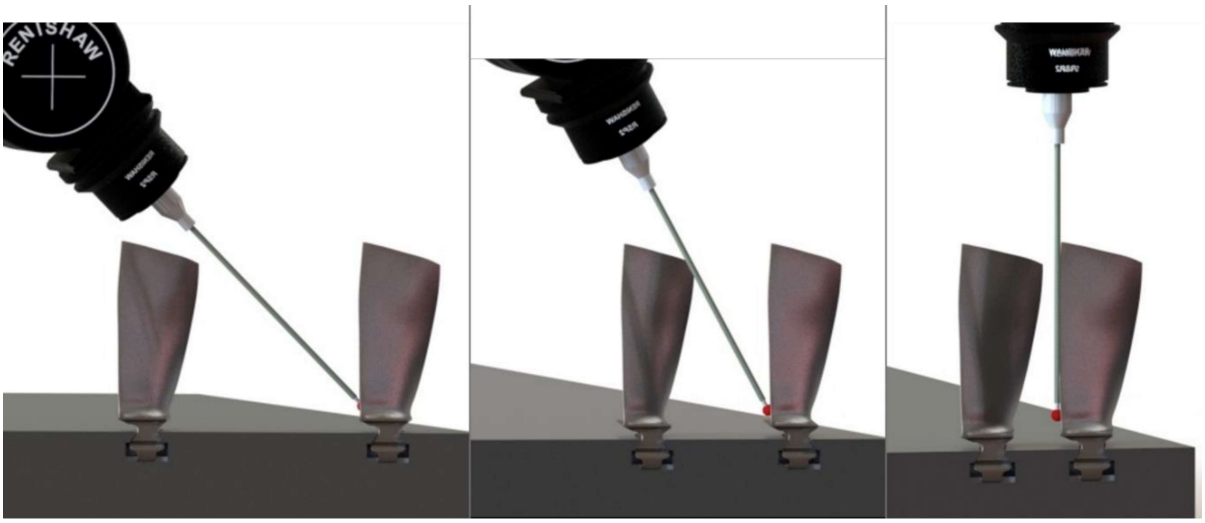

Figure 5.29 - Blade's Distance Influence on the Probe's Accessability

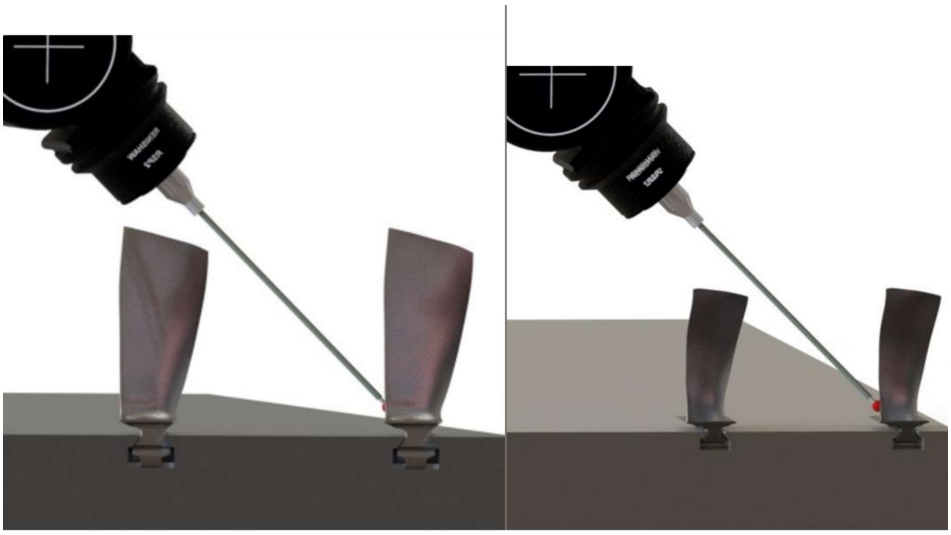

Figure 5.30 - Blade's Height Influence on the Probe's Accessability

With this in mind, it is possible to develop a simple mathematical expression that gives us the required minimal distance between blades knowing the probe and blade dimensions. Looking at this problem two-dimensionally, it is possible to consider a rectangular region that encloses the blade's airfoil and platform sections as highlighted in green in Figure 5.31. Using simple trigonometry, blade distance, d, as illustrated in Figure 5.31, is calculated by (10) where h corresponds to the blade's maximum height and b to the considered block width.

$$d = b + h.\tan\theta \tag{10}$$

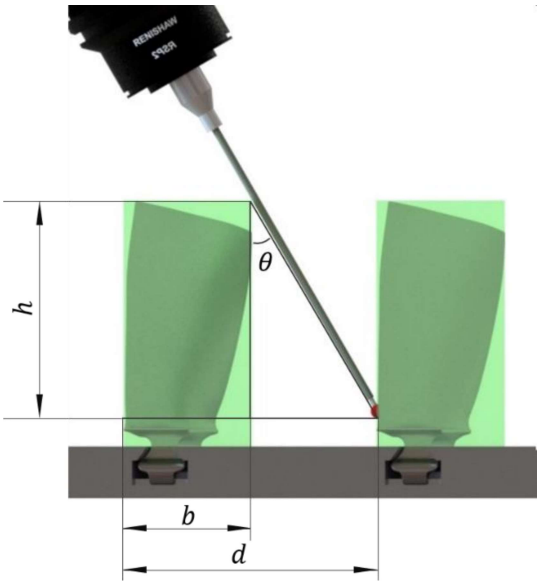

Figure 5.31 - Blade Distance Dimensions with Two-dimensional Approach

However, this two-dimensional approach is rather conservative and space economy in the fixture tool should be prioritized given the large number of blades per set. This way, using the 3D software *SolidWorks* it is possible to identify the closest distance between the blades surfaces as depicted in Figure 5.32. With these reference points the true minimal distance required between blades can be obtained similarly to what was done above, by using the blade's dimensions that are illustrated in Figure 5.33, the required distance d is determined by:

$$d = b + h.\tan\theta\,.\cos\beta \tag{11}$$

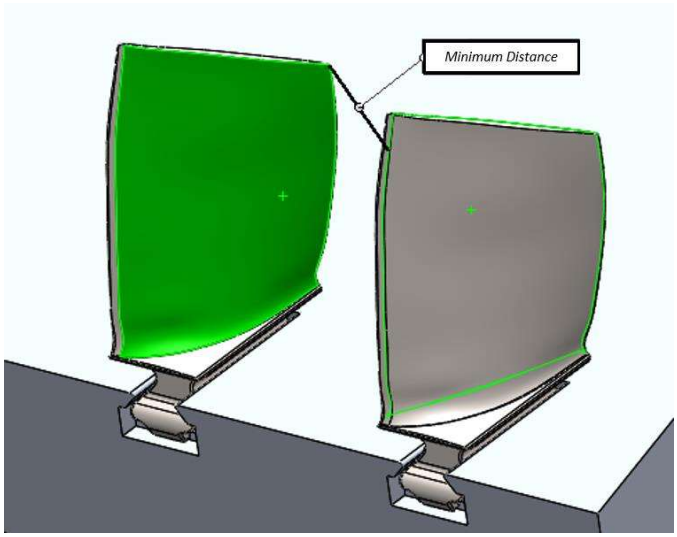

Figure 5.32 – *SolidWorks'* Minumum Distance Feature

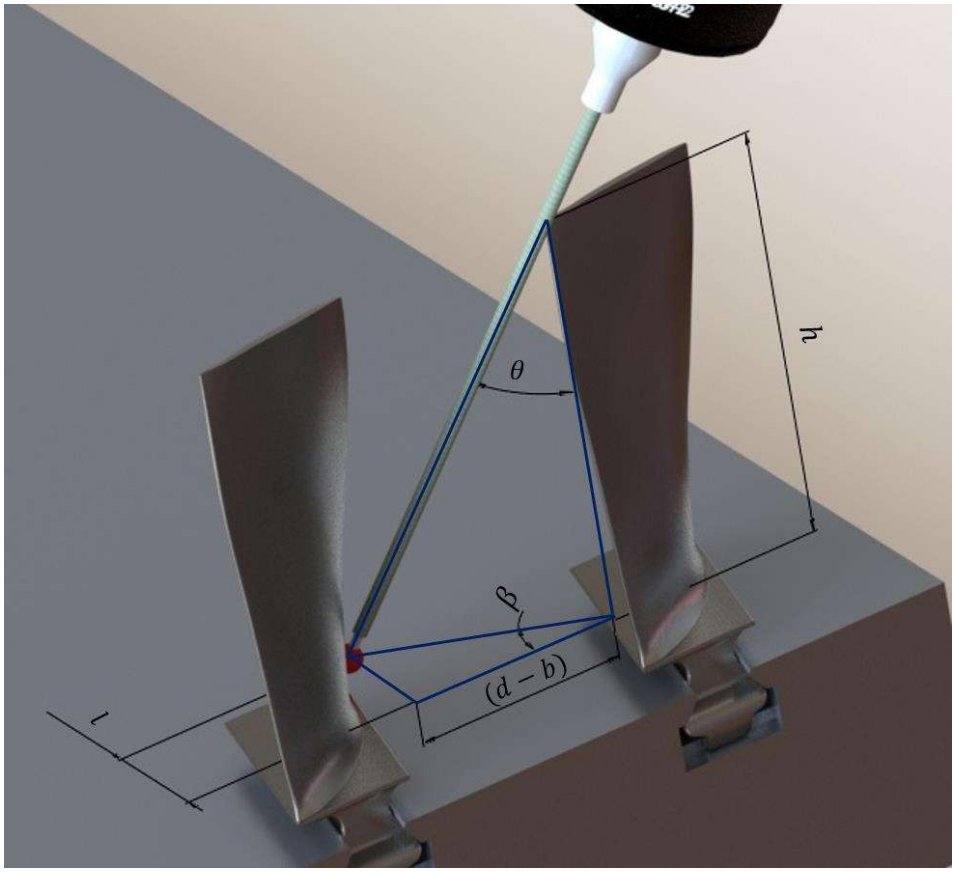

Figure 5.33 - Blade Distance Dimensions with Three-dimensional Approach

However, the angle β displayed still depends on the blade's distance so dimension l provides us this dimensional information based on the blade's platform dimension. Applying Pythagoras Theorem to the bottom triangle it is possible to obtain:

$$\sqrt{l^2 + (d-b)^2} = \mathrm{h}.\tan\theta \tag{12}$$

$$d = b + \sqrt{(h.\tan\theta)^2 - l^2} + C \tag{13}$$

Simplifying (12), blade distance is obtained through (13). Dimension C represents an established clearance of 5mm in order to compensate for calculation approximations, manufacturing deviations or reference model incoherencies.

In short, by knowing probe position for angle θ and with access to the blade's dimensions through the CAD models (developed in chapter 4.2) for dimensions b (block width – Fig.5.33), h (partial blade height) and l (tip-platform airfoil width), it is possible to obtain the minimum required distance between blades for probe inspection.

Angular position for angle θ is assumed as 30° as it should allow for proper airfoil inspection or scanning while the other dimensions will be obtained through measuring features in 3D CAD software *SolidWorks*. The values calculated for the required distance between blades are documented in Table 5-4 where the distance values for both the three-dimensional (13) and two-dimensional (11) estimates are displayed.

Table 5-4 - Blade Distance Calculation and Measured Dimensions

Blade Stage	$\boldsymbol{\theta}$ [°]	*Dim.* $\boldsymbol{h}$ [mm]	*Dim.* $\boldsymbol{l}$ [mm]	*Dim.* $\boldsymbol{b}$ [mm]	*Dim.* $\boldsymbol{d}$ [mm] (11)	*Dim.* $\boldsymbol{d}$ [mm] (13)
1	30	86.15	41.45	51.74	106.48	**85**
2	30	61.41	27.35	35.66	76.12	**64**
3	30	46.69	20.62	29.94	61.90	**53**
4	30	36.93	13.42	25.69	52.02	**48**
5	30	29.89	12.99	20.73	42.99	**38**

Apart from other dimensions which were obtained directly, dimension h was obtained through a measurement of platform to tip blade height with an offset of -6mm in order to account for the probe's ball access. All dimensions were rounded upwards apart from dimension l in favour of an approximation by excess for blade distance. Finally, dimension d which will be used as a blade distancing parameter was obtained according to (13) and rounded to integer.

Note that using (11) corresponding to the 2D iteration, the required distance between blades was between 9% and 21% higher resulting in a lower space economy. After testing the values obtained through (13) using the 3D models, the three-dimensional approach was confirmed as the best functionally acceptable option.

At last, in order to fit complete blade sets to the available area for the tool established in chapter 5.2, slot rows were repeated laterally in conjunction with some extruded cuts for blade assembly. For each stage, 4 rows of slots were enough for the whole set. In the case of the tool that will be used for both stage 4 and stage 5 blades, the distance between blades was defined according to stage 4 while slot number was defined according to stage 5 as the number of blades in the fifth stage is greater while the distance calculated for the fourth stage blades is larger.

Figure 5.34 illustrates the blade display for the first stage fixture tool, which in this case accommodates 40 blades whereas the complete set requires only 38. The distance between blade rows, despite representing different relative positions between blades, is also considered as the distance d established, providing more than the necessary space for the probe's access. With this in mind the slot spacing was dimensioned accordingly to required distance d as Figure 5.35 illustrates for the first compressor stage.

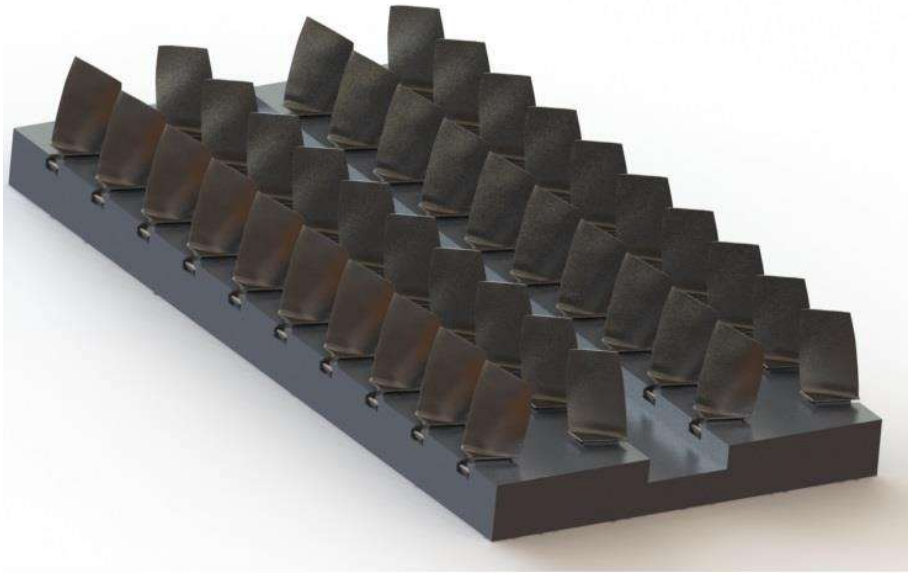

Figure 5.34 – 1st Stage Tool Design Final Blade Display

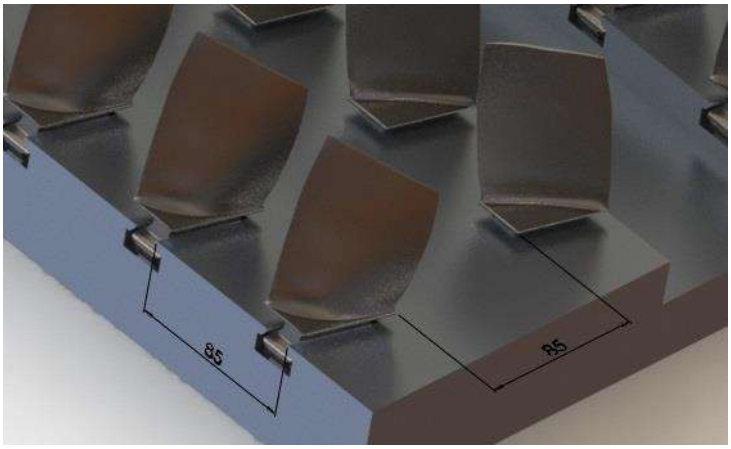

Figure 5.35 - Blade Display Dimensions for 1st Stage Tool

To conclude, the same procedure was applied to the following three tool designs obtaining the same blade display for each stage with adequate dimensioning. With this designed, the tool should be ready for the assembly of full sets of blades.

5.3.3 Fixture Tool's positioning features

As stated in subchapter 5.1, in the interest of using a CNC program to command the CMM through the measurements of the full set of blades mounted on the tool, the machine's software needs to be aware of the position of the blades and consequently of the fixture tool itself.

Commonly, when using the CMM to inspect a part, the first commands have the purpose of locating the geometry that will be inspected. For example, when inspecting a datum for roundness tolerance, three points are measured firstly to locate the circumference centre and then the CNC program may sweep or measure a desired number of points automatically.

Following the same methodology, the fixture should include a fixture that will allow the software to locate the tool with the required precision. Only then may the CNC program run the commands that will provide the desired blade dimensions. This program may be based on CAD models or on a "learn and repeat" mode, still a positioning reference is required either way.

The base concept for the alignment of a workpiece on the CMM is to define a coordinate system on the workpiece so that the machine is able to locate it in reference to its own coordinate system. For this, Chapter 9 of the *Mitutoyo's User's Manual* for *GEOPAK* [17] provides us the complete insight on the necessary requirements for the alignment of a workpiece to generate a part program.

The user's manual states that the reference coordinate system can be created by different means but the most common is to identify a pattern of different geometries of which there are eight different possibilities. These possibilities are displayed in Figure 5.36.

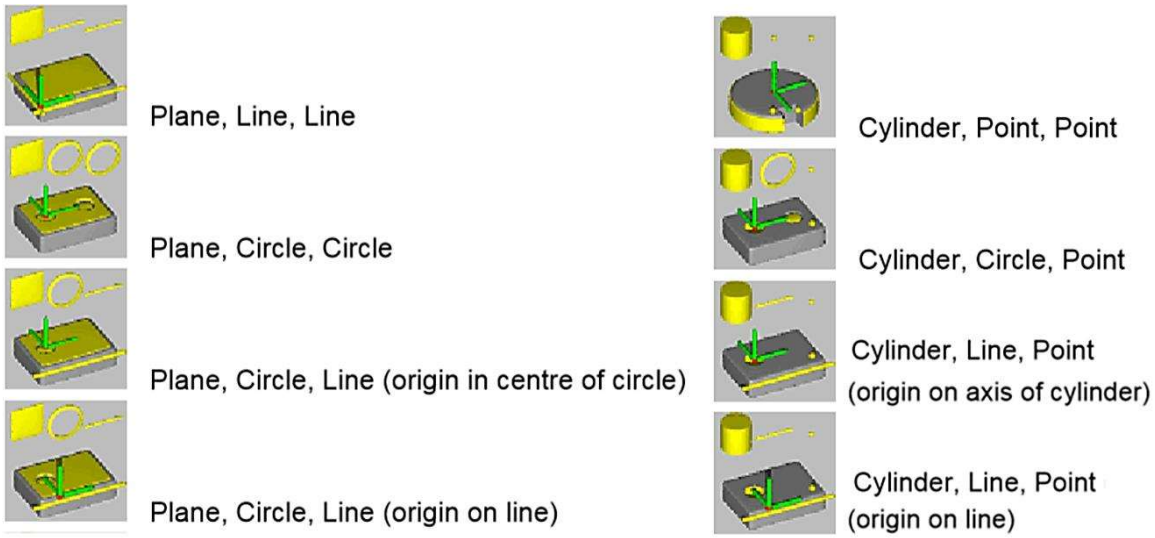

Figure 5.36 - CMM's Part Alignment Options [17]

Analysing Figure 5.36, all these patterns would be possible to implement by including the required geometries in the tool's design. However, this could introduce new concerns regarding the tool's GD&T (Geometric Dimensioning and Tolerancing) which means that the best option is to work with the tool's available geometries. For this, the tool's features that will serve as reference to the position of the blades should also be used as the features of reference for the geometries of the pattern.

At the current stage of the design, the blade slot display has already been defined and the overall geometry of the workpiece was set as a parallelogram. For this geometry, the first option of "Plane-Line-Line" seems to be the most adequate.

In the case of the tools designed, slots are displayed in rows following the right and frontal surfaces of its overall geometry. This makes the first option a wise choice as these surfaces may also serve as geometric references or, as they are going to be referred to in the GD&T chapter, datums. Figures 5.37 illustrates the application of this pattern option highlighting the geometries used for virtual alignment while Figure 5.38 demonstrates the coordinates referential created.

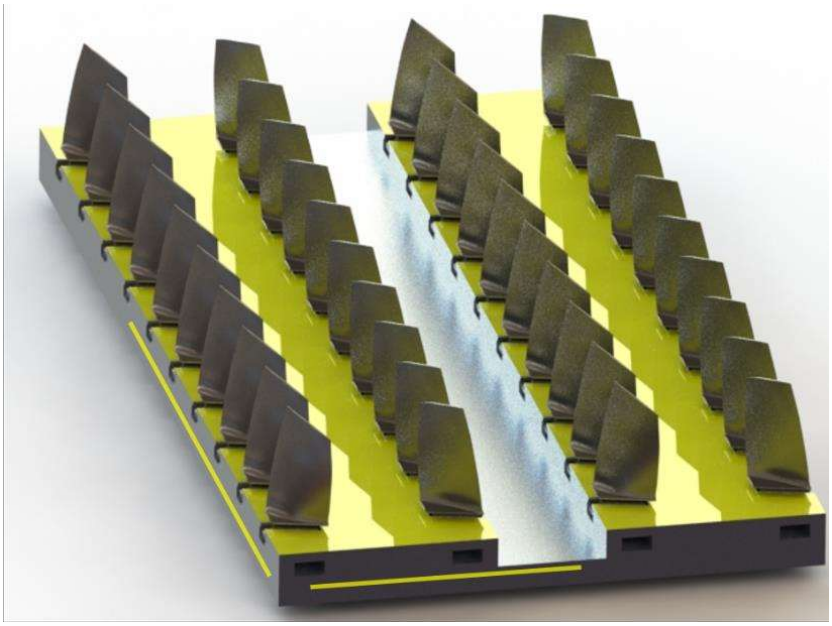

Figure 5.37 - Tool's Plane-Line-Line Corresponding Features

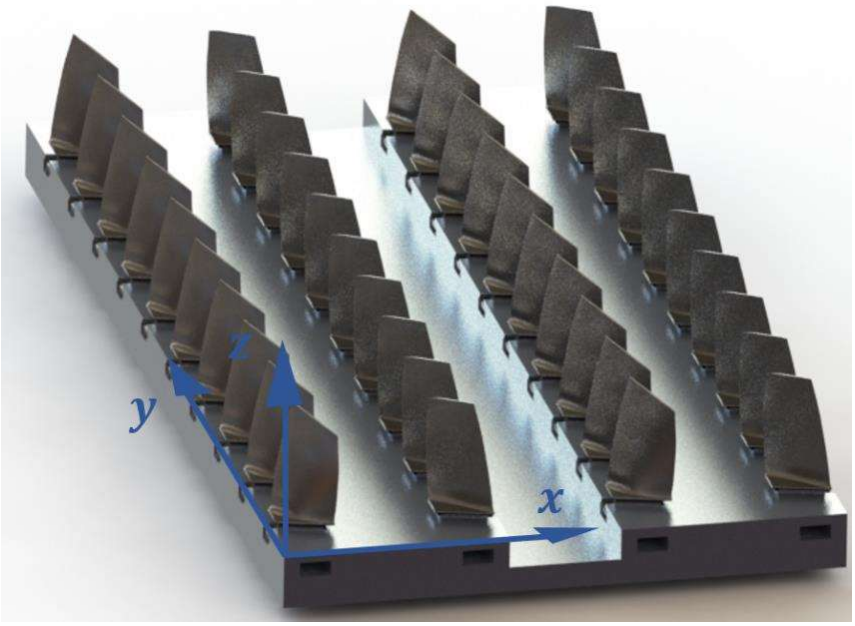

Figure 5.38 - Tool's Defined Co-ordinate System

This also means that, from a “design for manufacturing” perspective, if we consider that the slots will be machined with the block attached to these surfaces, the deviations between the slots and these references will be minimal. Therefore, the right and left or front and back surfaces of the tool must be distinguished to relay the orientation of the tool on manufacturing and on the CMM placement.

For this, a chamfer will be added to mark the front left edge of the tool which will correspond to the origin of the *X* and *Y* axis of the tool’s coordinate referential thus indicating the front and left surfaces where the “lines” of the alignment pattern will be defined as displayed in Figure 5.37.

However, unlike these surfaces, the top face of the tool should not be a reference surface for the slot’s machining process. This means that any geometric deviations caused in manufacture which may be reflected in the slot’s dimensions might also present themselves in the top surface as both geometries could correspond to consecutive machining operations. In any case, these reference surfaces should require appropriate GD&T in order to get the best possible alignment of the workpiece.

Mitutoyo’s User’s Manual [17] also stated the possibility of loading a previously saved coordinate system. To use this feature, the coordinate system would be saved after its definition through the procedure described above. After that, the tool would have to be placed in the CMM table in the exact same position and location each time. For this purpose, a grid of threaded holes, about 15.75 inches apart from each other, is available on the CMM.

In these holes, cylindrical head screws can be fastened providing two cylindrical surfaces on which the tool can be leaned against for placement. With this, there is the option to incorporate features in the

bottom of the tool that would allow for exact placement and for this purpose the following geometry displayed in Figure 5.39 was created.

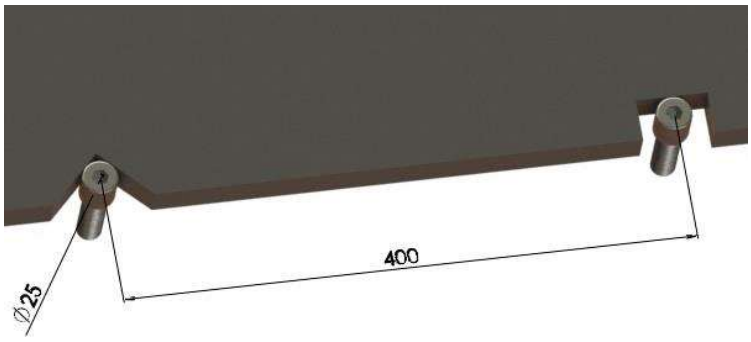

Figure 5.39 - Tool's Bolted Pin Positioning Feature

As this image illustrates, this feature is composed of two geometries, a *V* shape slot and a rectangular slot. The *V* shaped slot presents a 45 degree angle where the cylindrical head of the screw can mate tangentially locking *X* and *Y* axis translatory movement. Then, with the tool's rotation around the screw's axis of revolution, the rectangular slot surface can be mated with the second screw. Naturally, as the tool's *Z* axis movement is disabled gravitationally by the CMM table, this presents a fully defined mating between the tool's and screw head surfaces.

This feature should be included on the tool's left surface which represents the *Y* axis in the workpiece alignment pattern described above and the slots depth is properly placed for the threaded holes position relative to the available workspace described in subchapter 5.1.2.

With this, the fixture tool should be designed to allow for proper alignment of the workpiece concerning the automated dimensional inspection routine used by the CMM. However, it is important to notice that, although the tool was designed to provide the most exact alignment possible, all manufacturing deviations may have implications on the true alignment of the workpiece and this has to be taken into consideration in the development the CMM program.

Furthermore, this chapter also implies that this design should cover a more in-depth analysis of the geometric dimensioning and tolerancing of the tool in order to minimize the impacts of these issues, which will be covered further down in this work.

5.3.4 Fixture Tool's Early Prototyping and Design Adjustments

Using 3D printing technology, PLA (Polylactic Acid) plastic prototypes of the first iteration of the blade attachment mechanism were tested for each of the for tools designed. Figure 5.40 portraits the four models for each stage (the fourth being compatible with both 4th and 5th stage blades) with the respective blades assembled.

Figure 5.40 - Tool's Early Prototypes for Slot Testing

Testing the blade's assembly using these prototypes revealed some interesting aspects on the spring fastening mechanism that would have to be changed in order to allow the blades to be easily mounted on the tool.

When sliding the blades in the slot, they seemed to get stuck rather than pushing the bars down. The blades displayed were also 3D printed using the models developed in subchapter 4.2.2, which do not include the RTV application which is commonly found in usable or new blades in shop. This would aggravate this problem even more as the RTV on the dovetail would make it impossible to slide the blades into the slot without damaging it.

This demanded for enough clearance in the slot which would mean that the bar would have to be pushed down with something other than the blade itself. For this the slot profile was adjusted by the *X* and *Y* dimensions according to Figure 5.41 in order to accommodate a custom designed type of wedge spacer.

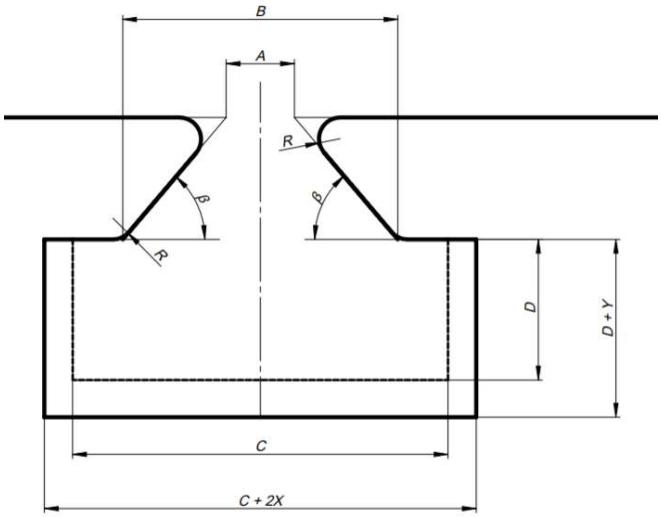

Figure 5.41 - Blade Slot Profile Dimensions Adjusted for Spacer

The spacers displayed in Figure 5.42 were designed to push the bar further down without surpassing the springs maximum displacement thus providing enough clearance for blade including RTV to slide in the slot. After this the spacer is taken out releasing the springs and locking the blade into position. The inverse procedure works also for the blade disassembly. Figure 5.43 provides illustration on the clearance displayed for the blade to slide in due to the spacer (displayed in green) for the case of the 2nd stage tool using the scanned model which includes the RTV silicone thickness.

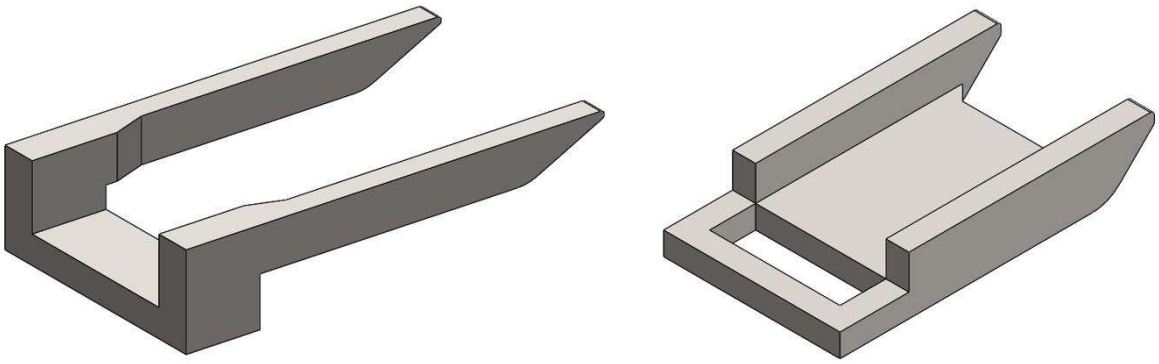

Figure 5.42 - Designed Spacers for 1st Stage Tool (left) and Remaining Stages (right)

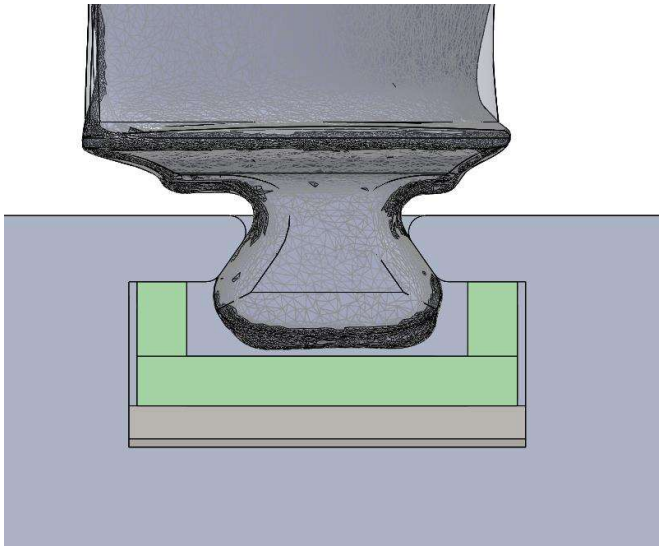

Figure 5.43 - RTV Clearance Provided by the Spacer

After this, new prototypes were printed in order to test the spacers. These seemed to work as intended in the way that the blades slide freely through the slot and are locked in position as the spacer is removed. Figure 5.44 portraits this iteration for the case of the 1st stage tool slot with the spacer in position without the blade (left) and with the blade in position without the spacer (right).

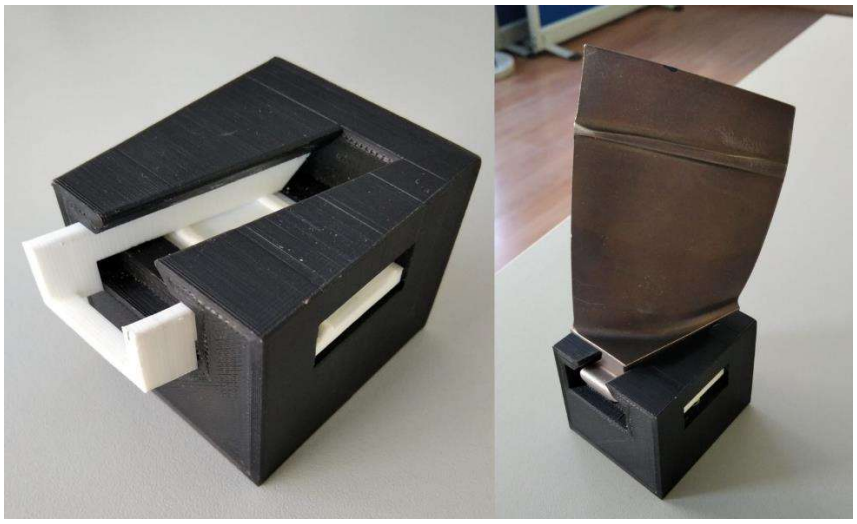

Figure 5.44 - 1st Stage Tool Prototype completed with the Spacer

In this Figure, both the spacer and the bar are displayed in white printed PLA while the tool is displayed in black printed PLA. The spacer causes the bar to go further down allowing for the blade to slide in and after the spacer is removed the bar presses against the bottom of the blade thus locking the blade into position. In this regard, the spacers designed were considered to be essential for the assembly of the blades onto the tool and, for this, were included in the design.

Despite the success of the spacers, this prototype iteration still revealed some issues regarding the spring's behavior in the fastening mechanism. When released, the springs have the tendency to buckle at the top even with them being housed in holes with more than half their height. This causes the bar to move sideways thus diverging some of the spring's force sideways rather that purely upwards as it is intended. Figure 5.45 demonstrates this subtle detail with the model for the 2nd stage tool where the bar can be seen displaced from its position and the spring buckling to the side.

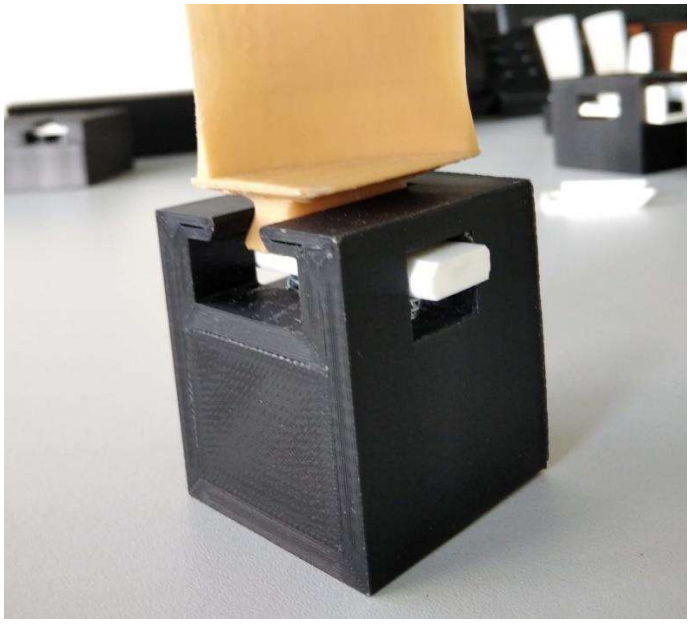

Figure 5.45 - Bar and Spring's Fault Demonstrated through 2nd Stage Tool Prototype

This issue brought up the necessity to guide the bars movement sideways thus guiding the springs displacement solely in the axial direction. This in conjunction with the housing hole designed in the subchapter 5.3.1 should constrain the spring enough to prevent any sort of buckling. Figure 5.46 illustrates the cut section view of the tool before (left) and after (right) the bar sideways constriction was applied.

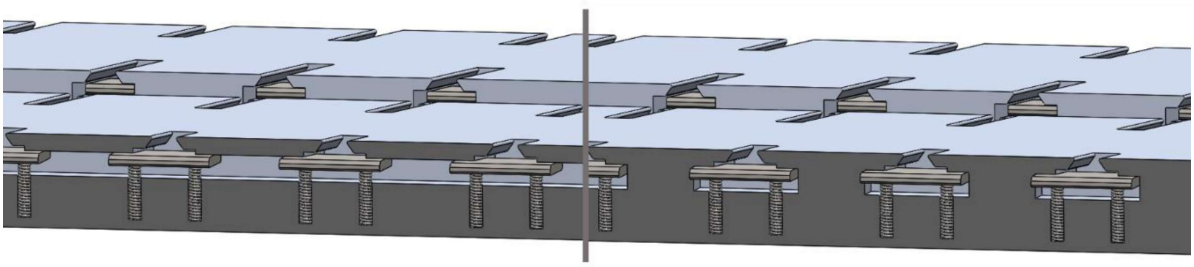

Figure 5.46 - Tool Design Adjustment for Bar Movement Constriction

Lastly, two larger scale prototypes for CMM testing were printed with the intention of validating the distances between blades. For this, models containing four blade slots were printed and assembled corresponding to a smaller section of the tool in true scale. These models were printed for the 1st stage tool and for the 4th and 5th stage tool which represent, respectively, the largest and the smallest of the tools designed. These prototypes, which can be seen in Figure 5.47, received very positive feedback and are currently being used for further testing.

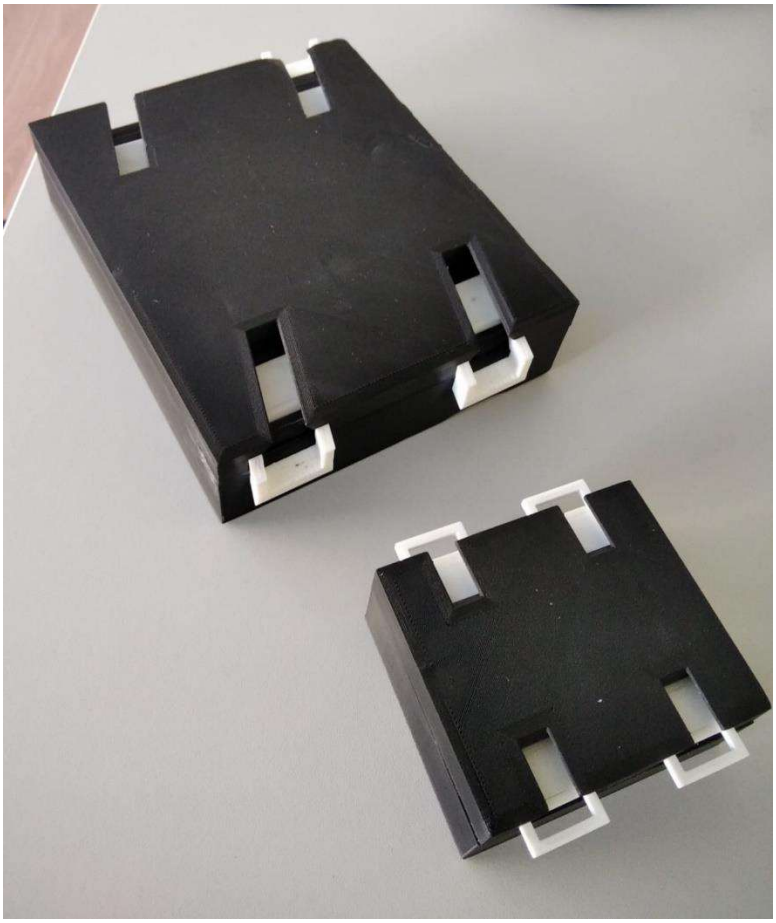

Figure 5.47 - Blade Distance Validation Prototypes

This concludes the fixture tool's design for the purpose of mounting a full set of blades for dimensional inspection. However, design is yet to be completed as the tool still presents features that would be inappropriate for manufacture. For this, in the following subchapters, some design adjustments will be made in order to cover the tool's manufacture and portability.

5.3.5 Design Adjustments for Manufacturing

The fixture tool was designed with CNC machining as the tool's manufacturing technology in mind. This way, every geometry included in design should be possible to produce through a 4-Axis CNC machining centre.

However, the tool's model, as of its current state, could not possibly be manufactured as some of the features are inaccessible for the machining tool. Concerning this, the tool's model was divided horizontally into two section which in turn result in three separate parts, two identical top components and one bottom component. Figure 5.48 illustrates this separation, as it is clear that some of the tool's features are now accessible for conventional machining operations.

The horizontal cut was placed purposely at the very bottom of the blade's slot's geometry, as the yellow plane in Figure 5.49 illustrates, to minimize the amount of different machining operations that would have to be performed for each of the components' manufacture. This cut is also essential for the tool's final assembly as neither the bars nor the springs could be placed in their position without it.

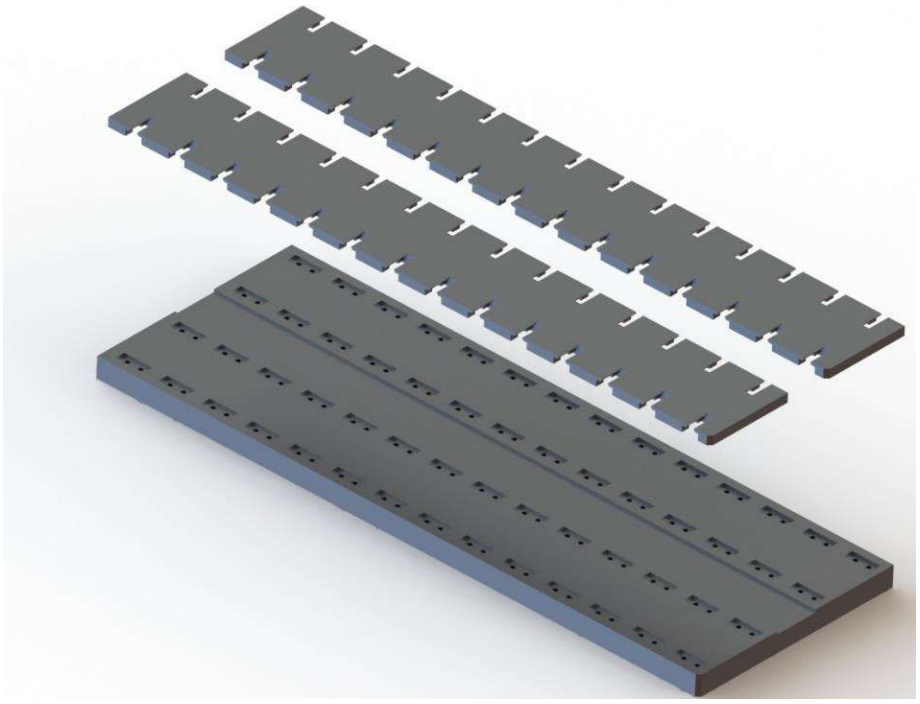

Figure 5.48 - Tool's Division in Top and Bottom Components

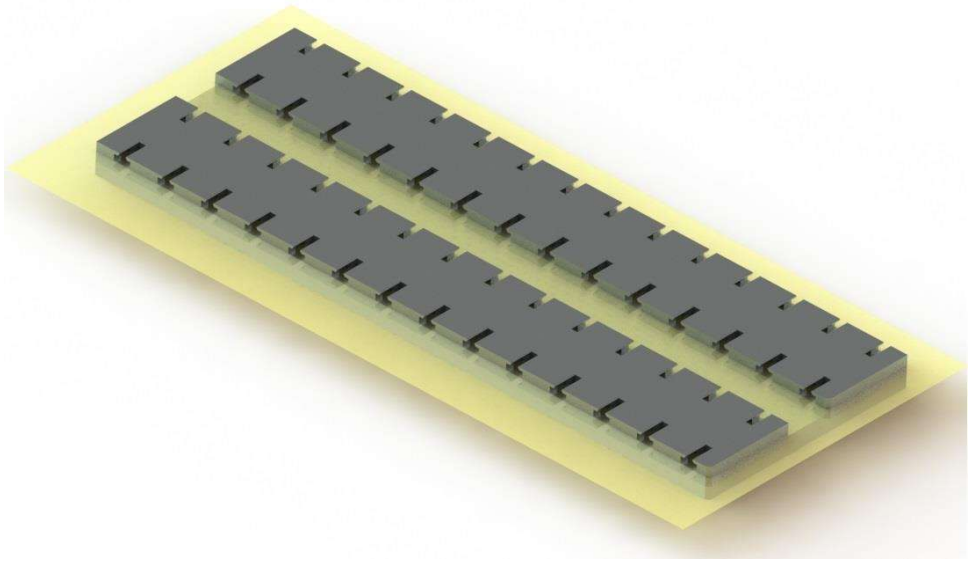

Figure 5.49 - Reference Plane for the Component's Separation

Now, each tool was divided into three components with both top components being completely identical apart from the reference chamfer. However, to simplify the manufacturing specifications and to define the reference surfaces on both components, the top components were considered as the same part thus making the assembly of the tool's main body comprised of only two distinct parts, one bottom component and two of the same top component.

Following this division, a bolted connection had to be included in the design to unite the bottom and top components. As the top pieces are subject to the spring forces, there was the concern for guaranteeing that the connection could withstand the combined force of all the springs when fully loaded. Considering this, the combined force of the fully loaded springs was taken into account in the calculation of the thread stresses for a M6 bolted connection between the top and bottom components.

For the case of the 4th and 5th stage tool which contains the larger amount of springs of the tool's designed, the combined force supported by the bolted connection is given by the maximum load of each spring, $\overrightarrow{F_n}$ (as displayed in the *Lesjöfors* Catalogue [11] times the number of springs mounted per top component, n_S. The total force will then be divided by the number of bolts included, *N,* in order to define the force supported by each bolted joint considering equal distribution. This leads us to force $\overrightarrow{F_j}$ as expression (14) conveys.

$$F_j = \frac{F_n . n_S}{N} \tag{14}$$

Knowing force $\overrightarrow{F_j}$ in terms of the number of bolts N allows us to dimension the bolted connection in terms of the stress on the thread fillets. For this, *Shigley's Mechanical Engineering Design* [4] eighth chapter on "*Screws, Fasteners, and the Design of Nonpermanent Joints*" was consulted for some guidance on the calculation of the stresses on the thread fillets.

The tool's material is defined as Aluminium Alloy 6061 which is going to be covered in detail in the following subchapter. This means that the tool's material is less resistant than the bolt's steel, therefor the bolted connection will be dimensioned according to the fillet stresses in the tool's thread by a criterion of least resistance.

As Figure 5.50 depicts in the cross section of the thread connection the upwards force caused by the springs is translated to $\vec{F_j}$ as an action-reaction pair in the top and bottom components respectively. This in turn can be translated into a shear stress, τ, on the thread fillet corresponding to the outermost facet of the male thread.

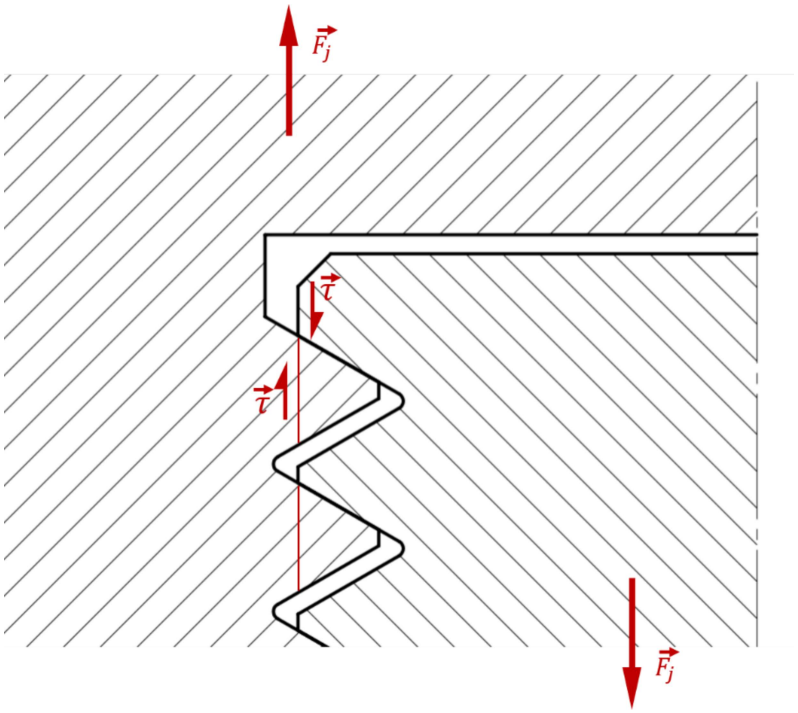

Figure 5.50 - Shear Stress in the Thread Fillets fo the Bolted Connection

This way, the shear stress on the thread fillets can be calculated knowing the thread dimensions by calculating the area of the fillet which is subjected to shear (section outlined by the red line in Figure 5.50. Considering the dimensions portrayed in Figure 5.51, this area can be calculated through expression (15).

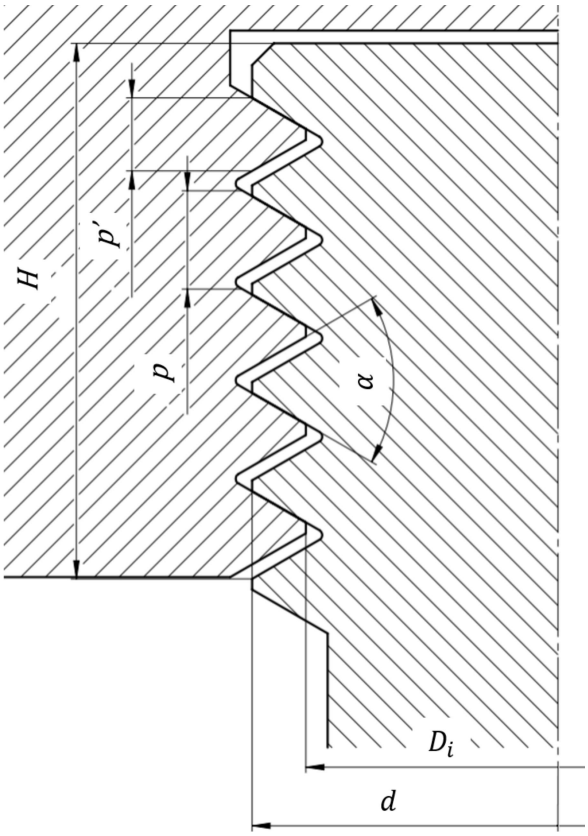

Figure 5.51 - Thread Dimensions

$$A_s = \pi . d . p' . f \tag{15}$$

Factor f is used to determine the number of fillets in the whole threaded length and therefor is given by the quotient between the threaded length and the thread's pitch, $f = H/p$. It is also important to note that ISO metric threads were considered and therefor this corresponds to a triangular thread with $\alpha = 60°$ and $p' \cong \frac{7}{8} . p$.

As stress is defined by force divided by area, the shear stress on the thread's fillets can be calculated by combining expressions (14) and (15) which results in:

$$\tau = \frac{F_j}{A_S} = \frac{F_n . n_S}{\pi . d . p' . f . N} \tag{16}$$

From this point, the bolted connection can be dimensioned using the yield tensile strength by calculating a correspondent tensile stress through *Tresca's Criterion*, $\sigma_{COM} = 2\tau$ which gives us:

$$\sigma_{COM} = 2\tau = \frac{2 . F_n . n_S}{\pi . d . p' . f . N} \tag{17}$$

With this, both threaded lengths, H and the number of bolts, N can be determined by establishing the limit condition for the admissible tensile stress with a factor of safety of 0.7 to the material's yield strength as follows:

$$\sigma_{adm} = 0.7\ \sigma_{yield} \tag{18}$$

$$\sigma_{adm} > \sigma_{COM} \tag{19}$$

Finally, by combining expression (17) and (18) with condition (19) it is possible to obtain the dimensioning condition for the bolted connection based on the thread dimensions, the spring's force and the tool's material. This allows us to determine, the minimum required amount of bolts, N in the connection as:

$$N > \frac{2\,.\,F_n\,.\,n_S}{\pi\,.d\,.p'.f.\ 0.7\sigma_{yield}} \tag{20}$$

Concerning the bolted connection design, the bolts will be fastened only to the top component passing through clearance holes in the bottom component with the bolts head concealed in a housing hole on its bottom surface as Figure 5.52 illustrates. This way, the bolts where defined as M6 with ISO threads corresponding to the dimensions displayed in Table 5-5 and a threaded length of at least 5mm.

Table 5-5 - Metric Thread Dimensions – M6 (*Desenho Técnico* Tabela 15.10 [34])

Nominal Diameter $[mm]$	Pitch $[mm]$	Fillet Diameter $[mm]$	Internal Diameter $[mm]$	Diameter for Tensile Stress area calculation $[mm]$	Tensile Stress Area $[mm^2]$
6	1	5.350	4.917	4.773	20.1

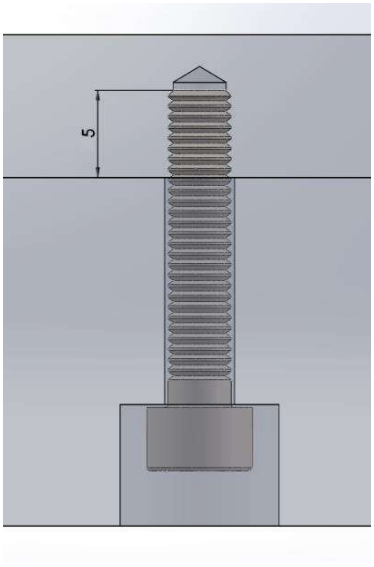

Figure 5.52 - Bolted Connection Design Illustration

Using this information, the minimum required number of bolts, N, to assembly one of the top components to the bottom component of the tool is calculated. The result shows that only three bolts are required in order to prevent shear failure on the top component's thread fillets.

In another case, the fillets on the tool's threaded holes might also be subject to pressure as Figure 5.53 illustrates. Therefore, similarly to what was done above, the minimum number of bolts will be calculated according to this scenario.

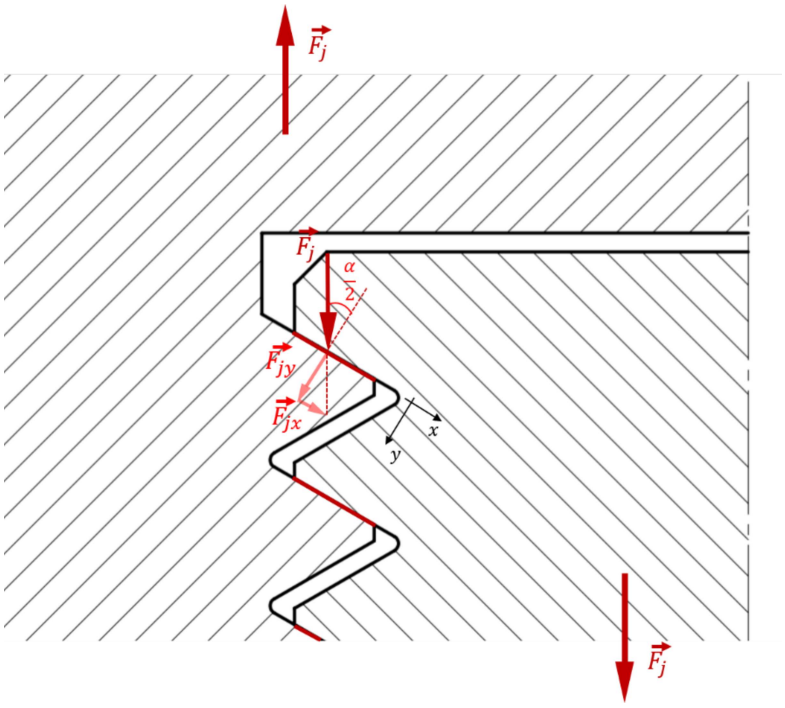

Figure 5.53 - Pressure on the Thread Fillet Surfaces for the Bolted Connection

Here, the area for the stress calculation refers to the contact surface between the male and female threads as the dark red lines illustrate in Figure 5.53. The area accountable for the stress calculation corresponds to the projection of the surface in the horizontal plane which results in:

$$A_p = (d^2 - Di^2).\frac{\pi}{4}.f \tag{21}$$

In turn, the pressure on the fillets of the top component's thread can be calculated similarly to (16) where only the force normal to the surface is considered, F_{jy} obtaining.

$$p = \frac{F_{jy}}{A_p} = \frac{F_n \,.\, n_S \,.\cos(\alpha/2)}{N \,.\, (d^2 - Di^2) \,.\, \frac{\pi}{4} \,.\, f} \tag{22}$$

Lastly, if the pressure is considered correspondent to a compression tensile stress in the thread fillets, the tensile stress is assumed as $\sigma_{COM} = p$ and conditions (18) and (19) may also be applied. This way the minimum number of bolts for this case can be calculated through:

$$N > \frac{F_n \,.\, n_S \,.\cos(\alpha/2)}{(d^2 - Di^2) \,.\, \frac{\pi}{4} \,.\, f \,.\, 0.7\sigma_{yield}} \tag{23}$$

Considering this, the pressure on the thread fillets requires a minimum of only two bolts per top component which is under the minimum required by shear stress. This seems less than expected and doesn´t justify that the tool should be assembled by only this amount bolt as this would potentially lead to the deformation of the top component due to the force of the springs furthest from said bolts.

For this, between 12 and 14 bolts will be placed connecting both parts equally distributed along the blade slots for each of tools. Figure 5.54 demonstrates the hole configuration highlighted in red on the top component for the case of the 2nd stage tool.

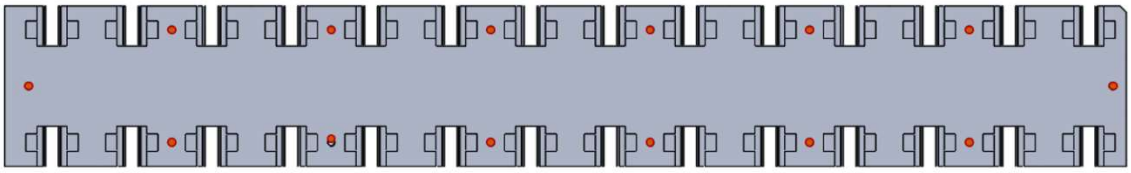

Figure 5.54 - Threaded Holes Display on the Top Component

However, the bolted connection by itself in not adequate for a precise assembly of two components as the clearances between the bolt and the holes on both the top and bottom components do not guarantee the proper alignment of both pieces. For this, dowel pins will be included to align both components as these provide a tighter fit on assembly.

The dowel pin's information was acquired from the *Technifast* Precision Engineered Components Catalogue [32] where one ISO 2338 (1998) dowel pin was chosen with a 10mm diameter and a 24 mm length for the alignment of the tool's components. Consequently, three pins will be used, placed in a line equally spaced to the centre of the top component as Figure 5.55 displays highlighted in red. To facilitate the assembly, 1 mm chamfers with 45º of inclination were added to the entrance of the holes to guide the pins.

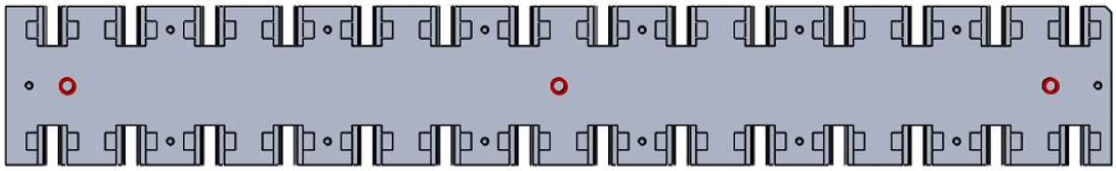

Figure 5.55 - Dowel Pin Holes Display on the Top Component

Appendix V provides the relevant information from the *Technifast* Catalogue [32] concerning the specifications for the dowel pin's tolerances, fittings and material. Although the pin's hole fitting and tolerances will be covered further ahead, this document states that when the dowel pin is to be fitted in blind holes (as in this case), there should be a flat ground along the full length of the pin to avoid air pressurization inside the hole. For this matter, a flat ground with 0.3mm depth will be included in design and will be provided along the tool's manufacturing specifications as displayed in the dowel pin's technical drawing – Appendix XXVIII.

At last, with both components fastened and aligned accordingly, the tool's adjustments for manufacturing are concluded. These adjustments will require special attention regarding dimensional and geometric tolerances, however, this topic will be covered ahead in the respective subchapter 5.3 along with other required tolerances for each manufactured component.

5.3.6 Fixture Tool's handling Features

With the tool's design features almost fully defined at this point, the tool's weight for each stage can be estimated through the 3D models developed so far. For this, *SolidWorks* calculates the total weight based on the components volume and its material's density. Once we have estimated the component's material and register each tool's total weight, we will be able to develop the most adequate features for the tool's handling in shop.

However, before that, the choice of the material for the tool's manufacturing has to consider both the manufacturing process and the tool's application which means that the material should be durable and adequate for machining. Between the most common materials that fit into these categories, there are two obvious choices that should be considered, aluminium and stainless steel.

Both aluminium and stainless steel are reasonable choices in terms of machinability and corrosion resistance. However, while stainless steel stands out for its strength and resistance, its density would increase the final tool's weight significantly. As the tool's stress resistance does not appear to be a determinant factor in design , aluminium seems the most appropriate choice for this situation despite its

ductility as the blade's assembly on the tool or the dimensional inspection of the blades do not imply considerable loads.

Considering this, 6061 aluminium alloy was defined as the tool's main body material as this is a very versatile and commonly used alloy due to its balance between machinability and cost. Even with cost not being a determinant factor for the material's choice, these alloys correspond to this design's necessities and still represent a lower cost option for the first design iteration of this project.

For design purposes, Table 5-6 displays some of the mechanical properties for different tempers of the 6061 aluminium alloy, where the first, *6061-O*, was already used for the bolted connection dimensioning in the subchapter above, as it represents the most conservative choice.

Table 5-6 – Aluminium 6061's Properties (Consulted from [13])

	Density [g/cm^3]	Tensile Strength, Yield [MPa]	Tensile Strength, Ultimate [MPa]	Shear Strength [MPa]	Modulus of Elasticity [GPa]	Shear Modulus [GPa]	Machinability (0-100% Scale of Aluminum Alloys)
Aluminum 6061 – O	2.70	55.2	124	82.7	68.9	26.0	30%
Aluminum 6061 – T4	2.70	145	241	165	68.9	26.0	50%
Aluminum 6061 – T6	2.70	276	310	207	68.9	26.0	50%

Other materials include the unalloyed spring steel EN10270-1-SH for the springs and AISI304 stainless steel or EN58E for the bars which is commonly used for machining. Taking this into account, each tool's total weight estimative is registered in Table 5-7 along with the tool's overall dimensions.

Table 5-7 - Tool's weight and dimensions by HPC stage

Blade Stage	Weight [Kg]	Width [mm]	Height [mm]	Depth [mm]
1	45.61	455.00	45.50	900.00
2	29.43	320.00	42.50	900.00
3	22.78	256.00	41.50	900.00
4 & 5	16.88	200.00	41.00	900.00

As Table 5-7 demonstrates, none of the tool's has significant weight and all estimates are well below the weight constraint of the CMM table, as specified in subchapter 5.2. Despite this, each tool's dimensions in conjunction with its weight would require a hoist to lift and place onto the CMM table which is available in shop.

Considering the hoist as an available mean to move the tool, lifting eye mounts will have to be included in the tool's design to connect to the hoist's hooks. For this, lifting eye bolts will be included in accordance with *DIN 580:2010* as this information was obtained from an extract compiled by the supplier *MecWolf SRL* [14]. From this same source, Appendix VI summarizes some specifications for lifting eye bolts with regards to *DIN 580:2018* in a brochure type of layout.

However, it is important to note that, as stated in this extract [14] and according to the respective normative, all the specifications that will be used in this segment apply only if:

"- the lifting eye bolt shank is fully engaged (assuming adequate thread length);

- the lifting eye bolt is firmly screwed down and the collar sits evenly on the contact surface;

- the material of the equipment is capable of accommodating the stresses induced without any deformation liable to impair safety;

- tapped holes have a threaded length sufficient to ensure that the lifting eye bolt shank is fully engaged and the collar fully seated (see DIN 76-1)."

To that end, two threaded holes will be included in the bottom component of the tool equally spaced to the tool's centre of mass provided by the *SolidWorks Mass Properties* feature. The lifting eye bolts were placed laterally to the centre of mass as Figure 5.56 illustrates for the case of the Stage 1 tool, following the guidelines in the quotation above.

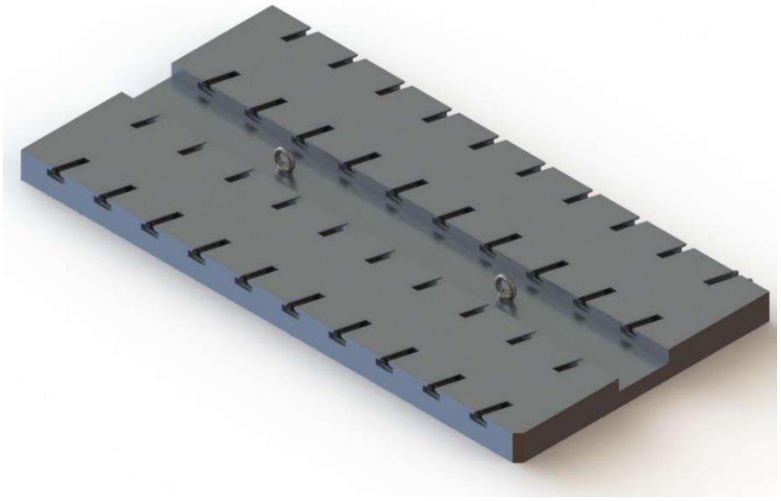

Figure 5.56 - 1st Stage Tool with Lifting Eye Bolts

This configuration allows for some rotation along the *Y* axis, allowing carefully place the tool on the CMM table. This should be done by laying one edge first and the lowering the tool gradually without turning completely sideways due to its inertia. Still, the lifting eye bolts must be mounted exactly as displayed and the tool must not be allowed to tilt too much in order to comply with *DIN 580:2010* as Figure 5.57 illustrates.

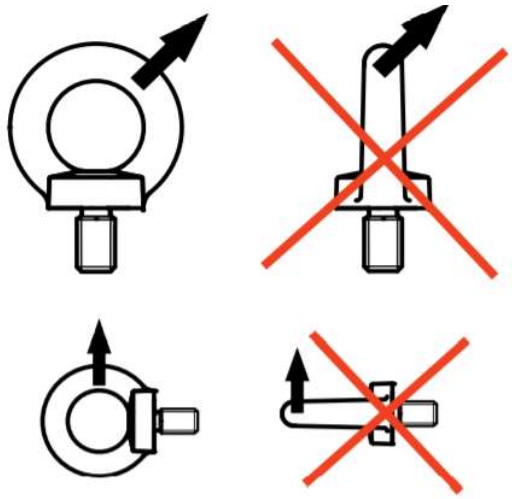

Figure 5.57 - Loads to be avoided according to *DIN 580:2010* [14]

However, similarly to the though process developed to include the bolted connection in the subchapter above, there are some concerns regarding failure in the tool's thread due to its aluminium alloy being weaker than the steel of the lifting eye bolt. Concerning this, the force on the thread fillet was calculated for the thread according to the free body diagram presented in the 1st stage tool section cut in Figure 5.58.

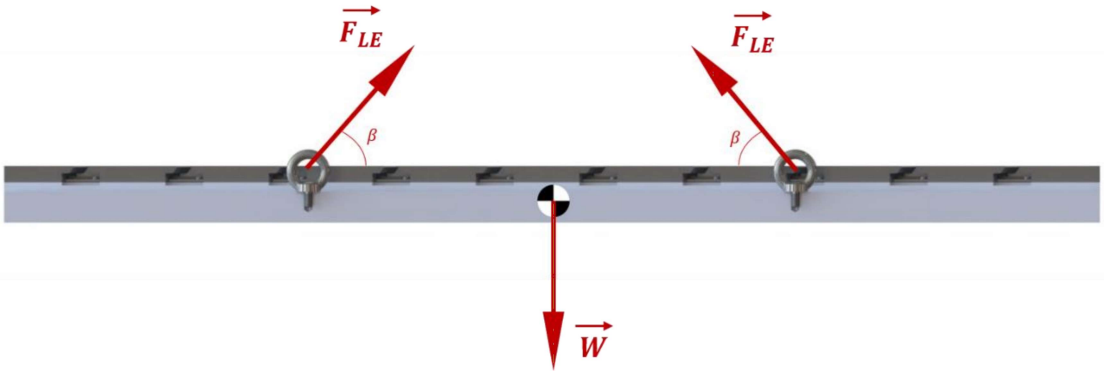

Figure 5.58 - Lifting Eye Bolts' Force Diagram

While the absolute value of force $\overrightarrow{W}$ is determined with the tools mass by Newton's Second Law of Motion, $F = m.g$, the absolute value of forces $\overrightarrow{F_{LE}}$ depends on the value of angle β as they are calculated through the equilibrium on forces which is displayed in Figure 5.58. In that regard, the equilibrium of forces for the vertical axis leads us to equation (24) that determines the force applied by the hoist on the lifting eye bolt as follows:

$$F_{LE} = \frac{m.g}{2.sen(\beta)} \tag{24}$$

In this regard, force F_{LE} was calculated for different values of angle β of 30°, 45° and 90° corresponding to the specified *DIN 580:2018* cases of the load angles 60°, 45° and 0° respectively. The values calculated are listed in Table 5-8 below while Figure 5.59 provides the lifting capacity (in Kg) of the lifting eye bolt according to its thread diameter and load angle.

Table 5-8 - Hoist force on the Lifting Eye bolt by angle β for the 1st Stage tool

Angle $\boldsymbol{\beta}$ [°]	Load angle [°]	$\boldsymbol{F_{LE}}$ $[N]$	$\boldsymbol{F_{LE}}$ $[Kgf]$
30	60	**447.4**	45.6
45	45	**316.4**	33.3
60	30	**258.3**	26.3
90	0	**223.7**	22.8

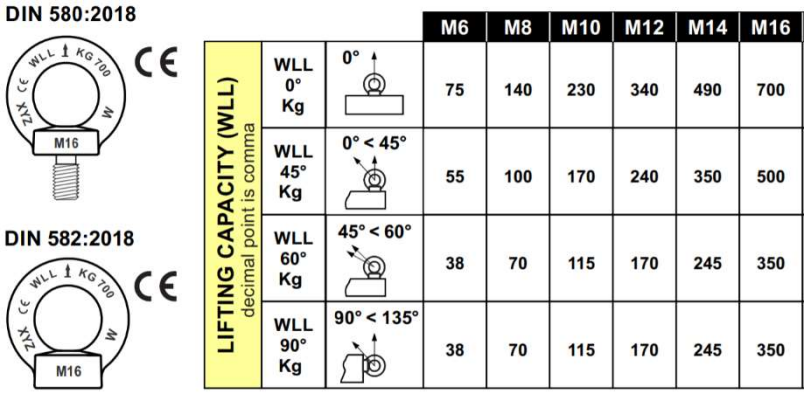

Figure 5.59 - Weight Lifting Capacity per Lifting Eye Bolt - Appendix VI

Combining the information from Table 5-8 and Figure 5.59, the M6 threaded lifting eye bolt is adequate for this design as its lifting capacity is greater that the load applied in the case of the heaviest tool. However, for safety purposes and to prevent failure due to non-predicted loads, the next largest bolt will be used.

Therefore, two M8 *DIN 580:2018 L*ifting Eye bolts will be included in the tool's design. For this, a non-exact model of the bolt was developed according to the dimensions provided in the *MecWolf SRL* extract [14] and two M8 threaded holes were incorporated into the tool's bottom component model with a length of *15mm* in compliance with the guidelines described before.

Finally, with the thread's dimensions it is possible to calculate the stresses on the tool's thread fillets similarly to what was done for the bolted connection in the subchapter above. Figures 5.60 and 5.61 illustrate this for the shear stress and pressure calculations on the thread fillets for this case specifically.

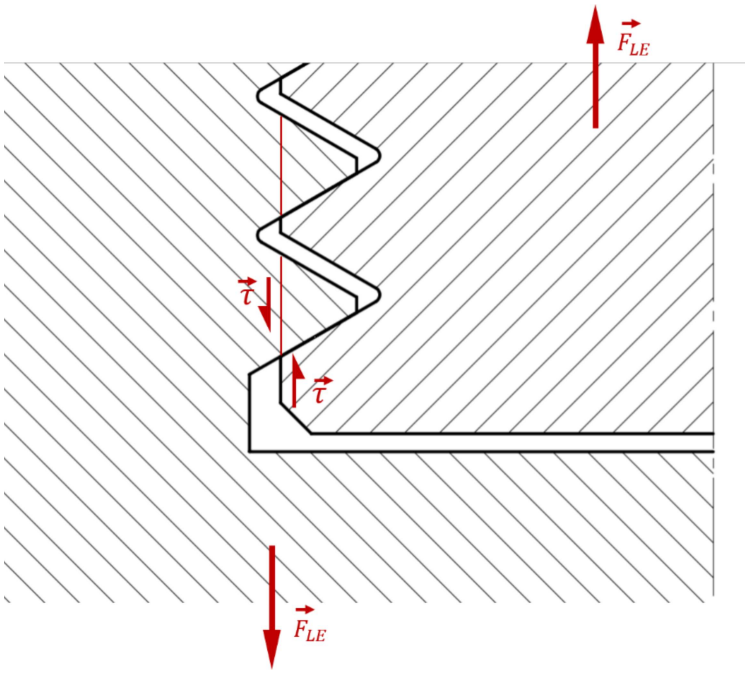

Figure 5.60 - Shear Stress in the Thread Fillets for the Lifting Eye Bolted Connection

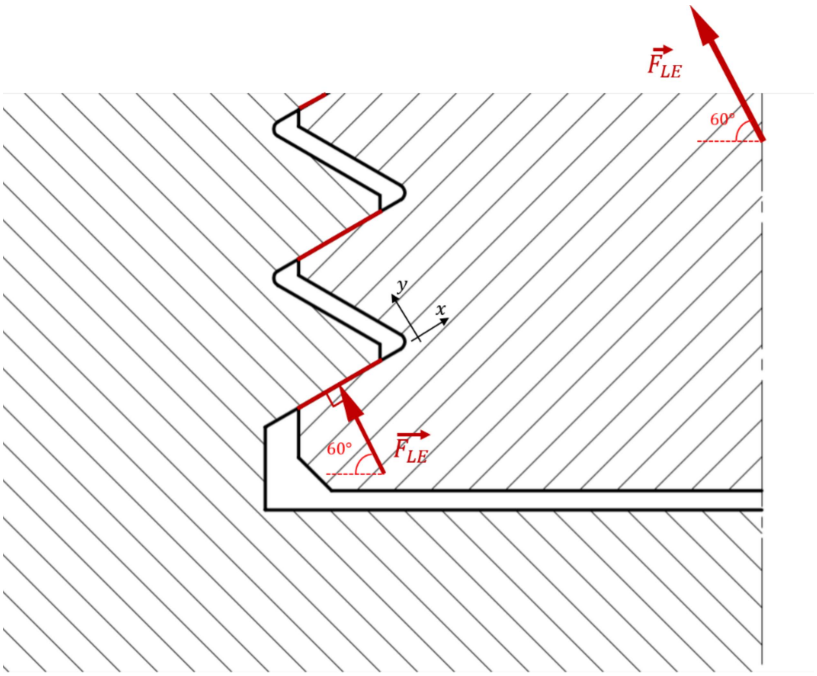

Figure 5.61 - Pressure on the Thread Fillet Surfaces for the Lifting Eye Bolted Connection

For the case of the shear stress, angle β was assumed as $90°$ as it represents the most demanding load case which is when the force applied in the lifting eye bolt is collinear with the stress. For the same reasons, the angle β of $60°$ was used to calculate the pressure on the thread fillets, however the area for pressure calculation considered covers only $1/3$ of the full circumference of the fillet. This consideration was made due to the fact that the load described is only true on the side of the fillet to which the force leans to. Figure 5.61 illustrates this for the side of the thread where the stress calculation is considered.

According to this and along the same line of thought that was used in the bolted connection, the values for the stresses on the fillets can be calculated through expressions (25) and (26) as it follows:

$$\tau = \frac{F_{LE}}{A_S} = \frac{F_{LE(90°)}}{\pi \,.d\,.p'.f} \tag{25}$$

$$p = \frac{F_{LE}}{\frac{Ap}{3}} = \frac{3\,.\,F_{LE(60°)}}{(d^2 - Di^2)\,.\,\frac{\pi}{4}\,.\,f} \tag{26}$$

Equally to what was done before, these stresses were converted to a tensile stress for comparison with the admissible Tensile stress for the aluminium alloy:

$$\sigma_{COM,Shear} = 2\tau \tag{27}$$

$$\sigma_{COM,pressure} = p \tag{28}$$

Table 5-9 - Metric Thread Dimensions– M8 (*Desenho Técnico* Tabela 15.10 [34])

Nominal Diameter $[mm]$	Pitch $[mm]$	Fillet Diameter $[mm]$	Internal Diameter $[mm]$	Diameter for Tensile Stress area calculation $[mm]$	Tensile Stress Area $[mm^2]$
8	1.25	7.188	6.647	6.466	36.6

In addition to the thread's dimensions documented in the table above, the threaded length was established as *10mm.* It is also known that for ISO metric threads, there is a correspondence between the threads pitches of $p' \cong \frac{7}{8}.p$ for the dimensions displayed in Figure 5.51 above.

Using this, the stress values calculated for comparison according to (27) and (28) are, respectively, approx. 2.1 MPa and 6.3 MPa. These values are nowhere near the admissible tensile stress of the aluminium alloy and thus, the lifting eye bolts are validated and included in the tool's design.

With this, the tool's design is considered completed for the first iteration of this project. At this stage, each tool designed is composed of 8 different components summing up to a total 343 individual components for the case of the 4th and 5th stage tool. Figure 5.62 displays the exploded view of the 1st stage tool with the designed spacer included.

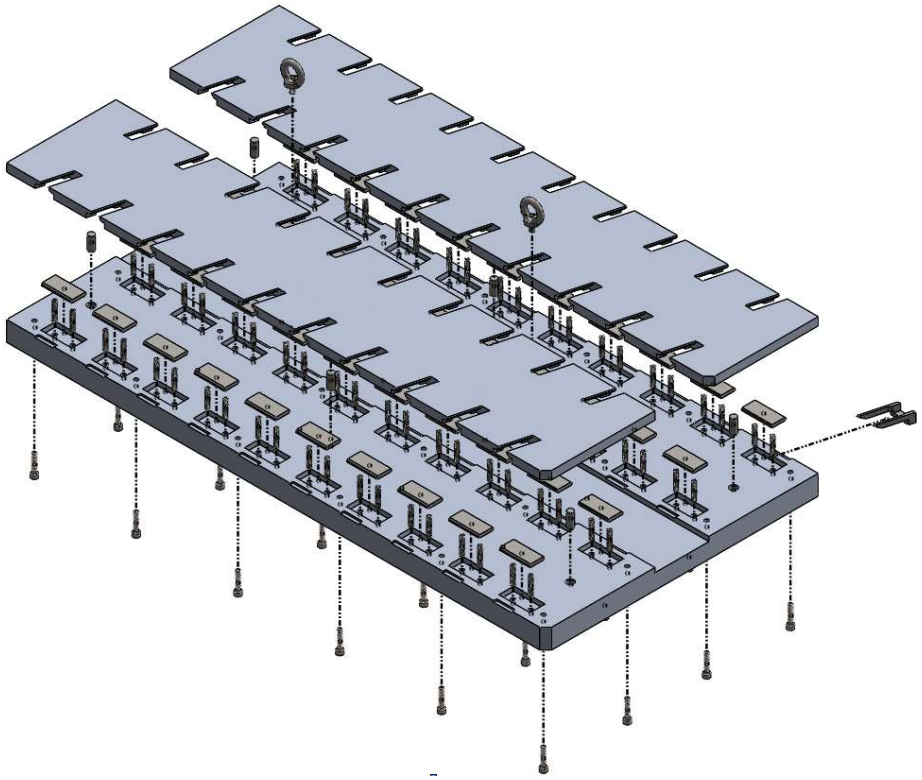

Figure 5.62 - 1st Stage Tool's Assembly Exploded View

The model conveyed above will be further developed in terms of design for manufacturing tolerances and functional dimensioning in the following chapter. Despite this, and in regards to some concerns with the tool's manoeuvrability, this subchapter is also includes the design of the handle bars and caster wheels to facilitate positioning on the CMM table which could be easily to the post manufactured tool with a few threaded holes.

In this sense, two handles will be added to the right surface of the tool while two caster wheels will be added its left surface as Figure 5.63 displays. These handles were designed from scratch and attach to the tool by a bolted connection of four M5 pan headed *Philips* screws, as displayed in Figure 5.64, which will be verified to its stress.

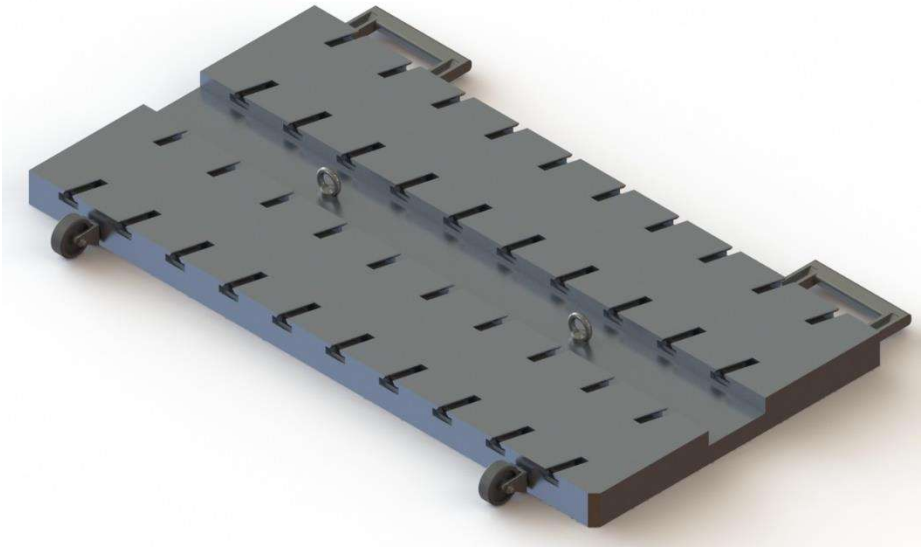

Figure 5.63 - 1st Stage Tool with Handle Bars and Caster Wheels

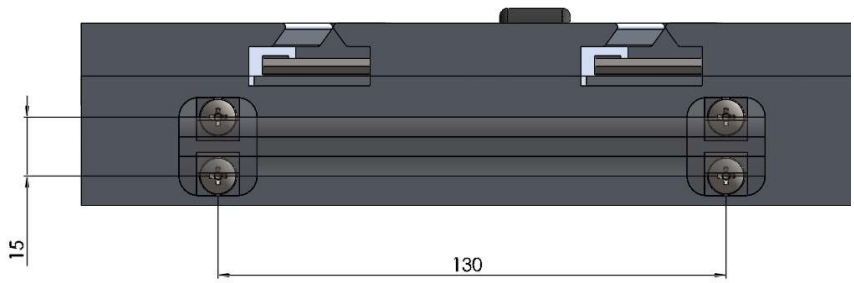

Figure 5.64 - Designed Handle Bars' Dimensions

The bolted connection on the handle will be verified against the necessary force to lift the tool pivoting on the caster wheels. For this the equilibrium of momentum will be used to determine the required force to lift the tool, $\overrightarrow{F_L}$, as Figure 5.65 demonstrates. However, force $\overrightarrow{F_L}$ depends on the angle to the CMM table surface as the component of $\overrightarrow{W}$ which causes momentum decreases as the tool is lifted. For this reason, the force required to lift the tool will be calculated for the exact moment when the tools lose contact with the CMM surface which is illustrated in Figure 5.66.

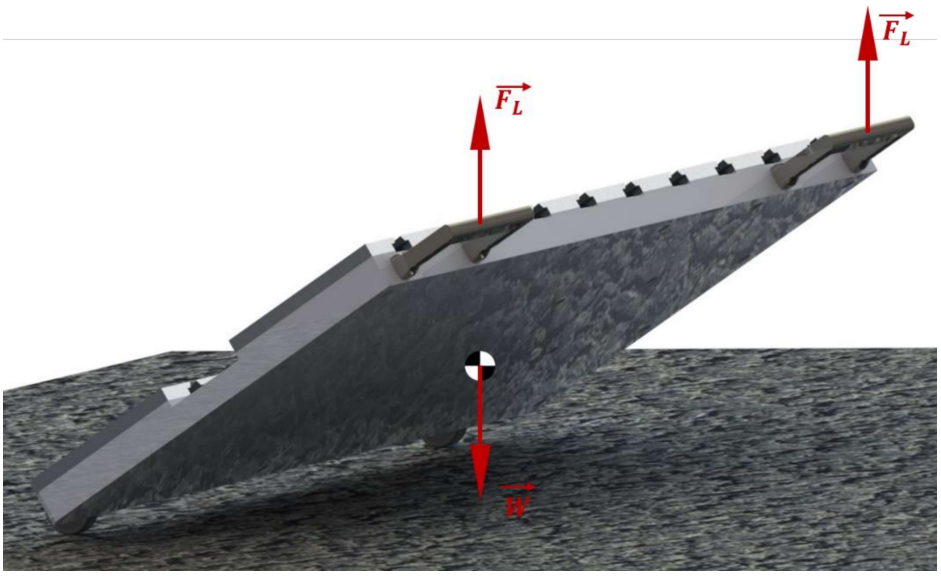

Figure 5.65 - Tool's Lifting Force Diagram

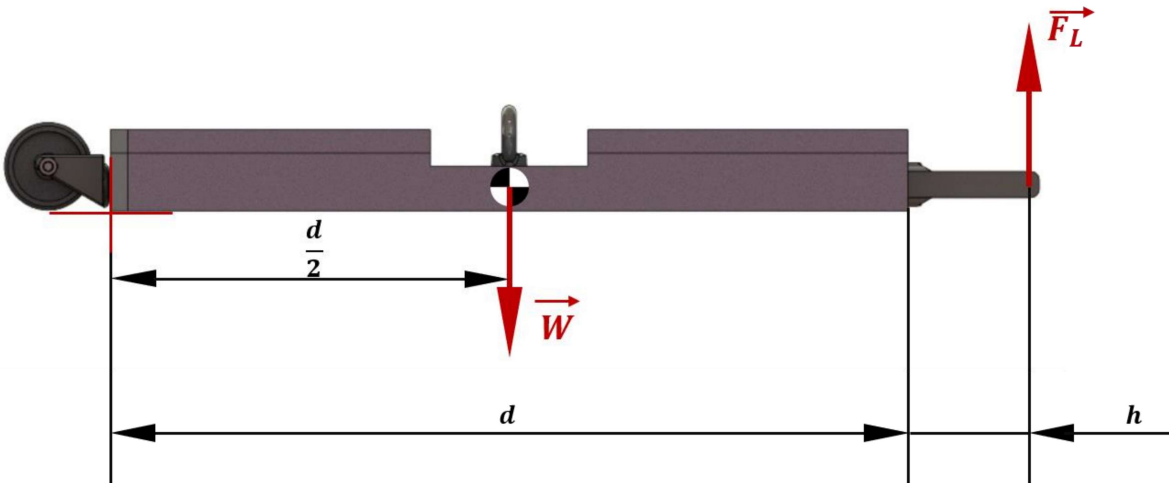

Figure 5.66 - Tool's Lifting Two-Dimensional Force Diagram with Dimensions

Provided the tool and handle's width in conjunction with the tool's mass, the force required to lift the tool by a single handle (ignoring any turning effects around the *X* axis) is calculated by:

$$F_L = \frac{m \,.\, g \,.\, \frac{d}{2}}{d+h} \tag{29}$$

With both the tools weight and width listed in the beginning of this subchapter and $h = 62.5mm$, the greatest lifting force required was calculated for the 1st stage tool which resulted in $F_L \cong 196.7N$.

Thereafter, the stress in the bolted connection is calculated following some guidelines presented in the eighth chapter "*Screws, Fasteners, and the Design of Nonpermanent Joints*" from *Shigley's Mechanical Engineering Design* [4] according to the momentum caused in the handle which translates to axial stress in the screws. Figure 5.67 illustrates this well as, depending on the handles force's direction, different screws can be considered to be subjected to either axial compression or traction.

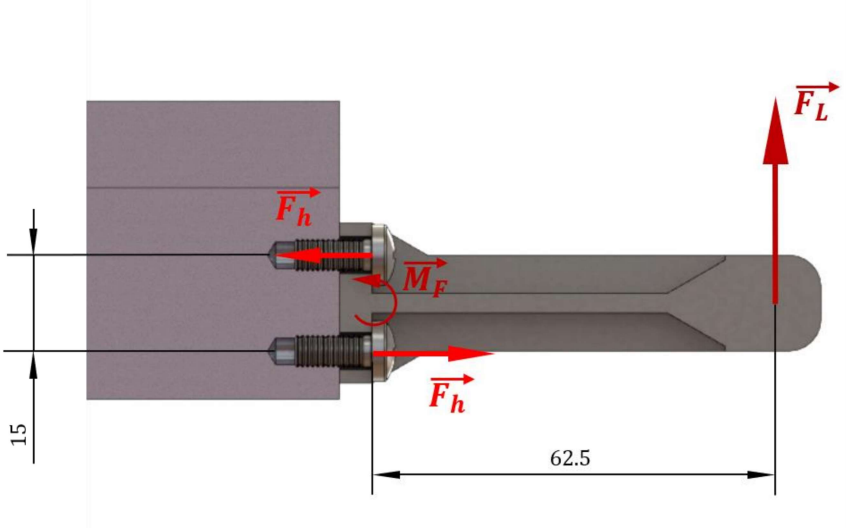

Figure 5.67 - Handle Bars' Bolted Connection Force Diagram

Forces $\overrightarrow{F_h}$ correspond to $\overrightarrow{M_F}$, the binary produced by the force on the handle. Concerning this, they can be calculated through the equilibrium of moments knowing the handle's dimensions as follows:

$$F_h = F_L \,.\, \frac{62.5}{15} \tag{30}$$

However, to be precise $\overrightarrow{F_h}$ does not translate directly into the screw and is, in fact, translated to the hole section of the handle which affects the forces applied on the screw. Figure 5.68 details this for both cases where the force on the handle eases the combined loads on the screw (left) and where the force on the handle contributes to aggravate traction on the screw (right).

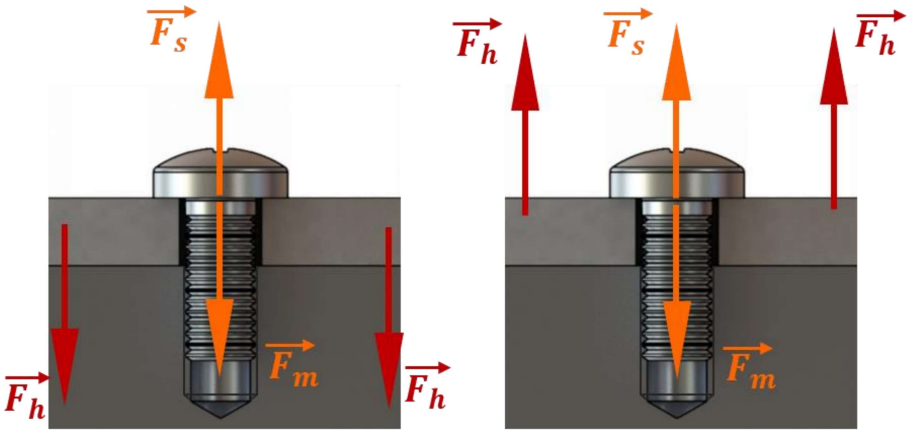

Figure 5.68 - Forces on the Bolted Connection Illustration

The forces displayed in orange refers to the loads resultant of the bolted connection. Force $\overrightarrow{F_s}$ represents the load applied on the screw while force $\overrightarrow{F_m}$ represents the load applied on the material. which constitute an action-reaction pair directly correlated to the torque applied to tighten the screw. However, with force $\overrightarrow{F_h}$ present, the load on the screw, $\vec{P}$, translates to expression (31) for the left case and (32) for the right case, with the last being obviously greater.

$$\vec{P} = \overrightarrow{F_s} - \overrightarrow{F_h} \tag{31}$$

$$\vec{P} = \overrightarrow{F_s} + \overrightarrow{F_h} \tag{32}$$

Focusing on the right case, the absolute values of forces $\overrightarrow{F_h}$ and $\overrightarrow{F_s}$ can be calculated separately in order to calculate the load on the considered screw. $\overrightarrow{F_s}$ is calculated through the required force to tighten the screw which can be estimated as the compression force that prevents the slippage between the handle and the tool's material in the presence of force $\overrightarrow{F_L}$. This avoids shear stress in the screw and can be easily estimated with the friction coefficient between both materials through the condition:

$$F_s \cdot \mu_{(Al-Steel)} \geq \frac{F_L}{n} \tag{33}$$

Although the static friction coefficient between aluminium and stainless steel is documented to be around 0.61 for clean and dry surfaces, for safekeeping, the friction coefficient of two lubricated steel surfaces of 0.15 will be used. Therefore, with the number of screws present in the connection, n , being 4, force F_s is estimated to be approx. $327.8N$ at the lower limit of condition (33).

With both absolute values of $\overrightarrow{F_h}$ and $\overrightarrow{F_s}$ determined, the traction load $\vec{P}$ on the screw is calculated at around $1147.4N$. However, this load is actually distributed to the component's material (tool and handle) as well as to the screw according to a ratio of these component's rigidity. Despite this, for simplicity and safekeeping, the tensile stress on the screw will consider the full load, disregarding the load on the compressed components.

$$\sigma_{COM} = \frac{P}{A_t} \tag{34}$$

Lastly, the tensile stress on the screw is calculated through expression (34) where A_t represents the area of the screw for tensile stress calculation registered in table 8-1 of *Shigley's Mechanical Engineering Design [4]* as $14.2\ mm^2$ for the M5 metric thread. This results in a tensile stress of around $80.8\ MPa\ [N/mm^2]$.

Also from *Shigley's* [4], table 8-11 documents some mechanical properties correspondent to different metric property classes of screws. In this table, the lower class 4.6 presents a tensile yield strength of $240\ MPa$ which in turns results in a admissible tensile stress $\sigma_{adm} = 168\ MPa$ with a factor of safety of 0.7. As it is evident, the estimated tensile stress on the bolts is approximately half of its admissible tensile stress. This demonstrates that for the designed handle connected through four M5 screws should be enough to lift the tool on its side without failure on the bolted connection.

At last, this completes the design of all the tool's features for the first iteration of this project which should cover all the functional requirements listed in the first segment of chapter 5. At this stage, the tool's CAD models are considered completed in terms of their geometry and features.

Despite this, further development is still required to guarantee the final product's quality. In this regard, the following chapter will cover this design's geometric dimensioning and tolerancing.

5.4 Geometric Dimensioning and Tolerancing

At this design stage, the CAD models for the tool's assembly and respective components are fully developed. However, it is still unconceivable that the final piece corresponds exactly to the CAD model as manufacturing deviations are inevitable. Due to this, the manufactured components may cause some problems in terms of assembly or of the final piece's quality.

Although many of these concerns can be prevented with good design practices and some of them where already avoided with the developments of subchapter 5.2, only through a careful analysis in terms of geometric dimensioning and tolerancing can we assure the final piece's quality.

For this purpose, the tool's assembly will be divided into relevant segments in order to cover all the possible issues caused in manufacturing the tool's components. Concerning this, the analysis will be divided into four main segments: the dowel pin fittings and positioning; the positioning of the holes for the bolts; the slot's profile tolerancing and the reference surfaces tolerancing.

These segments will be developed following guidelines from *Mourão, 2004* [18], which is based on *Chevalier, 1989* [6], and in conjunction with the lecture notes from FCT-NOVA's Mechanical Engineering Subject "*Toleranciamento de Sistemas Mecânicos*". In some cases, tolerancing will be attributed according to documented values for acceptable manufacturing deviations according to *Agostinho et al* [1] for the milling process which seemed to be the most adequate choice in comparison to the CNC machine cutting technology considered in this design.

In addition to this, these sections will also include justification for the tolerances considered as well as for the surface finishes that will be attributed to the relevant surfaces. As the outcome of this subchapter, the final technical drawings of each component and the assembly of each tool will be concluded and provided in Appendixes VIII to XXVII.

It is also important to note that, GD&T for mass production presents a much greater challenge in terms of guaranteeing the assembly for each combination of components. As this is a unique design, many of the tolerances applied are not required for assembly purposes yet are still important for the final piece's quality.

5.4.1 Dowel Pin Fitting and Tolerancing

According to the dowel pin's technical specifications provided by *Technifast* [32] and summarized in Appendix V, the recommendations for the fitting tolerances can be chosen according to the hole component's material. Three categories for the hole tolerance guide are provided, hardened steel, mild steel and aluminium/zinc/brass.

For each of these categories, it is possible to choose the type of fitting desired according to design requirements. For aluminium's case, the recommendations provided present the largest tolerances of the

three categories which include lower limits for the diameter of $-35\ \mu m$ for an interference fit, $-5\ \mu m$ for a transition fit and a range of $+25$ to $+60\ \mu m$ for the clearance fit.

In addition to this, the dowel pin selected is manufactured to a $m6$ tolerance which allows us to study the hole-pin fitting tolerances. This way it is possible to determine the hole's standard tolerance according to the manufacturer guidelines. For example, considering each fit, the dimension tolerances are depicted as follows.

Table 5-10 - Pin-Hole Fitting Tolerances

	Pin $(d_{-di}^{+ds})\ [mm]$	Hole $\left(D_{-di}^{+ds}\right)\ [mm]$
Interference Fit	$10\ m6 = 10_{-0.003}^{+0.006}$	$10_{-0.035}^{+dx}$
Transition Fit	$10\ m6 = 10_{-0.003}^{+0.006}$	$10_{-0.005}^{+dx}$
Clearance Fit	$10\ m6 = 10_{-0.003}^{+0.006}$	$10_{-dx}^{+0.025}$ to $10_{-dx}^{+0.060}$

As Table 5-10 demonstrates, the dimension limits for the hole tolerances have yet to be set according to tolerance class determined by design. For this purpose, Table 14.1 of Veiga da Cunha [34] was consulted to obtain the fundamental tolerances for each class according to the Portuguese standard NP 189:1962. This table lists a tolerance of $9\ \mu m$ for class IT6 and a tolerance of $15\ \mu m$ for class IT7 regarding a 10mm dimension.

Classes IT6 and IT7 are both medium precision classes and usually correspond to a standard mill cutting capability. As an option, the class IT7 was considered for conservative reasons as the dowel pin holes will also be subjected to the geometric position tolerance as will be covered ahead. This way, considering the tolerance of $15\ \mu m$ for class IT7, values for the tolerance limit dx listed in Table 5-11 can be calculated which results in:

Table 5-11 - Hole Adjusted Standard Tolerances

	Hole $\left(D_{-di}^{+ds}\right)\ [mm]$	Standard Fitting Tolerance $\left(D_{-di}^{+ds}\right)\ [mm]$
Interference Fit	$10_{-0.035}^{-0.020}$	$10_{-0.034}^{-0.019} = 10\ R7$
Transition Fit	$10_{-0.005}^{+0.010}$	$10_{-0.005}^{+0.010} = 10\ J7$
Clearance Fit	$10_{+0.010}^{+0.025}$ to $10_{+0.045}^{+0.060}$	$10_{+0.040}^{+0.055} = 10\ D7$

The values for the hole tolerances for each type of fitting were adjusted to the standard according to ISO 286-1:1988 as the right column of Table 5-11 depicts. With this information, the transition fit was selected for the bottom component while a clearance fit was selected for the top component. These fittings should be adequate for the tool's assembly requirements and result in a diameter of $10\ J7\ mm$ for the bottom component's pin hole and $10\ D7\ mm$ for the top component.

Nevertheless, concerning the dowel pin's assembly, a geometric tolerance for the hole's position is required. This tolerance will constrict the position of the hole's axis to a tolerance cylinder of a determined diameter, thus controlling the position of each hole and reassuring the components compatibility in terms of alignment.

The geometric tolerance needs to be set according to the tolerance on the fitting between the pin and the hole. This is related to the compatibility of the alignment of the holes in both the top and bottom components, which depends directly on the clearance between the pin and the hole. To determine the tolerance, expression (35) is for the calculation of the geometric tolerance of a set of holes is equal to the sum of the minimum clearance in each hole's assembly.

$$\sum t_i = \sum c_{min} \tag{35}$$

For this case, as every hole is identical in terms of assembly, the calculation of the geometric tolerance can be treated individually and then applied to all of them. The minimum clearance is easily calculated as the difference between the maximum diameter of the pin and the minimum diameter of the hole for the clearance fit, which translates to $0.034\ mm$ in the top component.

At last, this tolerance was divided equally between the top and bottom components resulting in a true position tolerance that requires the axis of the holes to be contained by a cylinder of $17\ \mu m$ diameter centered in its true position.

Furthermore, the maximum material condition was applied to the top component's tolerance, corresponding to the interference fit, while the bottom component is toleranced to the projected dimension of the top component's hole. This has the purpose of guaranteeing that the bottom hole is aligned to the full length of the pin while the maximum material condition represents the least favourable diameter for assembly. In the cases where the material is not in the maximum material condition, a "bonus" tolerance will be available further facilitating the dowel pin's fitting.

Surface finish was also added to both the dowel pin holes due to the tight fit assembly. For these surfaces, the class $N6$ according to ISO 1302-1978 was attributed, which corresponds to a surface roughness of $0.8\ \mu m$. This class corresponds to a medium precision adequate to the manufacturing technology considered.

All this information is displayed accordingly in Figure 5.69 which summarizes the tolerances applied in the top and bottom component's drawings.

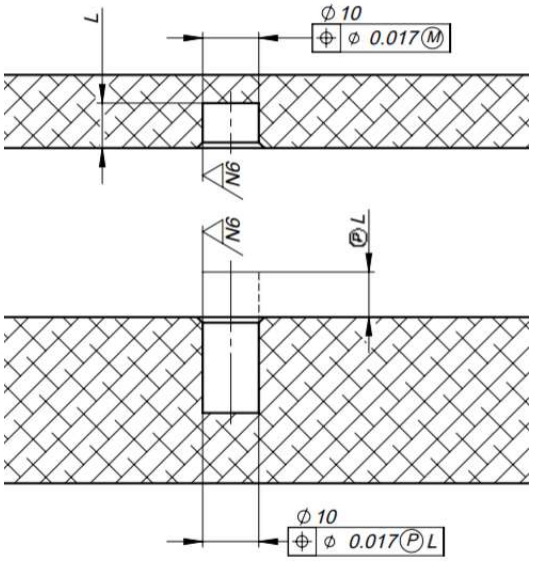

Figure 5.69 - Dowel Pin Holes Geometric Tolerancing

In addition to this, the datums corresponding to the reference surfaces of the tool were added to the geometric tolerance as these surfaces convey the true dimensions of the holes in the components drawing.

5.4.2 Bolted Connection Tolerancing

The bolted connection holes are almost identical to the dowel pin holes in terms of tolerance analysis. The holes for the bolts will also be toleranced to their true position relative to the reference surfaces.

However, in order to use expression (35), the minimum clearance that dictates the tolerance for the true position does not refer to fitting dimensions. In this case, the minimum clearance refers to the difference between the clearance hole on the bottom tool and the thread's nominal diameter as displayed by dimension *c* in Figure 5.70.

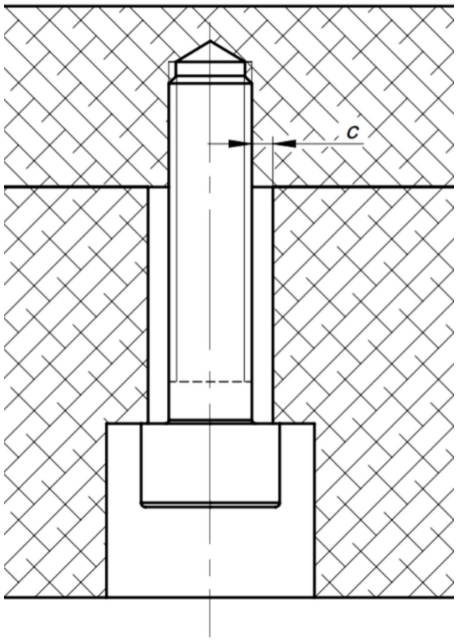

Figure 5.70 - Clearance for the Bolted Connection's True Position Tolerance Calculation

The clearance hole in the bottom tool was dimensioned according to *tabela 15.18* of Veiga da Cunha [34] which gives us recommendations for bolt clearance hole's diameters according to ISO 273:1979. Considering this, for the M6 threads the hole was dimensioned with a diameter of $6.6mm$ with an $H8$ tolerance which corresponds to a minimum dimension $c = 0.3mm$.

Not accounting for the clearance present between the bolt and top component threads, the following expression derived from (35) is valid to calculate the true position tolerances for the bolt holes.

$$t_{top} + t_{bottom} = 0.3mm \tag{36}$$

With this, it is possible to determine the required geometric tolerance for the bolt hole's position by distributing the available $0.3mm$ between the top and bottom component. This distribution is usually made according to the manufacturing operation of each feature by enlarging the tolerance where manufacturing is more demanding.

As it was done for the dowel pin holes, as both components have similar manufacturing procedures, it seemed adequate to divide the tolerance equally between both components, thus attributing a true position tolerance for the bolt holes of $0.150mm$.

This means that the threaded holes in the top component and the clearance holes on the bottom component are required to have their axis positioned inside a cylinder of $0.150mm$ diameter with its axis in the hole's true position.

Furthermore, similarly to what was done for the dowel pin holes, the maximum material condition was attributed to the bottom component clearance hole while the threaded hole in the top component was subjected to the projected dimension tolerance.

All this results in the tolerancing displayed in Figure 5.71 with true position dimensions and the datums correspondent to the reference surfaces attributed in the respective component's drawing provided in Appendixes VIII to XXVII.

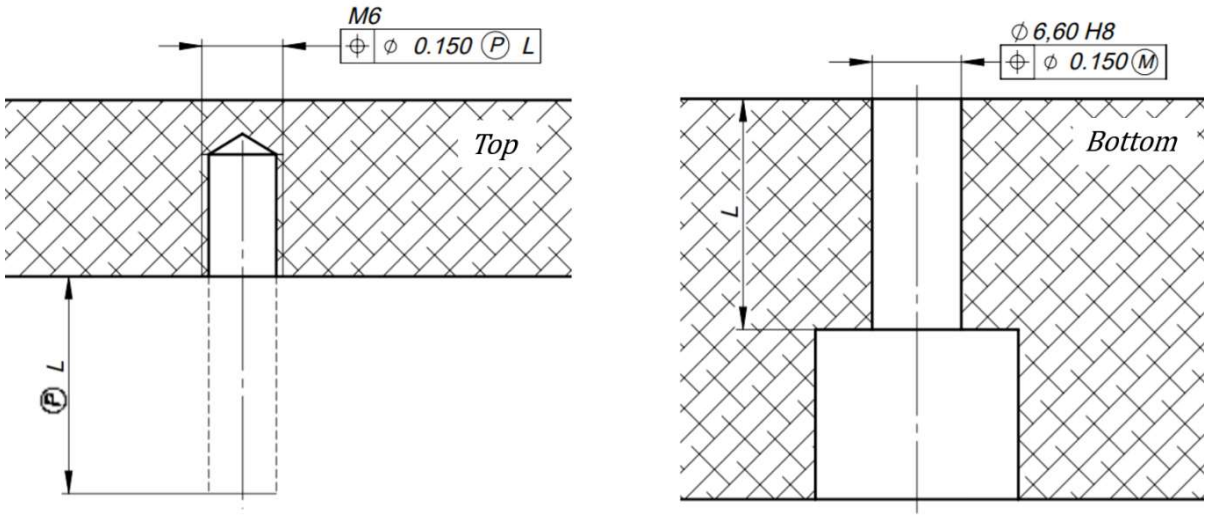

Figure 5.71 - Bolted Connection Hole's Geometric Tolerancing

5.4.3 Blade Slot's Profile Tolerancing

In this segment, the blade's slot profile developed in subchapter 5.3.1 will be covered. Although this feature is very important for the blade's assembly on the tool, its geometry was designed to require minimal tolerancing as it simplifies the fastening of the blades.

In terms of blade assembly, the only dimension relevant for this analysis is the angle of the slots mating surfaces which in turn corresponds to the blade's dovetail angle of aperture as referred to in chapter 4 covering the HPC blade's reference dimensions. This is also valid for the 1st stage blade dovetail inclination angle γ displayed in Figure 5.14, however in this case, the reference value for the angle will be based on the CAD reference models.

In this segment, the slot's symmetry plane will also be analysed as a means to achieve the desired blade's position when assembled on the tool. For this, the symmetry plane of the slot will be toleranced to its perpendicularity against the bottom and lateral reference surfaces as it will be demonstrated further ahead.

Regarding the slot's profile mating surfaces, angle β previously displayed in Figure 5.13, will now be referring to the angle between both surfaces as Figure 5.72 illustrates. This angle has a direct effect on how the blade is positioned when assembled in the slot.

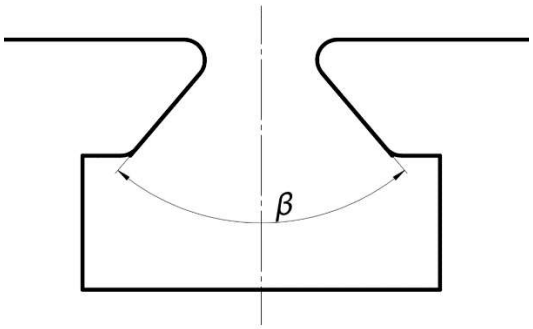

Figure 5.72 - Slot's Profile Toleranced Angle

Considering manufacturing variations in this angle in both the blade and slot's geometry, there are two situations that can be considered as Figure 5.73 illustrates by exaggeration. In the left, when the blade's angle is greater that the tool's and, in the right, when the tool's angle is wider than the blade's.

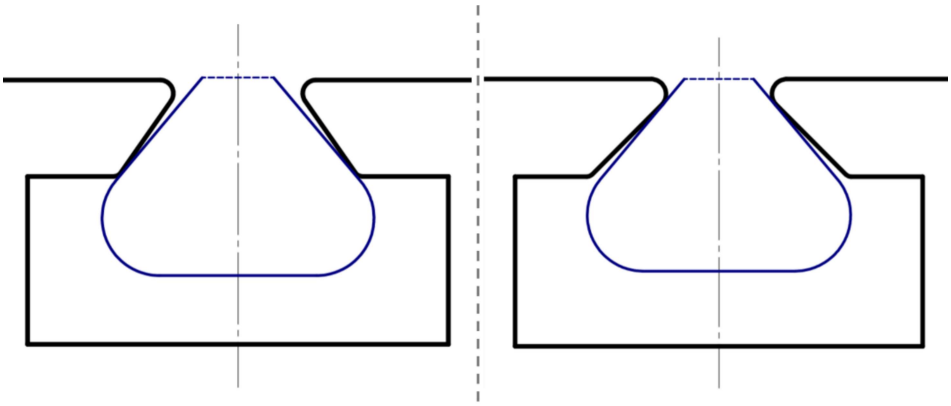

Figure 5.73 - Slot's Angle Deviation effects on Blade Attachment

Although Figure 5.73 exaggerates this, the manufacturing variations in this angle directly affect the position of the blade when mounted on the tool. According to the images this seems to have an impact on how high the blade sits in the *V* shaped slot. However, the situation on the right was considered to be the most favourable as it promotes slippage between the surfaces when the spring upwards force is applied, thus favouring the assembly of the blade to the same position every time.

This way, a unilateral tolerance will be attributed to angle β where only a superior deviation will be allowed for this dimension as follows.

$$\beta^{+ds}_{-0.000} \tag{37}$$

Yet, to quantify an appropriate value to apply to this tolerance required a different approach as the manufacture of these angled surfaces might present different challenges. These angles can be achieved, for example, through a 4th axis on CNC machining centre by rotating the tool or through a specially designed chamfer machining tool. In both these cases, there is the issue of producing the desired angle as well as maintaining this angle throughout the whole length of the surface.

To better grasp this, the tolerances for classes IT6 and IT7 corresponding to the length of these surfaces for each tool were consulted from Table 14.1 of Veiga da Cunha [34] and the PPT (Parts Per Thousand) value of this tolerance correspondent to the length of the slot was calculated as Table 5-12 lists.

Table 5-12 - Slot Length Tolerance Class Analysis

Blade Stage	Slot Length $[mm]$	IT6 Tolerance $[\mu m]$	IT6 PPT [‰]	IT7 Tolerance $[\mu m]$	IT7 PPT [‰]
1	46.6	16	0.34	25	0.54
2	32	16	0.50	25	0.78
3	25	13	0.52	21	0.84
4 & 5	18	11	0.61	18	1.00

As Table 5-12 demonstrates, considering the PPT values, the tolerance attributed seems to decrease with larger length dimensions while the actual tolerance value is greater for larger dimensions. This leads us to consider the height of these angled surfaces as these also have implications on the possible angle variations from manufacturing.

Table 5-13 - Surface Height Tolerance Class Analysis

Blade Stage	Surface Height (mm)	IT6 Tolerance (μm)	IT6 PPT [‰]	IT7 Tolerance (μm)	IT7 PPT [‰]
1	4.94	8	1.62	12	2.43
2	2.44	6	2.46	10	4.10
3	1.22	6	4.91	10	8.20
4 & 5	4.66	8	1.72	12	2.58

In Table 5-13, the PPT values of tolerance attributed for the smaller dimension of these surface are much greater than the ones obtained considering the slot length. Regarding this, a PPT of 1.5‰ tolerance seemed adequate to attribute to the slot's angle resembling the IT6 tolerance class.

At last, the tolerance value was calculated according to a $90°$ angle considered as reference since the angle of the surface itself does not influence the precision on manufacturing and therefore should not influence the tolerance value. This way, a tolerance of $8'6''$ was attributed to the slot's angle of each model which corresponds to a $0.135°$ tolerance.

Furthermore, a surface finish specification was attributed to these surfaces according to a $N6$ class according to ISO 1302-1978 which corresponds to a surface roughness of $0.8\,\mu m$. The parallel restriction was then added to the surface finish requirement as it complies with the blade's assembly on the tool.

Following this, two more perpendicularity geometric tolerances have yet to be applied, concerning the slot's symmetry plane. As Figure 5.74 demonstrates, the symmetry plane of the slot will be toleranced against the two lateral reference surfaces to assure the slot's orthogonal position on the tool.

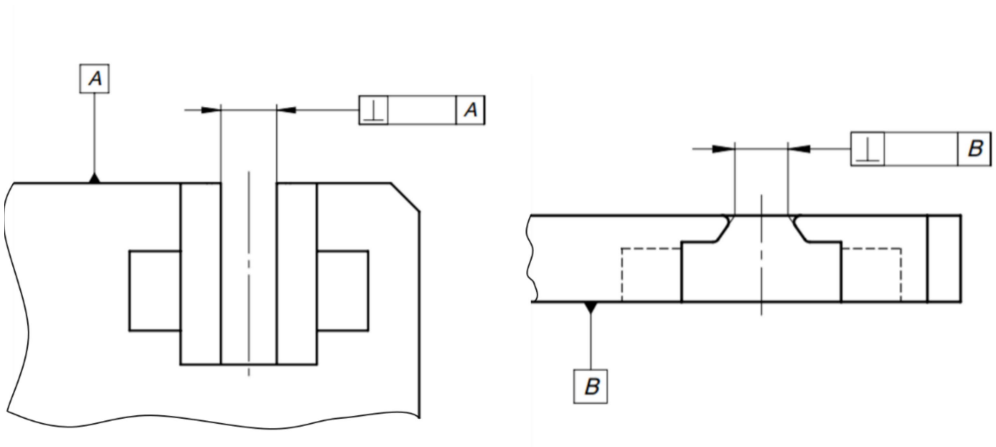

Figure 5.74 - Blade Slot Geometric Tolerances Representation

These tolerances are attributed for quality purposes and therefore will be dimensioned according to appropriate values known for the intended manufacturing technology. For this Agostinho et al [1] was consulted which documents permissible perpendicularity deviations regarding mill machining. These tables are also available for consultation in Appendix VII.

According to this, for the most conservative hole milling operation, table 3.12 lists an economic value of 0.08mm and a minimum value of 0.05mm of perpendicularity deviation per 100mm. This way, the symmetry plane was toleranced to be within two planes 0.050mm apart, equally spaced to a plane perfectly perpendicular to the top component's base surface as Figure 5.74 depicts on the right.

In addition, the tolerance displayed on the left of Figure 5.74 was attributed according to the class IT6 corresponding to the slot's length dimension. This results in tighter tolerances than those referred to above thus promoting the perpendicularity of the blades to the lateral reference surface.

All this information was then added to the manufacturing drawings provided in Appendixes VIII to XXVII concerning the top components of each tool. Figure 5.75 illustrates this with the slot's tolerancing for the case of the 2nd Stage tool.

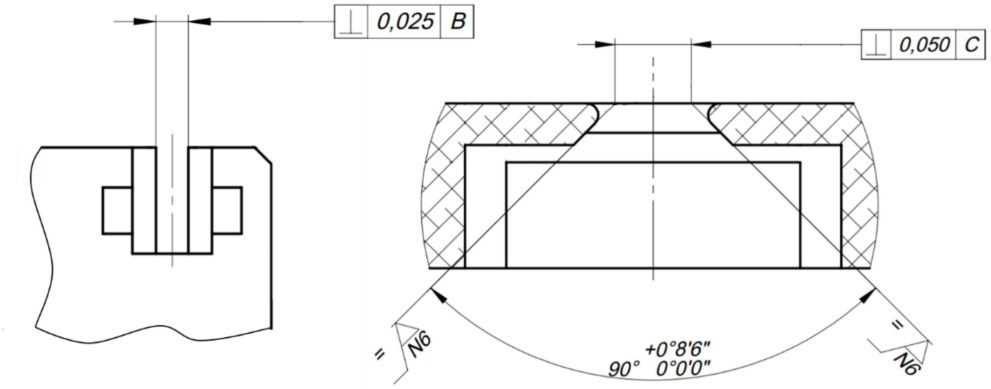

Figure 5.75 - Blade Slot's Symmetry Plane Geometric Tolerancing

Lastly, there is the case of the 1st stage tool slot which, due to the blade's geometry, is not perpendicular to the tool's lateral surfaces. In place of the geometric tolerance for perpendicularity between the slot's symmetry plane and the lateral surface, a dimensional tolerance was applied to the slot's inclination angle, γ.

With a similar approach to the one taken for the *V* shaped surfaces of the slot, the tolerance was attributed as a PPT of 2.5‰ relative to the reference 90° angle, which corresponds to a tolerance of 0.225°. This value may seem too conservative considering the depth of the slot, however this decision is attributed to the fact that large deviations on this angle could result in a faulty assembly of the blades on the tool.

In this case, however, the tolerance was applied as bilateral and symmetric setting the mean dimension value as the value of the inclination angle of the reference model of the 1st stage blade. This results in a tolerance of $\gamma \pm 6'45''$ applied as displayed in Figure 5.76.

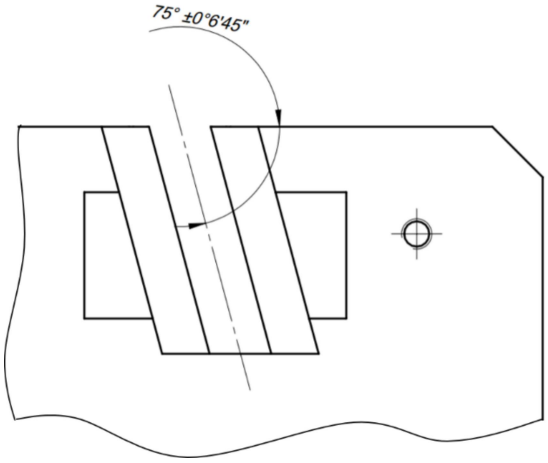

Figure 5.76 - 1st Stage Blade Slot's Angle of Inclination Tolerancing

5.4.4 Reference Surfaces Dimensional Tolerancing

At last, this design should include dimensional tolerances regarding the reference surfaces which include the top, front and left surfaces marked by the matching chamfer as explained in subchapter 5.3.3. However, these surfaces' placement in terms of manufacturing deviations also depends on other surfaces which will have to be toleranced as well.

Firstly, concerning the top reference surface, its alignment with the CMM table depends on the bottom surface of the tool, as well as on the mating surfaces linking the top and bottom components. Taking the manufacturing process into account, each component may be manufactured by machining the mating surface first, which refers to the top surface in the bottom component and bottom surface in the top component.

This way, considering the machining order of the surfaces, the mating surface of each component will be toleranced to its flatness while the top and bottom surfaces of the assembly will be toleranced to their parallelism to said mating surfaces. For a clearer understanding, Figure 5.77 demonstrates this in a partial cut section drawing of the top and bottom components.

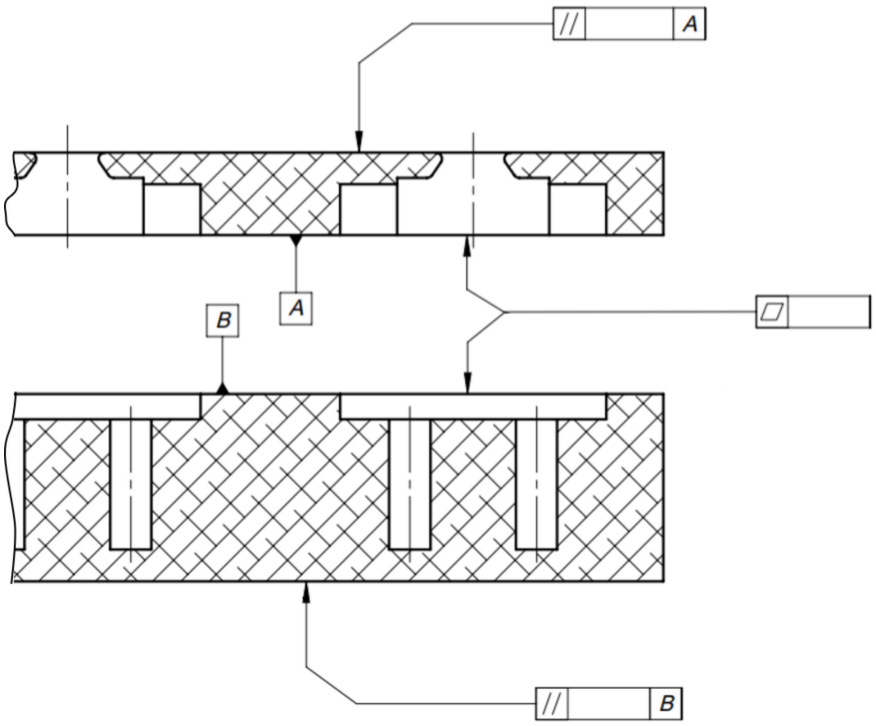

Figure 5.77 - Top and Bottom Component's Mating Surfaces' Geometric Tolerances Representation

However, similar to was presented in the subchapter above, there is no clear guideline on how to calculate this tolerance to meet assembly requirements. For this, these tolerances will be attributed according to documented values for permissible deviations concerning mill machining technology.

As it was done above, *Agostinho et al* [1] was consulted for permissible deviation values for flatness regarding face milling operations and rectification through face grinding. The minimum values documented in Table 3.6 from [1] for flatness deviation are $30\ \mu m$ for milling and $20\ \mu m$ for face grinding, each per $100\ mm$ of length.

For reference, these values were compared to the tolerance classes IT6 and IT7 corresponding to $100\ mm$ length and the largest dimension of the surface toleranced, $900\ mm$. Table 5-14 lists these values for comparison.

Table 5-14 - Flatness Tolerance Values Comparison

	Tolerance Class		Flatness Permissible Deviation [1]			
			Precision Grinding		**Face Milling**	
Dimension	**IT6** [μm]	**IT7** [μm]	**Economic** [μm]	**Minimum** [μm]	**Economic** [μm]	**Minimum** [μm]
100	22	35	50	20	50	30
900	56	90	—	—	—	—

As we can see, the precision grinding minimum value may be associated with an IT6 class while the face milling minimum value is closer to the IT7 class. With this in mind, to maintain the high quality standard desired for the tool's manufacturing concerning mill machining, a flatness geometric tolerance of $30\ \mu m$ will be attributed to the mating surfaces of both components per $100\ mm$ of length.

In addition, a flatness tolerance of $100\ \mu m$ will be attributed without length restriction. This tolerance was attributed resembling the class IT7 following the correspondence to the face milling process as described above.

Following this, a similar thought process was applied for the parallelism tolerance attributed to the top and bottom surfaces of the tool's assembly. Table 3.8 from *Agostinho et al* [1] documents the respective parallelism deviation values for plane surfaces concerning different manufacturing technologies. As listed, precision grinding was attributed an economic value of $30\ \mu m$ and a minimum value of $10\ \mu m$ while face milling presents an economic value of $50\ \mu m$ and a minimum value of $20\ \mu m$, each situation per $100\ mm$ of length.

Accordingly, the top surface of the top component and the bottom surface of the bottom component were attributed a tolerance of $100\ \mu m$ per $100\ mm$ of length for parallelism to their respective mating surfaces. To avoid confusion, Figure 5.78 displays the partial cut section of both the top and bottom components, now with the respective tolerances attributed.

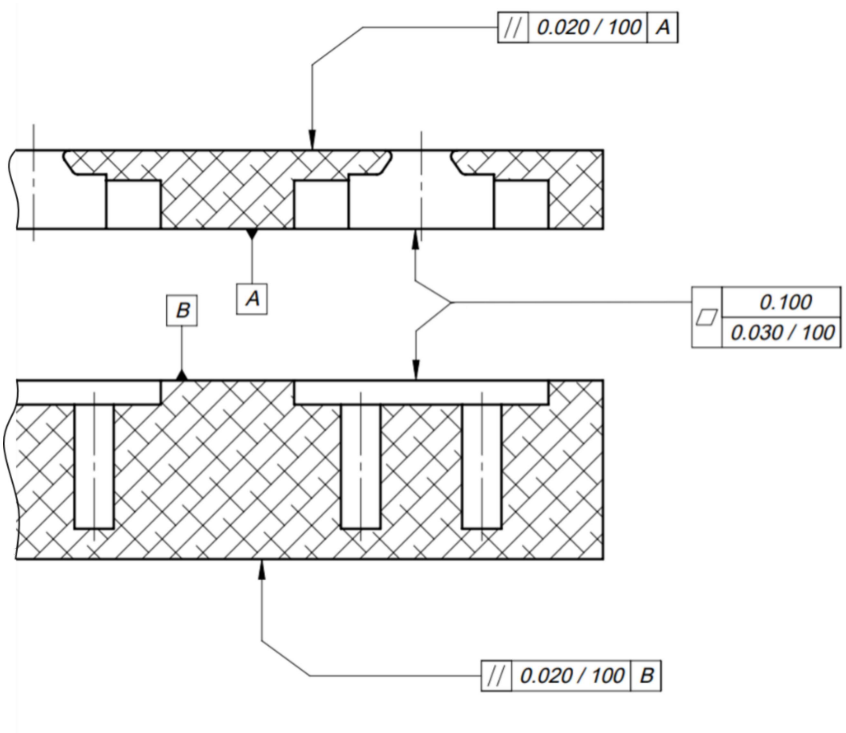

Figure 5.78 - Top and Bottom Component's Mating Surfaces' Geometric Tolerancing

Finally, the front and lateral surfaces will be attributed a perpendicularity geometric tolerance to the top reference surface of the tool to assure the orthogonality of the reference surfaces which also affects the slot's positioning. This will allow us to set a tool's referential in the CMM as it was already explained. With this in mind, these tolerances should also be attributed concerning face milling capability minimum values.

However, *Agostinho et al* [1] only documents permissible deviations for the perpendicularity of hole's axis to a certain surface. Still, the values concerning surface parallelism were taken as reference as these refer to a relative position of two surfaces as it is intended for the perpendicularity.

Considering this, the values abovementioned for parallelism deviation were used, with the minimum value attributed for the *X* axis reference surface (front) and the economic value to the *Y* axis reference surface (left) on the top component, both per $100\ mm$**.** This difference is due to the surfaces reference "hierarchy" which will also be considered when attributing the tolerance's datums.

Also, similarly to what was done to the flatness geometric tolerance, a condition without length restriction was added to these tolerances containing larger tolerance values, thus attributing a $200\ \mu m$ tolerance to the front surface and a $250\ \mu m$ tolerance to the lateral surface.

Figure 5.79 depicts the result of this though process with the tolerances and respective datums used in the manufacturing drawings of the top components in a partial top and side view.

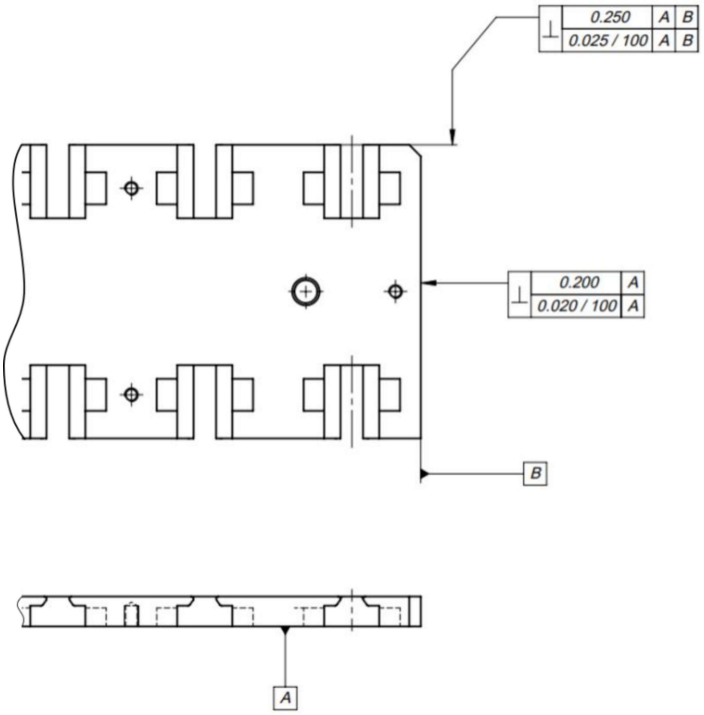

Figure 5.79 - Top Component's Refference Surfaces Geometric Tolerancing

At last, this concludes the tool's design and the final drawings adequately labelled should be available for manufacturing. These drawings will be provided in Appendixes VIII to XXVII next to the respective tool's assembly drawing. The assembly's drawing, in turn, displays the bill of materials illustrating all the components and their respective quantities.

For the manufacturer, the drawings were provided in conjunction with the CAD model files of the components and final assembly of each tool. The CAD models were submitted in ".step" format as requested.

6 HPC Blade Dimensional Inspection using the Coordinate Measuring Machine

In the final chapter of this project's development, the dimensional inspection of the HPC blades will be covered concerning the fixture tools designed. This chapter is going to cover some of the CMM's features as well as some available software modules for dimensional inspection.

As a first note, there are two main approaches that could be taken for this development. One is to create a program using the Part Manager of the *MCOSMOS* software which is commonly used in the TAP M&E shop. This option should require the localization of the piece's coordinate referential through a set of measurements as described in subchapter 5.3.3. After this, the operator could manually input the movements for dimensional inspection in "learn mode". This program uses a learn and repeat technology to record the inputs from the operator and then repeats them whenever desired.

The second option is to use the CAD models of the piece that will be placed in the CMM, which in this case refers to the CAD models of the fixture tools fully assembled with a whole set of blades. Then, using *Mitutoyo's CAT1000* software, the automatic inspection program could be developed virtually using all this software's dedicated features.

Still, despite the availability of the CAD models for the second option, there are some concerns about how the virtually developed program might react to the inconsistency between the CAD models and the real piece which are inevitable due to the tool's manufacturing deviations or to the blade model's deviations.

Regardless of this, this chapter will focus on the use of CAD models to develop the inspection program as a mean to reach the CMM's full potential. This way, the following sections should provide clear explanation on the type of CNC dimensional inspection program that was considered when developing the fixture tools, as well as providing some guidelines to the development of this program.

With this in mind, this chapter will be divided into two main sections. The first will introduce the CMM by providing a very brief description of the main equipment and software. The second section will refer to the more relevant *Mitutoyo*'s expansion software modules and their potential to improve dimensional inspection.

Yet, even though this was taken into consideration when developing some of the fixture tool's features, this chapter will not cover the surface scanning feature of the CMM. Despite this being a very interesting feature available in other software expansion modules, there is some priority in developing simpler inspection programs first in order to test the CMM's capability and the fixture tool's effectiveness.

Nevertheless, this is still something that may be implemented in the future as it provides many new opportunities to improve MRO procedures through this type of dimensional inspection. For this, *Mitutoyo* provides other software modules such as SCANPAK for scanning or CAT1000S for surface sweeping.

6.1 *Mitutoyo*'s Coordinate Measuring Machine and Equipment Brief Description

The coordinate measuring machine is a very important asset for an aircraft engine MRO facility as it allows to inspect the numerous geometries of the various engine parts with greater precision and in less time, thus determining if these meet the manufacturers' requirements for serviceability. Dimensional inspection is a very important part of the engine's overhaul process and, in some cases, the CMM is the only solution to inspect the part for dimensional and geometrical flaws.

TAP M&E MRO shop has at its disposal a *Mitutoyo's* CMM commanded by CNC (Computer numerical control), portrayed in Figure 6.1, which reads the desired coordinates by a mechanical touch triggered mechanism. This model was subject to some modifications which are going to be covered in this chapter. In this regard, this chapter will be mostly based in *Ferreira, E* [7] which provides an introduction and guidelines to the shop's CMM operation while documenting some of the machine's technical specifications.

Figure 6.1 - *Mitutoyo*'s CMM Available in TAP's Engine's Shop

This *Mitutoyo's* model in particular has a workvolume of $1200 \times 1200 \times 1000\ mm$ as it was already described in subchapter 5.2 and was retrofitted with a *RENISHAW's REVO-2* probing head. It has 5 axis of motion available, three translation axis and two rotation axis.

The three translation axis (*X*, *Y* and *Z*) correspond to the co-ordinate system described in subchapter 5.2 and represent three orthogonal axis of linear movement as Figure 6.2 illustrates.

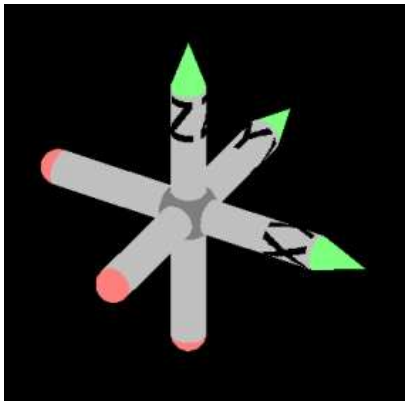

Figure 6.2 - CMM's Co-ordinate System Referential [7]

In addition to these, the probe head also has two rotation axis (*A* and *B*) available which correspond to the angular position of the stylus in the probe. Figure 6.3 illustrates the angular orientation of the *A* axis of rotation displayed in a schematic top view of the CMM while Figure 6.4 displays the angular orientation for the *B* axis corresponding to the probe's position.

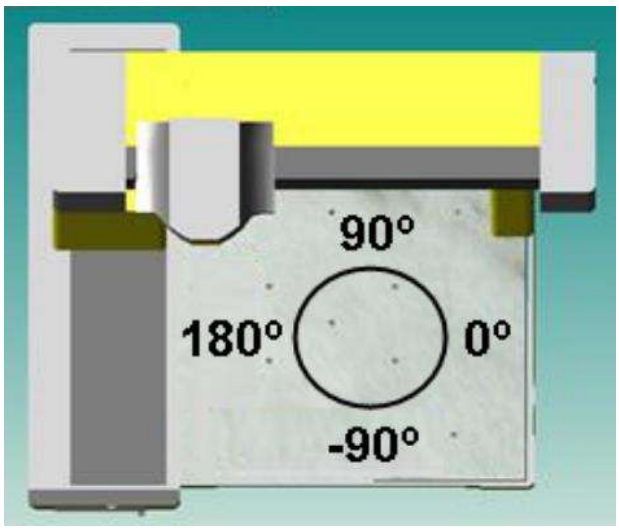

Figure 6.3 - CMM's *A* Rotation Axis Orientation [7]

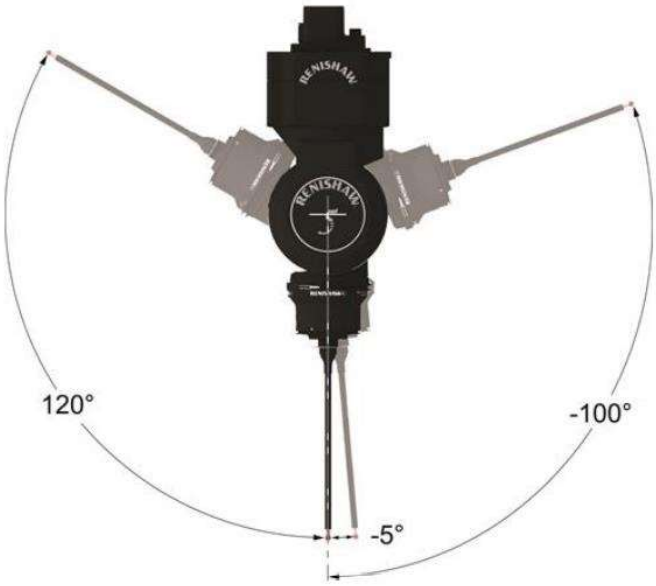

Figure 6.4 - CMM's *B* Rotation Axis Orientation [7]

The probe can be controlled through the *MCU5-2* (Manual Command Units) which allows the operator to control the probe's linear and angular movements as well as the probe's velocity. This MCU is commonly used to take measures manually, whether to locate the piece for a part program or to fully inspect an engine part according to the Engine's Shop Manual. This command unit is displayed in Figure 6.5 and is controlled mainly through the joystick for the movement and the dials to adjust the velocity.

Figure 6.5 - *RENISHAW*'s Manual Command Unit

Also, positioned on top of the CMM's granite table, there is a probe rack available with different options of Renishaw's *RSP2* and *RSP3* probes compatible with the *REVO-2* system. These probes are properly configured in the CMM's software and require calibration when installed. Currently the probe rack has six different probe configurations available and is placed at the centre of the leftmost part of the CMM table as Figure 6.6 depicts. Chapter 4 of *Ferreira, E* [7] provides a more detailed description of this and other CMM related equipment.

Figure 6.6 - CMM's Probe Storage Rack

The CMM is currently operated through the *Mitutoyo's MCOSMOS* software program. This grants access to the *GEOPAK* module which is used to create a part inspection program through the *Part Manager*. When accessing the *Part Manager,* many options are provided to manage the stored programs or to create new ones.

After login, the option to create new part inspection programs becomes available, as well as the option to edit stored ones. Also, in this section, we're able to access both the Learn Mode and Repeat Mode which may be useful to develop a CNC commanded inspection program with minimal use of computer programming but with extensive manual input.

Lastly, *MCOSMOS* also includes the very important CMM System Manager module which is where we are able to configure different settings for the probe rack and the different styli, as well as run automatic probe calibration.

However, for this work, the functionalities mentioned are not going to be referred to in this work, as they are already commonly used to develop an inspection program at the TAP shop. Also, *Ferreira, E* [7] does a remarkable job in describing the step-by-step procedure to develop a part inspection program using these modules in chapters 6, 7 and 8. The following subchapter will cover a brief introduction to some of the software modules that are more relevant to this work.

6.2 *Mitutoyo*'s software for CMM programing

As an *MCOSMOS* software expansion module, *Mitutoyo's CAT1000P* has great potential to the TAP Engine Shop especially in terms of dimensional inspection using the CMM. Its many features may allow TAP engineers to fully assess the various engine parts' condition according to the ESM's specifications and even improve the Shop's MRO capability by studying the correlation of said part's condition to the engine's performance.

All this could be accomplished with relative ease as this software is designed to require minimal manual data input. However, this software's potential lies heavily on the use of the engine parts' CAD models which are held by the manufacturer. This is where the recently obtained 3D Scanner will be very useful as it allows TAP engineers to obtain 3D models of any engine part they possess in the shop by developing the respective CAD models, just like it was done for the HPC blades in subchapter 4.2 of this work.

In addition to this, *Mitutoyo* also provides an airfoil analysis dedicated software, *MAFIS*. This software is prepared to fully inspect the typical airfoil profile and its many features such as the already mentioned leading edge, trailing edge, camber line and chord.

This section will present a summary of this software's relevant features for this work. All the information provided was taken from *Mitutoyo*'s Product Information Manuals [15] and [16] and does not provide step-by-step guidance on how to develop the dimensional inspection program.

In any case, this segment should hopefully provide the framework necessary to learn and explore said modules. Furthermore, *Mitutoyo*'s representative company in Portugal, *Emílio de Azevedo Campos, S.A.* could also provide employee training for the use of these softwares as it was already done in other occasions as part of costumer support.

6.2.1 CAT1000P – Creating GEOPAK Part Program with Help of CAD Data

CAT1000's software module may significantly facilitate the programming of CMM measurements. In particular, *CAT1000P*'s features are designed to program CMM measurements with a few mouse clicks provided that the CAD models for the inspected part are available.

Similar to what happens in CAM (Computer Assisted Manufacturing) software with the tool path, *CAT1000P* allows to generate and simulate the probe's path for a set of measurements thus optimizing the CMM's usage. Through this simulation of movement, it is possible to understand the whole measurement program through a virtual 3D view of the work environment while avoiding any collision with the model.

In terms of possible measurements, *CAT1000P* supports all basic elements already available in the GEOPAK module and some more. However, in the first stage of the development of the HPC blades

dimensional inspection program, only the line and point elements should be required to meet with the ESM's specifications, namely to measure chord length or edge thickness.

Concerning this, once the CAD data is provided, the measurements can be created and edited by clicking on the model's features and adjusting the dialogue window's options. Figure 6.7 illustrates the example of the dialogue window that pops up for the line element measurement.

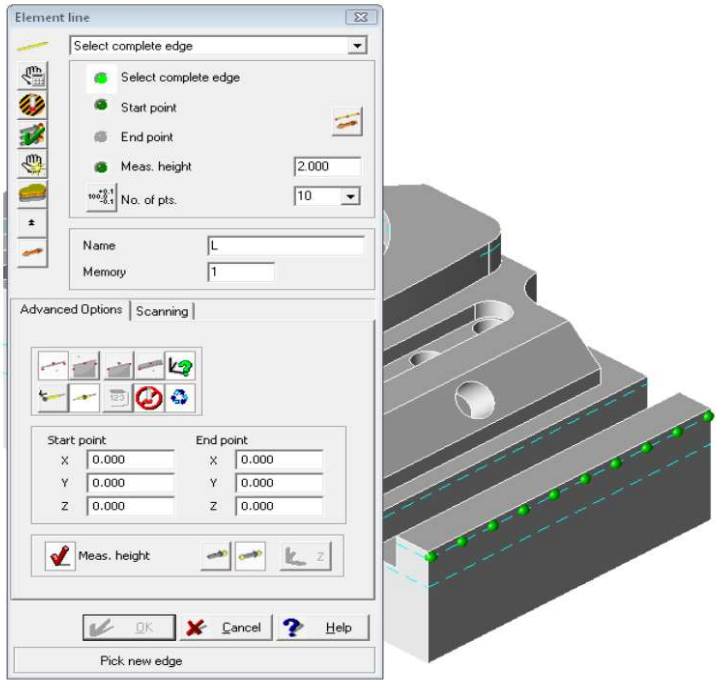

Figure 6.7 - *CAT1000P*'s Line Element Pop-up Window [16]

Following this, the various model features are available for click-on selection or tree view selection as displayed in Figure 6.8. For the purpose of this work, the top surface of the platform of the HPC blade in conjunction with the airfoil's profile at a specified height from this surface should represent the two main elements of relevance. These should allow us to inspect the blade according to the ESM's specifications. Figure 6.9 highlights these features in SolidWorks in comparison to what would be done in CAT1000.

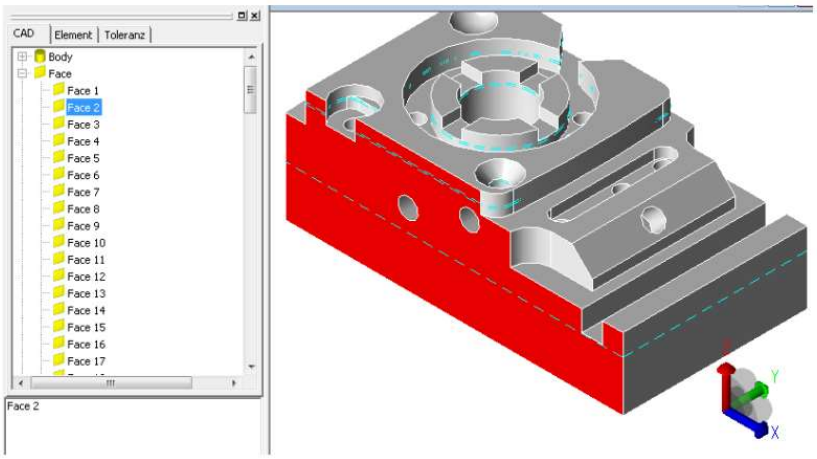

Figure 6.8 - *CAT1000*'s Tree View Selection [16]

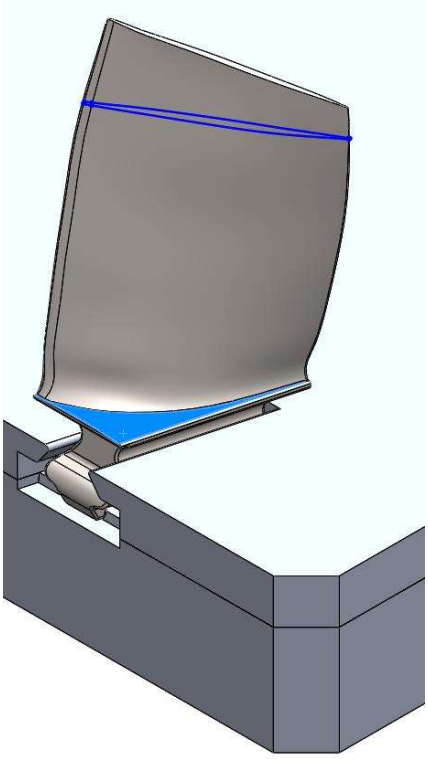

Figure 6.9 - HPC Blade's Inspection Suggested Reference Surfaces for *CAT1000* Programming

These elements could then be used to measure the airfoil's edge thickness or chord length at a determined blade height as it was the main purpose of this work. Furthermore, the airfoil's surface on the model may also be used for as a reference for surface sweeping with the probe for more complex CMM inspection programs which may be addressed in future developments of the airfoil's dimensional analysis.

At this stage, the software should be able to generate the probe's movements automatically based on the CAD data and the measurements defined by the user. For this, there are three main features that should be considered for the generation of the probe's path. One of these features should allow us to define intermediate probe positions thus granting the user some control on the generated probe's path. Another feature gives us the option to define fixtures, as the one developed in this work, which could then be used to improve collision control while minimizing CAD data processing.

Finally, this software allows to simulate the complete part program, granting the user the opportunity to inspect the part program for collisions or to tune parameters according to what is desired. This is possible through a graphical representation of both the workpiece and the probe as Figure 6.10 illustrates. For this, however, it is important to note that the probe's specifications should be accurately defined in the *CMM System Manager* Module.

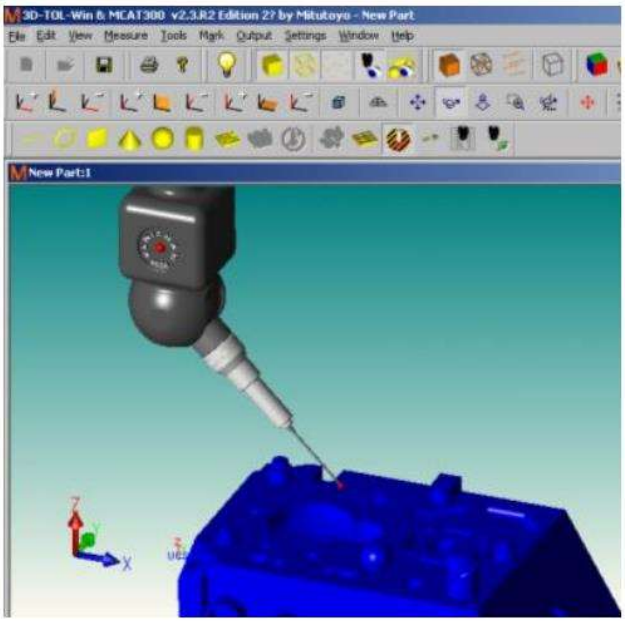

Figure 6.10 - *CAT1000*'s Probe Movement Simulation [16]

This concludes the main features for the offline development of the part program using CAD models. Naturally, as the part program will be saved and ran through the *GEOPAK* module, there is still the opportunity to use this module's feature to edit the part program generated.

Also, as it is currently done in *GEOPAK* based part programs which were developed through Learn and Repeat modes, the synchronization of the parts co-ordinate system with the CAD model's referential. This procedure was already described in segment 5.3.3 which demonstrated how it is possible to perform the virtual alignment of the workpiece.

There are several other features available within the *CAT1000P* module. This chapter only briefly describes the ones which were considered more relevant for the first iteration of the HPC blade's inspection part program. To complete this work, this software will have to be explored further and tested in order to achieve the wanted results.

6.2.2 MAFIS – Airfoil Profile Analysis

MAFIS stands for *Mitutoyo Airfoil Inspection System* and was especially developed by the company to simplify complicated airfoil analysis procedures. This module allows us to examine the most common features of the airfoil profile and to evaluate the output measurement results.

The *MAFIS* module is accessible as an option of the *SCANPAK* module in the *GEOPAK*-Editor, via the menu function "Contour/Airfoil Analysis". It requires the user to load an airfoil profile to calculate the airfoil dimensions.

This means that, in order to use this feature, the airfoil first needs to be scanned by the CMM using the *SCANPAK* module which isn't going to be covered in this thesis. Concerning this, this section will be developed with the purpose of demonstrating the full potential that the *Mitutoyo*'s CMM can reach in the inspection of compressor, turbine or even fan blades.

After running a *SCANPAK* part program that scans one or more airfoil profiles, the system stores the profile's data as Figure 6.11 illustrates. This data will then be loaded into the airfoil analysis tool which will calculate the airfoil's dimensions as illustrated in Figure 6.12.

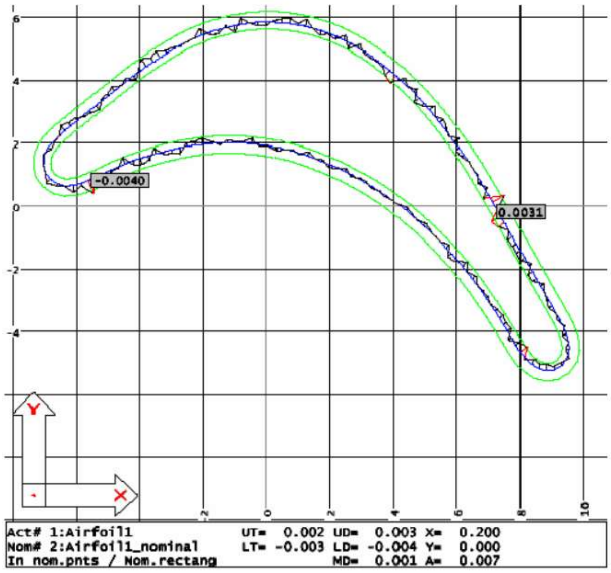

Figure 6.11 - Airfoil Profile Data From *SCANPAK*-based Inspection [15]

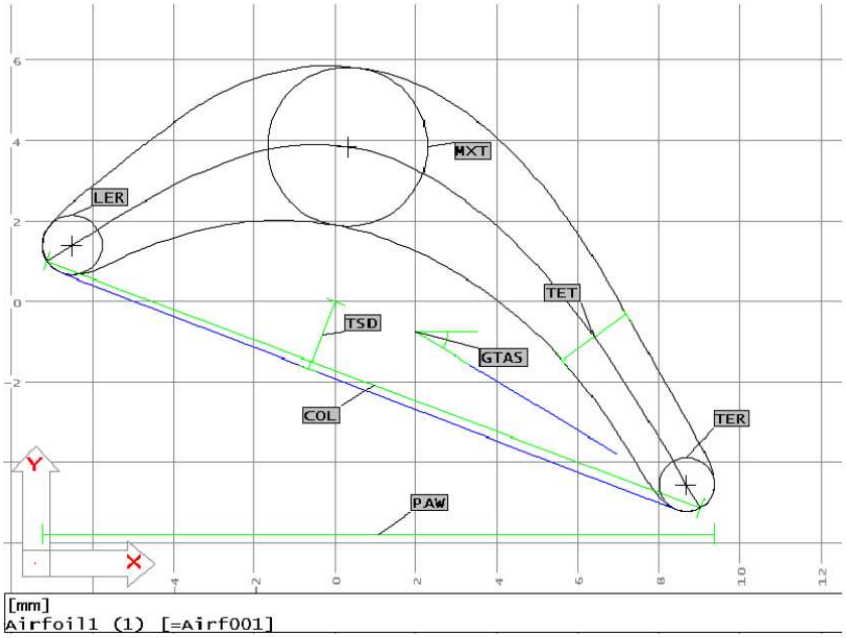

Figure 6.12 - *MAFIS* Airfoil Profile Analisys Output [15]

Through the pop-up dialogue window illustrated in Figure 6.13, the user should be able to select the analysis functions corresponding to the airfoil dimensions that are relevant to inspect. The calculated values will be stored in the computer system and could possibly be exported to a database.

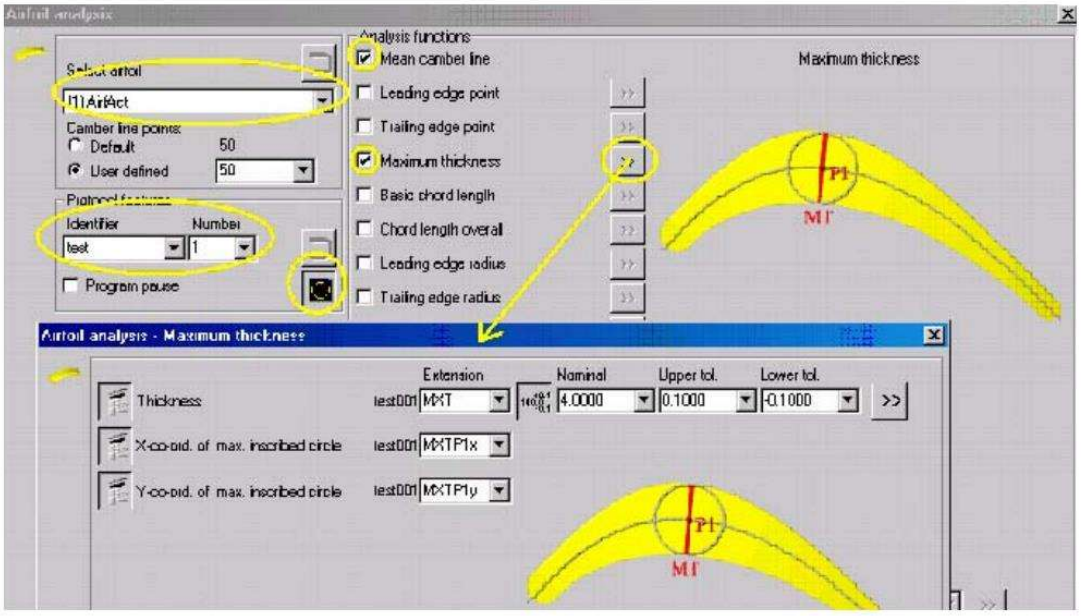

Figure 6.13 - *MAFIS* Profile Analisys Settings [15]

Through this tool, it is possible to convert the airfoil profile in an array of values corresponding to the relevant airfoil dimensions allowing TAP to assess the blade's dimensions according to the ESM specifications. Furthermore, by building a database of this information from both used and new blades, TAP may be able to develop a considerably precise correlation study between the HPC blade's main features and the engine's performance as it was the ultimate goal of this work.

If TAP achieves this, similar work could be developed for other engine parts, namely fan blades which, similarly to the HPC blades, are thought to have a great impact in the engine's performance. The knowledge taken from these correlation studies could ultimately be used to optimize MRO procedures concerning the repair and substitution of these blades.

However, the processing of several airfoil profiles as well as the memory capacity to store the amount of information required by the software raises some concerns. Although MAFIS provides tools that correspond to what TAP is looking to include in airfoil inspection, it may generate some unpredicted challenges.

All in all, the various CMM software modules should be explored following the order of their complexity in terms of programming. This would allow us to determine which one works best for the whole set assembled on the fixture tool and which one fits the dimensional inspection requirements better. Hopefully, the final HPC blade's dimensional program will be able to provide the shop with the desired information for the correlation study without extending the blade's inspection time.

7 Conclusions

The initial proposal for this work's development was to develop a fixture tool for the dimensional inspection of HPC blades. However, to fulfill TAP's main goal of developing a correlation study between the HPC blade's dimensions and the turbofan engine's performance output, there was the need to implement a new dimensional inspection procedure in order to provide TAP engineers with the data necessary for this study.

This goal was largely associated with the use of the Coordinate Measuring Machine available in shop to inspect the blade's airfoil geometry due to this component's geometric complexity and quantity. This resulted in the development of a fixture tool that would display a full set of blades of an HPC stage for the CMM to inspect.

However, this tool's design and its potential for the CMM inspection program required knowledge of the blade's dimensions, some of which TAP engineers did not have access to. For this and other reasons, TAP Engine's Shop acquired a 3D scanner that allowed the development of CAD models for the blades. These models were essential in the design of the fixture tool's and may be very helpful in the development of the CMM's dimensional inspection program based on these model's CAD data.

With both the CAD models for the HPC blades and the fixture tools to display a full set of blades on the CMM table, this work accomplished two of the three stages that are required to acquire the dimensional data for the correlation study mentioned, which are displayed in the diagram below.

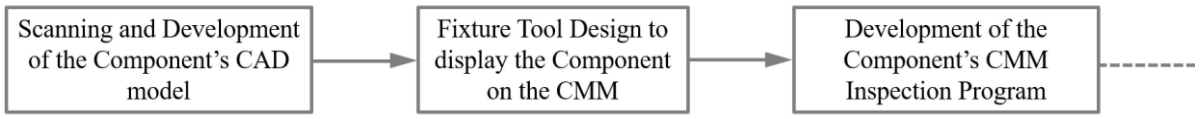

Figure 7.1 - Early Stage Developments for Airfoil Dimensional Data Acquisition

Once the CMM inspection program is fully developed and tuned, TAP's main intention is to inspect the sets of blades before HPC rotor assembly and then associate the results of this inspection with the performance output results from the engine's performance test. This analysis could provide new information concerning the recommended airfoil dimensions thus allowing TAP engineers to adjust said values. Concerning this, these stages described could follow the developments of this work as illustrated in the diagram below.

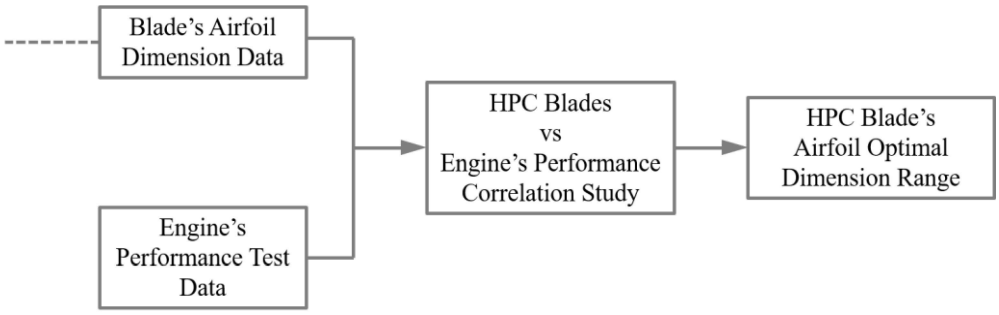

Figure 7.2 - HPC Blade's and Engine's Performance Correlation Study End Stages

Given the compressor role in the engine's performance, this could help TAP's Engine Shop get better results. Ultimately, this means that the engine's overhaul contract specifications could be achieved in less time and with fewer resources, thus providing TAP M&E with more profit margin on engine MRO services.

Even if these benefits are somewhat farfetched at such an early stage of these project, this still proves the potential that lies in the development of this work and the interest of TAP's Engine's Shop in such study. Furthermore, the process described in the conjunction of both diagrams above could be repeated to any other engine's component with similar characteristics further enhancing the potential that lies in the development of such projects like these.

7.1 Achievements

Concerning this project's potential as abovementioned, this work completes the two first stages of the implementation of a CMM dimensional inspection program for the HPC blades. These refer to the development of the HPC blade's CAD models and the design of a fixture tool to display the blades for CMM dimensional inspection.

The models for the blades were developed by tracing different blade profiles through the mesh models provided by the 3D Scanner. However, the mesh models themselves presented dimensional deviations from the real blade caused by the conversion from the point cloud acquired by the scanner to the mesh model used in *SolidWorks*.

In addition to this, the profiles of the blades that were traced also deviate from the mesh model which causes the final CAD models to be inaccurate both in terms of blade geometry and its dimensions. This becomes more noticeable in the blade's airfoil geometry due to its higher difficulty to scan and model.

However, with the help of some dimensions provided by the blade's chapter in the Engine's Shop Manual, the blade's profiles and respective dimensions were adjusted to better correspond to their real counterparts. With this, the CAD models developed may be accurate enough to serve as reference models to use in the fixture tool's design and CMM programming.

For this work, the reference CAD models were developed for the first five compressor stages as displayed in Figure 7.3. Other compressor stages were discarded as latter stages have less impact in compressor efficiency partly because these stages are subject to less deterioration. Regardless of that, this work presents a step-by-step explanation on how to develop the blade's reference models which can still be applied to the remaining stages.

Figure 7.3 - Rendered Imagem of HPC Blade's CAD Reference Models (Stages 1 to 5)

With these models, slot profiles were designed to fit each blade's dovetail section emulating the mating surfaces used in the compressor's rotor assembly. Then, these profiles in conjunction with other features were developed concerning the established design parameters that would meet the functional requirements for the fixture tools.

As a result of this work's design segment, four fixture tools were developed to display a full set of each of the first five stages of the HPC blades. These tools display the blades in such position that allows the CMM to inspect the blade's most relevant features, namely the airfoil dimensions.

These tools were designed to meet TAP's Engine's Shop needs and for this purpose, this design's main goal was to allow for an automated CMM inspection of a full set of blades while requiring low setup times for the blades inspection program. Primarily, this meant that large quantities of blades would have to be easily assembled on the tools while the tool itself would have to be easily maneuvered.

This culminated in the development of aluminum machined tools with four rows of blade slots distanced accordingly to the requirements for the CMM probe's access and to the available workvolume of the CMM. Other features were then added to allow for the tool's manufacturing and transportation thus resulting in the final pieces as displayed in Figure 7.4.

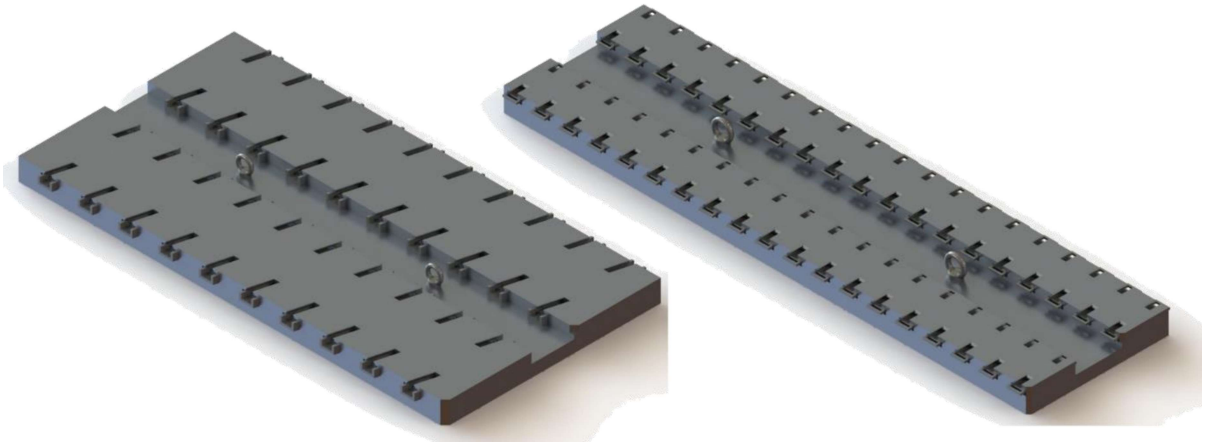

Figure 7.4 - Rendered Images of the Designed Fixture Tools (Stage 1 and Stage4/5)

Prototypes from sections of some of these tools were built from 3D printed models and were tested in shop for some design validation with positive feedback from TAP Engineers. Despite this, the full pieces designed have yet to be manufactured and may require some adjustments that were not yet noticed through the virtual models.

All in all, this work is considered successful for this first iteration of the tools' design. Nevertheless, there are still many things to be tested concerning the tool's usage in conjunction with the CMM which can only be done after these tools have been manufactured. In this regard, the CAD models of both the tools and respective blades will be saved for future changes and adaptations.

7.2 Future Work

As it was already stated, although this work accomplishes much of what was intended, it is only part of a larger scale project with the purpose of improving TAP's Engine's Shop dimensional inspection of the HPC blades. Concerning this goal, there is still many aspects of this project to be explored especially concerning the use of the Coordinate Measuring Machine.

Firstly, this work's development only covers the compressor rotor stages 1 to 5 due to their decreasing relevance in compressor performance. In this case, however, the tools and their respective blade models for the remaining stages could be easily developed following the CAD models and design

procedures described in this work's development. For this, the CAD files developed may be used as a template, requiring few adjustments to include the latter of the nine compressor stages.

Secondly, but perhaps more important, the CMM automated program for the dimensional inspection of the HPC blades must be developed. For this, there are many possible approaches that one can choose depending on the complexity of the inspection program. Chapter 6 covers some of these possibilities that could present great potential for this future development.

Despite this, it is recommended to develop an inspection program based on the machine's *Learn and* Repeat mode at the first stage of this work as a means to test the tool and provide this whole project some validation to continue further.

Nevertheless, for future developments, the CAD models of the tools with the blades assembled may be key to develop more complex CMM part programs. These models, as the one depicted in Figure 7.5, will enable offline programming of the CMM and will allow the developer to accurately probe certain blade dimensions which wasn´t possible using *Learn and Repeat*.

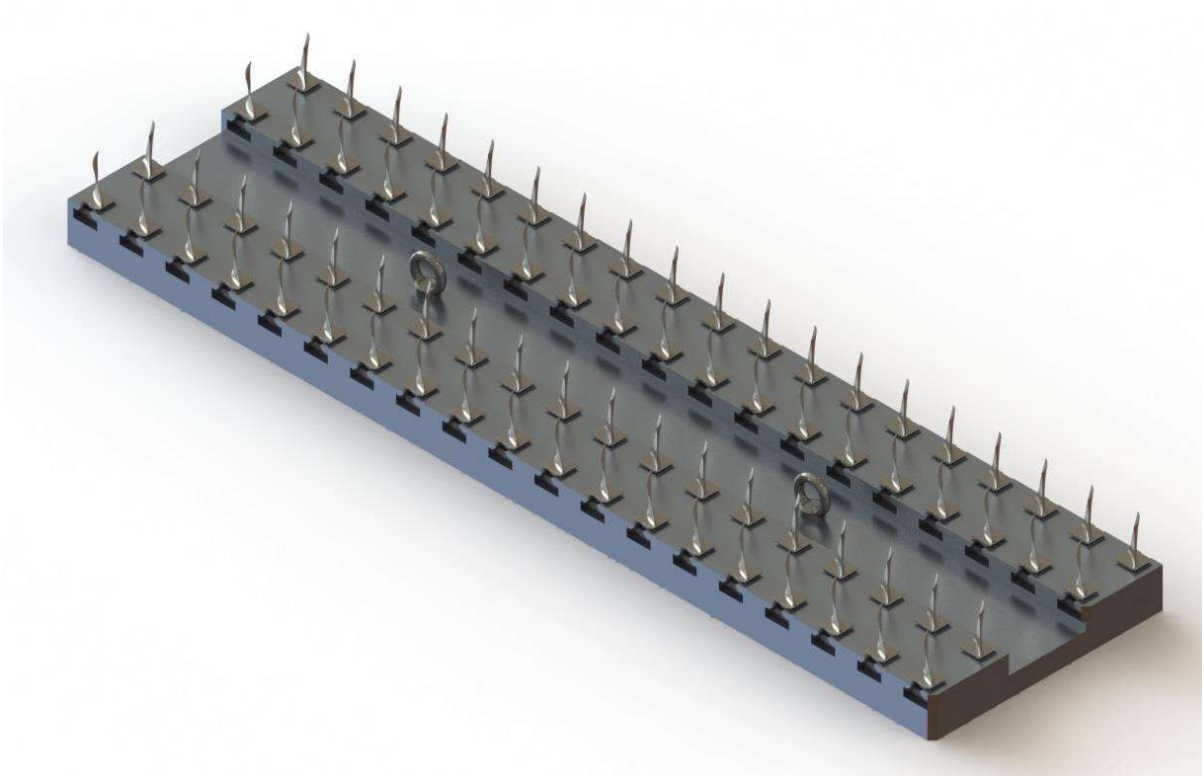

Figure 7.5 - Rendered Image of Fixture Tool with Blades Assembled

Once the CMM inspection program is developed and tuned, the blade's airfoil dimensional data can be acquired for the blade sets used in an engine's compressor rotor assembly. This information should be paired with the engine's performance test results.

Once TAP engineers acquire this information for a number of engines, a correlation study on the data obtained could be developed. The ultimate goal of this study would be to determine the optimal range for the airfoil dimensions and apply this knowledge when arranging these sets of blades. This could also result in changes in the rotor assembly procedures as blades within the optimal range would be evenly spaced along the compressor, for example.

Eventually, analyzing and discussing the data for this correlation study will require a lot of experimenting as several other engine's modules will influence the engine's test results. However, if enough resources are allocated to this study, this factor could be eliminated by maintaining other engine modules and varying only the compressor's rotor module.

In sum, although this work focuses on the implementation of the CMM inspection program for HPC blades, it is part of a larger project to improve TAP engine's shop MRO effectiveness concerning the high pressure compressor rotor. Also, the project envisioned in this work could also be applied similarly to many other engine's components that are thought to play a big role in the engine's efficiency. Fan blades are a great example of this, as they are known for their impact in the engine's performance and, similarly, lack a highly detailed dimensional inspection.

This project, despite requiring considerable time and resources to conclude, would give TAP engineers the tools they need to better understand the engine's behavior, thus allowing to adjust the engine's MRO procedure. Ultimately, this would save TAP's time and resources when overhauling the engines and could ultimately allow the company to accept more contracts with greater profit margins.

References

[1] AGOSTINHO, O., RODIRGUES, A., LIRANI, J. – *Princípios de Engenharia de Fabricação Mecânica – Tolerâncias, Ajustes, Desvios e Análise de Dimensões.* Editora Edgard Blucher, Ltda, São Paulo, 1977.

[2] BAMMERT, K., & WOELK, G. U. - *The Influence of the Blading Surface Roughness on the Aerodynamic Behavior and Characteristic of an Axial Compressor. ASME Journal of Engineering for Power, Vol. 102(2), 283. Germany. April 1980.*

[3] BAPTISTA, F. M. C. - *A 0-D Off-Design Performance Prediction Model of the CFM56-5B Turbofan Engine*. Instituto Superior Técnico. Lisboa, Portugal. October 2017.

[4] BUDYNAS, RICHARD G. AND NISBETT, J. KEITH – *Shigley's Mechanical Engineering Design*. McGraw-Hill, Ninth Edition.

[5] CFMI Customer Training Center - *Training Manual CFM56-5B, Basic Engine*. December 2000.

[6] CHEVALIER, A. – *Guide du Dessinateur industriel*. Hachette Technique, Paris 1989.

[7] FERREIRA, E – *Guia de Apoio à Operação com a CMM Mitutoyo*. TAP Maintenance and Engineering, Fevereiro, 2020.

[8] GIEBMANNS, A., SCHNELL, R., STEINERT, W., HERGT, A., NICKE, E. and WERNER-SPATZ, C. - *Analyzing and Optimizing Geometrically Degraded Transonic Fan Blades by Means of 2D and 3D Simulations and Cascade Measurements.* Proceedings of ASME Turbo Expo 2012. Copenhagen, Denmark. June 2012.

[9] KRONE, J. H.,FRIEDRICHS, J., STADING, J. - *Performance Study Of Deterioration Effects Of A Jet Engine High Pressure Compressor Stage*. DLRK Conference. Berlin, Germany. 2012.

[10] LAKSHMINARAYANA, B. AND HORLOCK, J. H. – Leakage and Secondary Flows In Compressor Cascades. Aeronautical Research Council Reports and Memoranda, R. & M. No. 3483. Liverpool, England. March 1965.

[11] LESJÖFORS GAS & STOCK SPRINGS – *The Spring Catalogue #15,* accessed June 8th, 2020. https://www.lesjoforsab.com/products/stock-springs/ .

[12] MARX, J., STADING, J., REITZ, G. AND FRIEDRICHS, J. - *Investigation And Analysis Of Deterioration In High Pressure Compressors*. DLRK Conference. Stuttgart, Germany. September 2013. [DOI 10.1007/s13272-014-0118-z]

[13] *MatWeb's Aluminum 6061 Material Property Data* – Retrieved from http://www.matweb.com/search/DataSheet.aspx?MatGUID=d5ea75577b1b49e8ad03caf007db5ba8&ckck=1 .

[14] MEC WOLF SRL - *Extract from standard DIN 580:2010, translation into and comment by the English company,* accessed July, 29th in https://www.mecwolf.today/en-download-documents.

[15] MITUTOYO – *Airfoil Analysis MAFIS - Short Instructions MCOSMOSv2.3*. Mitutoyo Europe GmbH, Neuss, issued in March, 2004.

[16] MITUTOYO –*User's Manual V4.2 - CAT1000PS.* Mitutoyo Europe GmbH, Neuss, issued in January, 2014.

[17] MITUTOYO –*User's Manual V4.2 - GEOPAK.* Mitutoyo Europe GmbH, Neuss, issued in June, 2017.

[18] MOURÃO, A. – *Cálculo de Tolerâncias Geométricas*. FCT-NOVA, Departamento de Engenharia Mecânica e Industrial. Liboa, Portugal, 2004

[19] RECRUDE, T. M. - *Desenvolvimento De Um Processo Para Correlacionar A Performance Do Motor CFM56-5B Com As Cordas Das Pás Do Seu Compressor De Alta Pressão*. FCT-NOVA. Lisboa, Portugal. December 2018.

[20] REID, K., DENTON, J., PULLAN, G., CURTIS, E. and LONGLEY, J. – *The Interaction Of Turbine Inter-Platform Leakage Flow With the Mainstream Flow.* ASME Journal of Turbomachinery Vol.129/303.Edmonton, AB, Canada. April 2007. [DOI: 10.1115/1.2162592]

[21] REITZ, G. and FRIEDRICHS, J. - *Procedure for Analyzing, Manipulating and Meshing of Compressor Blades to Simulate their Flow*. International Journal of Gas Turbine, Propulsion and Power Systems Vol.8 Nr.1. Braunschweig, Germany. May 2016.

[22] REITZ, G., DWINGER, K., SCHLANGE, S., FRIEDRICHS, J. and KAPPEI, F. - *Analysis of jet engine compressor deterioration and capturing correlations between geometric parameters. 16th International Symposium on Transport Phenomena and Dynamics of Rotating Machinery.* ISROMAC. Honolulu, United States. April 2016.

[23] REITZ, G., FRIEDRICHS, J., MARX, J. and STADING, J. - *Performance Analysis Of Deteriorated High Pressure Compressor Blades*. Proceedings of ASME Turbo Expo 2014: Turbine Technical Conference and Exposition GT2014. Düsseldorf, Germany. June 2014.

[24] RENISHAW – *REVO-2's RSP2 system*. Retrieved from https://www.renishaw.com/cmmsupport/knowledgebase/en/rsp2--22120

[25] RENISHAW – *Styli and accessories.* Technical Specifications H-1000-3200-16-B issued in September 2016.

[26] ROBERTS, W. B., ARMIN, A., KASSASEYA, G., SUDER, K. L., THORP, S. A. and STRAZISAR, A. J. – *The Effect Of Variable Chord Length On Transonic Axial Rotor Performance.* ASME Journal of Turbomachinery Vol.124/351. Cleveland, OH, United States. July 2002. [DOI: 10.1115/1.1459734]

[27] ROLLS-ROYCE – *The Jet Engine*. Fifth Edition, Derby, England. Rolls-Royce Plc, 1996. ISBN 0902121 235.

[28] SALLEE, G. P., KRUCKENBERG, H. D. and TOOMEY E. H. – *Analysis Of Turbofan Engine Performance Deterioration And Proposed Follow-On Tests*. Prepared for National Aeronautics and Space Administration. pp. 22-32. July 1975.

[29] SOGUT, M. Z., YALCIN, E. AND HIKMET KARAKOC, T. - *Assessment of degradation effects for an aircraft engine considering exergy analysis*. Energy, Volume 140, Part 2. ISSN 0360-5442. 2017.

[30] TABAKOFF, W., LAKSHMINARASIMHA, A. N., PASIN, M. - *Simulation Of Compressor Performance Deterioration Due To Erosion*. ASME Paper No. 89-GT-182. Toronto, Canada. June 1989.

[31] TAP M&E – *CFM56 Series -3/-5A/-5B/-5C/-7B Formação Profissional*. December 2015.

[32] TECHNIFAST – *Precision Engineered Components*, accessed July 29th, 2020. https://technifast.co.uk/dowel-pins

[33] TREAGER, I. – *Aircraft Gas Turbine Technology*. Glencoe Aviation Technology Series. McGraw-Hill, Third Edition.

[34] VEIGA DA CUNHA, L. – *Desenho Técnico*. Fundação Calouste Gulbenkian, 15ª Edição.

[35] WOZNIAK, A., DOBOSZ, M. – *Factors Influencing Probing Accuracy of a Coordinate Measuring Machine, in* IEEE Transactions on Instrumentation and Measurement 54(6):2540-2548. December 2005.

Appendix I – HPC Efficiency Concerning New Blade Percentage Per Stage – [3]

Appendix II –Dimensions from ESM's Repair Procedures for HPC Blades

Appendix III –Summary of ESM's Dimensional Inspection Specifications

Appendix IV – *Lesjofors*' Spring Catalogue Relevant Information – [11]

Appendix V – *Technifast*'s Dowel Pin Specifications – [32]

Appendix VI –Lifting Eye Bolts/Nuts DIN580 Summary Brochure – [14]

Appendix VII –Economic and Maximum Manufacturing Deviations – [1]

Appendix VIII – Stage 1 Tool's Assembly Technical Drawing

Appendix IX – Stage 1 Tool's Bottom Component Technical Drawing

Appendix X – Stage 1 Tool's Top Component Technical Drawing

Appendix XI – Stage 1 Tool's Upwards Force Bar Technical Drawing

Appendix XII – Stage 1 Tool's Spacer Technical Drawing

Appendix XIII – Stage 2 Tool's Assembly Technical Drawing

Appendix XIV – Stage 2 Tool's Bottom Component Technical Drawing

Appendix XV – Stage 2 Tool's Top Component Technical Drawing

Appendix XVI – Stage 2 Tool's Upwards Force Bar Technical Drawing

Appendix XVII – Stage 2 Tool's Spacer Technical Drawing

Appendix XVIII – Stage 3 Tool's Assembly Technical Drawing

Appendix XIX – Stage 3 Tool's Bottom Component Technical Drawing

Appendix XX – Stage 3 Tool's Top Component Technical Drawing

Appendix XXI – Stage 3 Tool's Upwards Force Bar Technical Drawing

Appendix XXII – Stage 3 Tool's Spacer Technical Drawing

Appendix XXIII – Stage 4&5 Tool's Assembly Technical Drawing

Appendix XXIV – Stage 4&5 Tool's Bottom Component Technical Drawing

Appendix XXV – Stage 4&5 Tool's Top Component Technical Drawing

Appendix XXVI – Stage 4&5 Tool's Upwards Force Bar Technical Drawing

Appendix XXVII – Stage 4&5 Tool's Spacer Technical Drawing

Appendix XXVIII – Adjusted Dowel Pin Technical Drawing

Appendix I

HPC Efficiency Concerning New Blade Percentage Per Stage

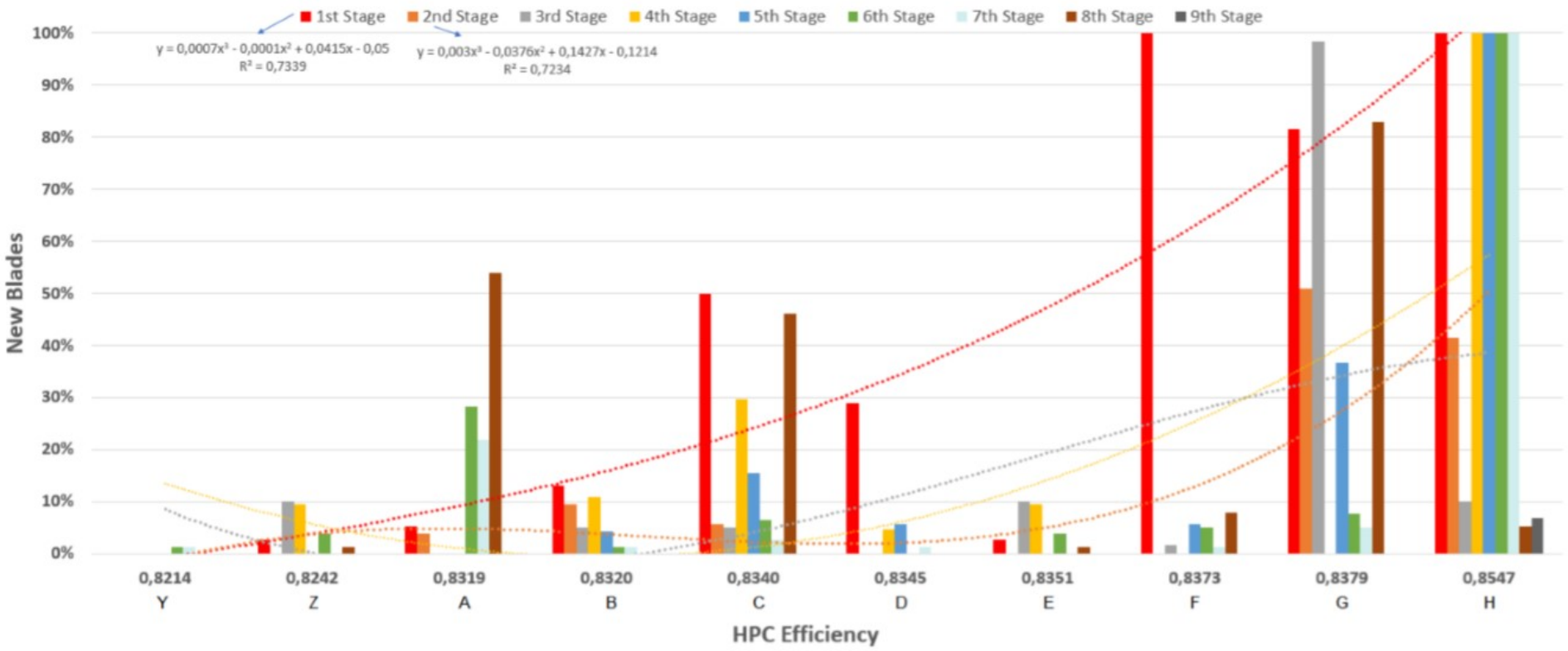
1st Stage
2nd Stage
3rd Stage
4th Stage
5th Stage
6th Stage
7th Stage
8th Stage
9th Stage
y = 0,0007x³ - 0,0001x² + 0,0415x - 0,05
R² = 0,7339
y = 0,003x³ - 0,0376x² + 0,1427x - 0,1214
R² = 0,7234
New Blades
100%
90%
80%
70%
60%
50%
40%
30%
20%
10%
0%
0,8214 Y
0,8242 Z
0,8319 A
0,8320 B
0,8340 C
0,8345 D
0,8351 E
0,8373 F
0,8379 G
0,8547 H
HPC Efficiency

Appendix II

Dimensions from ESM's Repair Procedures for HPC Blades

HPC STG 1 Blade

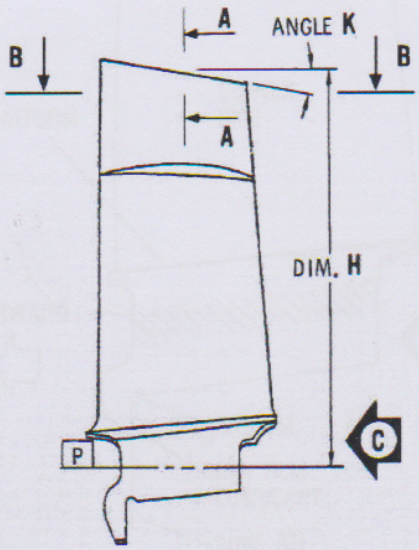

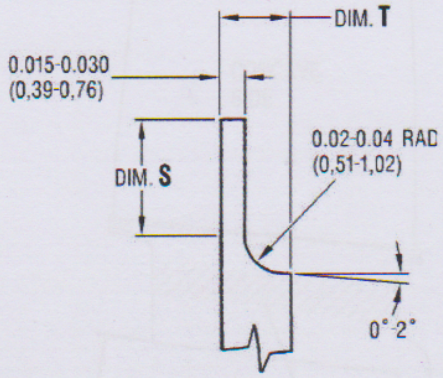

SECTION A-A

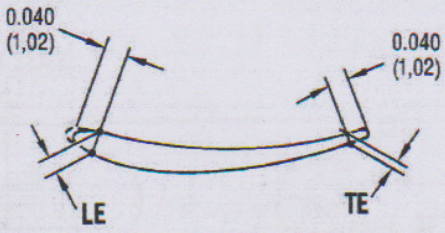

SECTION B-B

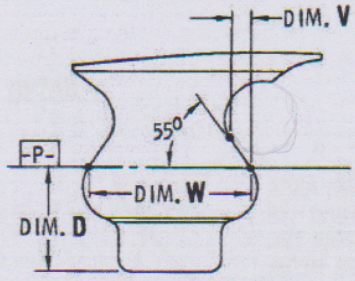

VIEW C

NOTE:
DIMENSIONS ARE IN INCHES WITH MILLIMETERS IN PARENTHESES.

Description	Minimum In-Process Dimension	Maximum In-Process Dimension	Minimum Finish Dimension	Maximum Finish Dimension	Reference Dimension
Dim. D	--	--	--	--	0.478 in. (12,14 mm)
Dim. H	3.636 in. (92,36 mm)	--	3.798 in. (96,47 mm)	3.828 in. (97,23 mm)	--
Angle K	--	--	14°35'	15°05'	--
Dim. S	--	--	0.090 in. (2,29 mm)	0.110 in. (2,79 mm)	--
Dim. V	--	--	--	--	0.052 in. (1,32 mm)
Dim. W	--	--	--	--	0.584 in. (14,83 mm)
Dim. LE	--	--	0.025 in. (0,64 mm)	--	--
Dim. TE	--	--	0.016 in. (0,41 mm)	--	--

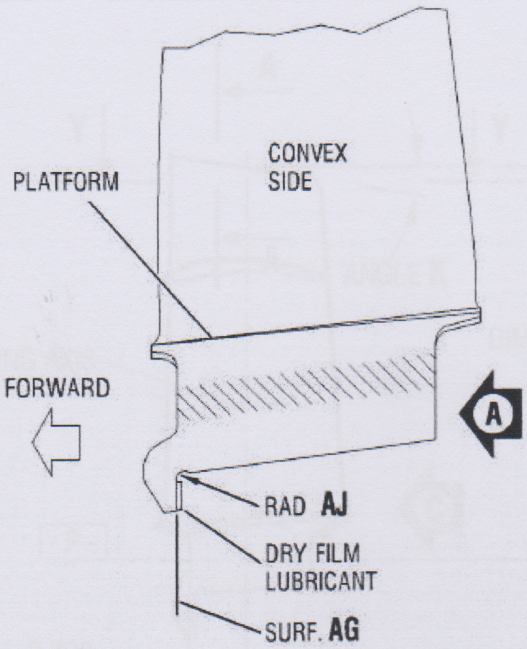

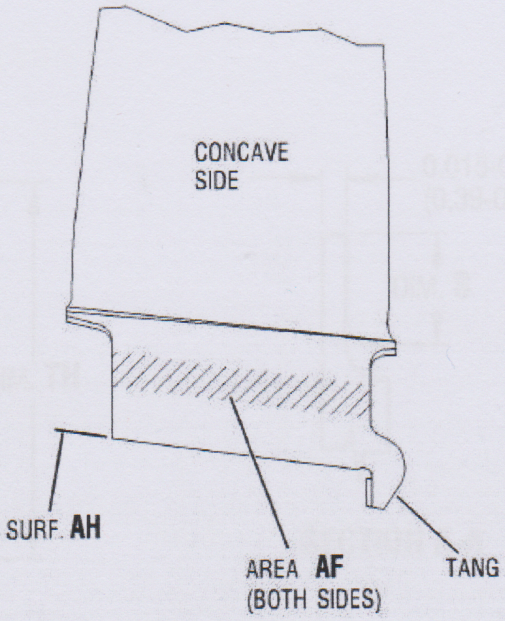

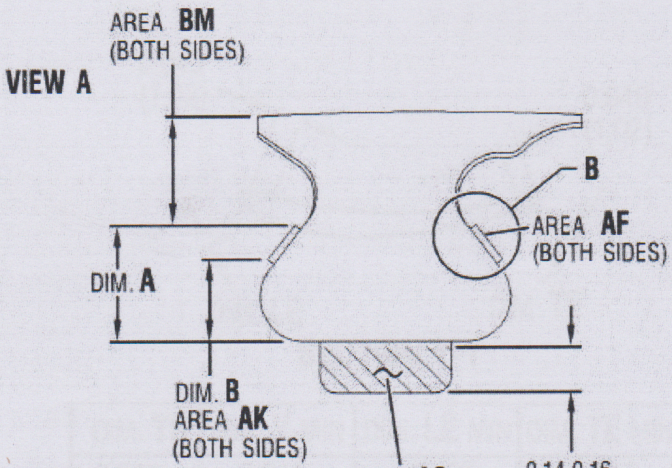

DIM. A	DIM. B
0.335-0.355 (8,51-9,02)	0.185-0.200 (4,70-5,08)

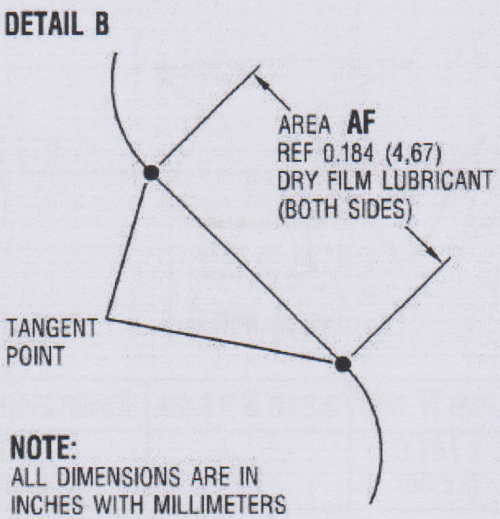

Description	Minimum In-Process Dimension	Maximum In-Process Dimension	Minimum Finish Dimension	Maximum Finish Dimension
Dim. A	--	--	0.335 in. (8,51 mm)	0.355 in. (9,02 mm)
Dim. B	--	--	0.185 in. (4,70 mm)	0.200 in. (5,08 mm)

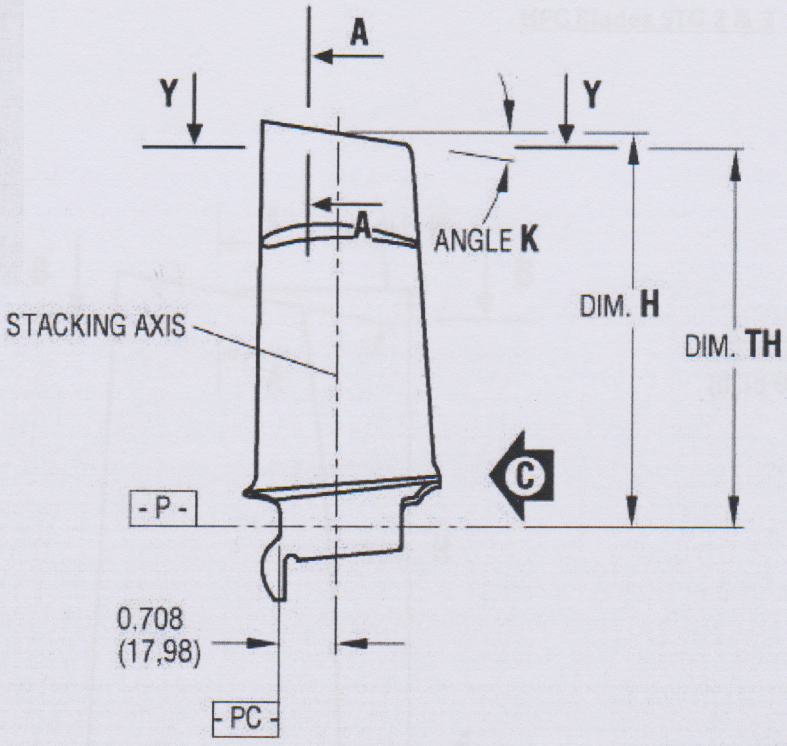

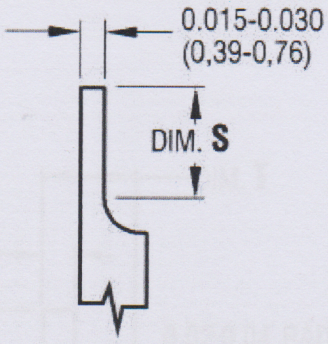

SECTION A-A

DETAIL C

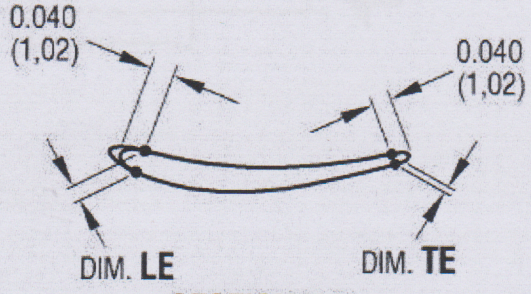

SECTION Y-Y

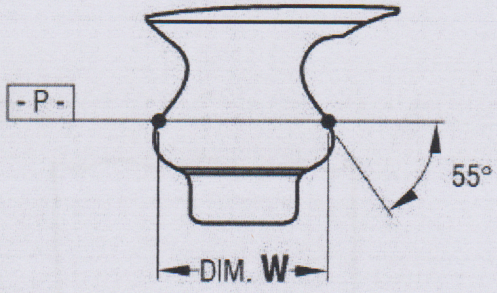

DIM. **TH**	DIM. **Y** MIN	DIM. **LE** MIN	DIM. **TE** MIN	DIM. **W** REFERENCE	ANGLE **K** BASIC	DIM. **H** MIN
3.287 (83,49)	2.241 (56,92)	0.025 (0,64)	0.017 (0,43)	0.584 (14,83)	15.50°	3.761 (95,53)

NOTE:
DIMENSIONS ARE IN INCHES WITH
MILLIMETERS IN PARENTHESES.

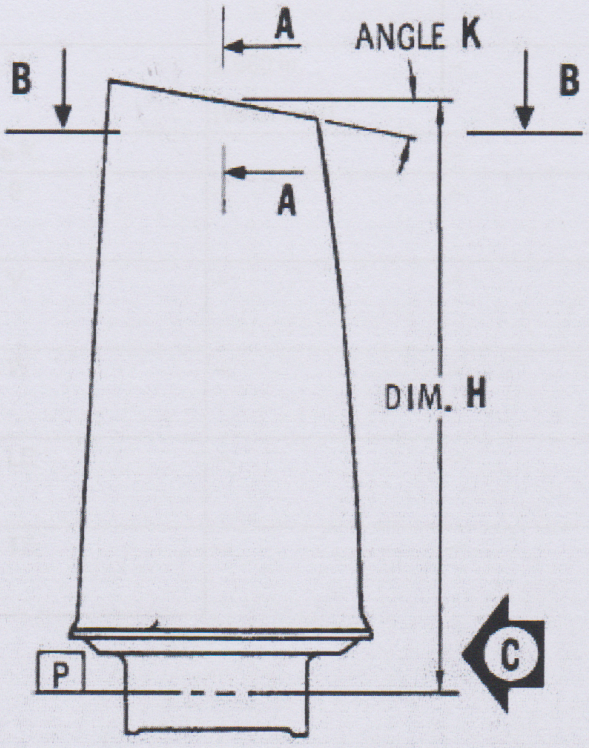

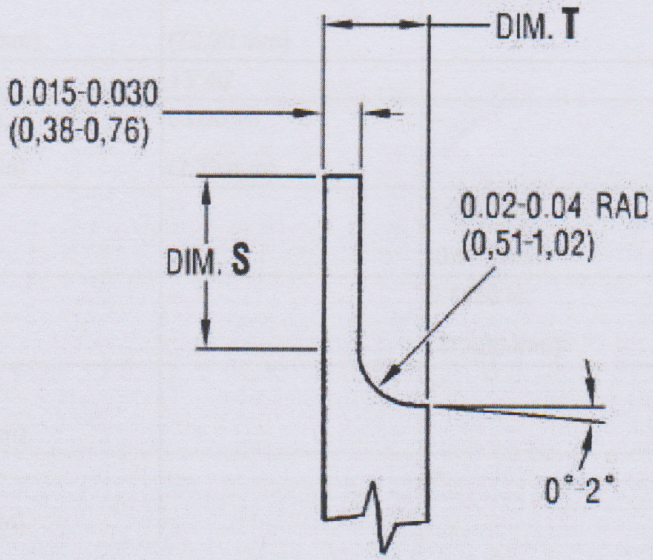

SECTION A-A

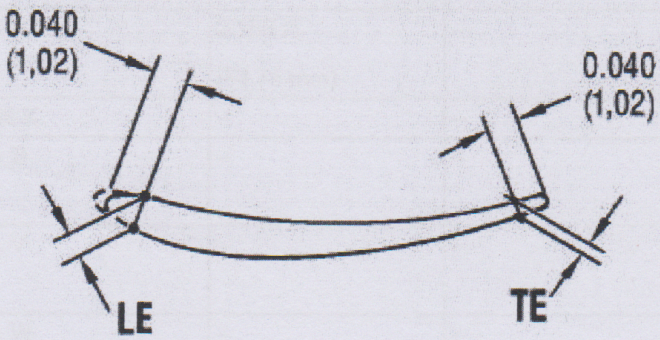

SECTION B-B

VIEW C

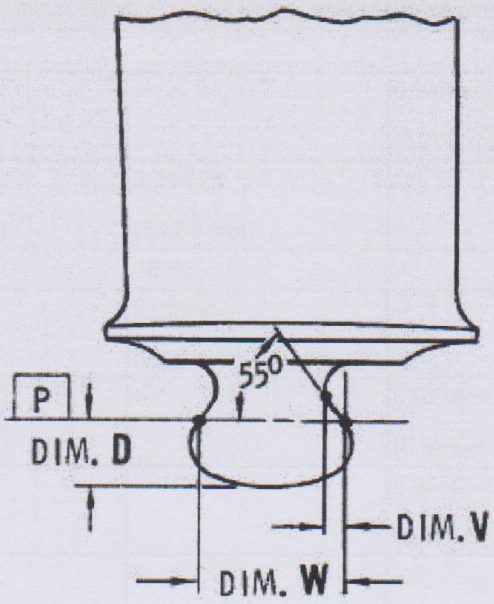

NOTE:
ALL DIMENSIONS ARE IN INCHES WITH MILLIMETERS IN PARENTHESES.

Description	Minimum In-Process Dimension	Maximum In-Process Dimension	Minimum Finish Dimension	Maximum Finish Dimension	Reference Dimension
Stage 2					
Dim. D	--	--	--	--	0.187 in. (4,75 mm)
Dim. H	2.680 in. (68,07 mm)	--	2.840 in. (72,14 mm)	2.870 in. (72,90 mm)	--
Angle K	--	--	13°16'	13°46'	--
Dim. S	--	--	0.070 in. (1,78 mm)	0.090 in. (2,29 mm)	--
Dim. V	--	--	--	--	0.0373 in. (0,947 mm)
Dim. W	--	--	--	--	0.4488 in. (11,400 mm)
Dim. LE	--	--	0.012 in. (0,30 mm)	--	--
Dim. TE	--	--	0.012 in. (0,30 mm)	--	--

Description	Minimum In-Process Dimension	Maximum In-Process Dimension	Minimum Finish Dimension	Maximum Finish Dimension	Reference Dimension
Stage 3					
Dim. D	--	--	--	--	0.1488 in. (3,780 mm)
Dim. H	2.156 in. (54,76 mm)	--	2.298 in. (58,37 mm)	2.318 in. (58,88 mm)	--
Angle K	--	--	9°46'	10°16'	--
Dim. S	--	--	0.065 in. (1,65 mm)	0.085 in. (2,16 mm)	--
Dim. V	--	--	--	--	0.0236 in. (0,599 mm)
Dim. W	--	--	--	--	0.3650 in. (9,271 mm)
Dim. LE	--	--	0.012 in. (0,30 mm)	--	--
Dim. TE	--	--	0.012 in. (0,30 mm)	--	--

Appendix III

Summary of ESM's Dimensional Inspection Specifications

HPC Rotor Blades Dimensional Inspection

Stage 1

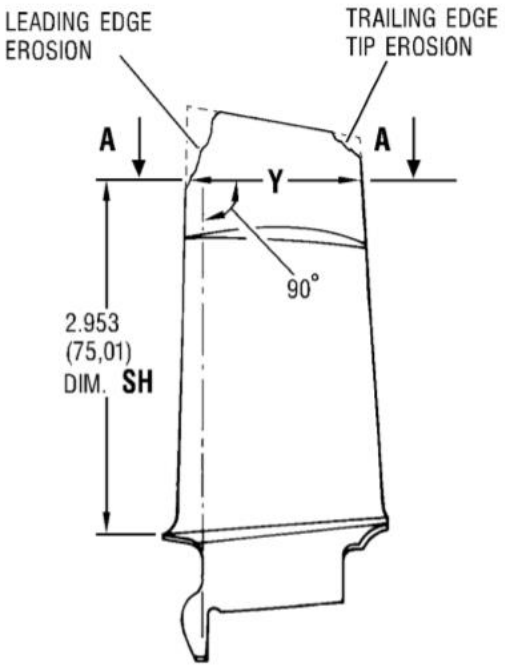

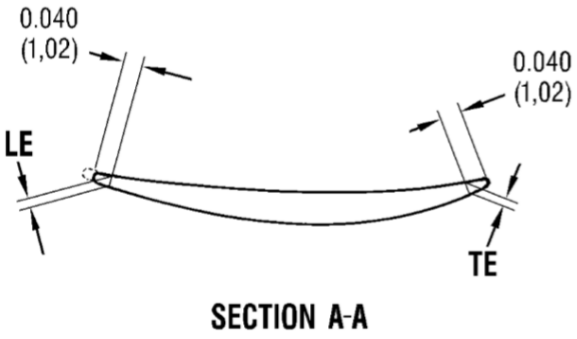

Effect -5B Non 3D DAC & SAC

	Min. Serviceable (in)	Max. Serviceable (in)	Max. Repairable (in)
DIM. Y (chord)	2.260	-	Non Rep.
DIM. LE	0.024	-	Any if Y
DIM. TE	0.016	-	Any if Y
DIM. H (tip length)	3.761	-	3.672

Effect -5B/P DAC.5B/P & SAC

	Min. Serviceable (in)	Max. Serviceable (in)	Max. Repairable (in)
DIM. Y (chord)	2.277	-	Non Rep.
DIM. LE	0.025	0.037	Any if Y
DIM. TE	0.015	-	Any if Y
DIM. H (tip length)	3.761	-	3.636

Effect -5B/3 SAC

	Min. Serviceable (in)
DIM. Y (chord)	2.241
DIM. LE	0.025
DIM. TE	0.0167

Ref. TH 3.287

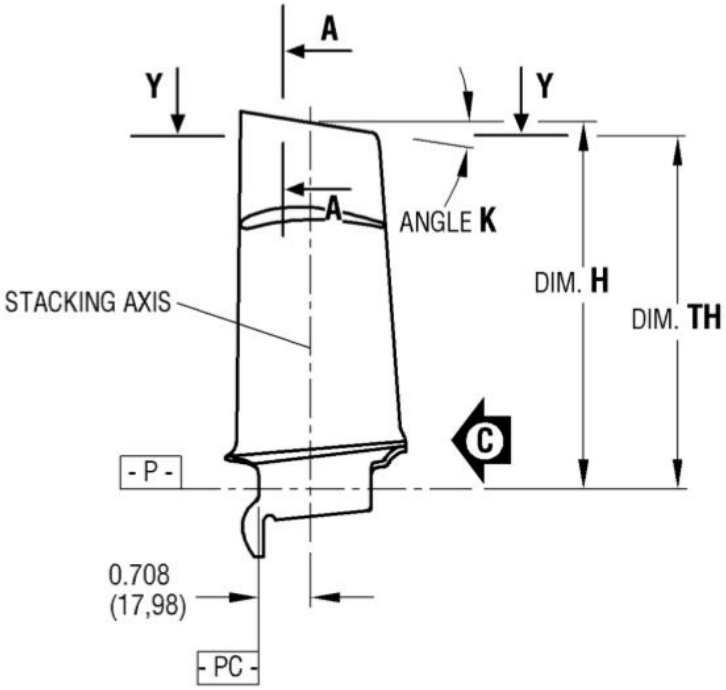

DETAIL C

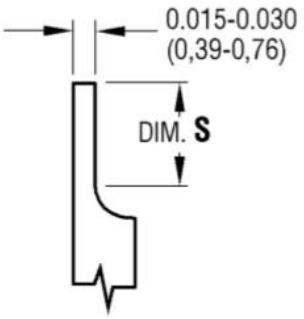

SECTION A-A

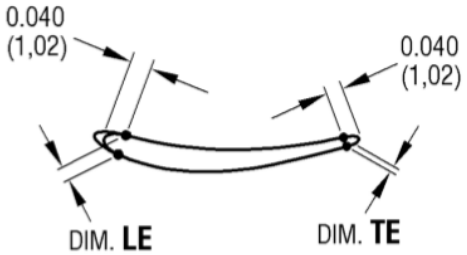

SECTION Y-Y

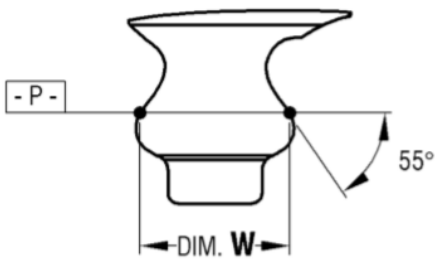

DIM. **TH**	DIM. **Y** MIN	DIM. **LE** MIN	DIM. **TE** MIN	DIM. **W** REFERENCE	ANGLE **K** BASIC	DIM. **H** MIN
3.287 (83,49)	2.241 (56,92)	0.025 (0,64)	0.017 (0,43)	0.584 (14,83)	15.50°	3.761 (95,53)

NOTE:
DIMENSIONS ARE IN INCHES WITH
MILLIMETERS IN PARENTHESES.

1295882-00

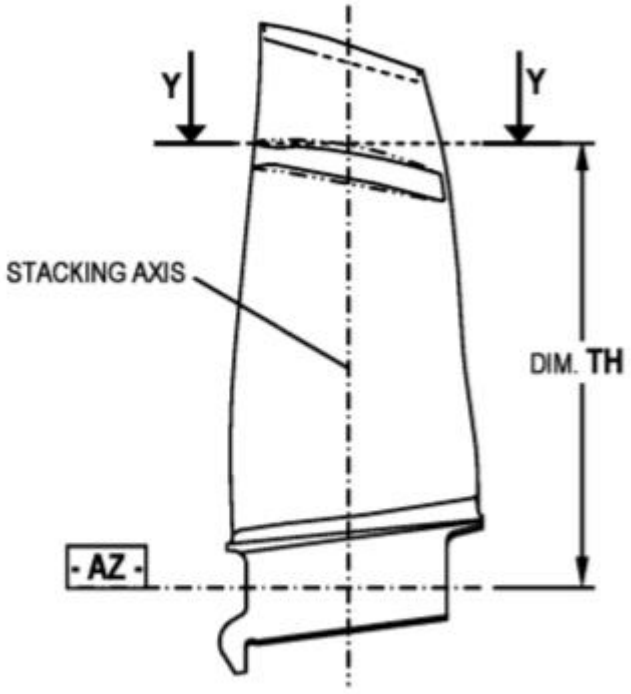

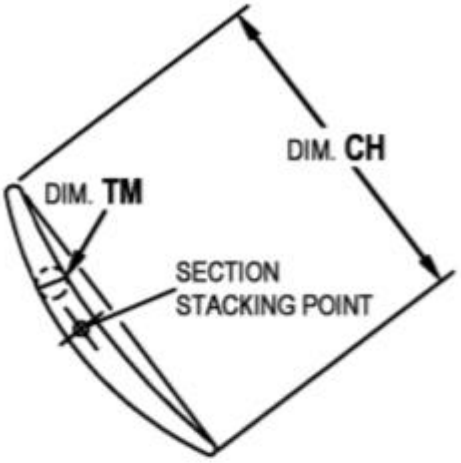

Y-Y

SECTION HEIGHT (DIM. **TH**) REF	MIN REPAIRABLE CHORD LENGTH (DIM. **CH**)	MIN REPAIRABLE AIRFOIL THICKNESS DIM. **TM**
3.455 (87,76)	2.192 (55,68)	0.080 (2,04)

Stage 2 and 3

FOR CFM56-5B SAC 3D Aero; CFM56-5B DAC 3D Aero

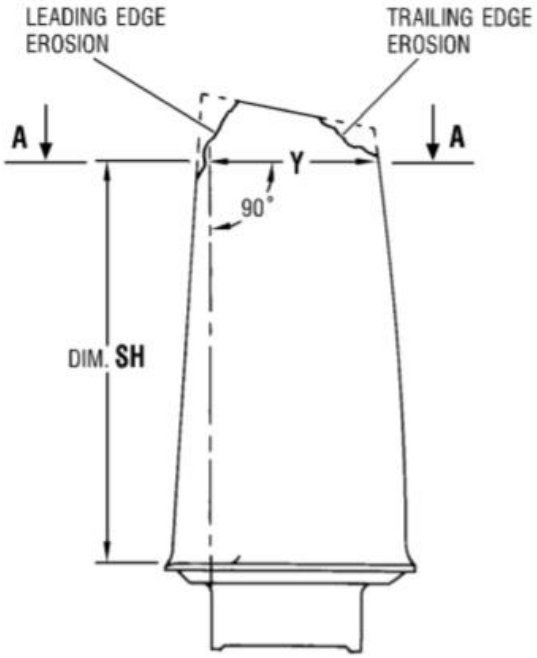

DIM. SH	
STAGE 2	2.033 (51,64)
STAGE 3	1.820 (46,23)

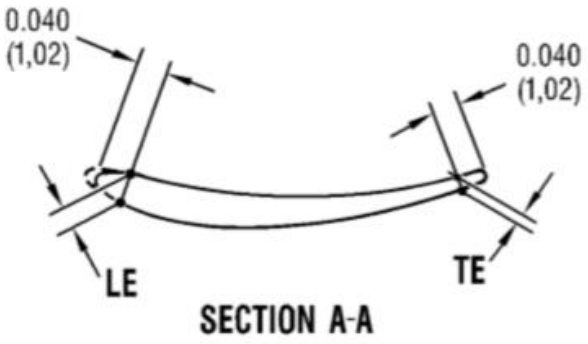

Stage 2

	Min. Serviceable (in)	Max. Serviceable (in)	Max. Repairable (in)
DIM. Y (chord)	1.623	-	Non Rep.
DIM. LE	0.012	0.023	Any if Y
DIM. TE	0.010	-	Any if Y
DIM. H (tip length)	2.826	-	2.700

Stage 3

	Min. Serviceable (in)	Max. Serviceable (in)	Max. Repairable (in)
DIM. Y (chord)	1.269	-	Non Rep.
DIM. LE	0.010	0,037	Any if Y
DIM. TE	0,009	-	Any if Y
DIM. H (tip length)	2.270	-	2.176

FOR CFM56-5B/3 SAC

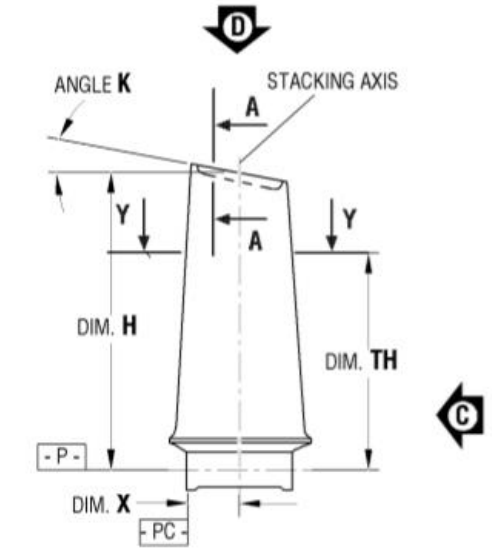

SECTION A-A
SQUEALER TIP

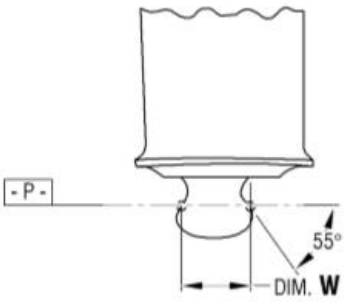

C

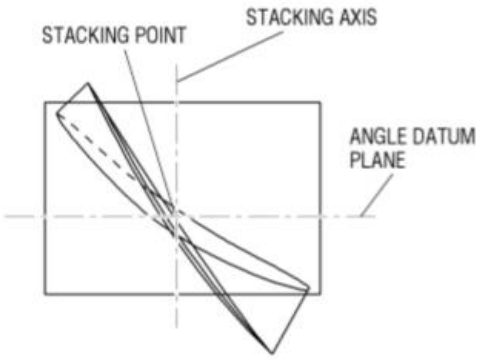

D

STAGE	DIM. TH	ANGLE TT REF	DIM. CH MIN	DIM. LE MIN	DIM. TE MIN	DIM. X REF	DIM. W	ANGLE K BASIC	DIM. H MIN
2	2.336 (59,33)	50.575°	1.602 (40,69)	0.013 (0,33)	0.010 (0,25)	0.490 (12,45)	0.4488 (11,399)	14.70°	2.813 (71,45)
3	2.067 (52,50)	49.303°	1.261 (32,03)	0.010 (0,25)	0.009 (0,23)	0.291 (7,39)	0.3650 (9,271)	11.88°	2.270 (57,66)

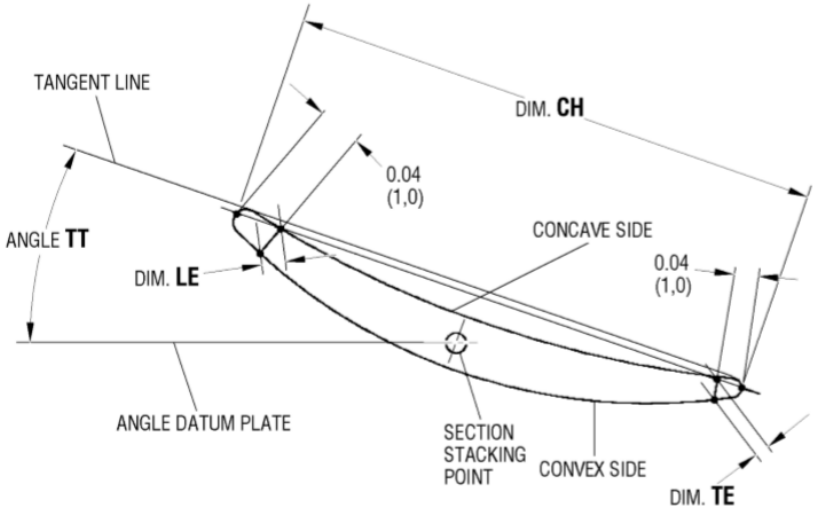

Y-Y

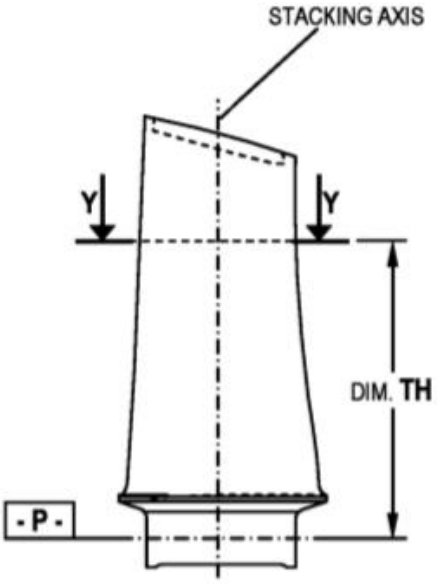

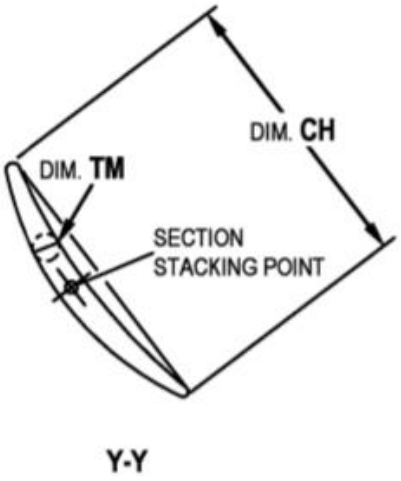

Y-Y

STAGE	SECTION HEIGHT DIM. **TH** REF	MIN REPAIRABLE CHORD LENGTH DIM. **CH**	MIN REPAIRABLE AIRFOIL THICKNESS DIM. **TM**
2	2.590 (65,79)	1.609 (40,87)	0.078 (1,99)
3	2.067 (52,50)	1.266 (32,16)	0.043 (1,10)

Stage 4-9

EFFECT CFM56-5B SAC Non 3D Aero

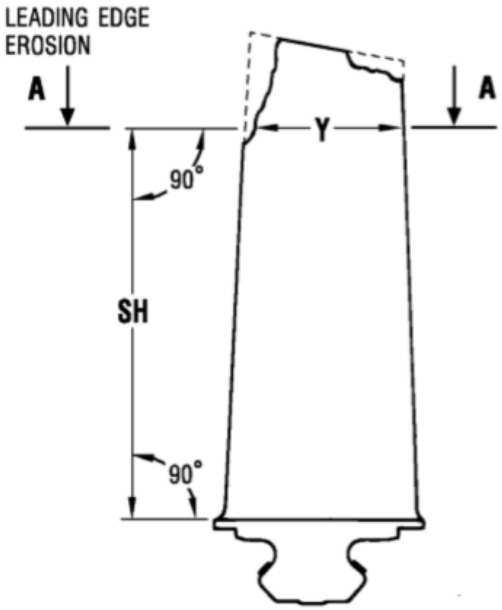

DIM. SH	
STAGE	
4	1.480 (37,59)
5	1.230 (31,24)
6	0.976 (24,79)
7	0.873 (22,17)
8	0.800 (20,32)
9	0.737 (18,72)

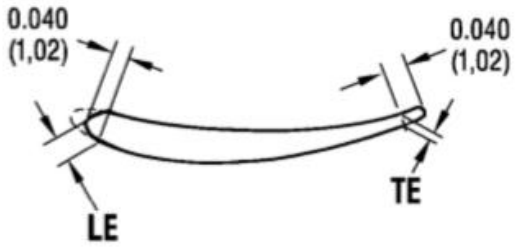

Stage 4

	Min. Serviceable (in)	Max. Serviceable (in)	Max. Repairable (in)
DIM. Y (chord)	1.021	-	1.010
DIM. LE	0.011	0.021	Any if Y
DIM. TE	0.011	-	Any if Y
DIM. H (tip length)	1.850	-	1.750

Stage 5

	Min. Serviceable (in)	Max. Serviceable (in)	Max. Repairable (in)
DIM. Y (chord)	0.871	-	0.862
DIM. LE	0.011	0,023	Any if Y
DIM. TE	0,011	-	Any if Y
DIM. H (tip length)	1.576	-	1.490

Stage 6

	Min. Serviceable (in)	Max. Serviceable (in)	Max. Repairable (in)
DIM. Y (chord)	0.765	-	0.755
DIM. LE	0.010	0.016	Any if Y
DIM. TE	0.010	-	Any if Y
DIM. H (tip length)	1.282	-	1.194

Stage 7

	Min. Serviceable (in)	Max. Serviceable (in)	Max. Repairable (in)
DIM. Y (chord)	0.757	-	0.747
DIM. LE	0.011	0,020	Any if Y
DIM. TE	0,011	-	Any if Y
DIM. H (tip length)	1.172	-	1.093

Stage 8

	Min. Serviceable (in)	Max. Serviceable (in)	Max. Repairable (in)
DIM. Y (chord)	0.800	-	0.790
DIM. LE	0.013	0.020	Any if Y
DIM. TE	0.008	-	Any if Y
DIM. H (tip length)	1.065	-	0.986

Stage 9

	Min. Serviceable (in)	Max. Serviceable (in)	Max. Repairable (in)
DIM. Y (chord)	0.820	-	0,810
DIM. LE	0.013	-	Any if Y
DIM. TE	0,008	-	Any if Y
DIM. H (tip length)	1.038	-	0.959

EFFECT CFM56-5B SAC 3D Aero; CFM56-5B DAC 3D Aero

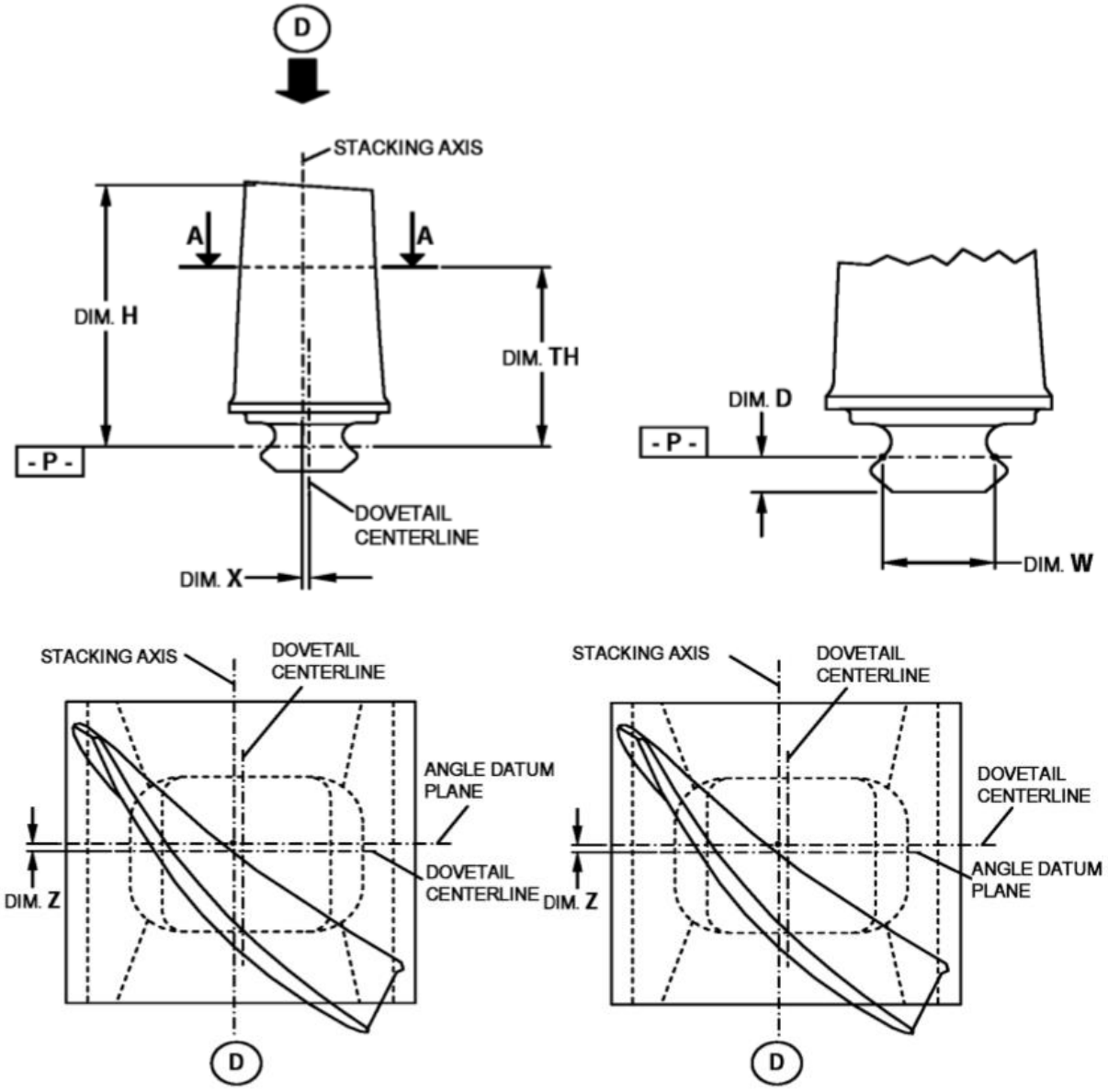

APPLIES FOR STAGES 4-6 AND 8

APPLIES FOR STAGE 7

STAGE	SECTION HEIGHT (DIM. TH)	TWIST ANGLE TT REF	DIM. D	DIM. X	DIM. W	DIM. Z
4	1.543 (39,19)	47.535°	0.160 (4,06)	0.027 (0,69)	0.4272 (10,851)	0.009 (0,23)
5	1.306 (33,17)	47.262°	0.130 (3,30)	0.027 (0,69)	0.4226 (10,734)	0.010 (0,25)
6	1.110 (28,19)	46.095°	0.140 (3,56)	0.032 (0,81)	0.3246 (8,245)	0.010 (0,25)
7	0.983 (24,97)	47.434°	0.140 (3,56)	0.031 (0,79)	0.3446 (8,753)	0.007 (0,18)
8	0.891 (22,63)	52.164°	0.140 (3,56) SEE NOTE 2 0.100 (2,54) SEE NOTE 3	0.045 (1,14)	0.2966 (7,534)	0.006 (0,15)

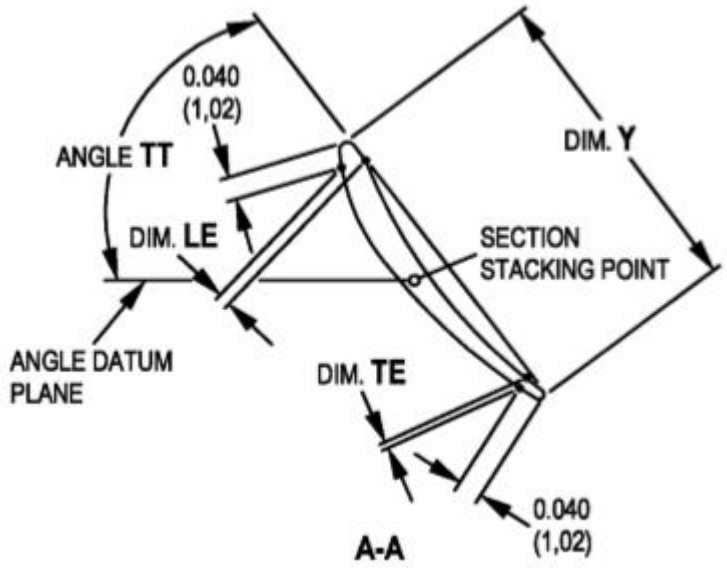

NOTES:

1. DIMENSIONS ARE IN INCHES WITH MILLIMETERS IN PARENTHESES.
2. APPLIES TO PART NUMBERS P338P01, P02, P05, P06, P09, P10, P13 AND P14
3. APPLIES TO PART NUMBERS P338P03, P04, P07, P08, P11, P12, P15 AND P16

Stage 4

	Min. Serviceable (in)	Max. Serviceable (in)	Max. Repairable (in)
DIM. Y (chord)	1.030	-	Non Rep.
DIM. LE	0.013	-	Any if Y
DIM. TE	0.010	-	Any if Y
DIM. H (tip length)	1.852	-	1.763

Stage 5

	Min. Serviceable (in)	Max. Serviceable (in)	Max. Repairable (in)
DIM. Y (chord)	0.869	-	Non Rep.
DIM. LE	0.016	-	Any if Y
DIM. TE	0,010	-	Any if Y
DIM. H (tip length)	1.535	-	1.441

Stage 6

	Min. Serviceable (in)	Max. Serviceable (in)	Max. Repairable (in)
DIM. Y (chord)	0.766	-	Non Rep.
DIM. LE	0.009	-	Any if Y
DIM. TE	0.007	-	Any if Y
DIM. H (tip length)	1.284	-	1.192

Stage 7

	Min. Serviceable (in)	Max. Serviceable (in)	Max. Repairable (in)
DIM. Y (chord)	0.751	-	Non Rep.
DIM. LE	0.013	-	Any if Y
DIM. TE	0,008	-	Any if Y
DIM. H (tip length)	1.160	-	1.069

Stage 8

	Min. Serviceable (in)	Max. Serviceable (in)	Max. Repairable (in)
DIM. Y (chord)	0.792	-	Non Rep.
DIM. LE	0.013	-	Any if Y
DIM. TE	0.007	-	Any if Y
DIM. H (tip length)	1.058	-	0.967

Stage 9

	Min. Serviceable (in)	Max. Serviceable (in)	Max. Repairable (in)
DIM. Y (chord)	0.816	-	0.810 if C rep.
DIM. LE	0.013	-	Any if Y
DIM. TE	0,008	-	Any if Y
DIM. H (tip length)	1.038	-	0.959

EFFECT CFM56-5B/3 SAC

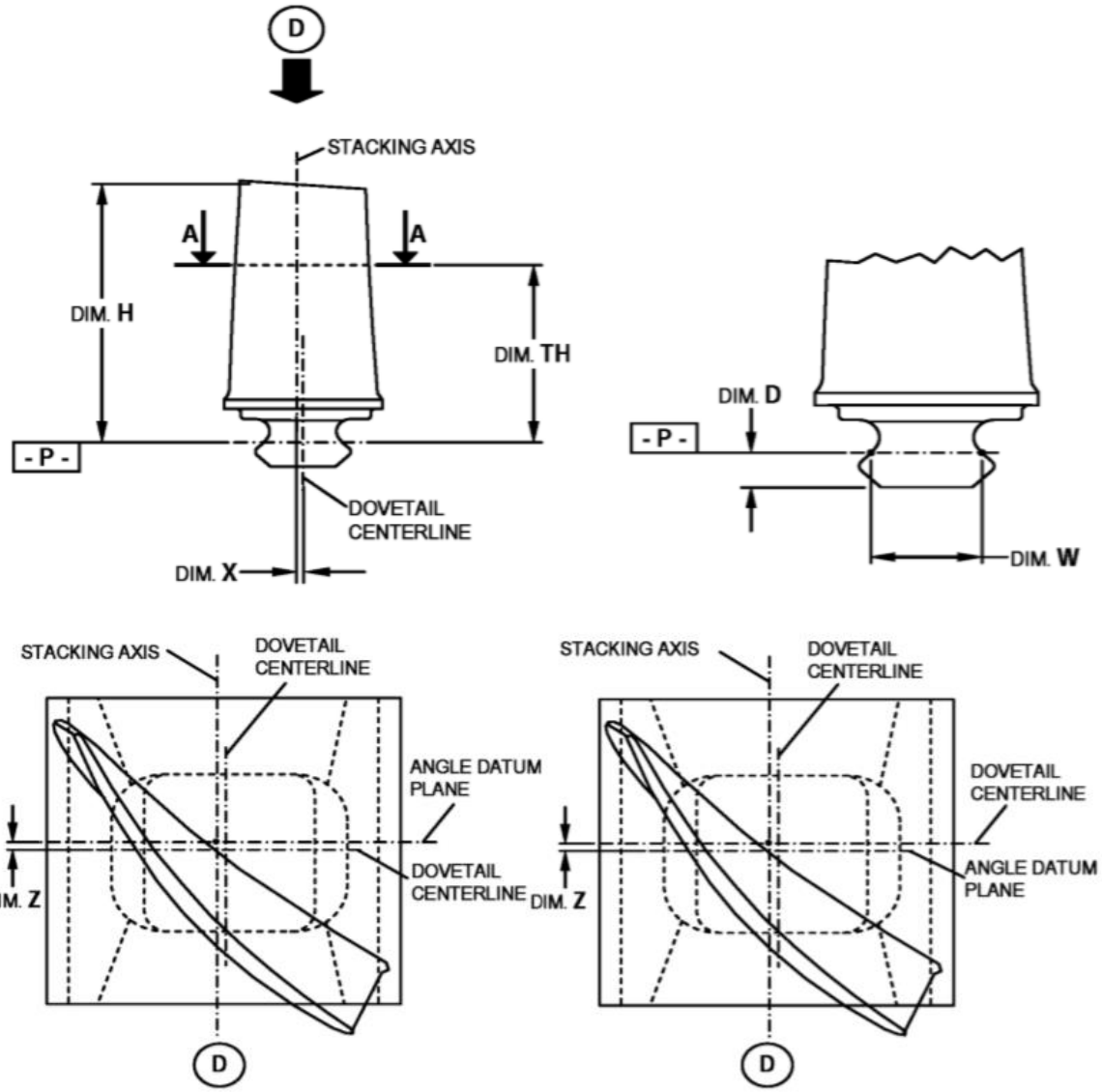

STAGE	DIM. TH	TWIST ANGLE TT REF	DIM. D	DIM. X AND DIM. Z SEE NOTE 4	DIM. W
4	1.543 (39,19)	47.155°	0.160 (4,06)	0.00	0.427 (10,85)
5	1.306 (33,17)	47.750°	0.130 (3,30)	0.00	0.423 (10,74)
6	1.110 (28,19)	44.040°	0.140 (3,56)	0.00	0.325 (8,26)
7	0.983 (24,97)	47.108°	0.140 (3,56)	0.00	0.345 (8,76)
8	0.891 (22,63)	51.760°	0.140 * (3,56)	0.00	0.297 (7,54)
			0.100 * (2,54)		
9	0.884 (22,45)	56.851°	0.100 (2,54)	0.00	0.317 (8,05)

* SEE NOTE 2

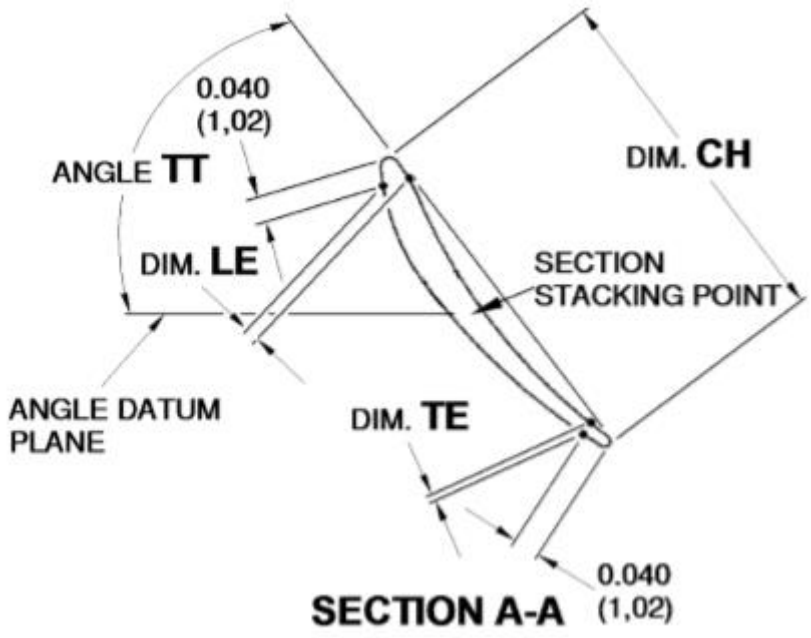

NOTES:

1. DIMENSIONS ARE IN INCHES WITH MILLIMETERS IN PARENTHESES.
2. APPLIES TO PART NUMBERS P398P01, P02, P05, AND P06.
3. APPLIES TO PART NUMBERS P398P03, P04, P07, AND P08.
4. FOR TECH INSERTION BLADES: DIM. **X** IS 0.00 BECAUSE THE STACKING AXIS AND DOVETAIL CENTERLINE ARE AT THE SAME LOCATION AND DIM. **Z** IS 0.00 BECAUSE THE ANGLE DATUM PLANE AND THE DOVETAIL CENTERLINE ARE AT THE SAME LOCATION. REFER TO FIGURE 804 SHEET 1.

Stage 4

	Min. Serviceable (in)	Max. Serviceable (in)	Max. Repairable (in)
DIM. CH (chord)	1.027	-	Non Rep.
DIM. LE	0.011	-	Any if CH
DIM. TE	0.011	-	Any if CH
DIM. H (tip length)	1.845	-	1.763

Stage 5

	Min. Serviceable (in)	Max. Serviceable (in)	Max. Repairable (in)
DIM. CH (chord)	0.869	-	Non Rep.
DIM. LE	0.014	-	Any if CH
DIM. TE	0,011	-	Any if CH
DIM. H (tip length)	1.529	-	1.441

Stage 6

	Min. Serviceable (in)	Max. Serviceable (in)	Max. Repairable (in)
DIM. CH (chord)	0.766	-	Non Rep.
DIM. LE	0.008	-	Any if CH
DIM. TE	0.009	-	Any if CH
DIM. H (tip length)	1.284	-	1.192

Stage 7

	Min. Serviceable (in)	Max. Serviceable (in)	Max. Repairable (in)
DIM. CH (chord)	0.750	-	Non Rep.
DIM. LE	0.015	-	Any if CH
DIM. TE	0,011	-	Any if CH
DIM. H (tip length)	1.161	-	1.069

Stage 8

	Min. Serviceable (in)	Max. Serviceable (in)	Max. Repairable (in)
DIM. CH (chord)	0.792	-	Non Rep.
DIM. LE	0.012	-	Any if CH
DIM. TE	0.006	-	Any if CH
DIM. H (tip length)	1.058	-	0.967

Stage 9

	Min. Serviceable (in)	Max. Serviceable (in)	Max. Repairable (in)
DIM. CH (chord)	0.808	-	0.810
DIM. LE	0.012	-	Any if CH
DIM. TE	0,006	-	Any if CH
DIM. H (tip length)	1.035	-	0,942

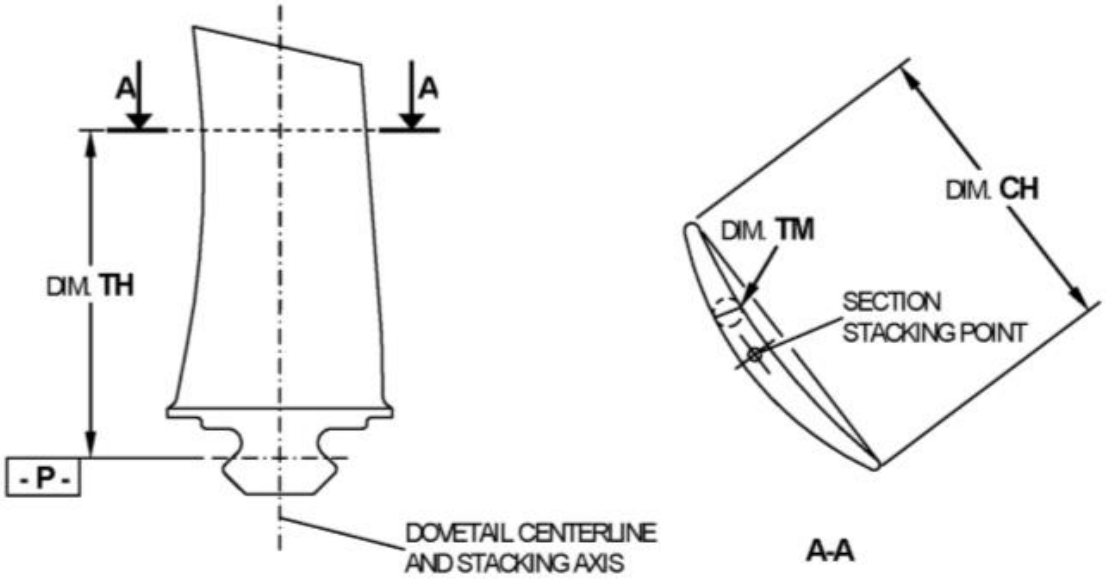

STAGE	SECTION HEIGHT (DIM. **TH**) REF	MIN REPAIRABLE CHORD LENGTH (DIM. **CH**)	MIN REPAIRABLE AIRFOIL THICKNESS DIM. **TM**
4	1.708 (43,38)	1.016 (25,81)	0.038 (0,97)
5	1.443 (36,65)	0.865 (21,98)	0.045 (1,15)
6	1.187 (30,15)	0.768 (19,51)	0.028 (0,72)
7	0.983 (24,97)	0.754 (19,16)	0.039 (1,00)
8	0.891 (22,63)	0.792 (20,12)	0.034 (0,87)
9	0.884 (22,45)	0.812 (20,63)	0.035 (0,89)

NOTES:

1. DIMENSIONS ARE IN INCHES WITH MILLIMETERS IN PARENTHESES.
2. REPAIRABLE AIRFOIL DIMENSIONS FOR TIP WELD REPAIR 016.

Appendix IV

Lesjofors' Spring Catalogue Relevant Information

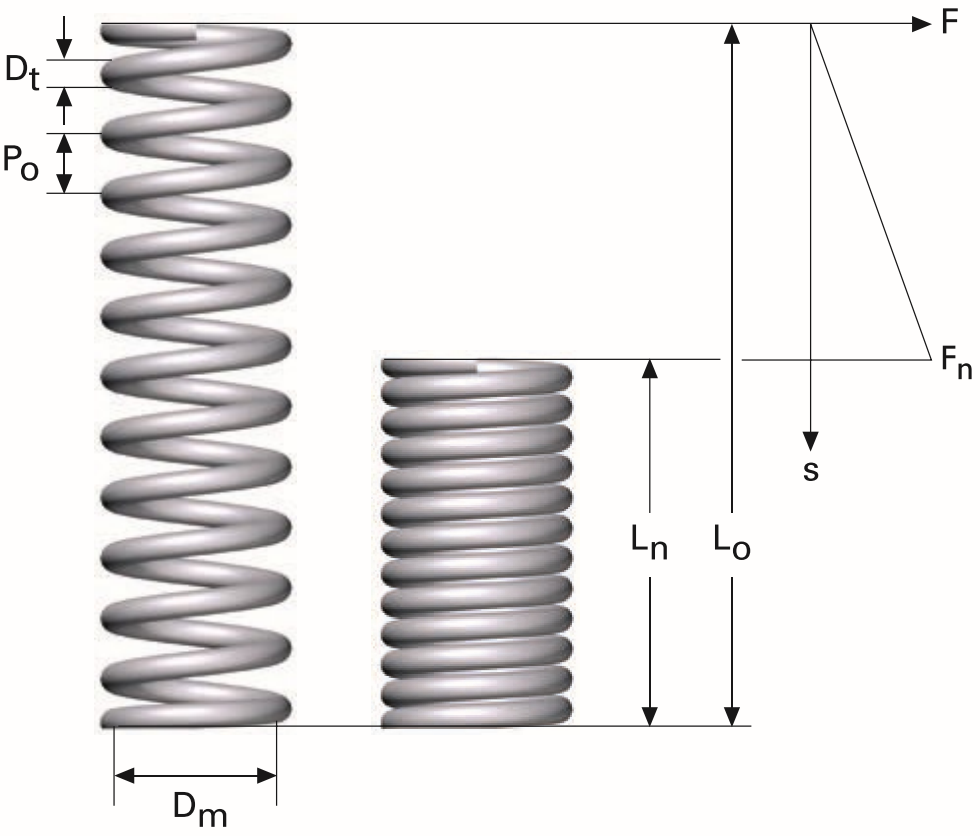

Compression springs for general use.
Dimensions according to international standards.
DIN2098, SS2387-2 & SF-TF

All dimensions are in mm

D_t = Wire diameter
D_m = Mean diameter
$D_{i\ min}$ = Inner diameter with smallest possible tolerance
L_o = Unloaded length
n_t = Total number of coils
L_n = Permitted loaded length for static load
F_n = Spring force in Newtons at L_n
R = Rate Newton / mm
P_o = Pitch
L_{st} = Solid length = $D_t \times n_t$
s = Deflection

Coiling: Right hand

Springs with Dt ≤ 0.4 do not have ground end coils, others have 3/4 end coils ground.

Springs with Dt ≥ 2.0 are shot peened.

Pre-setting
Springs having a calculated high stress under load to L_n are pre-set to solid length.

Material:
Lesjöfors standard compression springs are produced with different material depending on design and application.

Unalloyed spring steel
EN 10270-1-SH, page 8-25
EN 10270-2-FDSiCr, page 14-21 (Code marked with *)

Stainless spring steel
SUS304WPB, page 26-27
EN10270-3-1.4310, page 28-35

Min load length and temperature
Minimum load length L_n applies for static or pseudo static loaded springs operating at temperature up to about 40°C for unalloyed springs and up to about 150°C for stainless steel springs.
The relaxation, i.e. the power loss over time, will then stay within acceptable values for most applications. At higher operating temperatures or dynamic life demands, more than 10,000 cycles, the spring should not be loaded as far as L_n.

Maximum permitted operating temperature
EN10270-1-SH ~120 °C
EN 10270-2-FDSiCr ~250 °C
EN10270-3-1.4310 ~250 °C
SUS304WPB ~250 °C

1 kp = 9.80665 Newtons, 1 Newton = 0.10197 kp

Material: EN 10270-1-SH

d_t	D_m	$D_{i\,min}$	L_0	n_t	L_n	F_n	R	Cat.no
0,75	4,95	4,00	10	7,3	6,1	19	5,0	1290
0,75	4,95	4,00	15	10,4	8,8	19	3,2	1291
0,75	4,95	4,00	20	13,5	12	20	2,3	1292
0,75	4,95	4,00	25	16,6	14	20	1,8	1293
0,75	4,95	4,00	30	19,8	17	19	1,5	1294
0,75	4,95	4,00	40	26,0	22	19	1,1	1295
0,75	5,95	5,00	10	5,9	5,0	20	3,9	1296
0,75	5,95	5,00	15	8,2	7,1	20	2,5	1297
0,75	5,95	5,00	20	10,6	9,2	19	1,8	1298
0,75	5,95	5,00	25	12,9	11	19	1,4	1299
0,75	5,95	5,00	35	17,6	15	19	0,98	1300
0,75	5,95	5,00	45	21,3	19	21	0,79	1301
0,75	5,95	5,00	55	27,0	24	19	0,61	1302
0,75	7,00	6,00	10	4,9	4,2	19	3,2	1303
0,75	7,00	6,00	15	6,8	5,9	18	2,0	1304
0,75	7,00	6,00	20	8,6	7,6	18	1,4	1305
0,75	7,00	6,00	25	10,5	9,3	17	1,1	1306
0,75	7,00	6,00	30	12,3	11	17	0,91	1307
0,75	7,00	6,00	40	16,0	14	17	0,67	1308
0,75	8,00	7,00	10	4,3	3,6	18	2,8	1309
0,75	8,00	7,00	15	5,7	5,0	17	1,7	1310
0,75	8,00	7,00	20	7,3	6,5	16	1,2	1311
0,75	8,00	7,00	25	8,7	7,9	16	0,94	1312
0,75	8,00	7,00	35	11,7	11	16	0,65	1313
0,75	8,00	7,00	45	14,6	14	16	0,50	1314
0,75	8,00	7,00	55	17,6	16	16	0,40	1315
0,75	8,00	7,00	65	20,6	19	15	0,34	4556
0,75	9,00	8,00	10	3,7	3,2	18	2,6	3259
0,75	9,00	8,00	15	4,9	4,4	16	1,5	1318
0,75	9,00	8,00	20	6,1	5,5	16	1,1	1319
0,75	9,00	8,00	25	7,3	6,7	15	0,83	1320
0,75	9,00	8,00	30	8,5	7,9	15	0,68	1321
0,75	9,00	8,00	40	11,0	10	15	0,49	1322
0,75	9,00	8,00	50	13,4	13	14	0,39	1323
0,75	9,00	8,00	60	15,8	15	14	0,32	1324
0,75	10,0	9,00	10	3,4	2,9	16	2,3	1325
0,75	10,0	9,00	15	4,4	4,0	15	1,3	1326
0,75	10,0	9,00	20	5,3	4,9	15	0,98	1327
0,75	10,0	9,00	25	6,4	6,0	14	0,73	3780
0,75	10,0	9,00	35	8,4	8,1	14	0,50	1329
0,75	10,0	9,00	45	10,4	10	13	0,38	1330
0,75	10,0	9,00	55	12,4	12	13	0,31	1331
0,75	10,0	9,00	65	14,4	14	13	0,26	1332
0,75	11,1	10,00	10	3,2	2,8	14	2,0	1333
0,75	11,1	10,00	15	3,9	3,5	14	1,3	1334
0,75	11,1	10,00	20	4,7	4,4	14	0,88	1335
0,75	11,1	10,00	25	5,6	5,3	13	0,66	1336
0,75	11,1	10,00	30	6,4	6,2	13	0,54	1337
0,75	11,1	10,00	40	8,1	8,0	13	0,39	1338
0,75	11,1	10,00	50	9,7	9,7	12	0,31	1339
0,75	11,1	10,00	60	11,5	12	12	0,25	1340
0,80	4,00	3,05	6	5,0	4,3	36	22	2889
0,80	4,00	3,05	6,9	5,5	4,8	39	19	5906
0,80	4,00	3,05	8,7	7,0	6,2	34	13	2890
0,80	4,00	3,05	9,7	7,5	6,6	37	12	5907
0,80	4,00	3,05	13	10,0	8,9	32	8,2	2891
0,80	4,00	3,05	14	10,5	9,3	36	7,7	5908
0,80	4,00	3,05	18	14,0	13	31	5,4	2892
0,80	4,00	3,05	20	14,5	13	34	5,2	5909
0,80	4,00	3,05	27	20,0	18	31	3,6	2893
0,80	4,00	3,05	28	20,5	18	34	3,5	5910

Material: EN 10270-1-SH

d_t	D_m	$D_{i\,min}$	L_0	n_t	L_n	F_n	R	Cat.no
0,80	5,00	4,00	7,2	5,0	4,4	32	11	2894
0,80	5,00	4,00	8,3	5,5	4,8	33	9,5	5911
0,80	5,00	4,00	11	7,0	6,2	30	6,7	2895
0,80	5,00	4,00	12	7,5	6,7	32	6,1	5912
0,80	5,00	4,00	16	10,0	9,0	28	4,2	2778
0,80	5,00	4,00	18	10,5	9,5	32	3,9	5913
0,80	5,00	4,00	23	14,0	13	28	2,8	2897
0,80	5,00	4,00	25	14,5	13	30	2,7	5914
0,80	5,00	4,00	33	20,0	18	27	1,9	2898
0,80	5,00	4,00	36	20,5	19	31	1,8	5915
0,80	6,30	5,30	9,3	5,0	4,5	27	5,6	2899
0,80	6,30	5,30	11	5,5	4,9	27	4,8	5916
0,80	6,30	5,30	14	7,0	6,4	25	3,3	2900
0,80	6,30	5,30	16	7,5	6,8	26	3,0	5917
0,80	6,30	5,30	21	10,0	9,2	24	2,1	2901
0,80	6,30	5,30	23	10,5	9,7	26	2,0	5918
0,80	6,30	5,30	30	14,0	13	24	1,4	2902
0,80	6,30	5,30	33	14,5	14	26	1,3	5919
0,80	6,30	5,30	44	20,0	19	23	0,93	2903
0,80	6,30	5,30	48	20,5	19	26	0,90	5920
0,80	8,00	6,95	13	5,0	4,6	22	2,7	2904
0,80	8,00	6,95	15	5,5	5,1	22	2,3	5921
0,80	8,00	6,95	19	7,0	6,6	20	1,6	2905
0,80	8,00	6,95	22	7,5	7,1	21	1,5	5922
0,80	8,00	6,95	29	10,0	9,6	20	1,0	2906
0,80	8,00	6,95	32	10,5	10	21	0,96	5923
0,80	8,00	6,95	42	14,0	14	19	0,68	2907
0,80	8,00	6,95	47	14,5	14	21	0,65	5924
0,80	8,00	6,95	61	20,0	20	19	0,45	2908
0,80	8,00	6,95	68	20,5	20	21	0,44	5925
0,80	10,0	8,95	18	5,0	4,8	18	1,4	2909
0,80	10,0	8,95	20	5,5	5,3	17	1,2	5926
0,80	10,0	8,95	27	7,0	6,9	17	0,83	2910
0,80	10,0	8,95	30	7,5	7,5	17	0,76	5927
0,80	10,0	8,95	41	10,0	10	16	0,52	2911
0,80	10,0	8,95	46	10,5	11	17	0,49	5928
0,80	10,0	8,95	60	14,0	14	16	0,35	2912
0,80	10,0	8,95	66	14,5	15	17	0,33	5929
0,80	10,0	8,95	88	20,0	21	16	0,23	2913
0,80	10,0	8,95	97	20,5	21	17	0,23	5930
1,00	5,00	3,80	7,4	5,0	5,4	55	27	2914
1,00	5,00	3,80	8,5	5,5	6,0	59	23	5956
1,00	5,00	3,80	11	7,0	7,7	51	16	2915
1,00	5,00	3,80	12	7,5	8,3	55	15	5957
1,00	5,00	3,80	16	10,0	11	49	10	2916
1,00	5,00	3,80	17	10,5	12	51	9,6	5958
1,00	5,00	3,80	23	14,0	16	47	6,8	2917
1,00	5,00	3,80	24	14,5	16	51	6,5	5959
1,00	5,00	3,80	33	20,0	22	47	4,5	2918
1,00	5,00	3,80	35	20,5	23	50	4,4	5960
1,00	6,20	5,00	10	5,9	6,5	38	11	1341
1,00	6,20	5,00	15	8,3	9,3	39	6,8	1342
1,00	6,20	5,00	20	10,8	12	38	4,9	1343
1,00	6,20	5,00	25	13,2	15	38	3,8	1344
1,00	6,20	5,00	35	18,0	21	39	2,7	1345
1,00	6,20	5,00	45	23,0	26	38	2,0	1346
1,00	6,20	5,00	55	27,8	32	38	1,7	1347
1,00	6,20	5,00	65	32,5	37	39	1,4	1348

Appendix V

Technifast's Dowel Pin Specifications

DOWEL PINS AND EXTRACTABLE DOWELS

Dowels are solid pins, usually precision ground to narrow limits to permit accurate fitting, they are traditionally used to hold parts together in a fixed alignment, relying on the tightness of fit to stay in place.

Some applications for solid pins require clearance or transition fits on at least one of the components to be fastened. There are three factors that determine the size of hole needed:

- **The tolerance on the dowel**
- **The tightness of fit needed**
- **The hardness of the components into which the dowel is to be fitted**

TOLERANCES AND FITS

Our range standardises on m6 tolerance, which corresponds to the ISO and DIN standards*. The m6 tolerance is a 'plus tolerance' range and is normally used for interference fits. Also available are the minus tolerance ranges, h7 and h8.

HOLE TOLERANCE GUIDE

Hole material	Hardened steel	Mild steel	Aluminium / zinc / brass
Interference fit	Pin Ø less 5 microns	Pin Ø less 25 microns	Pin Ø less 35 microns
Transition fit	Pin Ø less 2 microns	Pin Ø less 5 microns	Pin Ø less 5 microns
Clearance fit	Pin Ø plus 25–60 microns	Pin Ø plus 25–60 microns	Pin Ø plus 25–60 microns

FITTING DOWELS INTO BLIND HOLES

When a dowel is interference-fitted into a blind hole, it increases the pressure of the air trapped in the hole. It is recommended that the dowel should have an air release flat ground along its full length to prevent the dowel being ejected under the pressure of compressed air, or bursting the component into which it is driven.

MATERIALS**

Through hardened steel	100Cr6, WS 1.3505 hardened and tempered to HV 550-650
Mild steel, unhardened	WS 1.0718 (9SMnPb28)
Stainless a2	WS 1.4305 or 303S31
Stainless a4	WS 1.4571 or 316S11

*See page 37 for full details.

**Other materials are listed under 'special pins'. See page 38 for material compositions.

STANDARDS

Dowel pins are made to several national or international standards, each with slight differences in chamfer forms, length tolerances and available materials.

STANDARD	STOCKED	MADE TO ORDER
DIN 6325 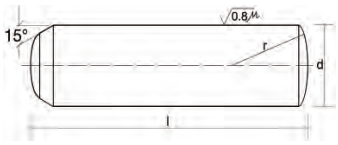	Diameters 1–20mm in steel, through-hardened and ground to m6	Other tolerances Stainless steel Diameters not shown overleaf
DIN 7 *Note; overall length is greater than nominal length. See dimension C and refer to table on next page* 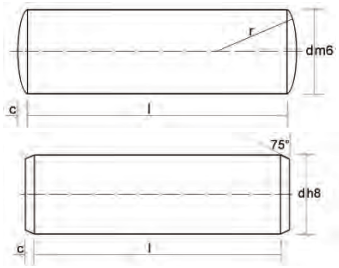	Diameters 1–30mm in mild steel ground to m6 Diameters 0.8–25mm in stainless A2 Diameters 1–12mm in stainless A4	Other tolerances Diameters not shown overleaf Dowels 14-25mm in stainless A4
ISO 2338 (1998) 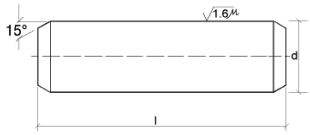	Diameters 1–25mm in mild steel ground to m6 Diameters 1–25mm in stainless A2	Other tolerances Stainless A4 Diameters not shown overleaf
ISO 8734 (1998) 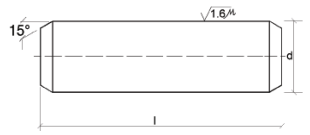		Diameters 1–20mm Through-hardened steel ground to m6 (8734A) Case-hardened steel ground to m6 (8734B) Through hardened martensitic stainless (8734C)
DIN 7979D 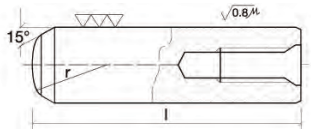	Diameters 4–20mm in steel, through-hardened and ground to m6 Diameters 4–20mm in stainless A2	

ADDITIONAL STANDARDS

BS 1804 PART 1	Solid dowels in inch sizes in low carbon steel, case-hardened for diameters 1/8”-1
BS 1804 PART 2	Solid dowels in metric sizes in low or high carbon steel, hardened for diameters of 4mm and above
BS 1804 PART 3	Extractable dowels and taper pins
BS 7055	Equivalent to ISO 8734
ISO 8733	Equivalent to DIN 7979A (unhardened)
ISO 8735	Equivalent to DIN 7979D (hardened)

T: +44 (0) 1536 461140 F: +44 (0) 1536 461662

SIZE RANGES

SIZE RANGE – DOWEL PINS TO ISO 2338 (1998)

Nominal Diameter, ISO 2338 (1998)	0.8	1	1.5	2	2.5	3	4	5	6	8	10	12	16	20	25	30
Available Materials	Mild Steel ground to m6 or h8 tolerance A2 Stainless, Grade 1.4305 ground to m6 or h8, 25 to m Ø															
Double Shear Strengths tested to ISO 8749, kN																
Mild Steel	0.4	0.7	1.6	2.85	4.25	6.15	10.6	16.5	22.8	40.5	63.2	91	156	220	300	390
Stainless Steel A2	0.4	0.7	1.7	2.9	4.4	6.6	11.7	18.1	26.0	47.0	64.1	92	160			
Lengths in mm																
3																
4																
5																
6																
8																
10																
12																
14																
16																
18																
20																
24																
28																
30																
32																
36																
40																
45																
50																
55																
60																
70																
80																
90																
100																
110																
120																
Length Tolerances	3 – 10 mm long ± 0.25						12 – 50 mm long ± 0.5					Over 50 mm long ± 0.75				

Appendix VI

Lifting Eye Bolts/Nuts DIN580 Summary Brochure

SAFETY REGULATIONS FOR THE USE OF LIFTING EYE BOLTS AND LIFTING EYE NUTS

The following working loads (WLL) are valid for eye bolts DIN 580:2018 and for eye nuts DIN 582:2018 made of C15E steel and A2/A3/A4 stainless steel.

DIN 580:2018

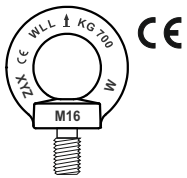

DIN 582:2018

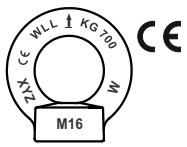

LIFTING CAPACITY (WLL) decimal point is comma

		M6	M8	M10	M12	M14	M16	M18	M20	M22	M24	M27	M30	M33	M36	M39	M42	M45	M48	M52	M56	M60	M64	M72	M80	M100
WLL 0° Kg	0°	75	140	230	340	490	700	850	1200	1400	1800	2100	3200	3200	4600	4600	6300	6300	8600	8600	11500	11500	16000	20000	28000	40000
WLL 45° Kg	0° < 45°	55	100	170	240	350	500	600	860	1000	1290	1500	2300	2300	3300	3300	4500	4500	6100	6100	8200	8200	11000	14000	20000	29000
WLL 60° Kg	45° < 60°	38	70	115	170	245	350	425	600	700	900	1050	1600	1600	2300	2300	3150	3150	4300	4300	5750	5750	8000	10000	14000	20000
WLL 90° Kg	90° < 135°	38	70	115	170	245	350	425	600	700	900	1050	1600	1600	2300	2300	3150	3150	4300	4300	5750	5750	8000	10000	14000	20000

INSTRUCTIONS FOR USE.

Lifting eye bolts or -nuts shall be completely tightened.The permissible working load limit (WLL) is allowed only if the bolt or nut is tightened to the part it's lifting. If you use mechanical tools for tightening, make sure not to over-strain the shank. Before lifting make sure that the rope and/or hook is stretched.

Lifting eye bolts -nuts must not be used with the ring's side pull.

The permissible working load limit (WLL) marked on bolts and nuts is valid only for straight lifting. The permissible working load limit for lifting on an angle at 45° or for orthogonal lifting at 90° is mentioned on the packing label (see dwg. at point 9 and 10). During lifting with more bolts or nuts, all rings shall be aligned by tightening. To achieve this, it may be necessary to use washers with at least the same diameter as the bearing area.

The permissible working load limit (WLL) applies to temperatures between -20°C to + 200°C (-4°F to + 392°F).

Before re-use make sure there are no surface flaws (ie: pits, voids, folds and seams, deformation of the ring, missing or broken threads, rust, etc..).

LEGEND OF THE LETTERS ON THE FASTENERS:

- A Thread / Dimension.
- B Lot.
- C Material.
- D Permissible working load limit (WLL) for straight lifting.
- E Manufacturer's Mark.

DIN 580:2018

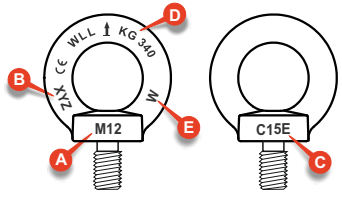

DIN 582:2018

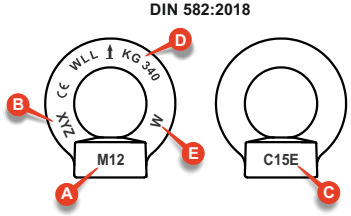

MANDATORY DOCUMENTATION:

Ensure that the pack always contains the user instructions and test certificate 3.1 EN 10204 relative to the production lot of Lifting Eye Bolts or –Nuts you are purchasing or installing.

For lifting eye bolts and lifting eye nuts to bear the CE marking, the manufacturer must issue a Declaration of Conformity stating that the parts meet the requirements of Machinery Directive 2006/42/EC (unless supplied separately, the declaration is included in certificate 3.1 EN 10204).

The chemical analysis of the hot-moulded Lifting Eye Bolts or –Nuts made of C15E steel must show an aluminium content (min. 0.025% - max. 0.050%).

Stainless steel Lifting Eye Bolts and –Nuts can be passivated and this surface treatment must be stated in certificate 3.1 EN 10204. Please note: stainless steel Lifting Eye Bolts and –Nuts must be hot-moulded and not die-cast.

If the Lifting Eye Bolts and –Nuts are to be exported (as equipment and/or machinery components) a Declaration of Origin issued by the manufacturer must also be provided. In this case too, unless supplied separately this declaration is usually included in certificate 3.1 EN 10204.

Please note: Lifting Eye Bolts and –Nuts are LIFTING ACCESSORIES and are not classed as common hardware. Safety regulations provide for a product's good quality as well as for the examination by the user of the product's compliance with the technical requirements provided for by the standards of reference and by Community regulation 2006/42/EC. Compliance must be declared by the manufacturer in certificate 3.1 EN 10204.

LEGEND OF THE SYMBOLS ON THE LABELS:

1. Standard / Table.
2. Type and dimension of thread.
3. Number of pieces per packing.
4. Lot number.
5. Surface treatment.
6. Material.
7. Chemical Analysis.
8. Permissible working load limit (WLL) (straight lifting) in kilograms - kg
9. Permissible working load limit (WLL) at 45° in kilograms - kg
10. Permissible working load limit (WLL) for orthogonal lifting at 90° in kilograms - kg
11. Tensile Strength (on the specimen).
12. Analysis Number/Certificate Number.
13. Draft of the fastener in the box.

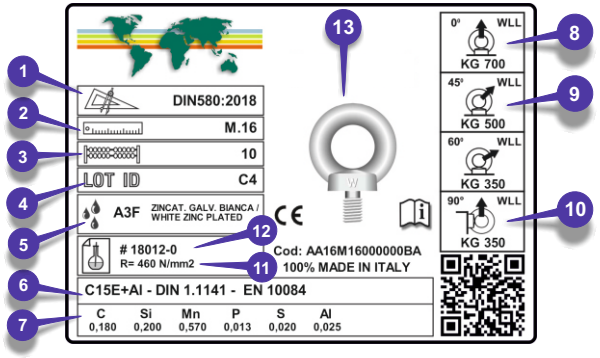

MEC WOLF SRL - Via Cascina California, 39
I-22036 ERBA (Co), ITALY
Ph. 0039-031-33303 - Fax 0039-031-3330411
infomec@wolf.it www.mecwolf.it

DIMENSIONS OF LIFTING EYE BOLTS -NUTS

LIFTING EYE BOLT DIN 580:2018

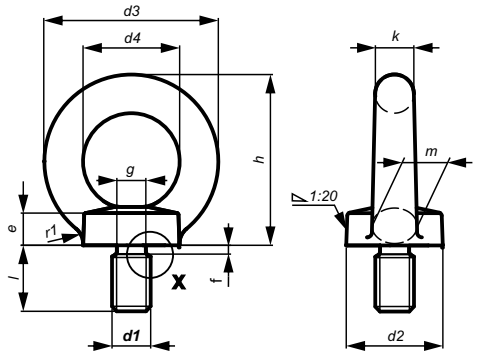

X Gola di scarico

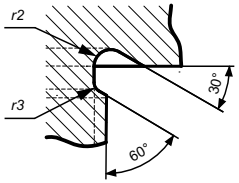

Machined surfaces: Ra 3,2

Dimensions in millimetres

d1 THREAD SIZE		M6	M8	M10	M12	M14	M16	M18	M20	M22	M24	M27	M30	M33	M36	M39	M42	M45	M48	M52	M56	M60	M64	M72x6	M80x6	M100x6
d2	Nominal size	20	20	25	30	35	35	40	40	50	50	65	65	75	75	85	85	100	100	110	110	120	120	150	170	190
	min.	19,5	19,5	24,5	29,5	34,5	34,5	39,5	39,5	49,4	49,4	64,3	64,3	74,3	74,3	84,3	84,3	99,2	99,2	108,9	108,9	118,9	118,9	148,8	168,5	188,5
	max.	20,9	20,9	25,9	30,9	36,1	36,1	41,1	41,1	51,2	51,2	66,3	66,3	76,5	76,5	86,5	86,5	101,7	101,7	112,1	112,1	122,1	122,1	152,4	173	193
d3	Nominal size	36	36	45	54	63	63	72	72	90	90	108	108	126	126	144	144	166	166	184	184	206	206	260	296	330
	min.	35,5	35,5	44,5	53,5	62,5	62,5	71,5	71,5	89,4	89,4	107,3	107,3	125,2	125,2	143,2	143,2	164,9	164,9	182,8	182,8	204,8	204,8	258,5	294,3	328,3
	max.	37,1	37,1	46,1	55,1	64,1	64,1	73,1	73,1	91,2	91,2	109,5	109,5	127,7	127,7	145,7	145,7	168,1	168,1	186,4	186,4	208,4	208,4	263	299,3	333,3
d4	Nominal size	20	20	25	30	35	35	40	40	50	50	60	60	70	70	80	80	90	90	100	100	110	110	140	160	180
	min.	19,1	19,1	24,1	29,1	33,9	33,9	38,9	38,9	48,8	48,8	58,7	58,7	68,5	68,5	78,5	78,5	88,3	88,3	98,1	98,1	107,9	107,9	137,6	157,3	177
	max.	20,5	20,5	25,5	30,5	35,5	35,5	40,5	40,5	50,6	50,6	60,7	60,7	70,7	70,7	80,7	80,7	90,8	90,8	100,9	100,9	111,1	111,1	141,2	161,3	181,5
e	Nominal size	6	6	8	10	12	12	14	14	18	18	22	22	26	26	30	30	35	35	38	38	42	42	50	55	60
	min.	5,5	5,5	7,5	9,5	11,5	11,5	13,5	13,5	17,5	17,5	21,4	21,4	25,3	25,3	29,3	29,3	34,2	34,2	37,1	37,1	41,1	41,1	48,9	53,8	58,8
	max.	6,9	6,9	8,9	10,9	12,9	12,9	14,9	14,9	19,1	19,1	23,2	23,2	27,3	27,3	31,3	31,3	36,7	36,7	39,9	39,9	43,9	43,9	52,1	57,4	62,4
f	max.	2,5	2,5	3	3,5	4	4	5	5	6	6	7	7	8	8	9	9	10	10	11	11	12	12	12	12	12
g h13	Nominal size	4,4	6	7,7	9,4	11	13	14,4	16,4	18,4	19,6	22,6	25	28	30,3	33,3	35,6	38,6	41	45	48,3	52,3	55,7	63,7	71,7	91,7
	min.	4,22	5,82	7,48	9,18	10,73	12,73	14,13	16,13	18,07	19,27	22,29	24,67	27,61	29,91	32,91	35,21	38,21	40,61	44,54	47,91	51,84	55,24	63,24	71,24	91,16
	max.	4,4	6	7,7	9,4	11	13	14,4	16,4	18,4	19,6	22,6	25	28	30,3	33,3	35,6	38,6	41	45	48,3	52,3	55,7	63,7	71,7	91,7
h	Nominal size	36	36	45	53	62	62	71	71	90	90	109	109	128	128	147	147	168	168	187	187	208	208	260	298	330
	min.	35,5	35,5	44,5	52,5	61,5	61,5	70,5	70,5	89,4	89,4	108,3	108,3	127,2	127,2	146,2	146,2	166,9	166,9	185,8	185,8	206,8	206,8	258,5	296,3	328,3
	max.	37,1	37,1	46,1	54,1	63,1	63,1	72,1	72,1	91,2	91,2	110,5	110,5	129,7	129,7	148,7	148,7	170,1	170,1	189,4	189,4	210,4	210,4	263	301,3	333,3
k	Nominal size	8	8	10	12	14	14	16	16	20	20	24	24	28	28	32	32	38	38	42	42	48	48	60	68	75
	min.	7,5	7,5	9,5	11,5	13,5	13,5	15,5	15,5	19,5	19,5	23,4	23,4	27,3	27,3	31,3	31,3	37,2	37,2	41,1	41,1	47,1	47,1	58,9	66,8	73,8
	max.	8,9	8,9	10,9	12,9	14,9	14,9	16,9	16,9	21,1	21,1	25,2	25,2	29,3	29,3	33,3	33,3	39,7	39,7	43,9	43,9	49,9	49,9	62,1	70,4	77,4
l js15	Nominal size	13	13	17	20,5	27	27	30	30	36	36	45	45	54	54	63	63	68	68	78	78	90	90	100	112	130
	min.	12,65	12,65	16,65	20,08	26,58	26,58	29,58	29,58	35,5	35,5	44,5	44,5	53,5	53,5	62,4	62,4	67,4	67,4	77,4	77,4	89,3	89,3	99,3	111,3	129,2
	max.	13,35	13,35	17,35	20,92	27,42	27,42	30,42	30,42	36,5	36,5	45,5	45,5	54,5	54,5	63,6	63,6	68,6	68,6	78,6	78,6	90,7	90,7	100,7	112,7	130,8
m	Nominal size	10	10	12	14	16	16	19	19	24	24	28	28	32	32	38	38	46	46	50	50	58	58	72	80	88
	min.	9,5	9,5	11,5	13,5	15,5	15,5	18,5	18,5	23,5	23,5	27,4	27,4	31,3	31,3	37,3	37,3	45,2	45,2	49,1	49,1	57,1	57,1	70,9	78,8	86,8
	max.	10,9	10,9	12,9	14,9	16,9	16,9	19,9	19,9	25,1	25,1	29,2	29,2	33,3	33,3	39,5	39,5	47,7	47,7	51,9	51,9	59,9	59,9	74,1	82,4	90,4
r1	~	4	4	4	6	6	6	8	8	12	12	15	15	18	18	20	20	22	22	25	25	25	25	35	35	40
r2	~	1	1	1	2	2	2	2	2	2	2	3	3	3	3	3	3	4	4	4	4	4	4	4	4	4
r3	~	1	1	1	1,2	1,2	1,2	1,6	1,6	2	2	2	2	2	2	2,5	2,5	2,5	2,5	3	3	3	3	3	3	3

LIFTING EYE NUT DIN 582:2018

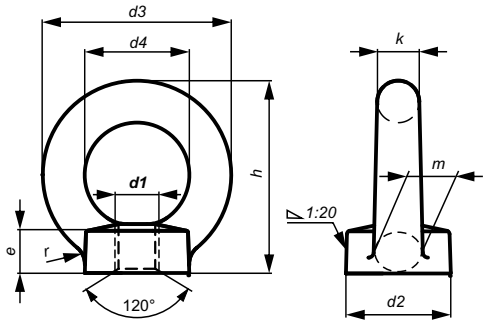

Machined surfaces: Ra 3,2

Dimensions in millimetres

d1 THREAD SIZE		M6	M8	M10	M12	M14	M16	M18	M20	M22	M24	M27	M30	M33	M36	M39	M42	M45	M48	M52	M56	M60	M64	M72x6	M80x6	M100x6
d2	Nominal size	20	20	25	30	35	35	40	40	50	50	65	65	75	75	85	85	100	100	110	110	120	120	150	170	190
	min.	19,5	19,5	24,5	29,5	34,5	34,5	39,5	39,5	49,4	49,4	64,3	64,3	74,3	74,3	84,3	84,3	99,2	99,2	108,9	108,9	118,9	118,9	148,8	168,5	188,5
	max.	20,9	20,9	25,9	30,9	36,1	36,1	41,1	41,1	51,2	51,2	66,3	66,3	76,5	76,5	86,5	86,5	101,7	101,7	112,1	112,1	122,1	122,1	152,4	173	193
d3	Nominal size	36	36	45	54	63	63	72	72	90	90	108	108	126	126	144	144	166	166	184	184	206	206	260	296	330
	min.	35,5	35,5	44,5	53,5	62,5	62,5	71,5	71,5	89,4	89,4	107,3	107,3	125,2	125,2	143,2	143,2	164,9	164,9	182,8	182,8	204,8	204,8	258,5	294,3	328,3
	max.	37,1	37,1	46,1	55,1	64,1	64,1	73,1	73,1	91,2	91,2	109,5	109,5	127,7	127,7	145,7	145,7	168,1	168,1	186,4	186,4	208,4	208,4	263	299,3	333,3
d4	Nominal size	20	20	25	30	35	35	40	40	50	50	60	60	70	70	80	80	90	90	100	100	110	110	140	160	180
	min.	19,1	19,1	24,1	29,1	33,9	33,9	38,9	38,9	48,8	48,8	58,7	58,7	68,5	68,5	78,5	78,5	88,3	88,3	98,1	98,1	107,9	107,9	137,6	157,3	177
	max.	20,5	20,5	25,5	30,5	35,5	35,5	40,5	40,5	50,6	50,6	60,7	60,7	70,7	70,7	80,7	80,7	90,8	90,8	100,9	100,9	111,1	111,1	141,2	161,3	181,5
e	Nominal size	8,5	8,5	10	11	13	13	16	16	20	20	25	25	30	30	35	35	40	40	45	45	50	50	60	70	80
	min.	8	8	9,5	10,5	12,5	12,5	15,5	15,5	19,5	19,5	24,4	24,4	29,3	29,3	34,3	34,3	39,2	39,2	44,1	44,1	49,1	49,1	58,9	68,8	78,8
	max.	9,4	9,4	10,9	11,9	13,9	13,9	16,9	16,9	21,1	21,1	26,2	26,2	31,3	31,3	36,5	36,5	41,7	41,7	46,9	46,9	51,9	51,9	62,1	72,4	82,4
h	Nominal size	36	36	45	53	62	62	71	71	90	90	109	109	128	128	147	147	168	168	187	187	208	208	260	298	330
	min.	35,5	35,5	44,5	52,5	61,5	61,5	70,5	70,5	89,4	89,4	108,3	108,3	127,2	127,2	146,2	146,2	166,9	166,9	185,8	185,8	206,8	206,8	258,5	296,3	328,3
	max.	37,1	37,1	46,1	54,1	63,1	63,1	72,1	72,1	91,2	91,2	110,5	110,5	129,7	129,7	148,7	148,7	170,1	170,1	189,4	189,4	210,4	210,4	263	301,3	333,3
k	Nominal size	8	8	10	12	14	14	16	16	20	20	24	24	28	28	32	32	38	38	42	42	48	48	60	68	75
	min.	7,5	7,5	9,5	11,5	13,5	13,5	15,5	15,5	19,5	19,5	23,4	23,4	27,3	27,3	31,3	31,3	37,2	37,2	41,1	41,1	47,1	47,1	58,9	66,8	73,8
	max.	8,9	8,9	10,9	12,9	14,9	14,9	16,9	16,9	21,1	21,1	25,2	25,2	29,3	29,3	33,3	33,3	39,7	39,7	43,9	43,9	49,9	49,9	62,1	70,4	77,4
m	Nominal size	10	10	12	14	16	16	19	19	24	24	28	28	32	32	38	38	46	46	50	50	58	58	72	80	88
	min.	9,5	9,5	11,5	13,5	15,5	15,5	18,5	18,5	23,5	23,5	27,4	27,4	31,3	31,3	37,3	37,3	45,2	45,2	49,1	49,1	57,1	57,1	70,9	78,8	86,8
	max.	10,9	10,9	12,9	14,9	16,9	16,9	19,9	19,9	25,1	25,1	29,2	29,2	33,3	33,3	39,5	39,5	47,7	47,7	51,9	51,9	59,9	59,9	74,1	82,4	90,4
r	~	4	4	4	6	6	6	8	8	12	12	15	15	18	18	20	20	22	22	25	25	25	25	35	35	40

Appendix VII

Economic and Maximum Manufacturing Deviations

Oswaldo Agostinho, Antônio Rodrigues, João Lirani, *Princípios de engenharia de fabricação mecânica – tolerâncias, ajustes, desvios e análises de dimensões*, Editora Edgard Blucher, Ltda., São Paulo, 1977.

DESVIOS DE FORMA E POSIÇÃO — Tabelas

Os desvios de forma e posição, como foram definidos, influem decisivamente na qualidade final do produto a ser produzido. Deverão ser especificados com a mesma constância e necessidade com que são as tolerâncias de ajuste. Projetos de produtos que não levam em consideração tolerâncias da forma teórica e de posição, inevitavelmente estarão comprometendo a precisão final da peça. Deve-se esta afirmação ao fato de que não será possível evitar, durante os processos de fabricação da peça, esses desvios.

Será, portanto, muito mais racional, ao invés de ignorá-los, enquadrá-los e controlá-los dentro de tolerâncias compatíveis com a funcionalidade e precisão esperadas para aquele produto.

As exigências de tolerâncias de forma e posição advindas do projeto do produto, deverão ser compatíveis com a capacidade do equipamento à disposição no parque industrial. Sempre que possível, caberá ao projetista enquadrar dentro das especificações de forma e posição, valores possíveis de serem obtidos na prática usual, de um modo geral. Particularmente, esses valores deverão atender, na medida do possível, as variações possíveis com as máquinas disponíveis dentro do parque industrial à disposição. Essa medida evitará investimentos adicionais em equipamentos mais precisos.

A seguir, são dadas diversas tabelas que servem como orientação para adoção de tolerâncias de forma e posição para os diversos processos de usinagem.

Os valores acima enumerados são médios, podendo variar de acordo com as condições de fabricação, qualidade e idade do equipamento, sofisticação do ferramental de fabricação, tais como dispositivos de fixação, ferramentas de corte, etc. São também bastante afetados pelos métodos de verificação utilizados. São, porém, valores que podem ser adotados, após a particularização para o caso um estudo, como bastante próximos de valores possíveis de serem obtidos na prática usual das fábricas.

Tabela 3.3 Desvios permissíveis da forma cilíndrica (cilindricidade)

Máquina	Peça		Desvio (0,001 mm)		
	Diâmetro (mm)	Comprimento (mm)	Ovalização	Concavidade	Conicidade
Torno com altura entre centros					
até 180 mm	—	300	5	20	10
até 400 mm	—	300	10	20	20
até 1,000 mm	—	300	20	20	20
Torno-revólver	—	—	10	20	30
Torno frontal	até 300	300	30	60	30
Torno vertical com uma coluna usinando com cabeçotes transversais	acima de 800	300	20	20	—
Torno vertical com uma coluna usinando com cabeçotes frontais	acima de 800	1 000	20	—	—
Mandriladora vertical com dois cabeçotes	até 300	300	20	20	20
Mandriladora vertical com dois cabeçotes	acima de 300	1,00	30	30	30
Retificadora cilíndrica	—	300	5	—	10

Tabela 3.4 Desvios permissíveis da forma cilíndrica com variações de dimensões

Diâmetro	Usinagem externa (eixos)		Usinagem interna (furos)		
	Torneamento	Retificação	Torneamento	Retificação	Mandrilamento
Até 50	0,01	0,003	0,02	0,003	0,02
De 50 a 120	0,02	0,005	0,03	0,005	0,025
De 120 a 250	0,04	0,06	0,05	0,008	0,040
De 250 a 500	0,05	0,01	—	—	—

Dimensões dadas em milímetros

Tabela 3.5 Desvios permissíveis de circularidade com variações de dimensões

Diâmetro	Operações de usinagem				
	Torneamento		Retificação		
	Entre pontos	Na placa ou mandril	Entre pontos	Na placa ou mandril	Sem centros
Até 10	0,003	0,005	0,002	0,003	0,003
De 10 a 50	0,005	0,015	0,002	0,005	0,005
De 50 a 120	0,008	0,030	0,003	0,008	0,008
De 120 a 250	0,01	0,05	0,005	0,01	0,01

Dimensões dadas em milímetros

Tabela 3.6 Desvios permissíveis da forma plana (planicidade)

Operações de usinagem	Precisão de fabricação	
	Valores econômicos	Valores máximos
	Desvio de planicidade por 100 mm	
Plainamento de superfícies planas e canais	0,3	0,1
Idem para plaina vertical	0,05 por 300 mm	0,02 por 300 mm
Fresamento com fresa de disco	0,3	0,08
Fresamento com fresa de topo	0,05	0,03
Torneamento em torno horizontal ou vertical	0,05	0,02
Retificação em retífica de superfície		
em sentido contrário ao avanço	0,1	0,05
no mesmo sentido do avanço	0,05	0,02
Retificação com a face lateral de rebolos	0,03 por 300 mm	0,01 por 300 mm
Retificação com o diâmetro externo de rebolos	0,03	0,01
Retificação em desbaste	0,2 por 300 mm	—
Brochamento	0,005	—

Tabela 3.7 Desvios permissíveis da forma plana com variações de dimensões

Maior comprimento L da superfície a ser usinada	Operações de usinagem				
	Lapidação	Retificação	Fresamento	Torneamento	Plainamento
Até 10	0,002	0,005	0,015	0,020	0,040
De 10 a 25	0,004	0,015	0,030	0,040	0,080
De 25 a 50	0,006	0,030	0,045	0,080	0,160
De 50 a 120	0,012	0,060	0,070	0,140	0,360

Dimensões dadas em milímetros
Os valores são válidos para *uma* fixação

Tabela 3.8 Desvios permissíveis de paralelismo entre duas superfícies planas

Operações de usinagem	Precisão de fabricação	
	Valores econômicos	Valores máximos
	Desvio de paralelismo por 100 mm	
Plainamento de superfícies planas e canais	0,1	0,05
Idem para plaina vertical	0,1 por 1,000 mm	0,02 por 1,000 mm
Fresamento com fresa de disco	0,1	0,03
Fresamento com fresa de topo	0,05	0,02
Retificação em retífica de superfície		
em sentido contrário ao avanço	0,1	0,03
no mesmo sentido do avanço	0,03	0,01
Retificação com a face lateral de rebolos	0,01	0,003
Retificação com o diâmetro externo de rebolos	0,05	0,01
Retificação em desbaste	0,2	—

Tabela 3.9 Desvios permissíveis de paralelismo entre duas superfícies planas com variação de dimensões

Maior comprimento L da superfície a ser usinada	Operações de usinagem			
	Torneamento	Fresamento	Plainamento	Retificação
Até 10	0,03	0,05	0,1	0,01
De 10 a 25	0,05	0,05	0,2	0,02
De 25 a 30	0,10	0,10	0,30	0,05
De 50 a 120	0,10	0,15	0,45	0,08
De 120 a 250	0,15	0,20	0,50	0,1

Dimensões dadas em milímetros
Os valores são válidos para *uma* fixação

Tabela 3.10 Desvios permissíveis de paralelismo de eixos de superfícies de revolução (T_{PLE_X} ou T_{PLE_Y})

Sistema de furação	Diâmetro da broca d, (mm)	Precisão de fabricação (mm)			
		Usual		Máxima	
		Desvio de distância entre centros	Desvio de paralelismo por 100 mm	Desvio de distância entre centros	Desvio de paralelismo por 100 mm
Furação por traçagem	Até 3	± 0,5	0,5	± 0,20	0,3
	3 a 6	± 0,6		± 0,25	
	6 a 10	± 0,8		± 0,30	
	10 a 18	± 1,0		± 0,35	
	18 a 30	± 1,2		± 0,40	
	30 a 50	± 1,6		± 0,45	
	50	± 2,0		± 0,50	

Tabela 3.11 Desvios permissíveis de perpendicularismo de furos com relação a uma superfície plana de referência

Operações de usinagem	Precisão de fabricação	
	Econômica	Máxima
	Desvio de paralelismo por 100 mm	
Furação		
por traçagem	0,5	0,3
com dispositivo	0,1	0,1
Mandrilamento		
em torno com a peça centrada por traçagem	1,0	0,5
centragem em placa angular	0,05	0,02
em mandriladora ou fresadora horizontal	0,05	0,02

Tabela 3.12 Desvios permissíveis de perpendicularismo de eixos ou furos com relação a um plano de referência

Operações de usinagem	Precisão de fabricação	
	Valores econômicos	Valores máximos
	Erro de perpendicularismo por 100 mm	
Furação		
com traçagem	0,5	0,3
com dispositivo	0,1	—
Usinagem em torno		
montagem ou traçagem	1,0	0,5
verificado com relógio comparador	0,5	0,2
furo e face em uma única usinagem	0,2	0,05
Usinagem de furo em fresadora vertical com a peça presa na mesa da máquina	0,05	0,02
Usinagem de furo em fresadora horizontal com a peça presa em ângulo com a mesa	0,08	0,03
Retificação interna com a peça presa em dispositivo	0,08	0,03

Tabela 3.13 Desvios máximos permissíveis de batida radial em torneamento e retificação externa ou em mandrilamento e retificação interna de furos para peças presas em placas

Tipo de centragem da peça	Precisão de fabricação			
	Usinagem externa		Usinagem interna	
	Torneamento	Retificação	Mandrilamento	Retificação
Usinagem em placa universal sem centragem subseqüente	1,0	0,5	1,0	0,6
Idem com centragem com graminho	1,0	—	1,0	—
Idem com centragem com relógio indicador	0,1	0,05	0,1	0,06
Idem para operação com castanhas moles	0,07	—	0,08	—

Tabela 3.14 Desvios permissíveis de batida radial, com variação de dimensões

Diâmetro	Operações de usinagem				
	Torneamento		Retificação		
	Entre pontos	Na placa ou mandril	Entre pontos	Na placa ou mandril	Sem centros
Até 5	0,03	0,05	0,005	0,03	0,03
De 5 a 10	0,05	0,08	0,01	0,05	0,05
De 10 a 50	0,08	0,1	0,015	0,1	0,1
De 50 a 120	0,1	0,15	0,02	0,15	0,15
De 120 a 250	0,15	0,2	0,025	0,20	0,20

Tabela 3.15 Desvios máximos permissíveis de batida radial com a peça entre centros

Tipo da usinagem	Precisão de usinagem mm	
	Torneamento	Retificação
Usinagem entre centros com uma operação	0,03	0,01
Usinagem entre centros com duas operações	0,05	0,015
Idem para duas operações com centro temperado sem lapidação posterior	—	0,05
Fixação em mandril previamente retificado	0,08	0,02
Idem para mandril sem retificação com ponto retificado ou torneado	0,10	0,04
Idem para mandril sem retificação e centro temperado sem retificação posterior	0,15	0,08

Appendix VIII

Stage 1 Tool's Assembly Technical Drawing

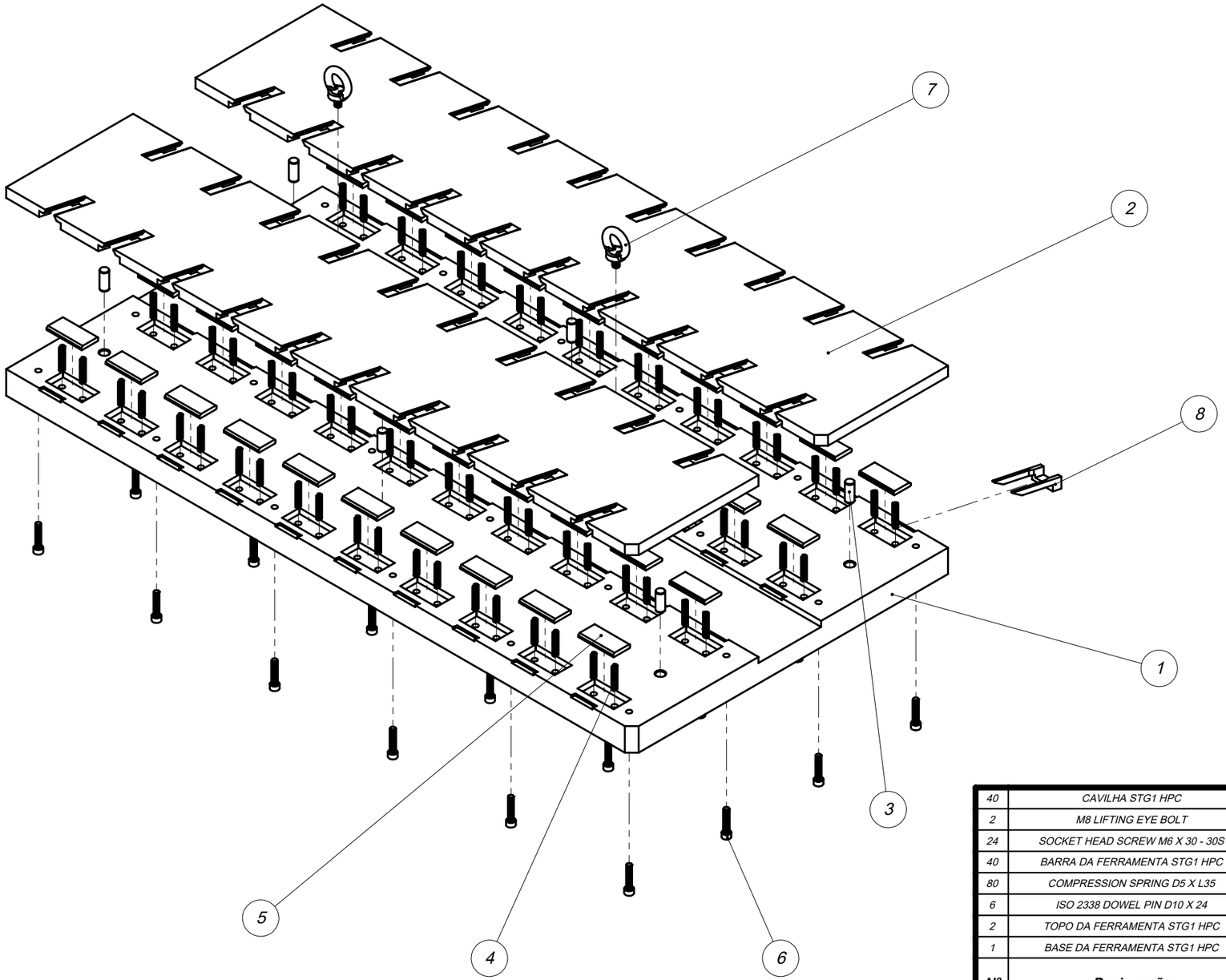

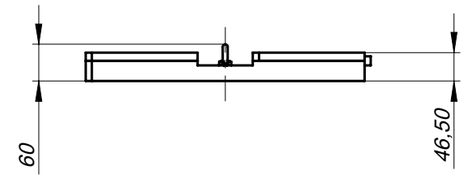

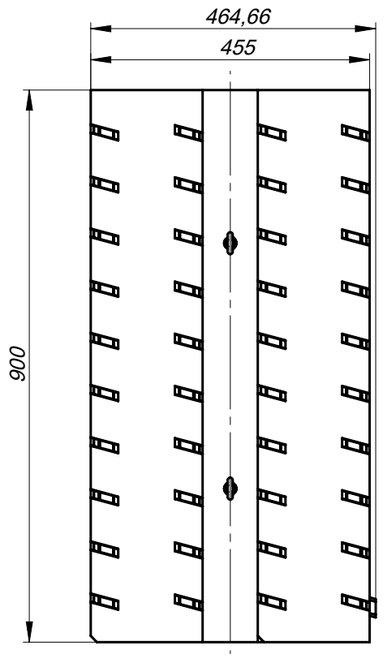

Nº	Designação	Nº da Norma Nº do Desenho	Material	Nº Ref	Prod. Semi Acabado Nº do Molde Nº da Matriz	Peso	Observações
40	CAVILHA STG1 HPC	F_HPC_0104	AÇO INOX AISI 304	8		32.01	MASSA EM GRAMAS
2	M8 LIFTING EYE BOLT	DIN 580		7		47.79	MASSA EM GRAMAS
24	SOCKET HEAD SCREW M6 X 30 - 30S	ISO 4762		6		1.137	MASSA EM GRAMAS
40	BARRA DA FERRAMENTA STG1 HPC	F_HPC_0103	AÇO INOX AISI 304	5		46.27	MASSA EM GRAMAS
80	COMPRESSION SPRING D5 X L35		EN 10270-1-SH	4	LESJOFORS CAT #15 - PART No. 5960	2.00	MASSA EM GRAMAS
6	ISO 2338 DOWEL PIN D10 X 24	F_HPC_PN01		3	TECHNIFAST DOWEL PIN	14.89	MASSA EM GRAMAS
2	TOPO DA FERRAMENTA STG1 HPC	F_HPC_0102	ALUMÍNIO 6061	2		5.04	MASSA EM KG
1	BASE DA FERRAMENTA STG1 HPC	F_HPC_0101	ALUMÍNIO 6061	1		33.40	MASSA EM KG

OBSERVAÇÕES

PESO ESTIMADO:
33.40 KG
(SEM CAVILHAS)

Projetou		2020-06-15
Desenhou		2020-08-31
Verificou		2020- -

UNL-FCT-DEMI TAP M&E
DISSERTAÇÃO DE MESTRADO

PEDRO RENDAS
MIEMc 47676

Escala 1:10

Tolerân. ISO 2768 m

FERRAMENTA STG1 HPC

F_HPC_0100

Substitui:

Substituido por:

Appendix IX

Stage 1 Tool’s Bottom Component Technical Drawing

SECÇÃO XX

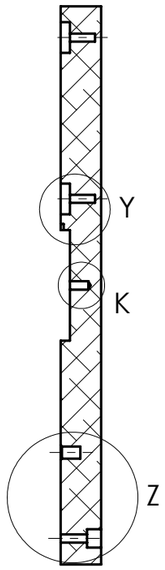

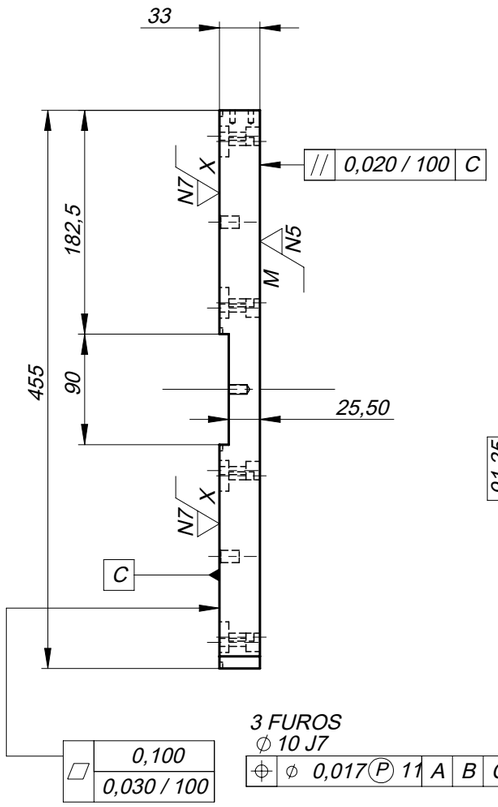

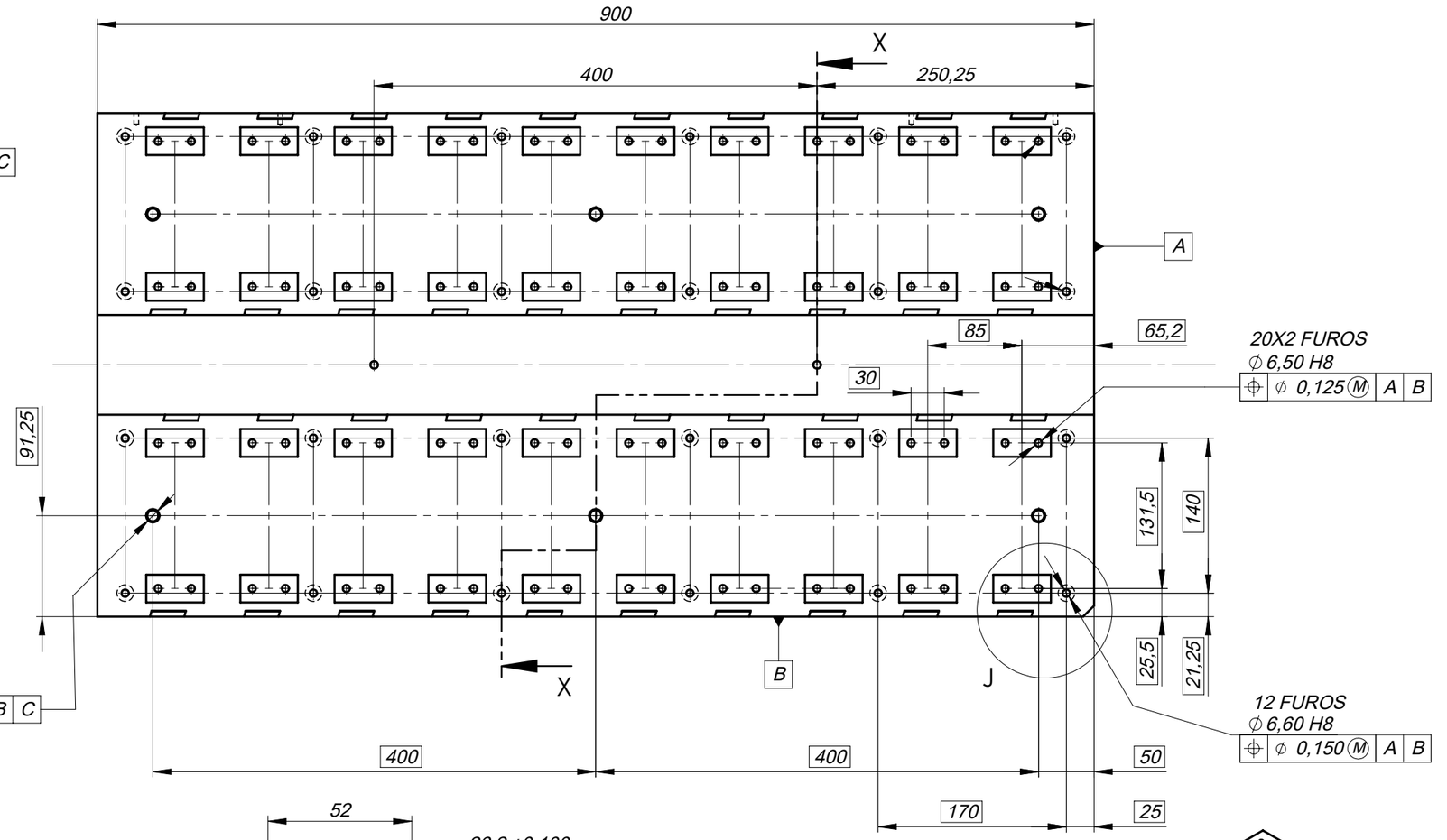

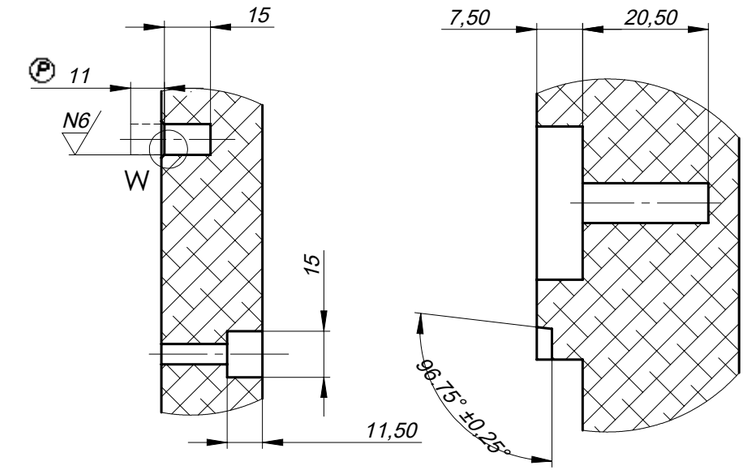

DETALHE Z
ESC. 1:2

DETALHE Y
ESC. 1:1

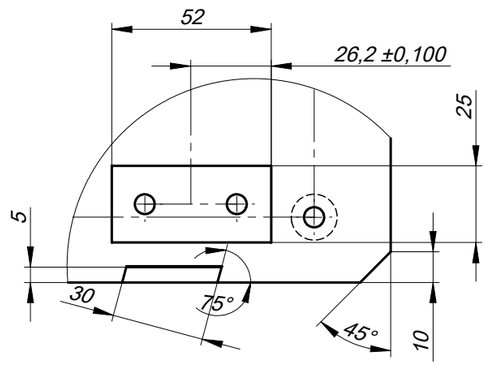

DETALHE J
ESC. 1:2

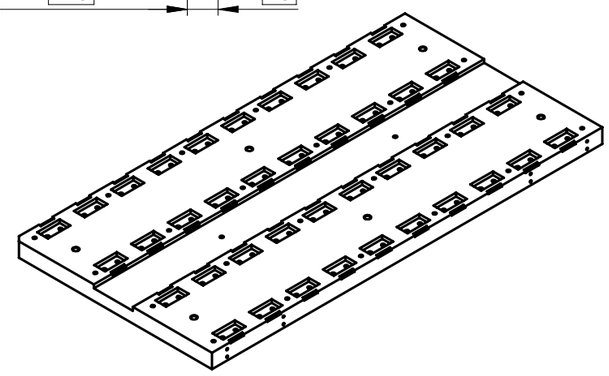

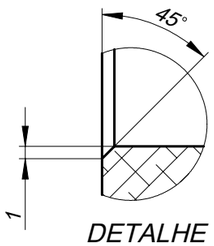

DETALHE W
ESC. 2:1

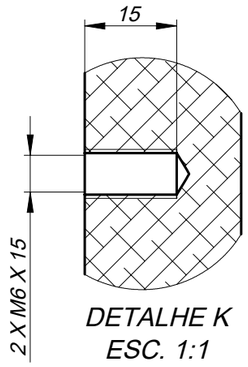

DETALHE K
ESC. 1:1

OBSERVAÇÕES - COTAGEM E TOLERANCIAMENTO EM CONFORMIDADE COM A SIMETRIA EM RELAÇÃO AO PLANO HOTRIZONTAL REPRESENTADO NA VISTA DE PLANTA. MATERIAL: ALUMÍNIO 6061	Projetou 2020-06-10 Desenhou 2020-08-29 Verificou 2020- - UNL-FCT-DEMI TAP M&E DISSERTAÇÃO DE MESTRADO Escala 1:5 Tolerân. ISO 2768 m BASE DA FERRAMENTA PARA AS PÁS DO 1º ANDAR DO HPC	PEDRO RENDAS MIEMc 47676 F_HPC_0101 Substitui: Substituido por:

Appendix X

Stage 1 Tool's Top Component Technical Drawing

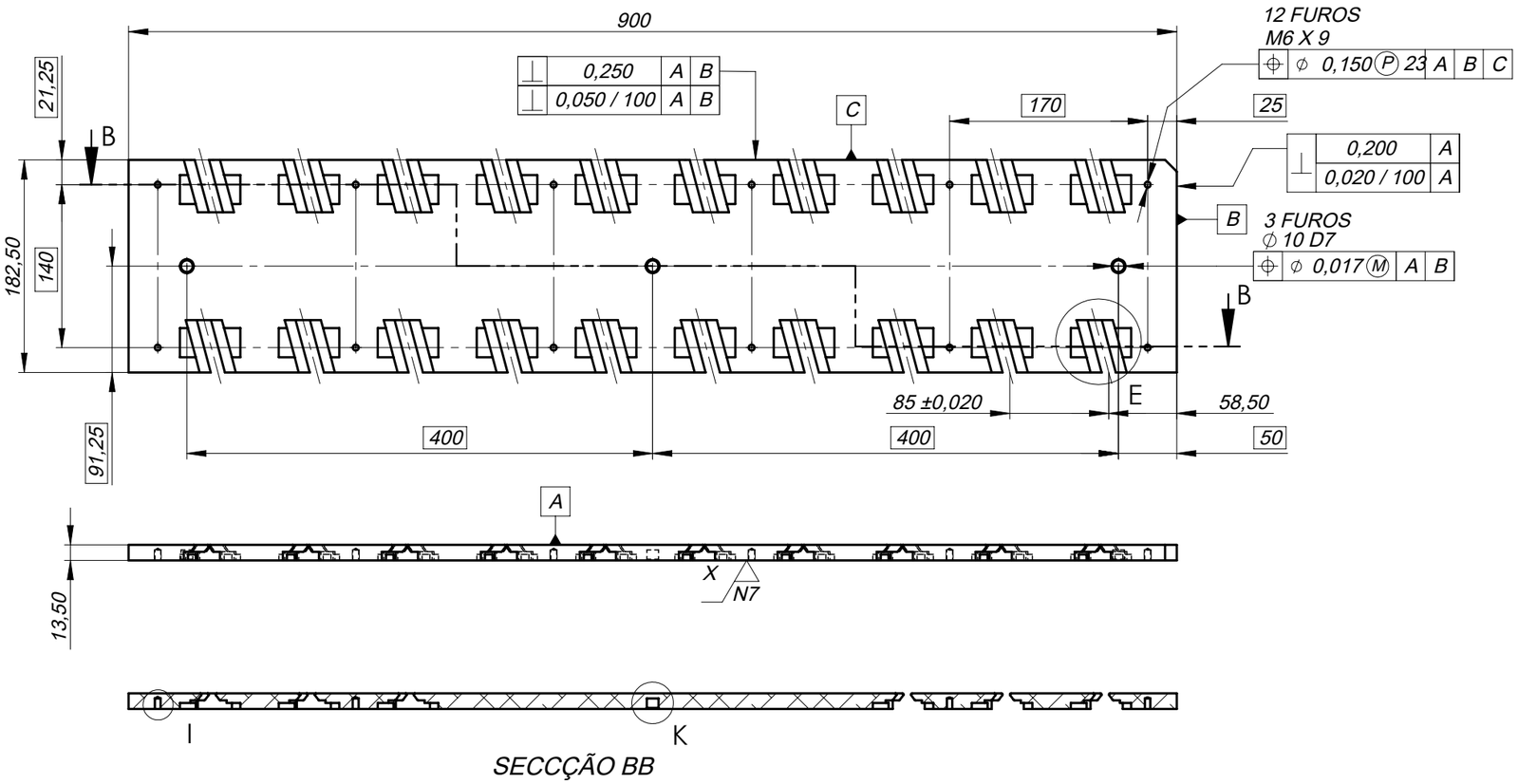

SECCÇÃO BB

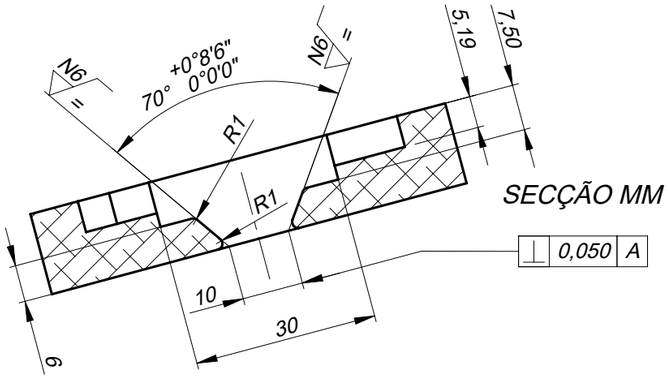

SECÇÃO MM

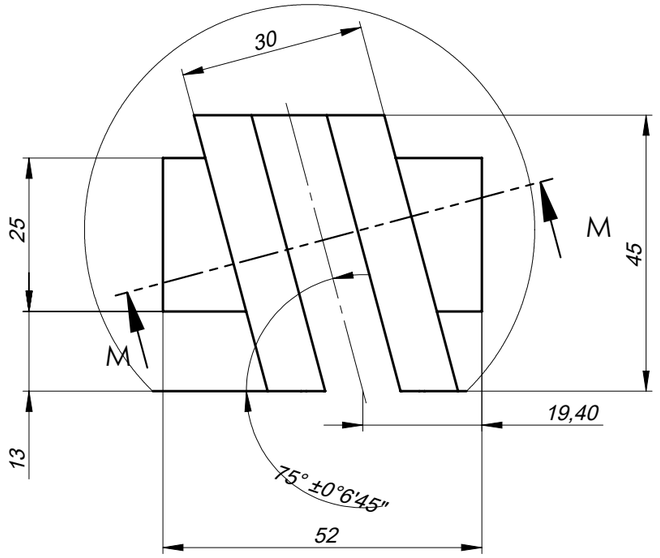

DETALHE E
ESC. 1:1

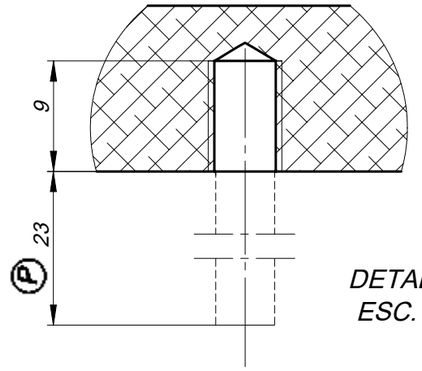

DETALHE I
ESC. 2 : 1

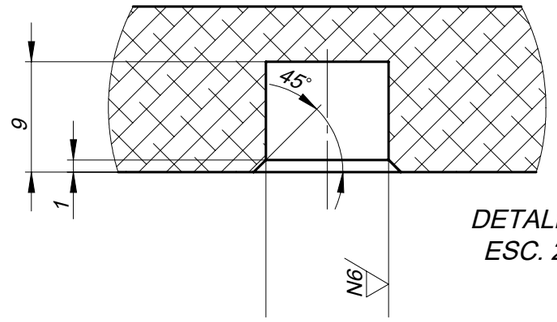

DETALHE K
ESC. 2 : 1

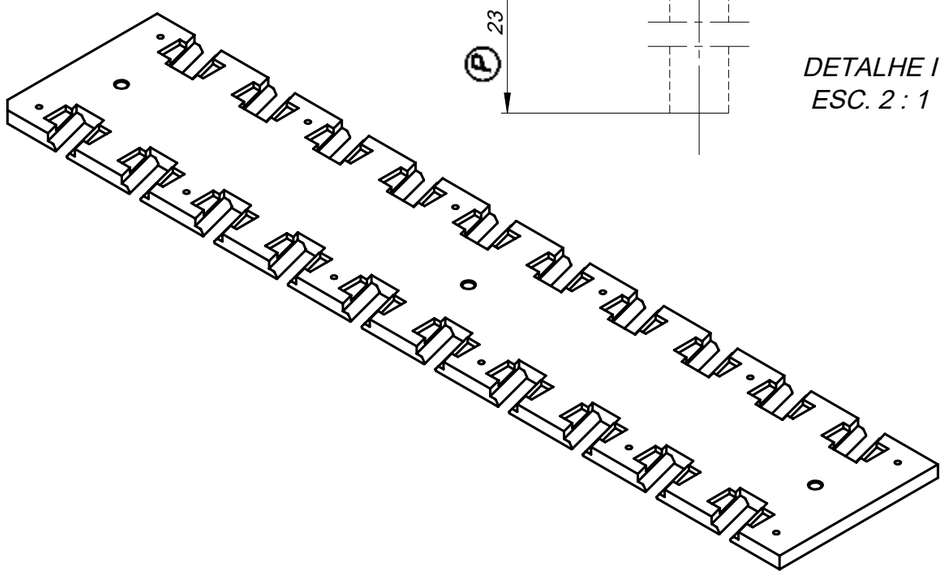

MATERIAL:
ALUMÍNIO 6061

Projetou		2020-06-11	UNL-FCT-DEMI TAP M&E
Desenhou		2020-07-29	DISSERTAÇÃO DE MESTRADO
Verificou		2020- -	

PEDRO RENDAS
MIEMc 47676

Escala 1:5

Tolerân. ISO 2768 m

COMPONENTE DE TOPO
PARA FERRAMENTA
DAS PÁS DO 1º ANDAR
DO HPC

F_HPC_0102

Substitui:

Substituido por:

Appendix XI

Stage 1 Tool's Upwards Force Bar Technical Drawing

Projetou		2020-08-31	UNL-FCT-DEMI TAP M&E DISSERTAÇÃO DE MESTRADO	PEDRO RENDAS MIEMC 47676
Desenhou		2020-06-10		
Verificou		2020- -		

SECÇÃO AA

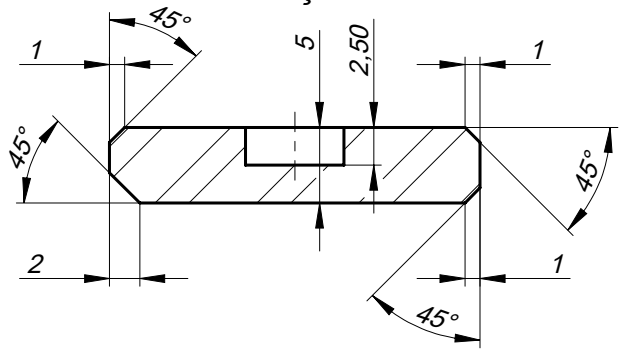

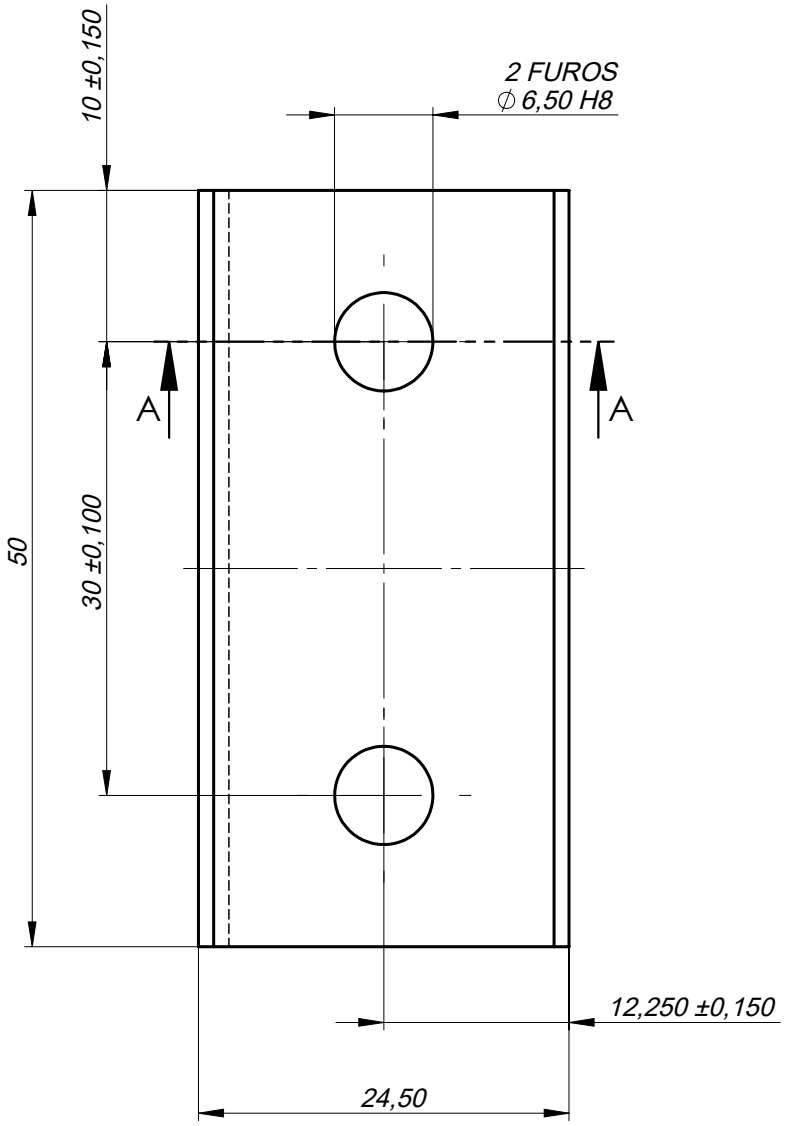

MATERIAL: AÇO INOX AISI 304	Esc. 2:1 Tolerância ISO 2768 m	BARRA DA FERRAMENTA STG1 HPC	F_HPC_0103 Substitui: Substituido por:

Appendix XII

Stage 1 Tool's Spacer Technical Drawing

Projetou		2020-08-31	UNL-FCT-DEMI TAP M&E DISSERTAÇÃO DE MESTRADO	PEDRO RENDAS MIEMC 47676
Desenhou		2020-07-12		
Verificou		2020- -		

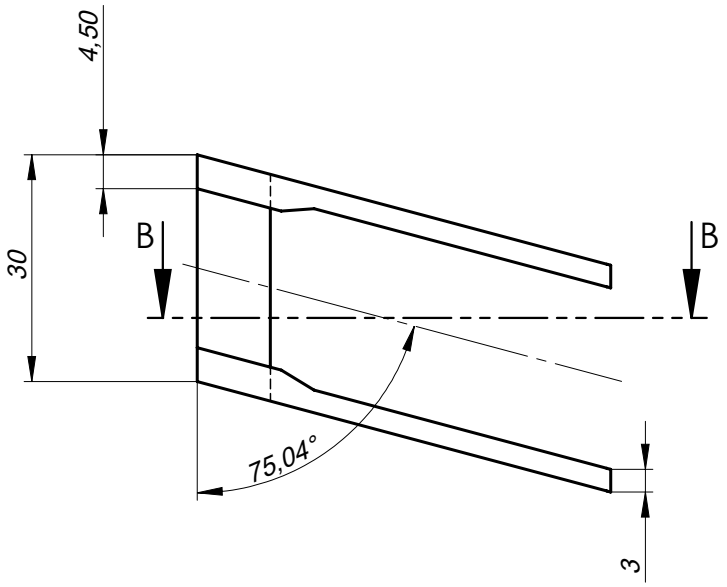

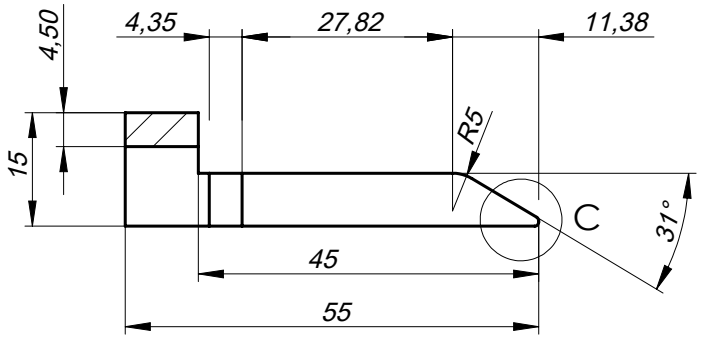

SECÇÃO BB

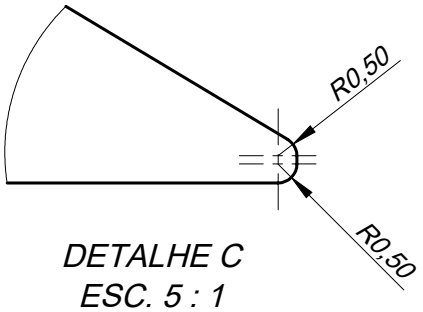

DETALHE C
ESC. 5 : 1

MATERIAL: AÇO INOX AISI 304	Esc. 1:1 Tolerância ISO 2768 m	CAVILHA STG1 HPC	F_HPC_0104 Substitui: Substituido por:

Appendix XIII

Stage 2 Tool's Assembly Technical Drawing

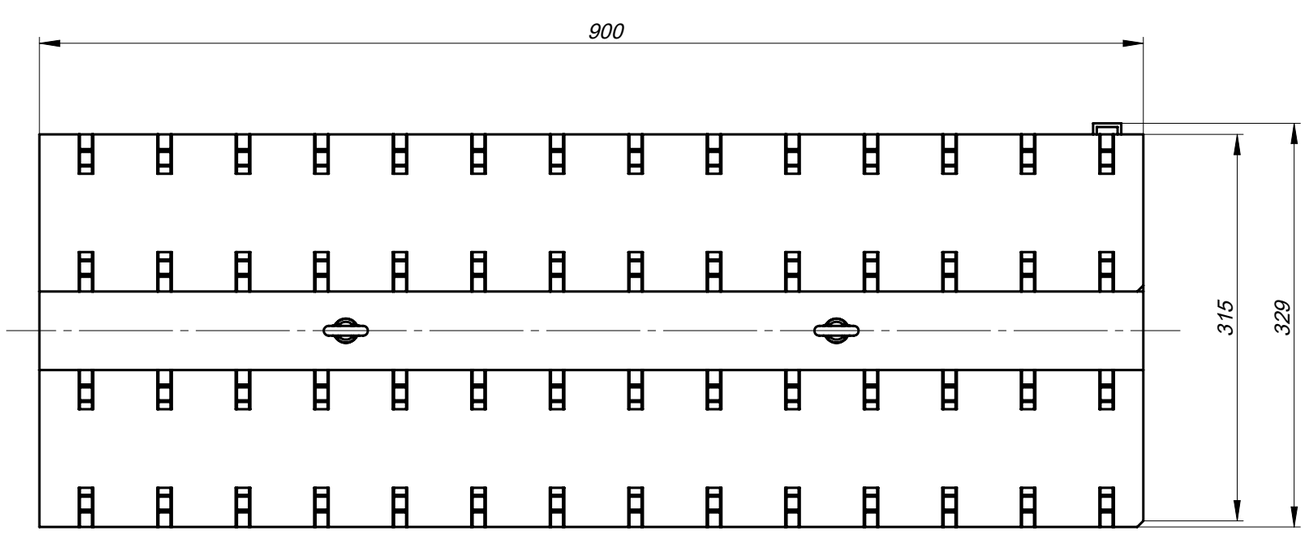

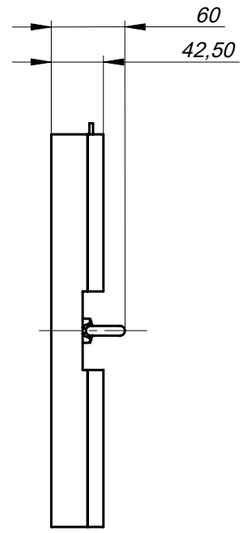

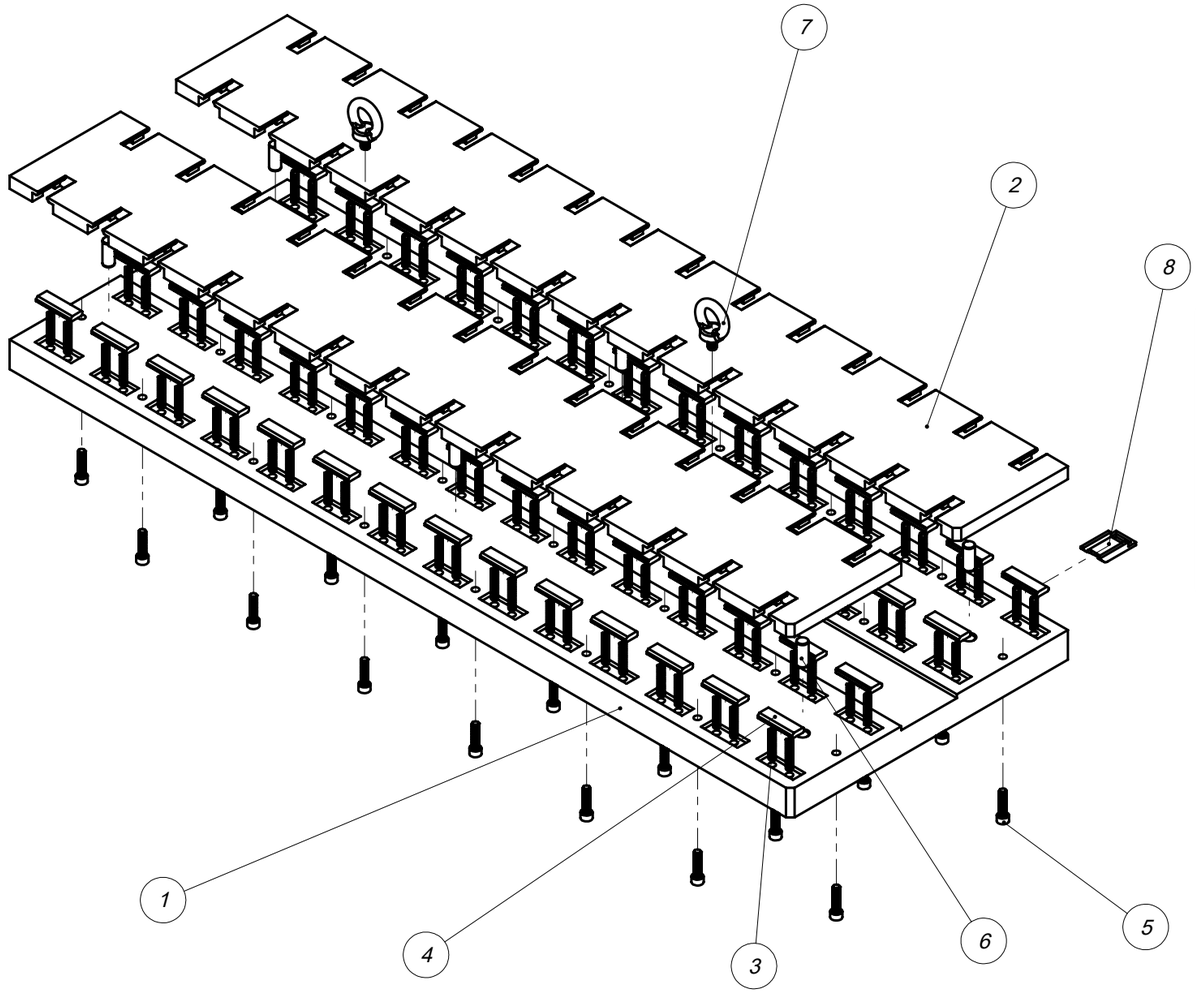

Nº	Designação	Nº da Norma Nº do Desenho	Material	Nº Ref	Prod. Semi Acabado Nº do Molde Nº da Matriz	Peso	Observações
56	CAVILHA STG2 HPC	F_HPC_0204	AÇO INOX AISI 304	8		23.43	MASSA EM GRAMAS
2	M8 LIFTING EYE BOLT	DIN 580		7		47.79	MASSA EM GRAMAS
6	ISO 2338 DOWEL PIN D10 X 24	F_HPC_PN01		6	TECHNIFAST DOWEL PIN	14.89	MASSA EM GRAMAS
28	SOCKET HEAD SCREW M6 X 25 - 25S	ISO 4762		5		1.014	MASSA EM GRAMAS
56	BARRA DA FERRAMENTA STG2 HPC	F_HPC_0203	AÇO INOX AISI 304	4		19.15	MASSA EM GRAMAS
112	COMPRESSION SPRING D5 X L35		EN 10270-1-SH	3	LESJOFORS CAT #15 - PART No. 5960	2.00	MASSA EM GRAMAS
2	TOPO DA FERRAMENTA STG2 HPC	F_HPC_0202	ALUMÍNIO 6061	2		3.25	MASSA EM KG
1	BASE DA FERRAMENTA STG2 HPC	F_HPC_0201	ALUMÍNIO 6061	1		21.52	MASSA EM KG

OBSERVAÇÕES

PESO ESTIMADO:
33.40 KG
(SEM CAVILHAS)

Projetou		2020-06-25
Desenhou		2020-08-31
Verificou		2020- -

UNL-FCT-DEMI TAP M&E
DISSERTAÇÃO DE MESTRADO

PEDRO RENDAS
MIEMc 47676

Escala 1:5

Tolerân. ISO 2768 m

FERRAMENTA STG2 HPC

F_HPC_0200

Substitui:

Substituido por:

Appendix XIV

Stage 2 Tool’s Bottom Component Technical Drawing

SECÇÃO XX

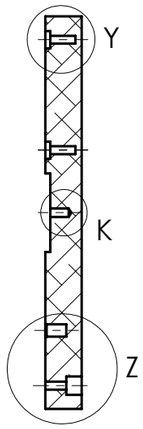

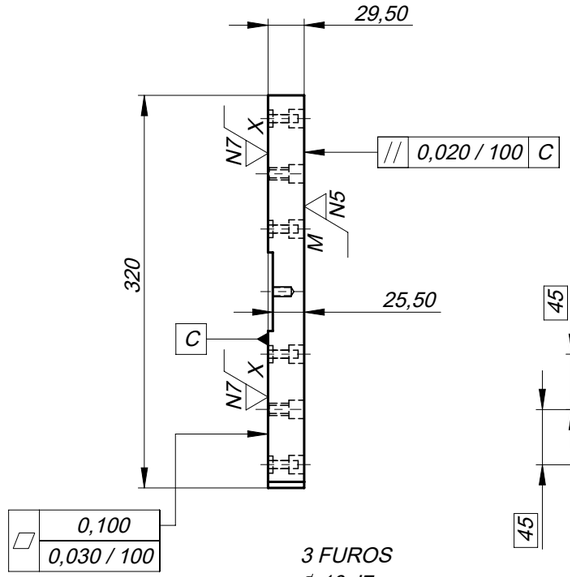

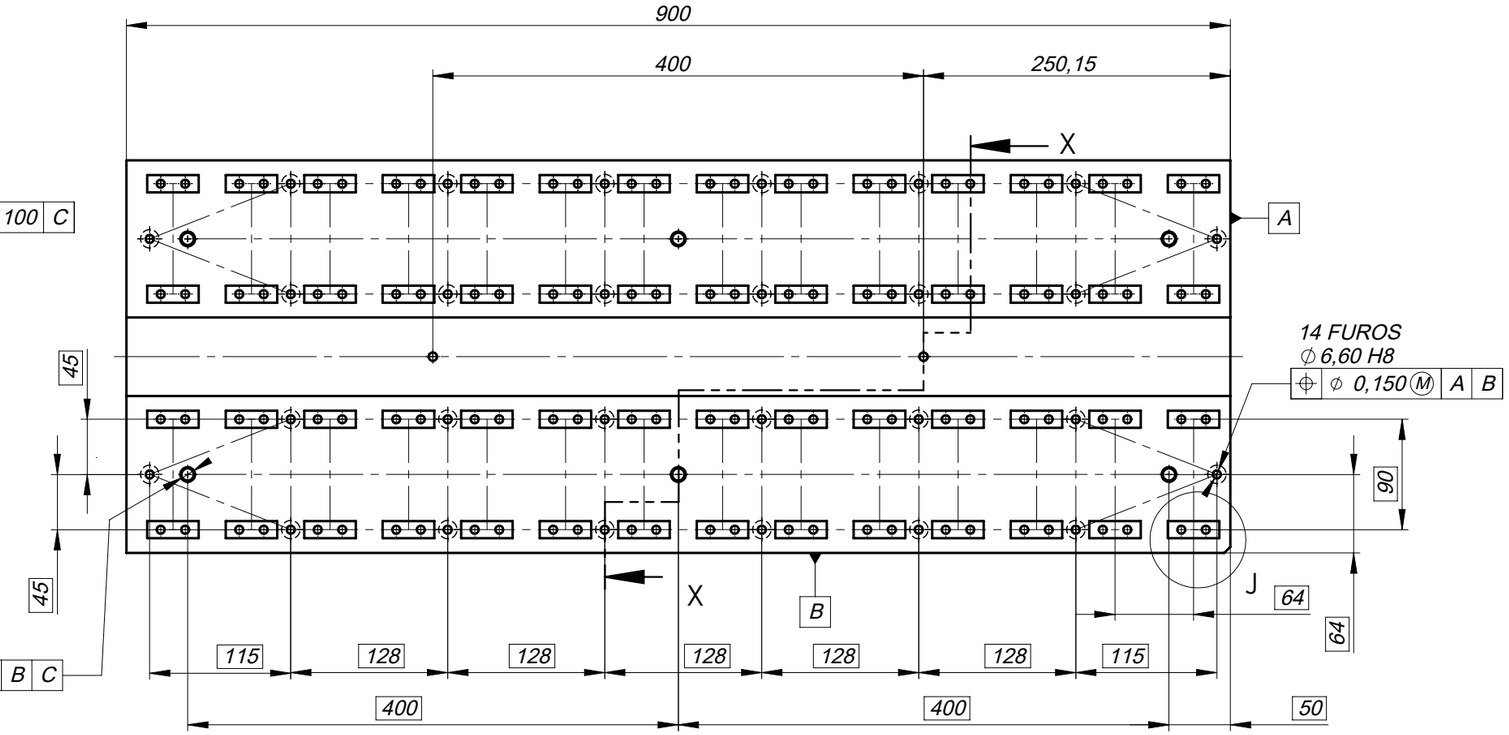

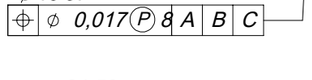

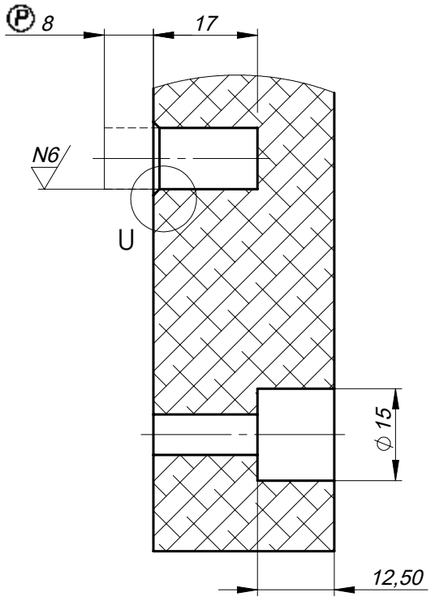

DETALHE Z
ESC. 1:1

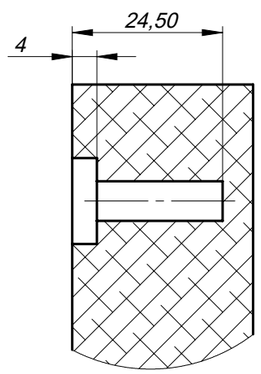

DETALHE Y
ESC. 1:1

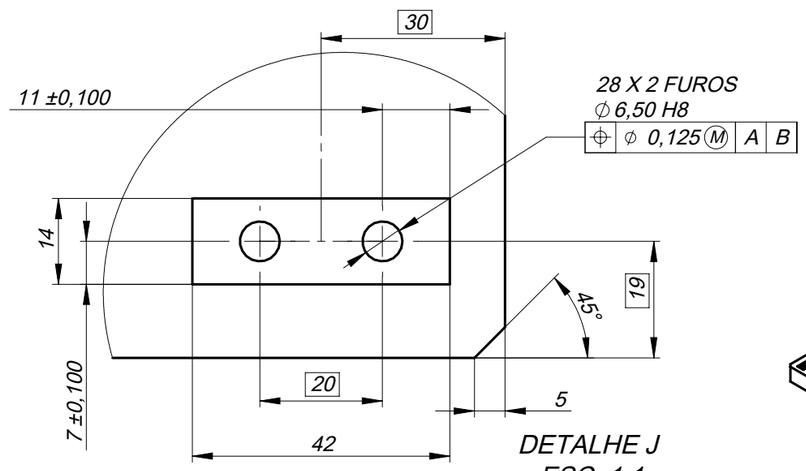

DETALHE J
ESC. 1:1

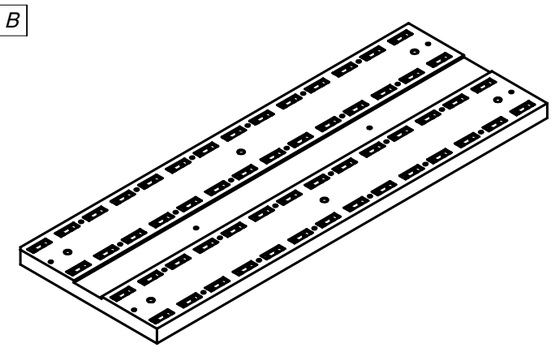

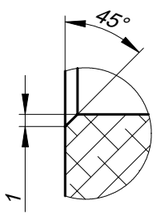

DETALHE U
ESC. 2:1

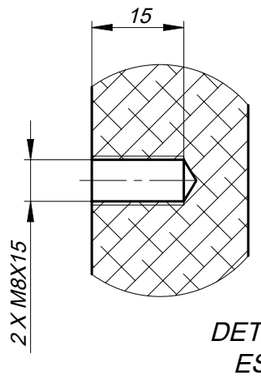

DETALHE K
ESC. 1:1

OBSERVAÇÕES				
- COTAGEM E TOLERANCIAMENTO EM CONFORMIDADE COM A SIMETRIA EM RELAÇÃO AO PLANO HOTRIZONTAL REPRESENTADO NA VISTA DE PLANTA.	Projetou		2020-06-15	UNL-FCT-DEMI TAP M&E DISSERTAÇÃO DE MESTRADO
MATERIAL: ALUMÍNIO 6061	Desenhou		2020-08-29	
	Verificou		2020- -	
	Escala 1:5			BASE DA FERRAMENTA PARA AS PÁS DO 2º ANDAR DO HPC
	Tolerân. ISO 2768 m			

PEDRO RENDAS
MIEMc 47676

F_HPC_0201

Substitui:

Substituido por:

Appendix XV

Stage 2 Tool's Top Component Technical Drawing

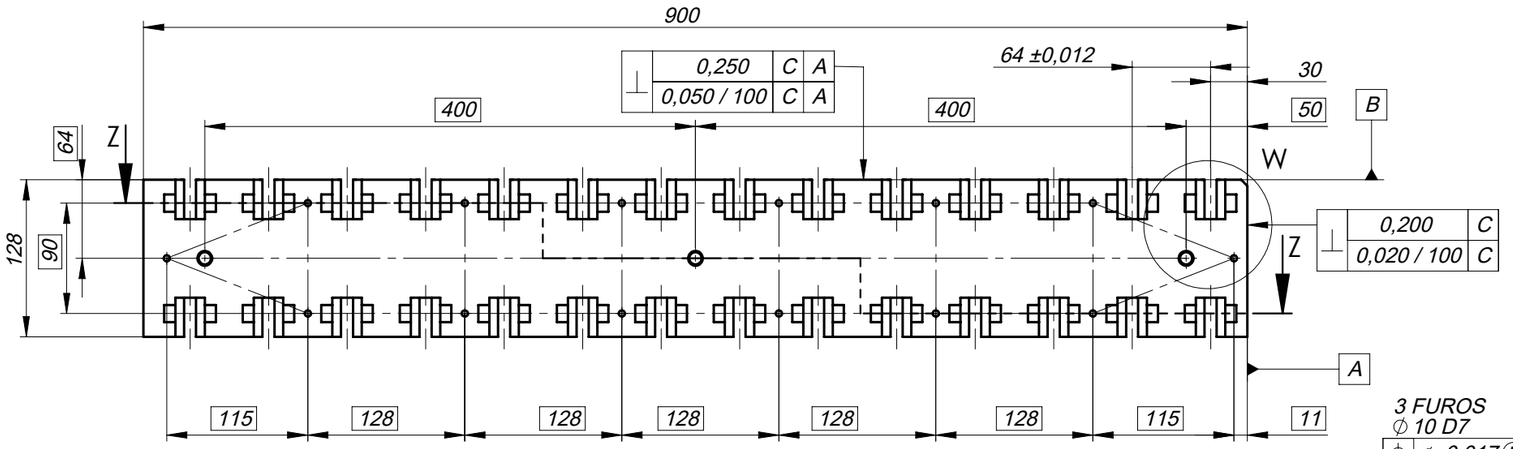

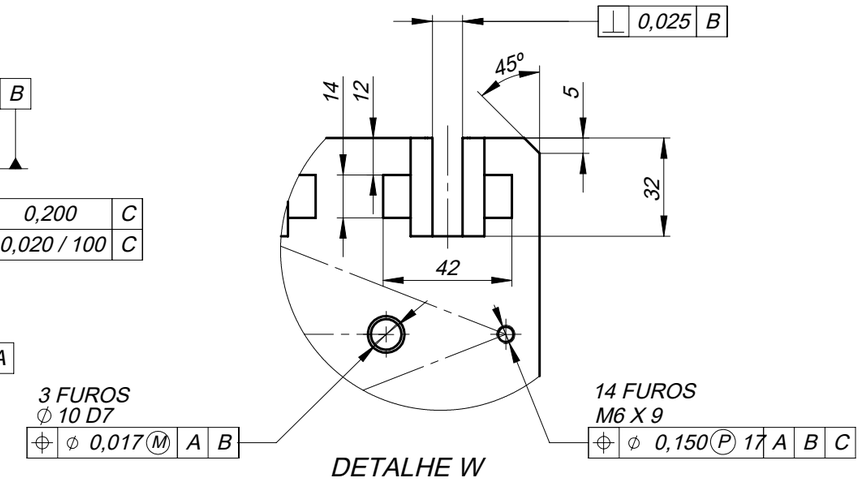

DETALHE W
ESC. 1:2

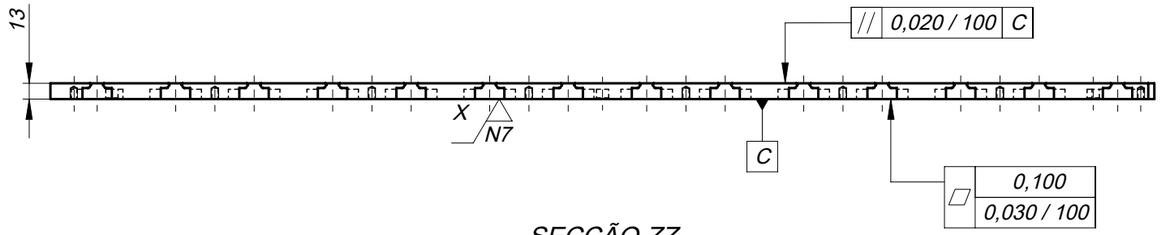

SECÇÃO ZZ

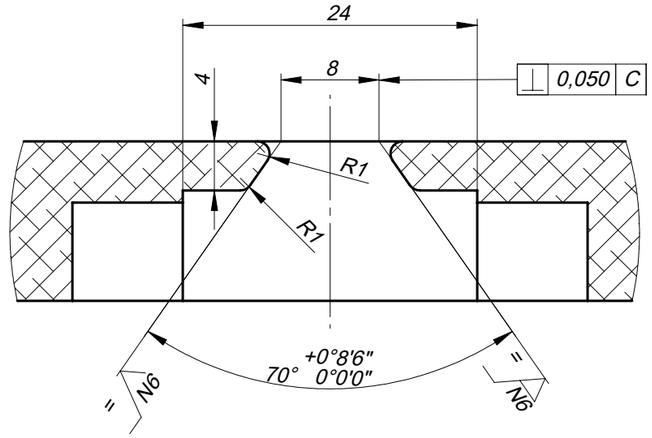

DETALHE Y
ESC 2:1

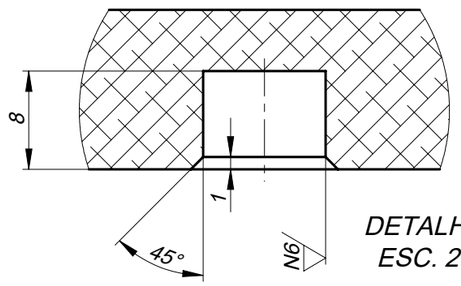

DETALHE X
ESC. 2 : 1

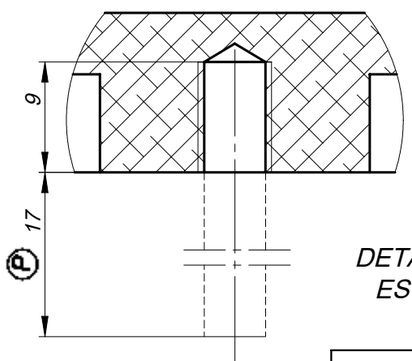

DETALHE K
ESC. 1:1

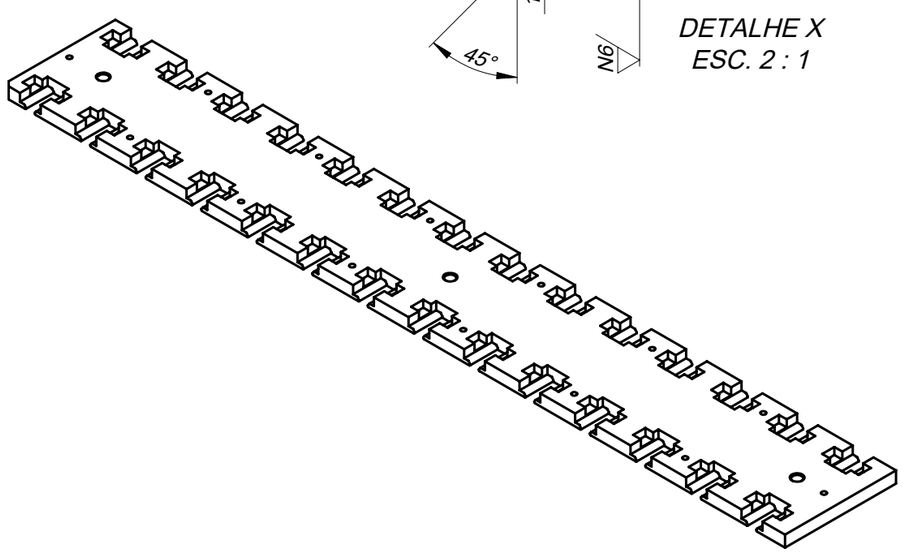

MATERIAL:
ALUMÍNIO 6061

Projetou		2020-06-15	UNL-FCT-DEMI TAP M&E	PEDRO RENDAS MIEMc 47676
Desenhou		2020-08-29	DISSERTAÇÃO DE MESTRADO	
Verificou		2020- -		
Escala 1:5	COMPONENTE DE TOPO PARA FERRAMENTA DAS PÁS DO 2º ANDAR DO HPC			F_HPC_0202
Tolerân. ISO 2768 m				Substitui:
				Substituido por:

Appendix XVI

Stage 2 Tool's Upwards Force Bar Technical Drawing

Projetou		2020-08-31	UNL-FCT-DEMI TAP M&E DISSERTAÇÃO DE MESTRADO	PEDRO RENDAS MIEMC 47676
Desenhou		2020-06-10		
Verificou		2020- -		

SECÇÃO AA

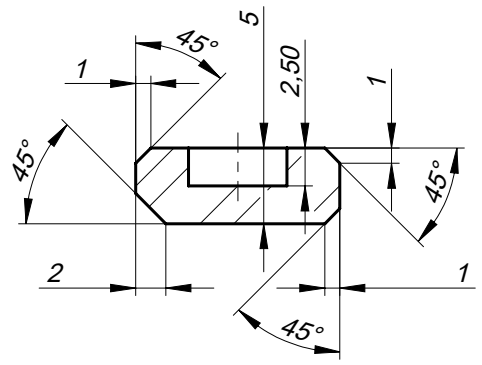

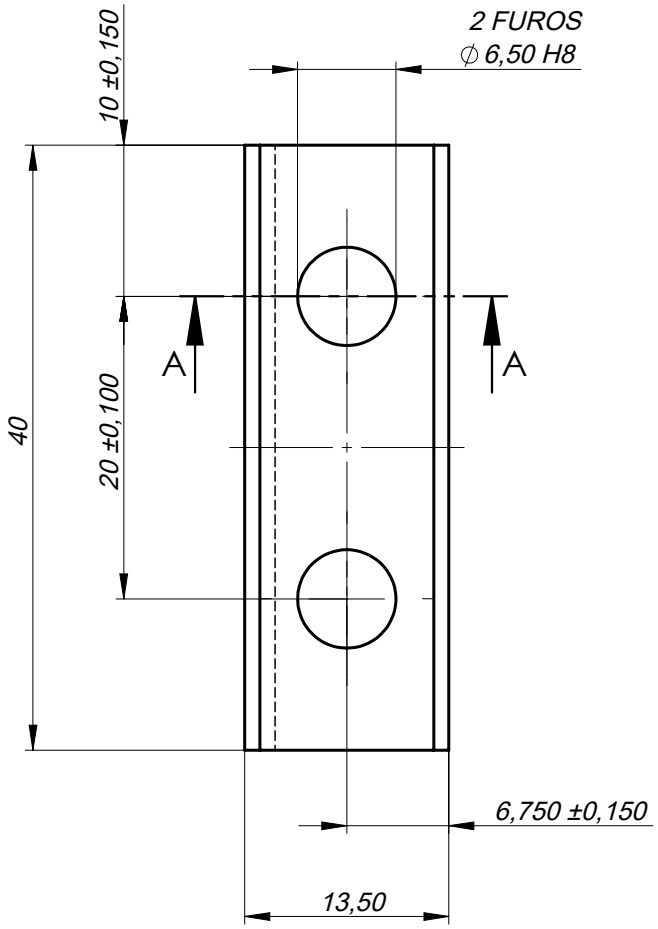

MATERIAL: AÇO INOX AISI 304	Esc. 2:1 Tolerância ISO 2768 m	BARRA DA FERRAMENTA STG2 HPC	F_HPC_0203 Substitui: Substituido por:

Appendix XVII

Stage 2 Tool’s Spacer Technical Drawing

Projetou		2020-08-31	UNL-FCT-DEMI TAP M&E DISSERTAÇÃO DE MESTRADO	PEDRO RENDAS MIEMC 47676
Desenhou		2020-07-12		
Verificou		2020- -		

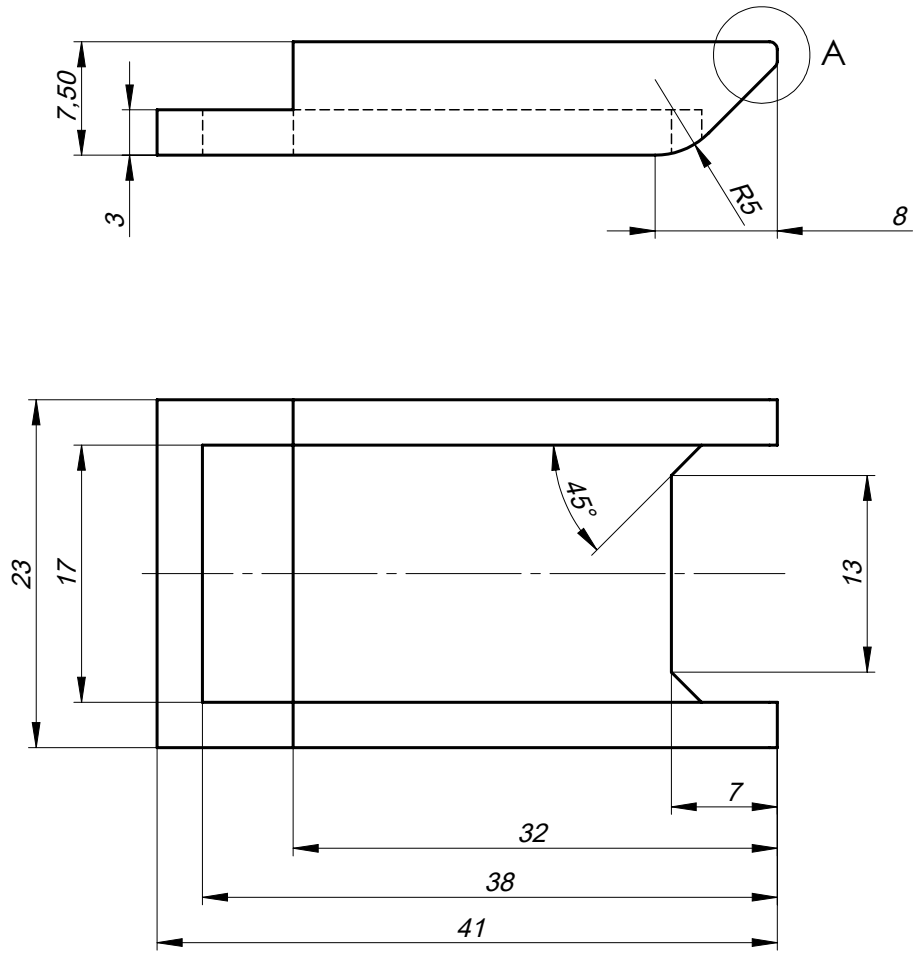

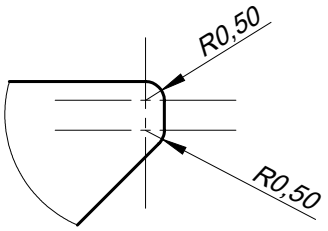

DETALHE A
ESC. 5 : 1

MATERIAL: AÇO INOX AISI 304	Esc. 2:1 Tolerância ISO 2768 m	CAVILHA STG2 HPC	F_HPC_0204 Substitui: Substituido por:

Appendix XVIII

Stage 3 Tool's Assembly Technical Drawing

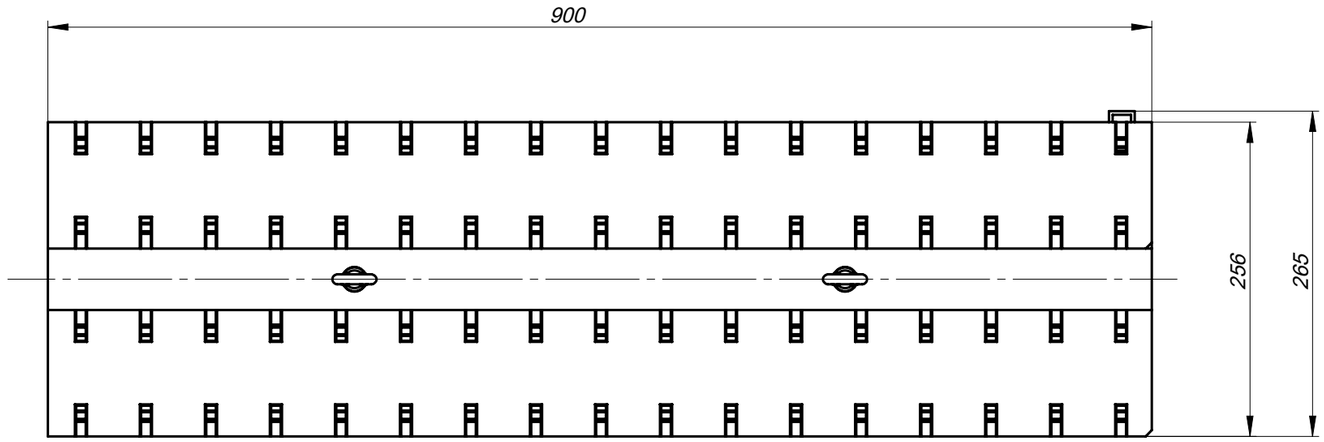

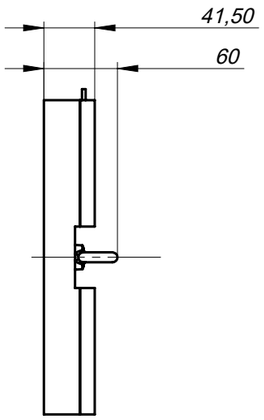

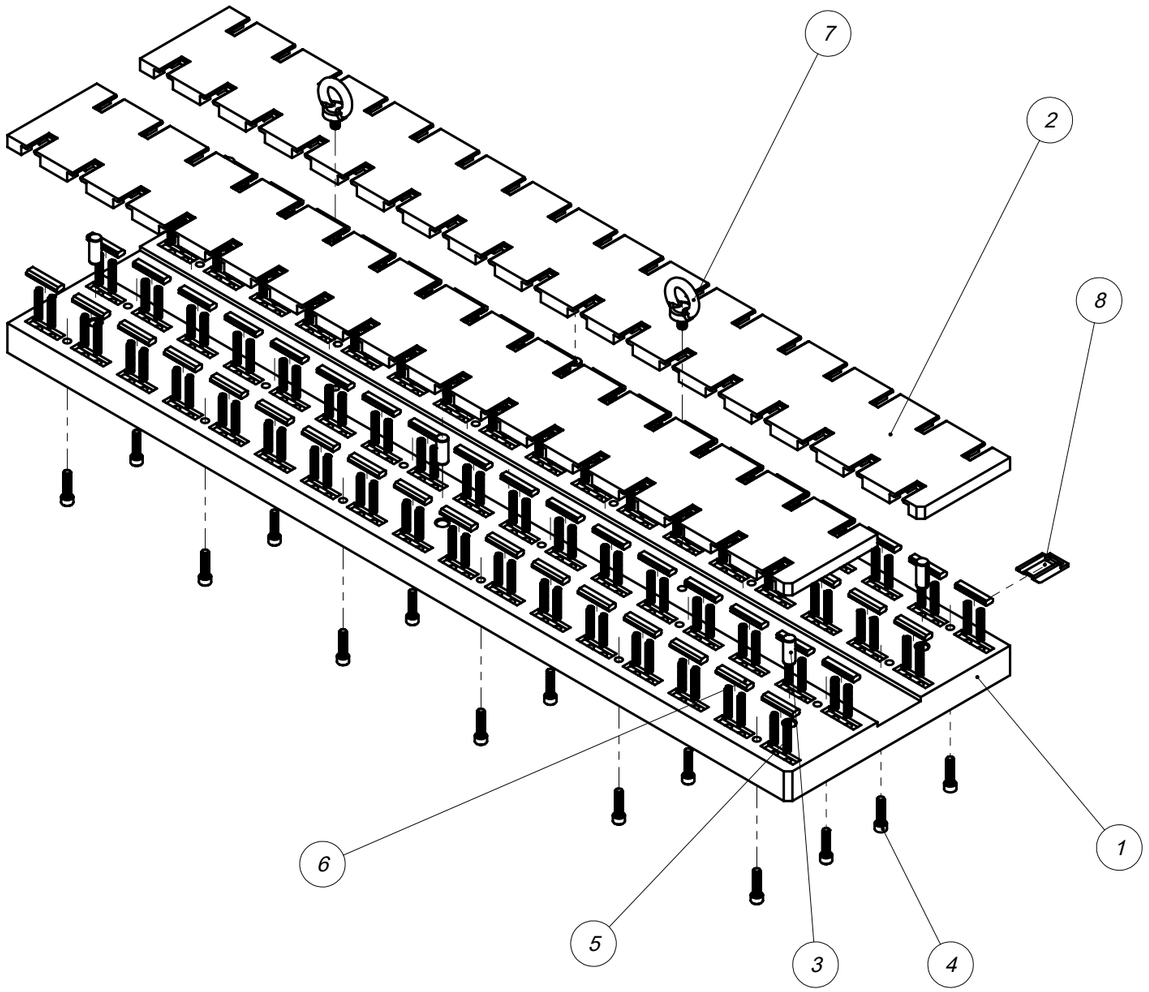

Nº	Designação	Nº da Norma Nº do Desenho	Material	Nº Ref	Prod. Semi Acabado Nº do Molde Nº da Matriz	Peso	Observações
68	CAVILHA STG3 HPC	F_HPC_0304	AÇO INOX AISI 304	8		19.25	MASSA EM GRAMAS
2	M8 LIFTING EYE BOLT	DIN 580		7		47.79	MASSA EM GRAMAS
68	BARRA DA FERRAMENTA STG3 HPC	F_HPC_0303	AÇO INOX AISI 304	6		9.59	MASSA EM GRAMAS
136	COMPRESSION SPRING D5 X L35		EN 10270-1-SH	5	LESJOFORS CAT #15 - PART No. 5960	2.00	MASSA EM GRAMAS
24	SOCKET HEAD SCREW M6 X 25 - 25S	ISO 4762		4		1.014	MASSA EM GRAMAS
6	ISO 2338 DOWEL PIN D10 X 24	F_HPC_PN01		3	TECHNIFAST DOWEL PIN	14.89	MASSA EM GRAMAS
2	TOPO DA FERRAMENTA STG3 HPC	F_HPC_0302	ALUMÍNIO 6061	2		2.29	MASSA EM KG
1	BASE DA FERRAMENTA STG3 HPC	F_HPC_0301	ALUMÍNIO 6061	1		17.16	MASSA EM KG

OBSERVAÇÕES

PESO ESTIMADO: 22.89 KG (SEM CAVILHAS)

Projetou		2020-06-10
Desenhou		2020-08-29
Verificou		2020- -

UNL-FCT-DEMI TAP M&E
DISSERTAÇÃO DE MESTRADO

PEDRO RENDAS
MIEMc 47676

Escala 1:5

Tolerân. ISO 2768 m

FERRAMENTA STG3 HPC

F_HPC_0300

Substitui:

Substituido por:

Appendix XIX

Stage 3 Tool’s Bottom Component Technical Drawing

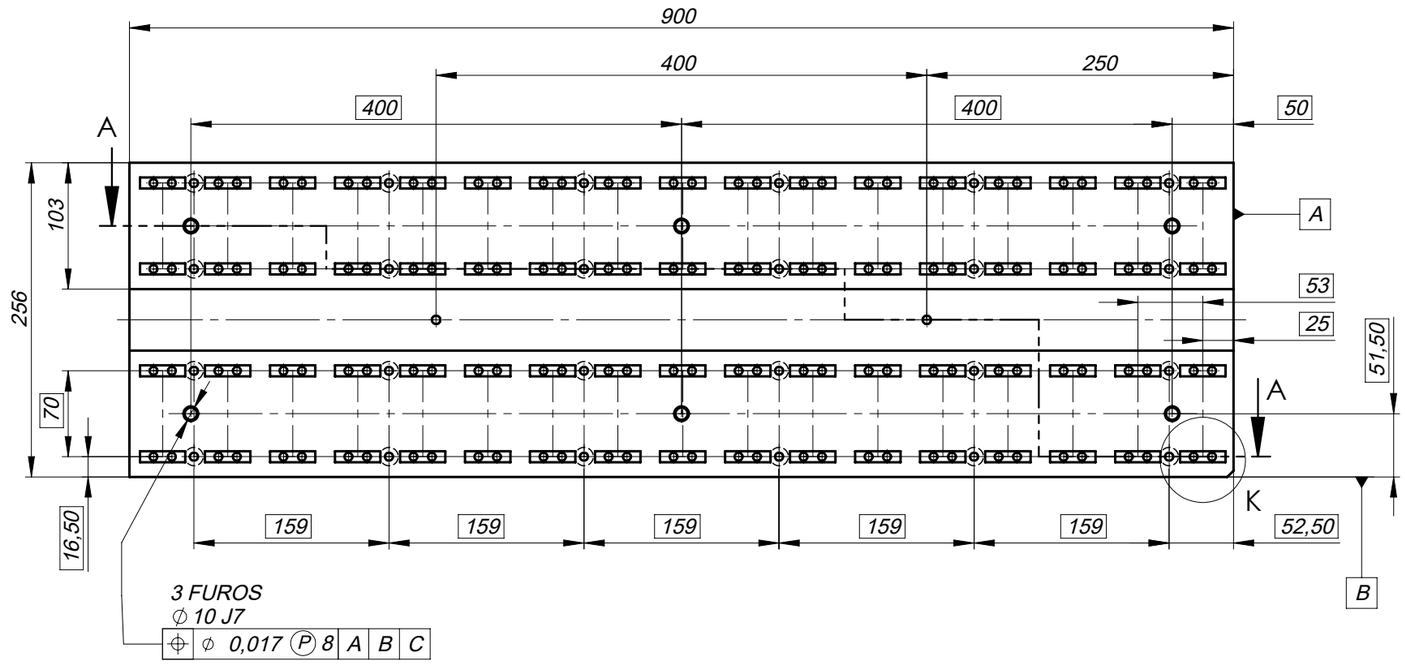

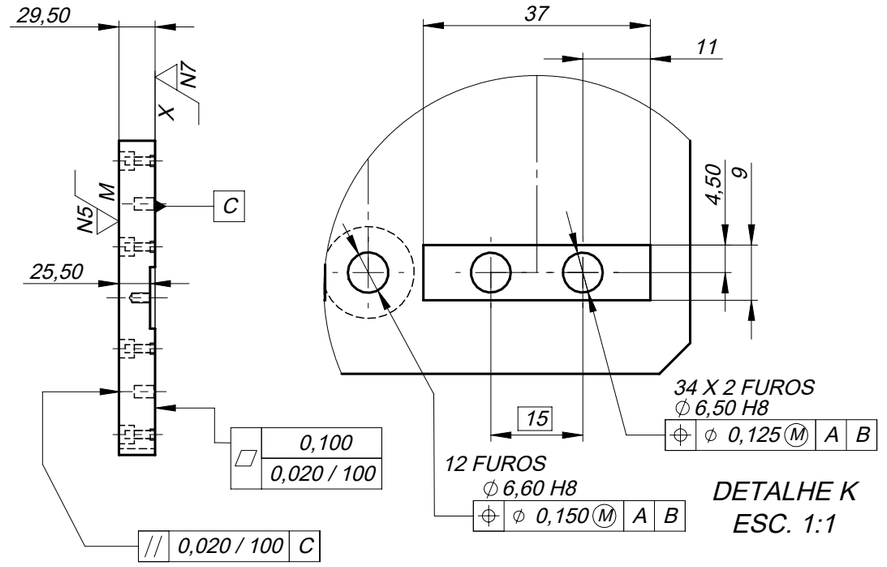

DETALHE K
ESC. 1:1

SECÇÃO AA

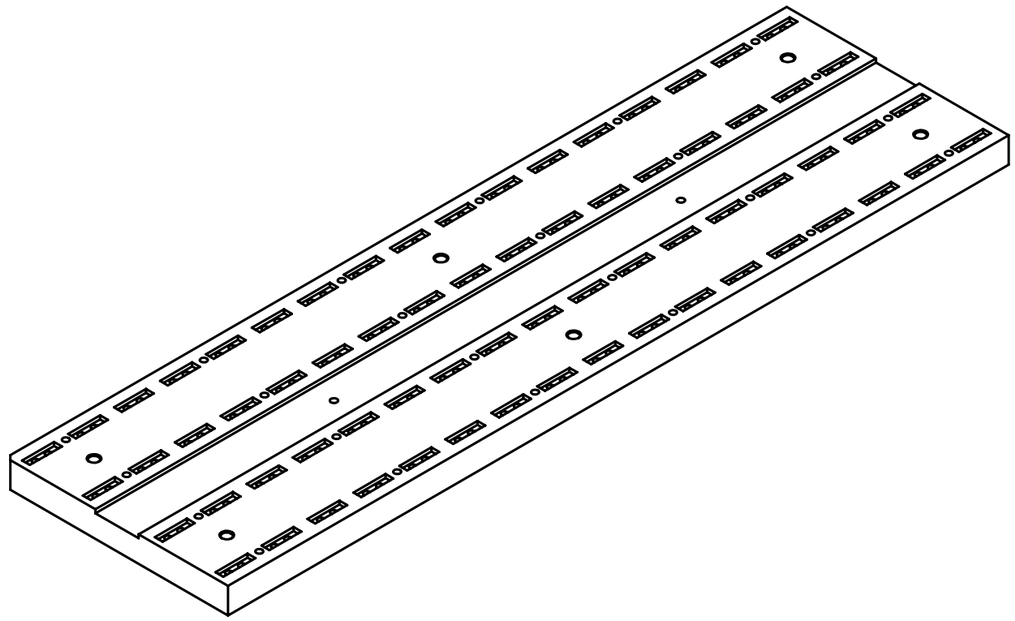

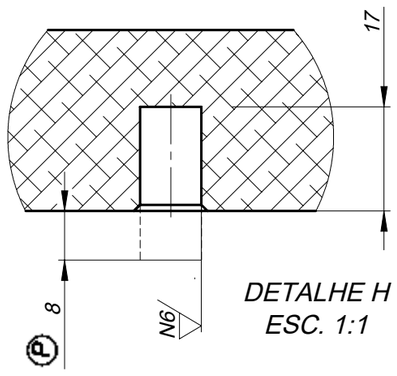

DETALHE H
ESC. 1:1

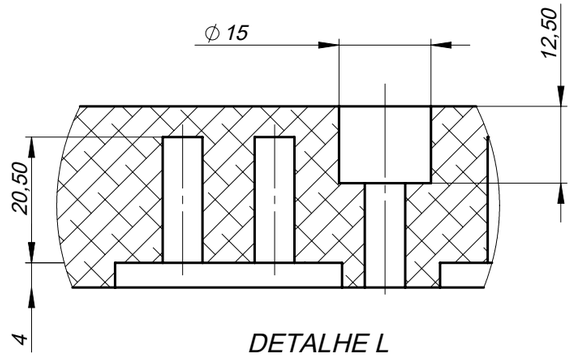

DETALHE L
ESC. 1:1

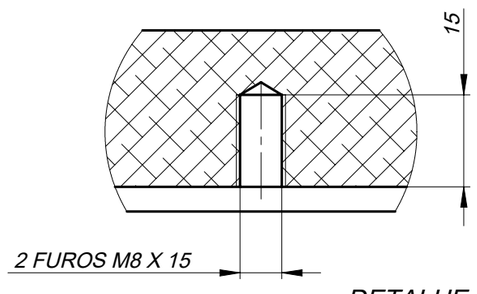

DETALHE J
ESC. 1:1

OBSERVAÇÕES

- COTAGEM E TOLERANCIAMENTO EM CONFORMIDADE COM A SIMETRIA EM RELAÇÃO AO PLANO HOTRIZONTAL REPRESENTADO NA VISTA DE PLANTA.

MATERIAL:
ALUMÍNIO 6061

Projetou		2020-06-22	UNL-FCT-DEMI TAP M&E DISSERTAÇÃO DE MESTRADO
Desenhou		2020-08-30	
Verificou		2020- -	

Escala 1:5

Tolerân. ISO 2768 m

BASE DA FERRAMENTA PARA AS PÁS DO 3º ANDAR DO HPC

PEDRO RENDAS
MIEMc 47676

F_HPC_0301

Substitui:

Substituido por:

Appendix XX

Stage 3 Tool's Top Component Technical Drawing

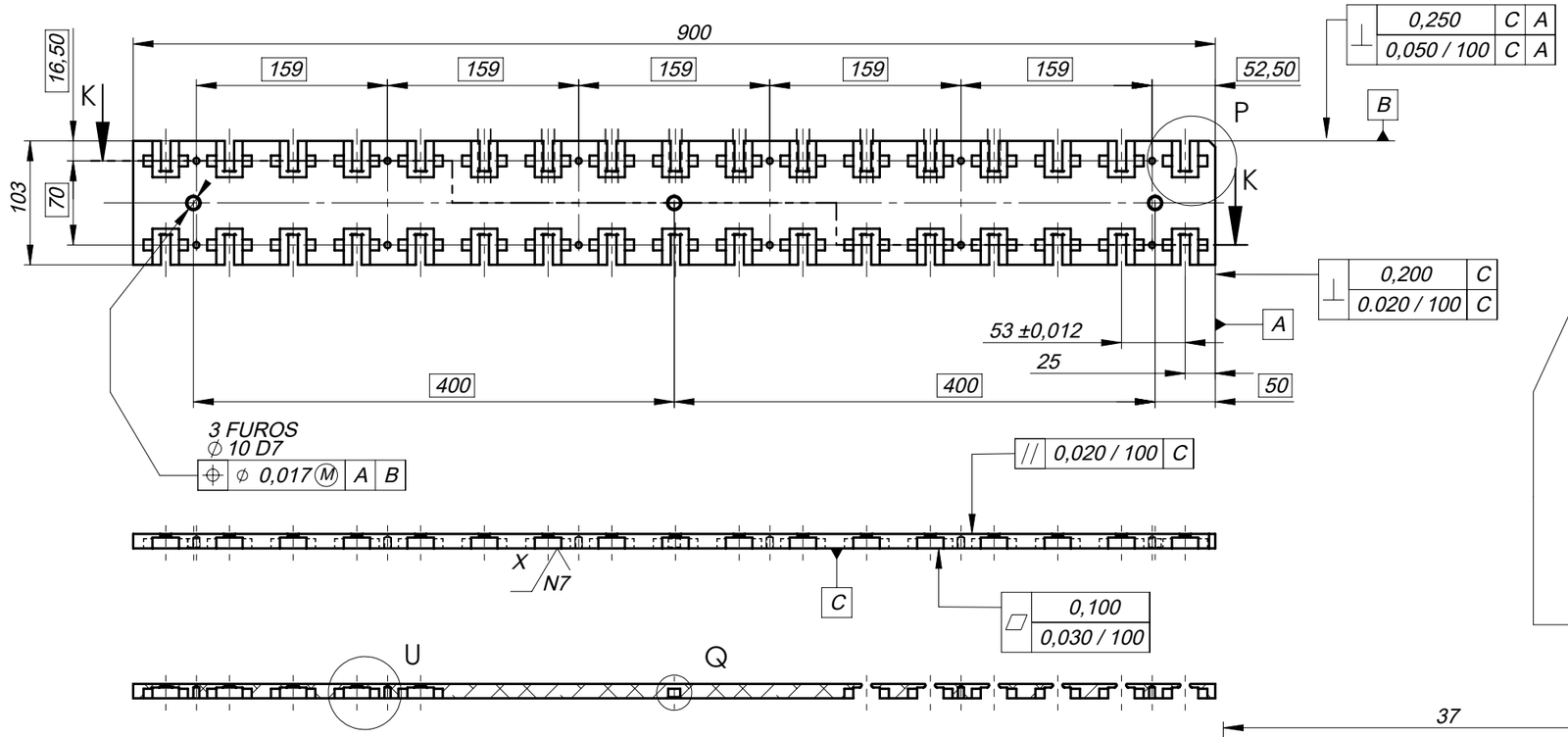

SECÇÃO KK

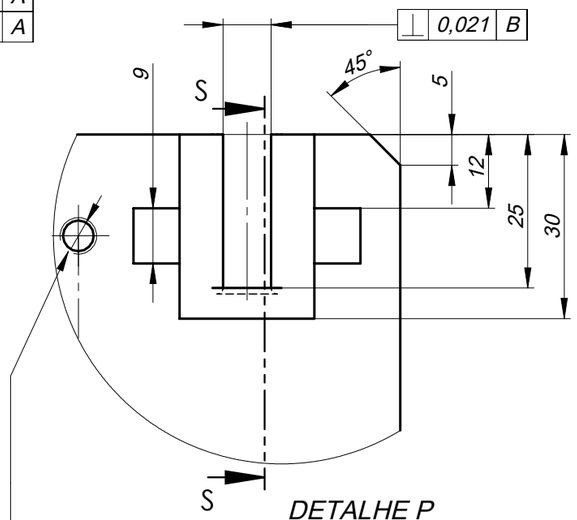

DETALHE P
ESC. 1:1

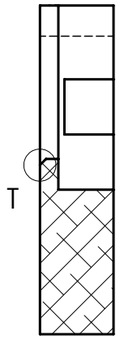

SECÇÃO SS

12 FUROS
M6 X 9
⌖ ⌀ 0,150 Ⓟ 17 A B C

DETALHE U
ESC. 2:1

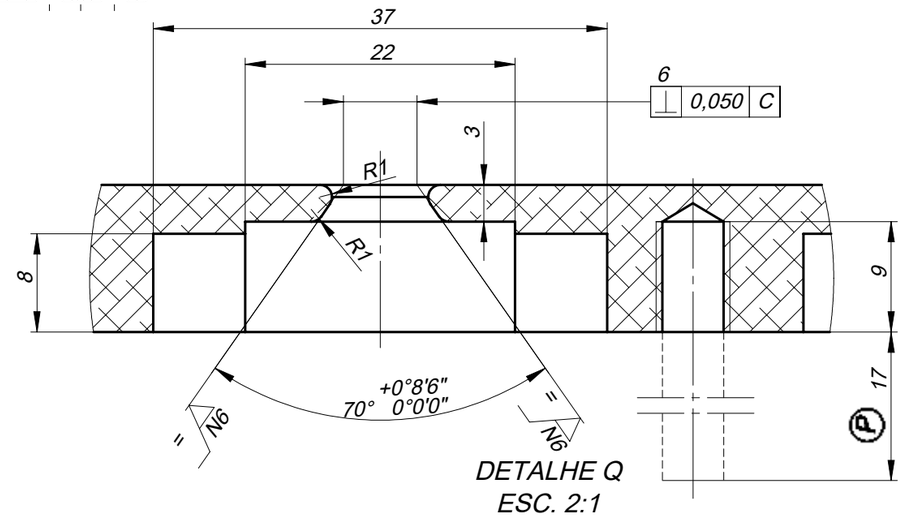

DETALHE Q
ESC. 2:1

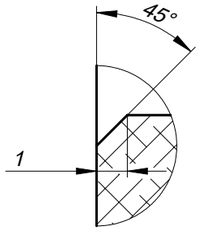

DETALHE T
ESC. 5 : 1

MATERIAL:
ALUMÍNIO 6061

Projetou		2020-06-22
Desenhou		2020-08-30
Verificou		2020- -

UNL-FCT-DEMI TAP M&E
DISSERTAÇÃO DE MESTRADO

PEDRO RENDAS
MIEMc 47676

Escala 1:5

Tolerân. ISO 2768 m

COMPONENTE DE TOPO
PARA FERRAMENTA
DAS PÁS DO 3º ANDAR
DO HPC

F_HPC_0302

Substitui:

Substituido por:

Appendix XXI

Stage 3 Tool's Upwards Force Bar Technical Drawing

Projetou		2020-08-31	UNL-FCT-DEMI TAP M&E DISSERTAÇÃO DE MESTRADO	PEDRO RENDAS MIEMC 47676
Desenhou		2020-06-26		
Verificou		2020- -		

SECÇÃO AA

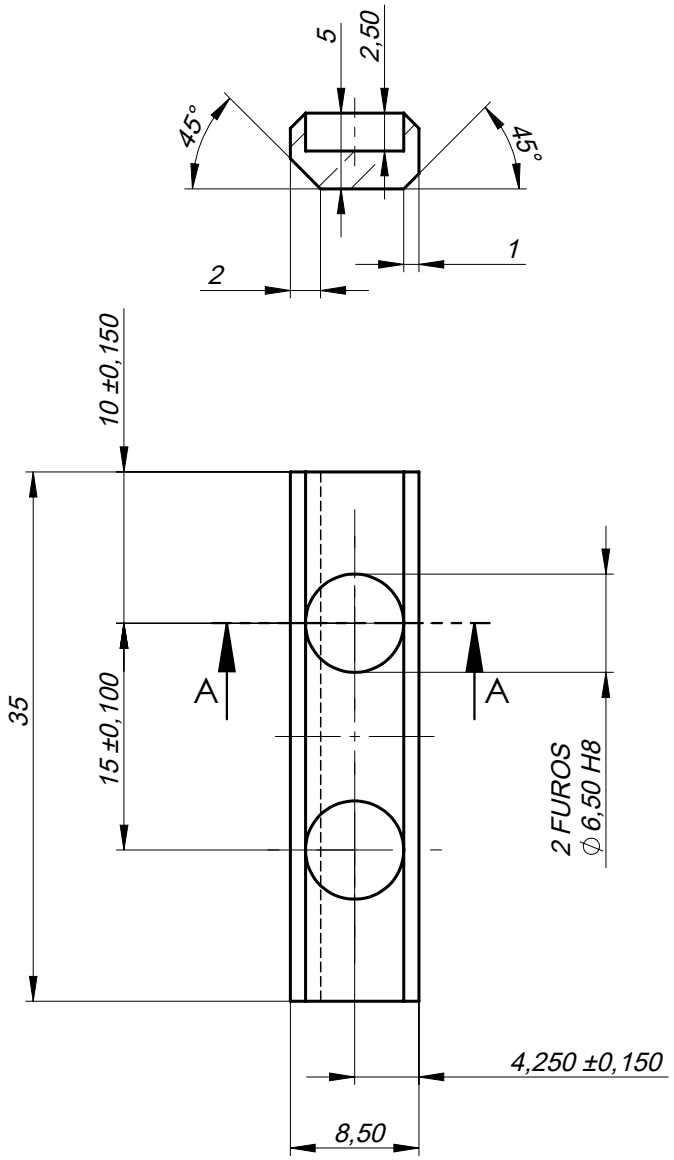

MATERIAL: AÇO INOX AISI 304	Esc. 2:1 Tolerância ISO 2768 m	BARRA DA FERRAMENTA STG3 HPC	F_HPC_0303 Substitui: Substituido por:

Appendix XXII

Stage 3 Tool's Spacer Technical Drawing

Projetou		2020-08-31	UNL-FCT-DEMI TAP M&E DISSERTAÇÃO DE MESTRADO	PEDRO RENDAS MIEMC 47676
Desenhou		2020-07-12		
Verificou		2020- -		

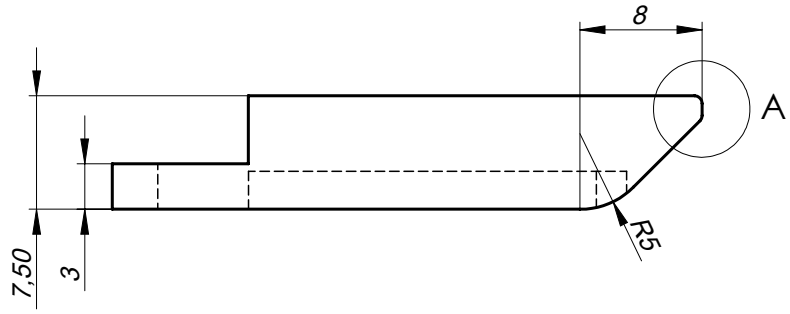

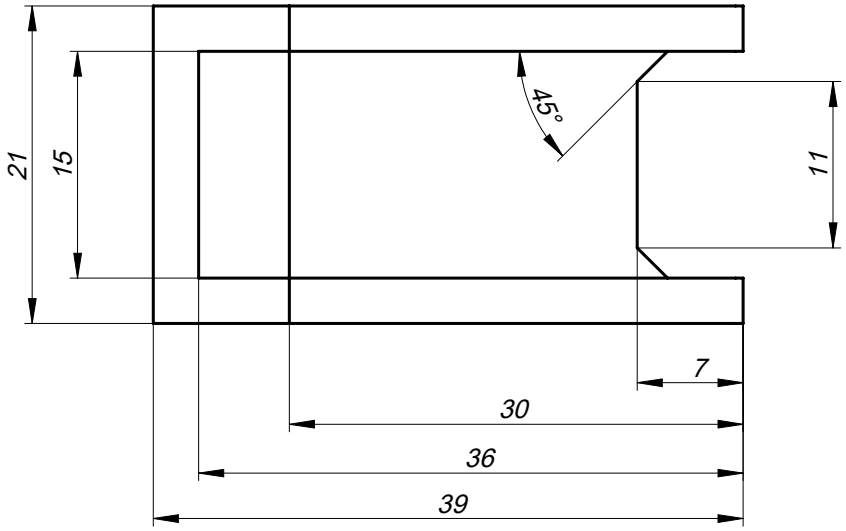

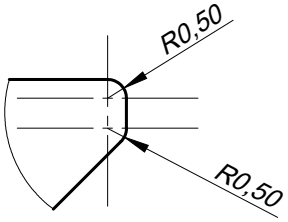

DETALHE A
ESC. 5 : 1

MATERIAL: AÇO INOX AISI 304	Esc. 2:1 Tolerância ISO 2768 m	CAVILHA STG3 HPC	F_HPC_0304 Substitui: Substituido por:

Appendix XXIII

Stage 4&5 Tool's Assembly Technical Drawing

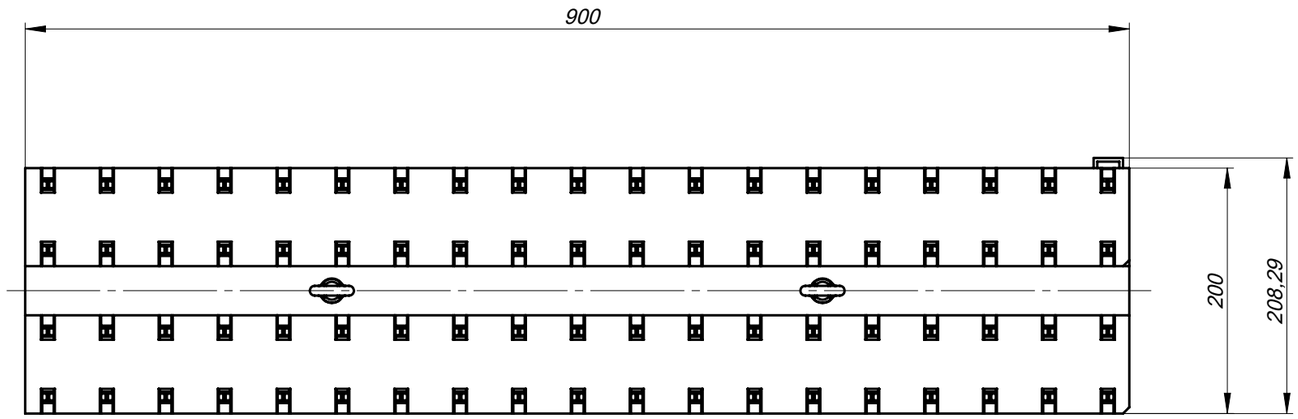

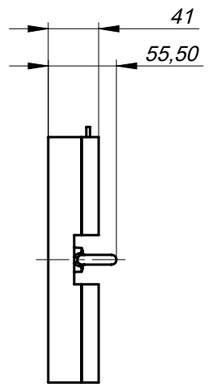

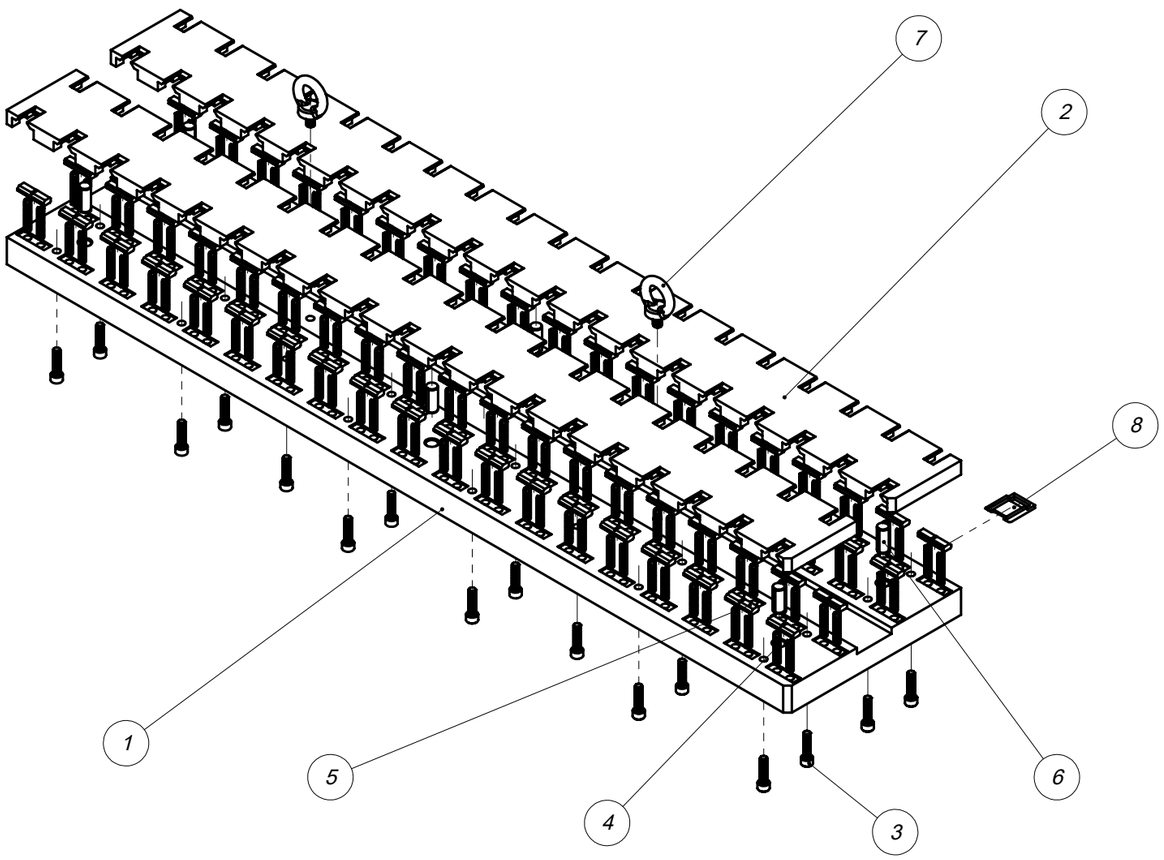

Nº	Designação	Nº da Norma Nº do Desenho	Material	Nº Ref	Prod. Semi Acabado Nº do Molde Nº da Matriz	Peso	Observações
76	CAVILHA STG4&5 HPC	F_HPC_0404	AÇO INOX AISI 304	8		13.20	MASSA EM GRAMAS
2	M8 LIFTING EYE BOLT	DIN 580		7		47.79	MASSA EM GRAMAS
6	ISO 2338 DOWEL PIN D10 X 24	F_HPC_PN01		6	TECHNIFAST DOWEL PIN	14.89	MASSA EM GRAMAS
76	BARRA DA FERRAMENTA STG4&5 HPC	F_HPC_0403	AÇO INOX AISI 304	5		8.00	MASSA EM GRAMAS
152	COMPRESSION SPRING D5 X L35		EN 10270-1-SH	4	LESJOFORS CAT #15 - PART No. 5960	2.00	MASSA EM GRAMAS
28	SOCKET HEAD SCREW M6 X 25 - 25S	ISO 4762		3		1.014	MASSA EM GRAMAS
2	TOPO DA FERRAMENTA STG4&5 HPC	F_HPC_0402	ALUMÍNIO 6061	2		1.94	MASSA EM KG
1	BASE DA FERRAMENTA STG4&5 HPC	F_HPC_0101	ALUMÍNIO 6061	1		11.97	MASSA EM KG

OBSERVAÇÕES

PESO ESTIMADO:
16.99 KG
(SEM CAVILHAS)

Projetou		2020-06-29
Desenhou		2020-08-31
Verificou		2020- -

UNL-FCT-DEMI TAP M&E
DISSERTAÇÃO DE MESTRADO

PEDRO RENDAS
MIEMc 47676

Escala 1:5

Tolerân. ISO 2768 m

FERRAMENTA STG4&5 HPC

F_HPC_0400

Substitui:

Substituido por:

Appendix XXIV

Stage 4&5 Tool's Bottom Component Technical Drawing

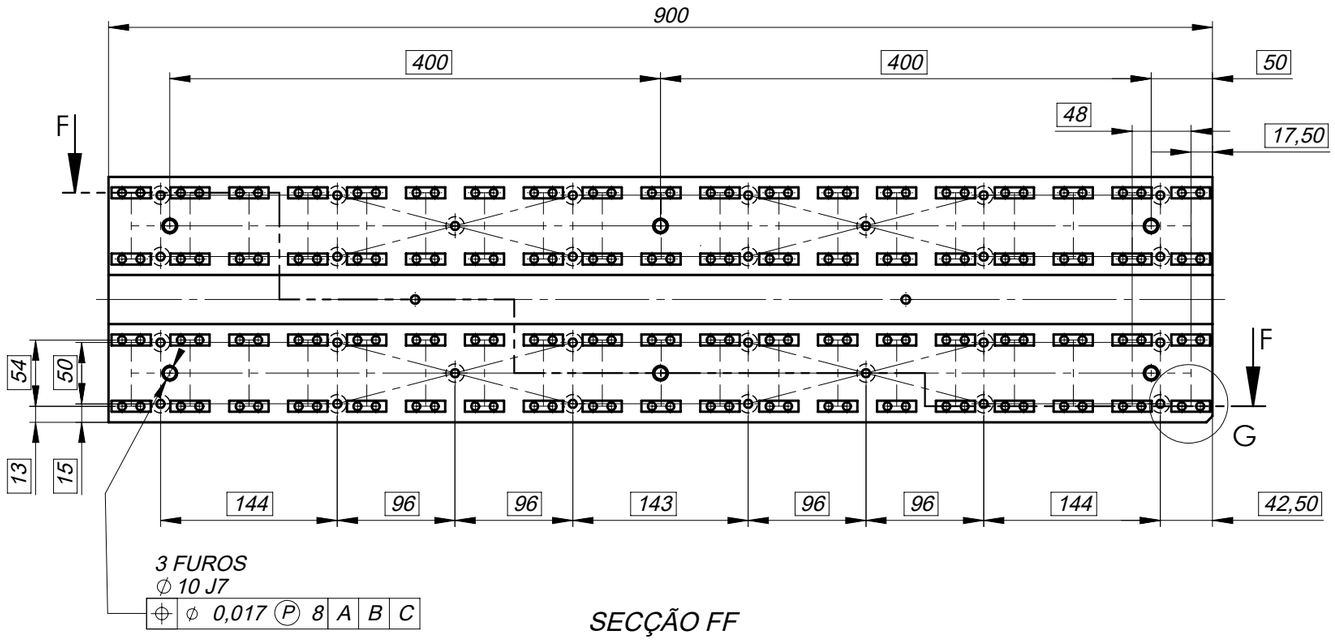

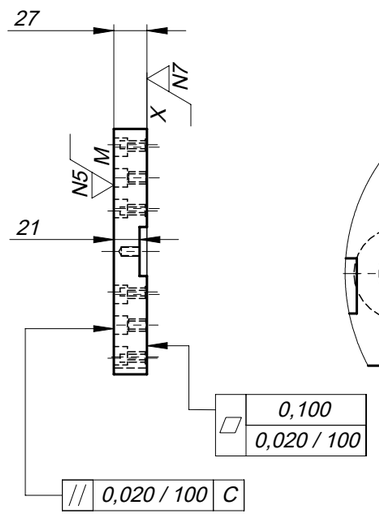

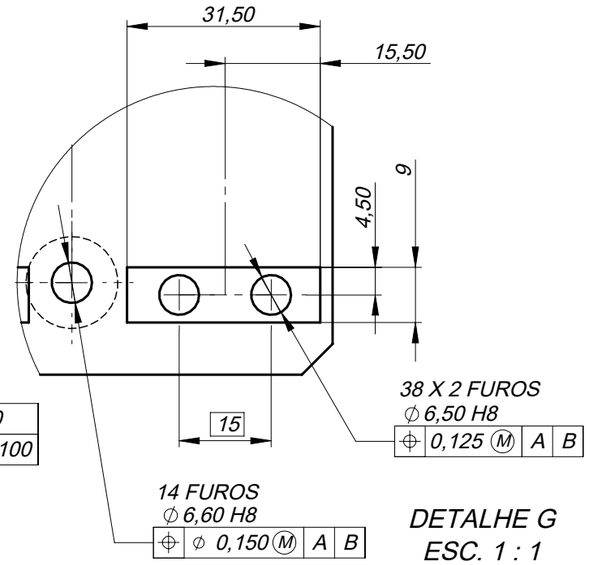

DETALHE G
ESC. 1 : 1

SECÇÃO FF

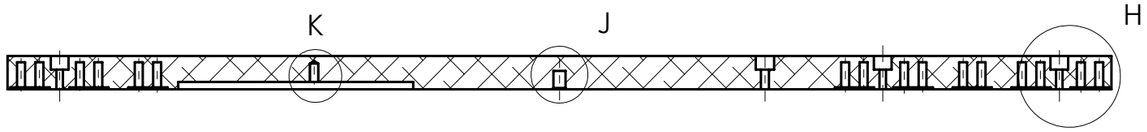

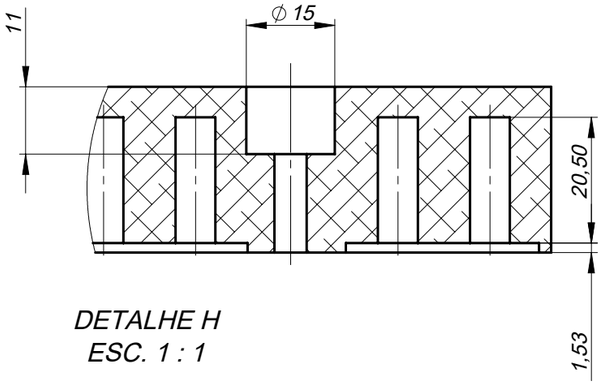

DETALHE H
ESC. 1 : 1

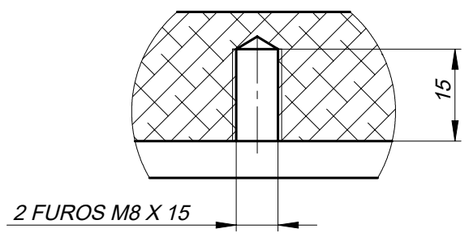

DETALHE K
ESC. 1 : 1

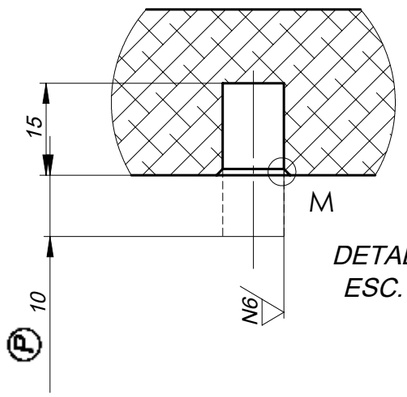

DETALHE J
ESC. 1 : 1

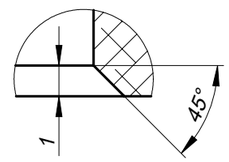

DETALHE M
ESC. 5 : 1

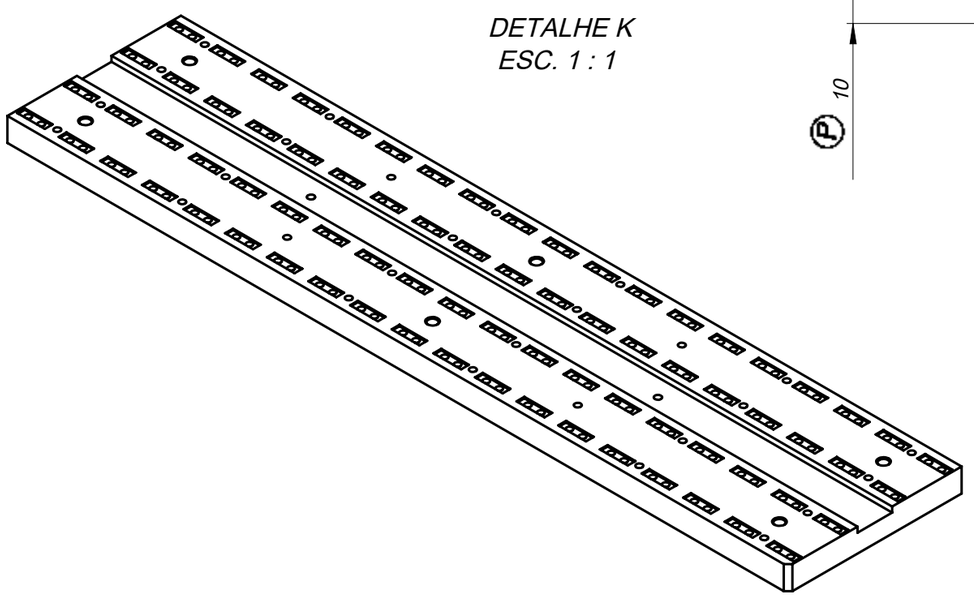

OBSERVAÇÕES

- COTAGEM E TOLERANCIAMENTO EM CONFORMIDADE COM A SIMETRIA EM RELAÇÃO AO PLANO HOTRIZONTAL REPRESENTADO NA VISTA DE PLANTA.

MATERIAL:
ALUMÍNIO 6061

Projetou		2020-06-25
Desenhou		2020-08-31
Verificou		2020- -

UNL-FCT-DEMI TAP M&E
DISSERTAÇÃO DE MESTRADO

PEDRO RENDAS
MIEMc 47676

Escala 1:5

Tolerân. ISO 2768 m

BASE DA FERRAMENTA PARA AS PÁS DO 4º E 5º ANDAR DO HPC

F_HPC_0101

Substitui:

Substituido por:

Appendix XXV

Stage 4&5 Tool's Top Component Technical Drawing

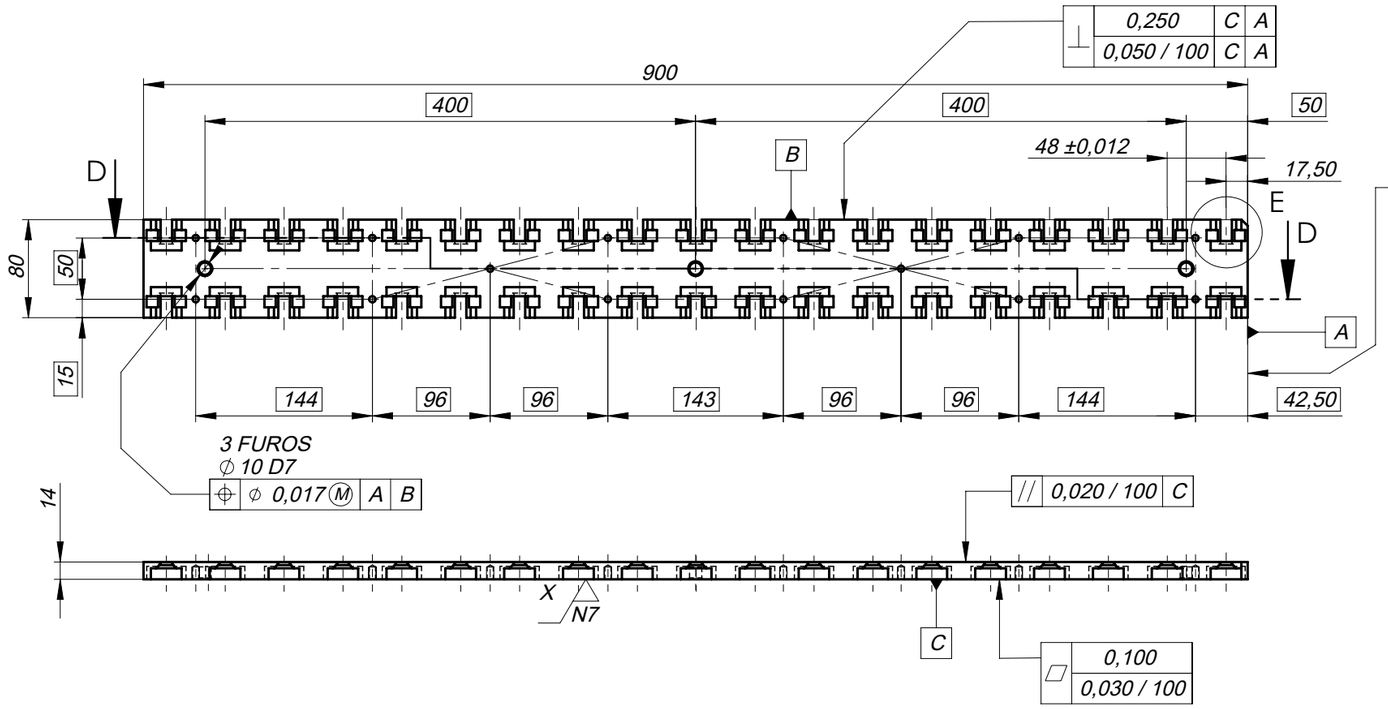

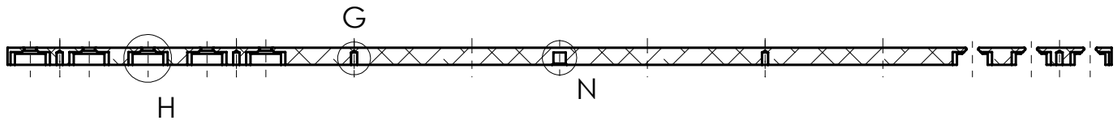

SECÇÃO DD

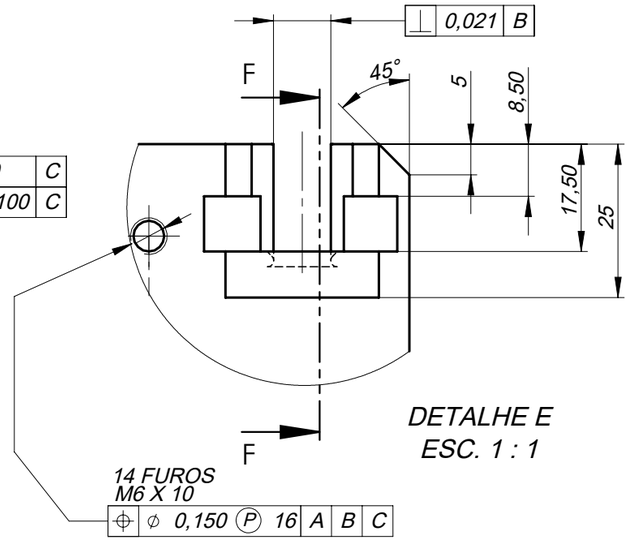

DETALHE E
ESC. 1 : 1

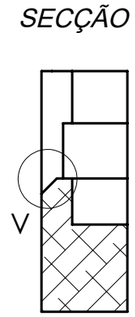

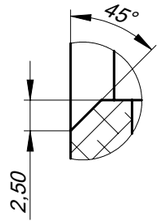

DETALHE V
ESC. 2 : 1

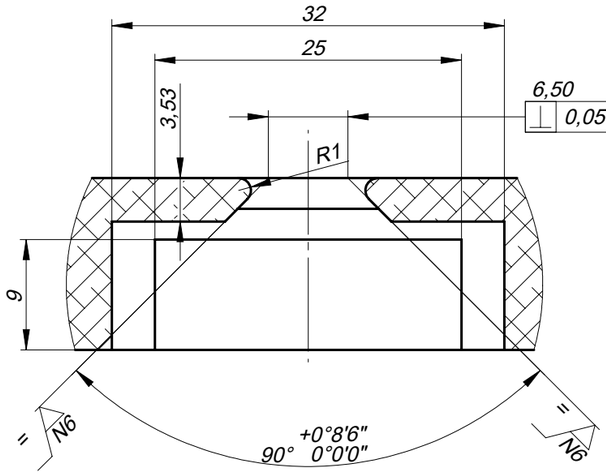

DETALHE H
ESC. 2 : 1

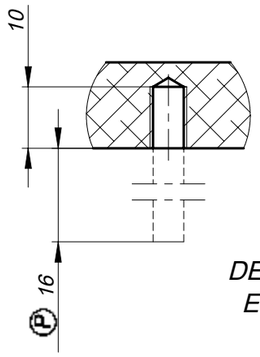

DETALHE G
ESC. 1 : 1

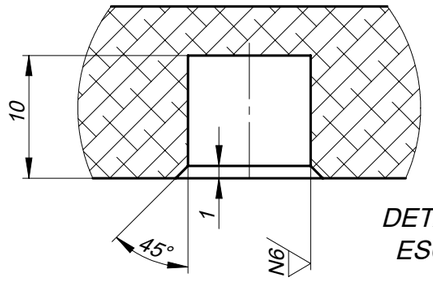

DETALHE N
ESC. 2 : 1

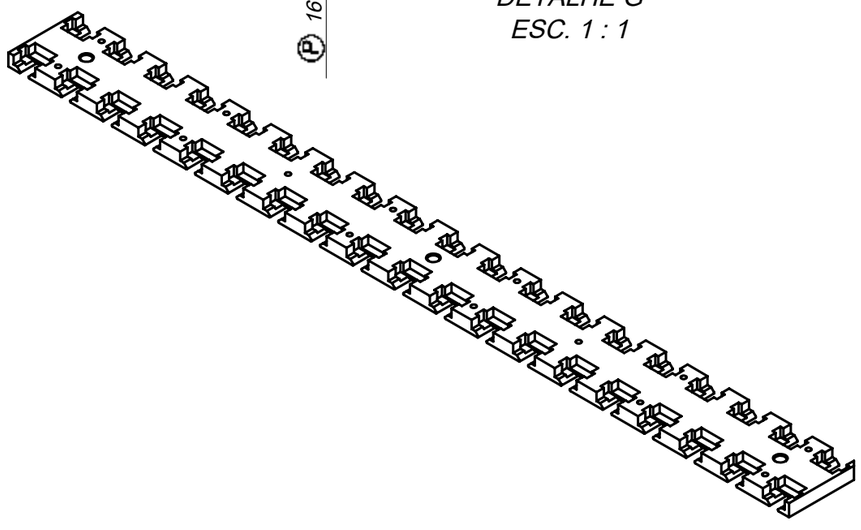

MATERIAL: ALUMÍNIO 6061	Projetou		2020-06-25	UNL-FCT-DEMI TAP M&E DISSERTAÇÃO DE MESTRADO
	Desenhou		2020-08-31	
	Verificou		2020- -	
	Escala 1:5			COMPONENTE DE TOPO PARA FERRAMENTA DAS PÁS DO 4º E 5º ANDAR DO HPC
	Tolerân. ISO 2768 m			

PEDRO RENDAS
MIEMc 47676

F_HPC_0402

Substitui:

Substituido por:

Appendix XXVI

Stage 4&5 Tool's Upwards Force Bar Technical Drawing

Projetou		2020-08-31	UNL-FCT-DEMI TAP M&E DISSERTAÇÃO DE MESTRADO	PEDRO RENDAS MIEMC 47676
Desenhou		2020-06-22		
Verificou		2020- -		

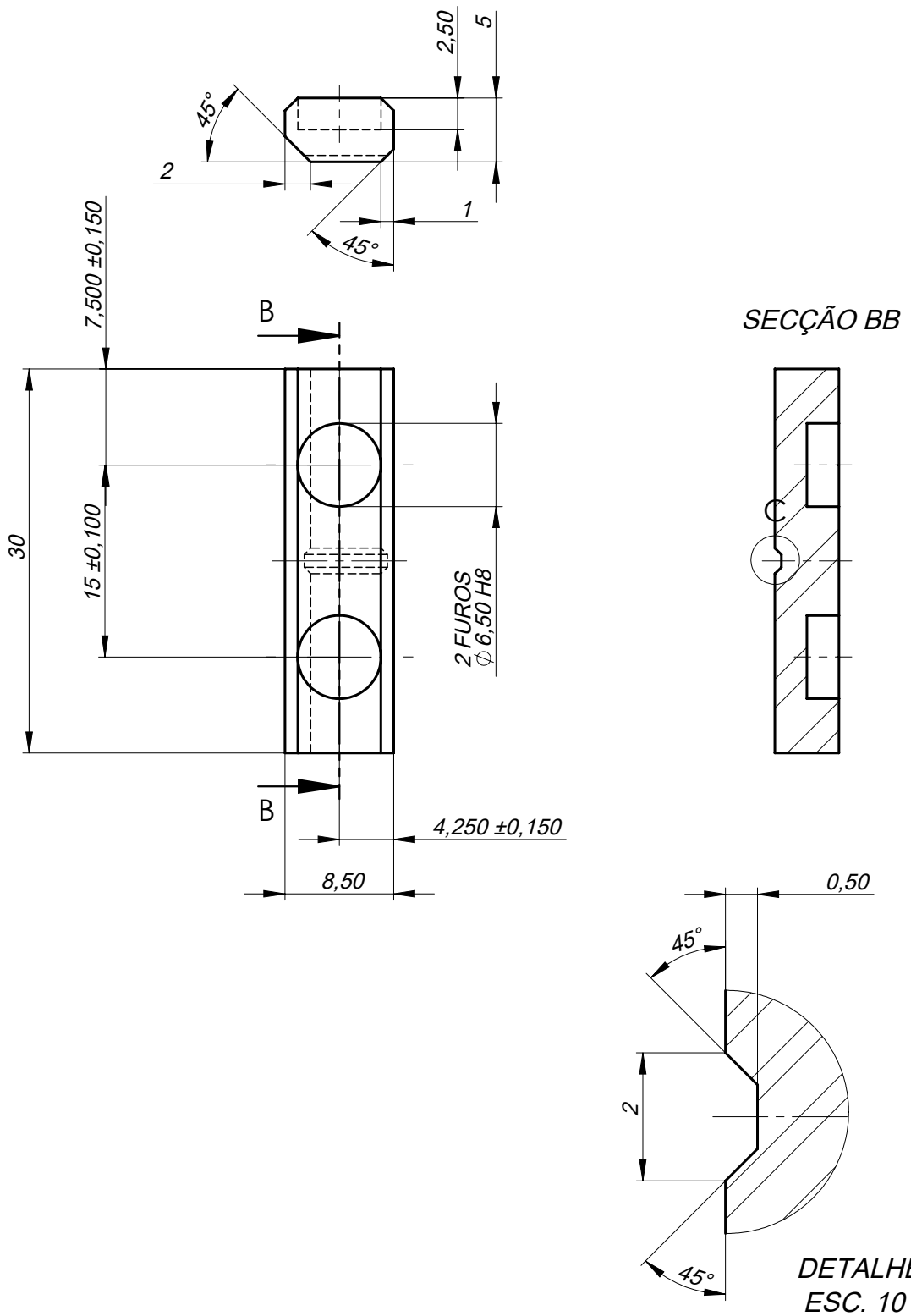

MATERIAL: AÇO INOX AISI 304	Esc. 2:1 Tolerância ISO 2768 m	BARRA DA FERRAMENTA STG4&5 HPC	F_HPC_0403 Substitui: Substituido por:

Appendix XXVII

Stage 4&5 Tool's Spacer Technical Drawing

Projetou		2020-08-31	UNL-FCT-DEMI TAP M&E DISSERTAÇÃO DE MESTRADO	PEDRO RENDAS MIEMC 47676
Desenhou		2020-07-12		
Verificou		2020- -		

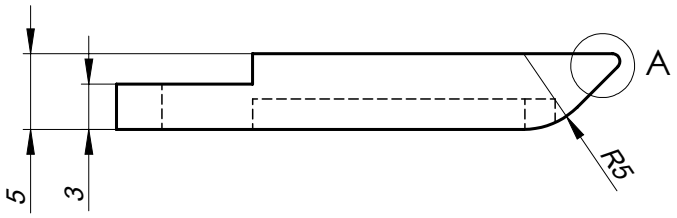

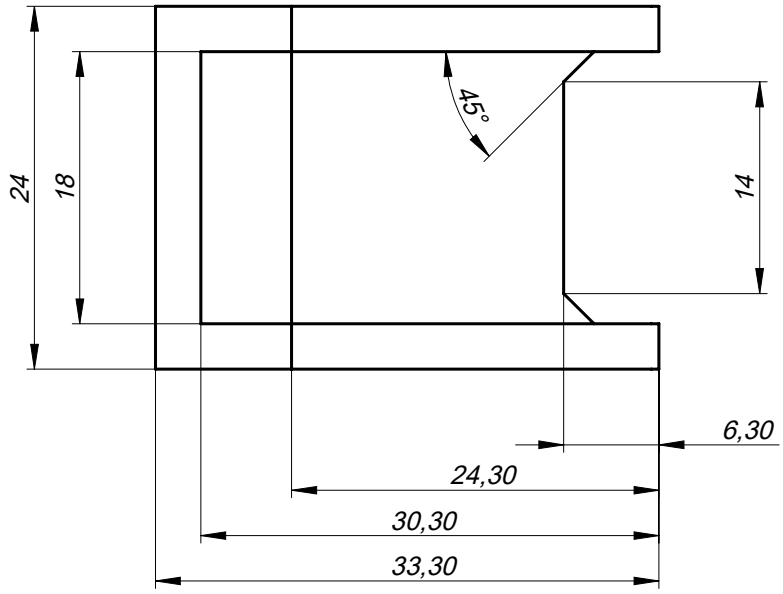

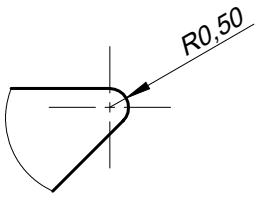

DETALHE A
ESC. 5 : 1

MATERIAL: AÇO INOX AISI 304	Esc. 2:1 Tolerância ISO 2768 m	CAVILHA STG4&5 HPC	F_HPC_0404 Substitui: Substituido por:

Appendix XXVIII

Adjusted Dowel Pin Technical Drawing

Projetou			UNL-FCT-DEMI TAP M&E DISSERTAÇÃO DE MESTRADO	PEDRO RENDAS MIEMC 47676
Desenhou				
Verificou				

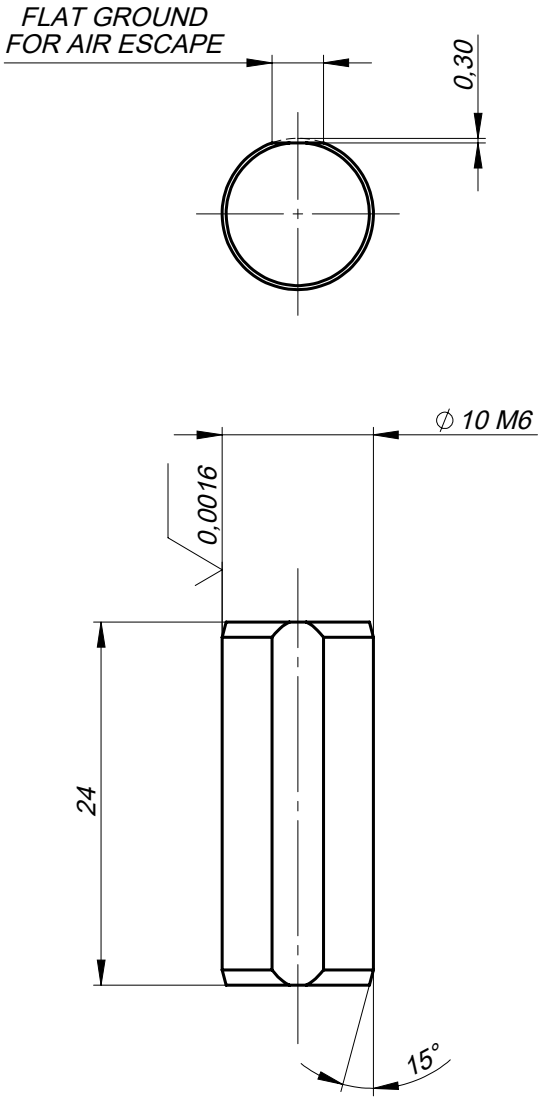

CORTE LONGITUDINAL PARA SAIDA DE AR NA MONTAGEM MODELO TECHNIFAST D10 X L24 A PARTIR DE ISO 2338 (1998)	Esc. 2:1 Tolerância	FLAT GROUND ON DOWEL PIN	F_HPC_PN01 Substitui: Substituido por: